Coil-ring-coil block copolymers as building blocks of supramolecular hollow cylindrical brushes

Dissertation

zur Erlangung des Grades

“Doktor der Naturwissenschaften“

am Fachbereich Chemie und Pharmazie

der Johannes-Gutenberg-Universität Mainz

Silvia Rosselli

born in Livorno

Mainz, 2001

Anyone who has never made a mistake
has never tried anything new.

Albert Einstein

To Cafer

for the unconditional support

for the warmth of his presence

Table of Contents

1 Introduction

1.1 State of the art and aim of the work

In recent years supramolecular science has received great attention[1] because supramolecular functional nanosystems are of primary importance both in material science and in biology. They serve as nanoscale devices in non linear optics, photonics[2], chemoselective sensing[3], as well as models for a better understanding of biological structures such as proteins, nucleic acids[4] and viruses.

Although chemists have been able to obtain complex molecules such as vitamin B_{12}[5] and palytoxin[6], synthesis of large and complex molecules through a stepwise formation of covalent bonds requires considerable effort and time. Polymerization reactions provide a simpler synthetic route for the formation of large molecules. New methodologies allow the synthesis of block copolymers and polymer lattices with more and more complex structures, but there are limitations concerning the introduction of functional groups at defined positions within the macromolecule in the final conformation[7]. A strategy that might overcome the disadvantages of the methods described above is molecular self-assembly. In this case, a relatively small, well defined molecule containing the appropriate functionalities is used as building block for the formation of a complex structure by noncovalent interactions.

Self-assembly strategies are well known and used in nature. Therefore, large effort has been put in the design of structures which imitate the complexity of biological systems both in structure and in function. One of the most intensively studied natural systems is the hollow cylindrical-shaped tobacco mosaic virus[8], and synthetic supramolecular architectures based on gallic acid derivatives show indeed superstructures, which are very similar to the natural model[9]. Nanoscale cylindrical objects have also been obtained by the organization of macrocyclic building blocks with orthogonal polar groups via specific interactions, e.g. hydrogen bonds as in cyclopeptides or in cyclosaccharides[10] (Figure 1.1).

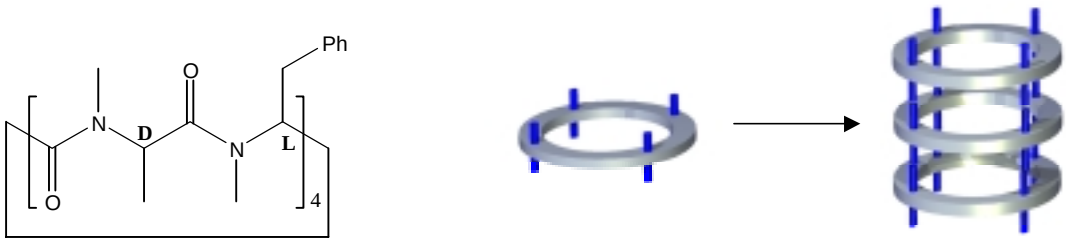

Figure 1.1: Columnar arrangement of cyclic moieties by specific interactions.

Functionalized shape-persistent macrocycles should also be suitable building blocks for the formation of nanoscale hollow cylinders. These structures are built up by a rigid, non collapsible backbone and have a lumen in the size range of a few nanometers. According to the convention describing polymer segments as rigid when their end-to-end distance is roughly the same as their contour length, shape persistent macrocycles have a diameter roughly equal the contour length of the backbone divided by π[11] (Figure 1.2).

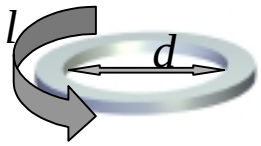

$$d = l / \pi$$

Figure 1.2

An objective of the present work is to facilitate aggregate formation of these macrocycles via non-specific interactions (e.g. solvophobic effects and shape complementary). This approach bears the possibility to organize functionalyzed macrocycles, while leaving the functional groups of the ring "free" and it opens therefore a new entry to intraannular functionalized rods. In other words, the functional groups shall not be used to organize the macrocycles, but the formation of the superstructure shall be used to organize the functional groups. For this purpose, side groups that are incompatible with the cyclic backbone of the ring were attached to the macrocycle and segregation of the different components of the copolymer (in a suitable solvent) should lead to aggregation into cylindrical objects (Figure 1.3).

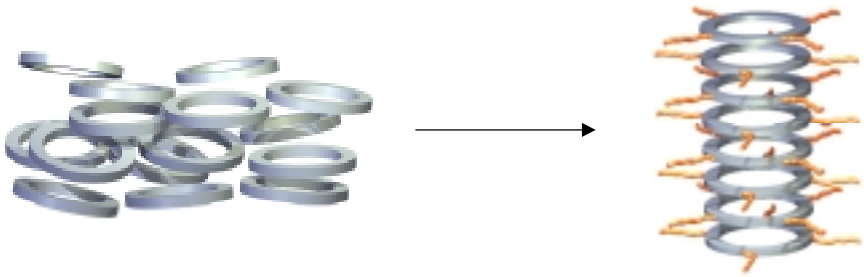

Figure 1.3: Aggregation of shape-persistent macrocycle by non-specific interactions.

Attempts by other groups have shown that π-π interactions can be used to aggregate phenyl-acetylene or phenyl-butadienyl macrocycles[12]. However, in those cases the occurrence of the aggregation strongly relies on the electronic structure of the molecules, only macrocycles with electron deficient core structures show the behavior of self aggregation[13].

Previous studies in Höger's group[14] on oligo-alkyl substituted shape-persistent rings have shown that their aggregation can also been enforced by solvophobic effects. For example, in solvents which act as good solvents for the rigid core and the flexible corona (e.g., CH_2Cl_2), no aggregation was observed. By adding a solvent which can solubilize only the alkyl corona (e.g., *n*-hexane) but not the rigid core, a solvophobic aggregation of the structures can be induced (Figure 1.4).

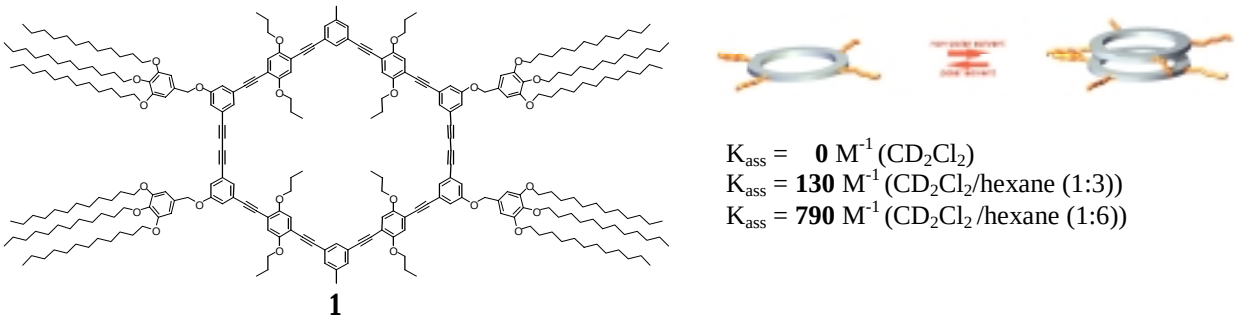

Figure 1.4: Formation of aggregates by solvophobic interactions.

However, this approach cannot be extended to the formation of higher aggregates due to the restricted compound solubility. Compound **1** just does not dissolve in a methylene chloride/hexane mixture with an higher hexane content.
In order to overcome the solubility problem, non-crystallisable side chains need to be attached to the ring. This might be either branched alkyl groups or, and this is the aim of the work presented here, oligomeric or polymeric side groups.

Figure 1.5: Schematic presentation of coil-ring-coil block copolymers.

When two coiled oligomers are attached to the rigid ring, the resulting structures can be described as coil-(rigid)ring-coil block copolymers (Figure 1.5) which are a specific case of rod-coil block copolymers. From those materials it is known that they microphase segregate to well ordered superstructures even at relatively low molecular weight, so that a similar behavior can be also expected for our structures.

2 Rod-coil block copolymers as a subclass of block copolymers

2.1 Properties and recent studies

Copolymers are defined as polymers containing two or more discrete types of monomer units. Copolymers in which blocks of one type of repeating units are attached to blocks of another type of repeating units, are called the block copolymers. Different block copolymers are distinguished by the number of blocks per molecule, for example, A_mB_n is referred as diblock and $A_nB_mA_n$ is referred as triblock copolymer, respectively. The architecture of block copolymers can be controlled by the synthesis.

The mixing of two different homopolymers leads in most cases to a two-phase blend. The reason why two polymers are usually not miscible becomes apparent from simple thermodynamic considerations. First, the enthalpy of mixing is usually small and positive. In low molecular weight compounds this is overcompensated by the entropy of the mixing. However the contribution of the entropic term to the total free mixing enthalpy becomes smaller and smaller as the molecular weight of the polymer increases making mixing an unfavorable process.

In block copolymers the different component blocks are bound together covalently, thereby segregation is prevented on the macroscopic scale. However, on the microscopic level the different block self-assemble in the melt into a variety of ordered structures with nanoscale periodicities via the process called *microphase segregation*. At high temperatures, the chains of the block copolymer are mixed homogeneously, as in any polymer melt. As the temperature is reduced, the tendency for the blocks to segregate is increased, i.e. the enthalpic process of demixing is favored. At the Order-Disorder Transition (ODT) temperature, the homogenous melt become ordered. Microphase segregation is driven by the enthalpy of demixing of the constituent components of the block copolymers, while macrophase separation is prevented by chemical connectivity of the blocks. This enthalpy is proportional to the Flory-Huggins segmental interaction parameter χ, which is found to be inversely proportional to the temperature. Microphase segregation leads to ordered structures with periods of several R_g, where R_g is the copolymer radius of gyration. The entropic penalty associated with the chains stretching is proportional to the degree of polymerization N. The product χN that express the enthalpic-entropic balance is then used to parameterize block copolymer phase behavior, along with the composition of the copolymer.

Remarkable are also the two basic processes that characterize the phase behavior of block copolymers in solution: micellization and gelation[15]. Micellization occurs when block copolymer chains associate into micelles in a solvent that is selective for one of the blocks. The core of the micelle is formed by the insoluble or poorly solvated block, while the corona contains the selectively

solvated block. The formation of micelles is one of the most important and useful properties of block copolymers. For example, micelles formed by block copolymers can solubilize otherwise insoluble substances, be used to microscopically "mix" incompatible substances and stabilize colloidal particles or form microemulsions. At a fixed temperature micellization occurs above a concentration called the critical micelle concentration (cmc). At higher concentrations, the micelle can order into a lattice above a critical gel concentration (cgc). In other words, in a semidilute or concentrate of block copolymer solution, micelles order into gels. As the concentration of the block copolymers in the solution increases, the polymer chains begin to overlap. This can lead to the formation of a liquid crystalline phase such as a cubic phase of spherical micelles, a hexagonal phase of a rod-like micelles or a lamellar phase. These ordered phases are considered lyotropic liquid crystal phases analogous to those formed by low-molecular-weight surfactants.

Diblock copolymers consisting of a rigid block attached to a coiled block are termed rod-coil block copolymers. The phase behavior of block copolymers formed by flexible polymer coils is remarkably rich. If one of the blocks is rigid, the copolymers can be expected to exhibit even more complex phase behaviors. For example, the rigid block may form a liquid crystal phase with its own phase behavior. This leads to the possibility of self-assembling of structures consisting of domains of a liquid crystalline material within a microphase-segregated block copolymer superstructure.

The first synthesis and characterization of rod-coil block copolymers was reported by Gallot and co-workers[16] in 1976. They studied AB diblock copolymers consisting of polybutadiene (PB) and the polypeptide poly(γ-benzyl-L-glutammate) (PBLG) or poly(N^5-hydroxy-propylglutammine) and found that their copolymers form a lamellar structure in concentrated solution and in the dry state (Figure 2.1).

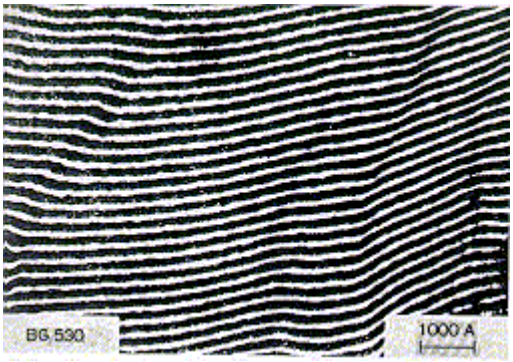

Figure 2.1: Electron micrograph of stained poly(butadiene-*block*-(γ-benzyl-L-glutammate)).

In this system the polypeptide chains are in α-helix conformation (rod block) and are assembled in a hexagonal array and folded while the PB chains are in a random coil conformation. PBLG is often used as a model rod like polymer, and forms liquid crystal phases in solution[17]. Later, Nakajiama[18]

investigated the phase behavior of ABA triblock copolymers consisting of PBLG as A blocks, and PB as B block. They reported lamellar, cylindrical and spherical domain morphologies as a function of the copolymer composition.

In the recent years the amount of different types of rod-coil block copolymers has remarkably increased. Examples are the synthesis of amylose-polystyrene block copolymers described by Stadler[19] and the preparation of poly(*para*-phenylene)-polystyrene or poly(ethylenoxide) block copolymers reported by Müllen[20].

Jenekhe[21] reported the synthesis of the poly(phenylquinoline)(PPQ)-*block*-polystyrene(PS) rod-coil copolymer. In a selective solvent for the rod block the copolymer forms micrometer size aggregates with various morphologies such as spheres, cylinders and lamellae, depending on the initial solvent composition and the solution dry rate, which can be observed by optical microscopy. Surprisingly, spherical molecules (C_{60}, C_{70}) can be solubilized to a large extend by solutions of the rod-coil block copolymers, resulting in the encapsulation of huge numbers of fullerene molecules into those hollow hard spheres. On the other hand, in a selective solvent for the coiled block it was possible to observe the formation of inverse micelles. Furthermore, these hollow soft spheres could order into two- and three-dimensional periodic structures leading to ordered microporous materials (Figure 2.2).

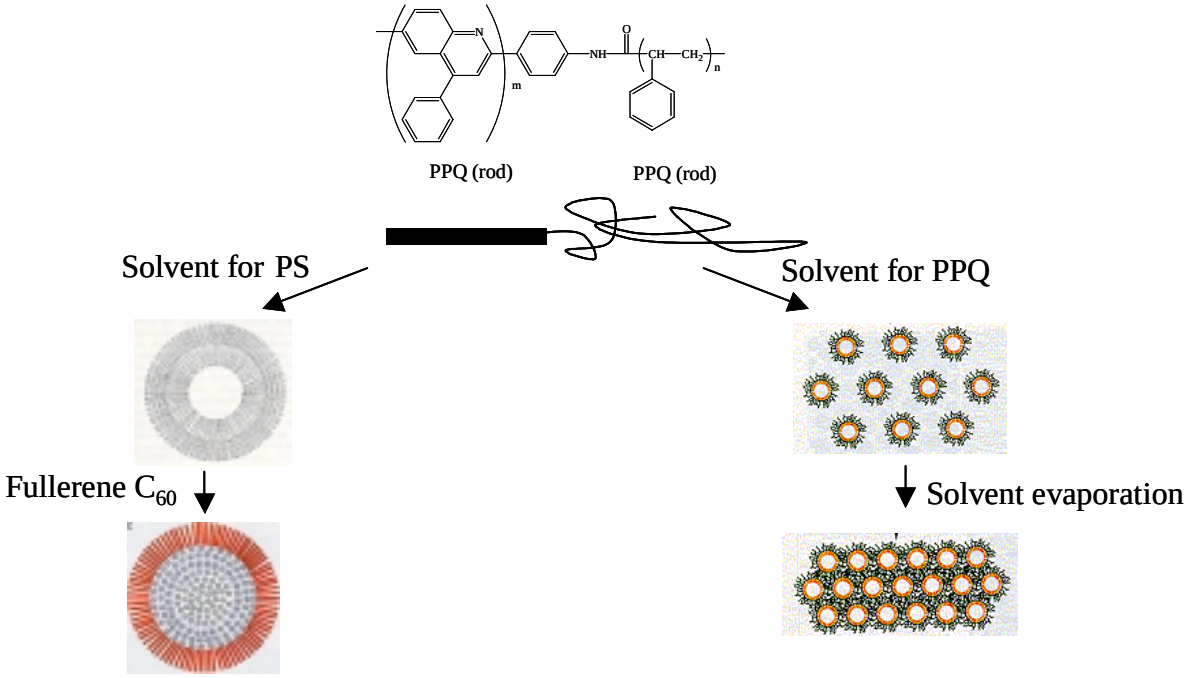

Figure 2.2: Schematic behavior of PPQ-*block*-PS rod-coil copolymers in different solvents.

The potential of the novel phase behavior in rod-coil block copolymers is illustrated by the recent work of Thomas on poly(hexyl-isocianate)(PHIC)-polystyrene (PS) rod-coil diblock copolymers[22]. PHIC, which adopts a helical conformation in the solid state, has a long persistence length (50-60 nm) and can form lyotropic liquid crystals in solution. The copolymer has a short PS block attached

to a long PHIC block. A number of morphologies were reported, wavy lamellar (WL), zigzag (ZZ) and arrowhead (AH) structures. Depending on the length of the rod block (by fixed length of the coiled block), it is tilted with respect to the layers in order to minimize free space between the rod (Figure 2.3). However, a complete understanding of these self-assembled morphologies is still ahead.

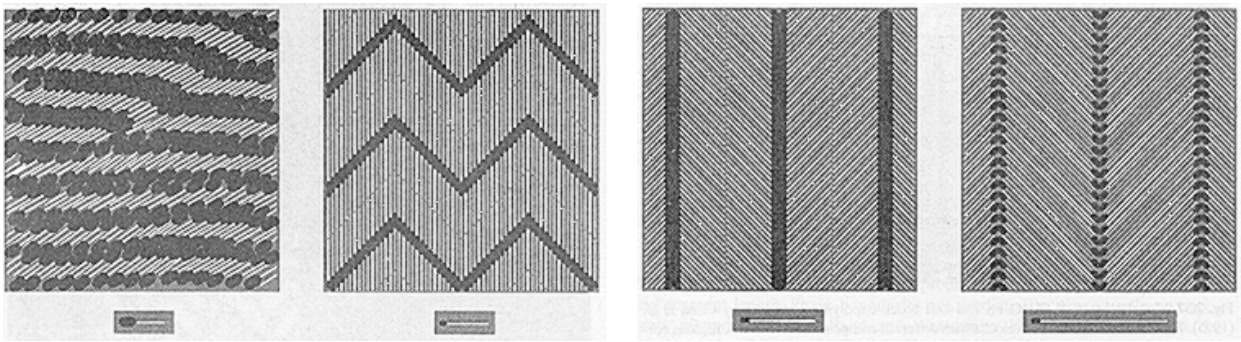

Figure 2.3: Schematic models show the packing arrangement of the rod-coil chains in the three solid state morphologies. For a given rod-coil molecule, the PHIC block is represented by the white rod and the PS block by the black ellipsoid. From the left to the right, WL, ZZ and AH morphology.

Stupp and co-workers reported the synthesis and electron microscopic structure characterization of the first rod-coil block copolymers in which the rod blocks were short (60Å) mesogenic compounds prepared by stepwise synthesis and the flexible block were poly(isoprene)s of different molecular weight[23] (Scheme 2.1). Films of these rod-coil block copolymers were casted from cyclohexane solution (a good solvent for the coil but poor for the rod) and showed nanophase segregation with a morphology, which depends on the rod volume fraction f_{rod}, as characterized by transmission electron microscopy (TEM). For f_{rod} = 0.36 and 0.30 a predominantly lamellar morphology with regularly spaced rod and coil domains is observed, which forms a fingerprint-like texture, while sample with f_{rod} = 0.25 showed a hexagonal packing.

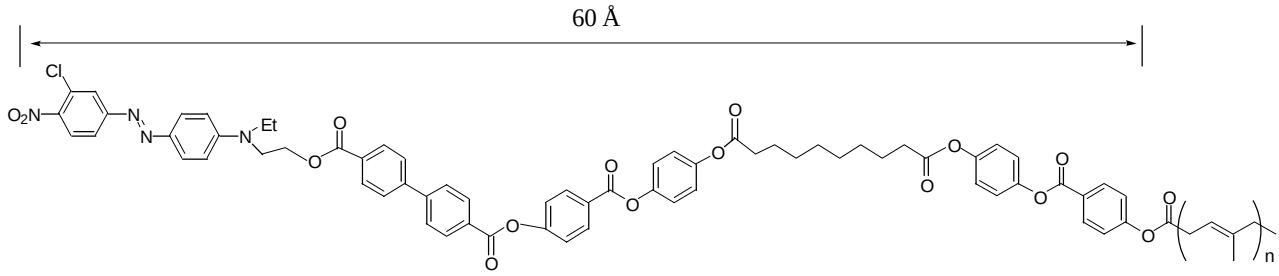

Scheme 2.1

Interestingly, the rod domains are not lamellae but form discrete channel-like long objects, 6-7 nm in diameter and a three dimensional staking order across the layers was found[24].

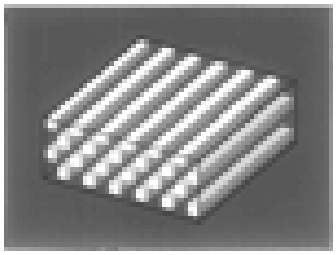

Figure 2.4 Schematic of the stacking arrangement of "strip" rod domains with a checkerboard cross section.

Two other examples of ABA rod-coil block copolymers in which the rod block is a monodisperse compound are poly-1,4-isoprene-[oligo(*p*-phenyleneethynylene)]-poly-1,4-isoprene] synthesized by Godt[25], and polystyrene-oligothiophene-polystyrene described by Hempenius[26]. In the latter case, the triblock copolymer forms spherical micelles with an average diameter of 12 nm, that corresponds to an aggregate of more or less 60 copolymer units.

Theoretical work has confirmed that various liquid crystalline (LC)-phase (supramolecular structures) such as nematic, layered smectic, and cylindrical phases could be observed in rod-coil block copolymers depending on the relative volume fraction of coiled block[27]. Unlike coil-coil block copolymers, rod-like molecules cannot form curved interfaces (in the melt state) due to the lack of conformational freedom associated with a rod-like chain. Lee and co-workers[28] have synthesized a rod-coil block copolymer consisting of (ethyl 4-[4'-oxy-4-biphenylcarbonyloxy]-4'-biphenylcarboxylate) as rod and poly-ethylene oxide (PEO) as the coiled block (Scheme 2.2). It organizes into a lamellar structure with nanoscale dimension and shows a layered smectic A phase in the melt. Upon complexation of the copolymer with lithium triflate a dramatic change of the phase behavior was observed. The complexes displayed successively lamellar smectic A, cubic and cylindrical micellar mesophases with increasing concentration of the triflate. This is a result of the increase of the coiled part of the structure as the salt concentration increases.

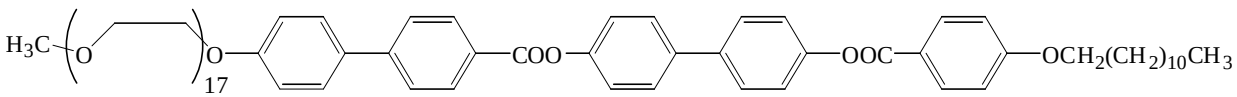

Scheme 2.2

When the poly-ethylene oxide is substituted by poly-propylene oxide, which can not crystallize, the copolymer organizes into a bicontinuous cubic or hexagonal columnar mesophase as function of the volume fraction of the coil segments and the temperature[29]. An interesting extension of this concept is described by the same authors (Figure 2.5).

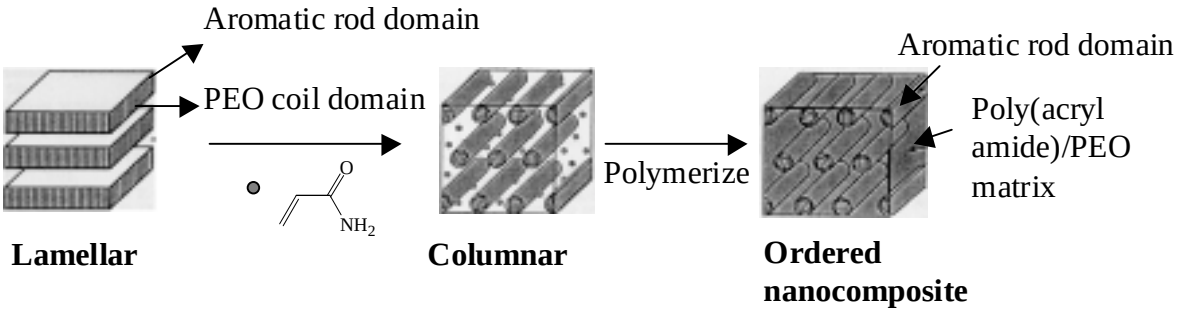

Figure 2.5: Schematic representation of the induction of a hexagonal columnar mesophase through polymerization.

They demonstrated that swelling of the block copolymer by acrylamide changes the morphology from lamellar to columnar, which can be conserved by polymerization of the amide[30]. This result is a novel strategy for the construction of ordered nanocomposite materials with well defined architectures.

Highly regular organizations of rod-coil block copolymers are presented by the work of Leclère and co-workers[31] based on poly(*p*-phenylene) (PPP)-*block*-polystyrene(PS) and poly(*p*-phenyleneethynylene) (PPE)-*block*-poly(dimethylsiloxane) (PDMS) copolymers. Atomic Force Microscopy (AFM) investigations of thin films show the presence of bright elongated structures with a length of a few micrometers (Figure 2.6).

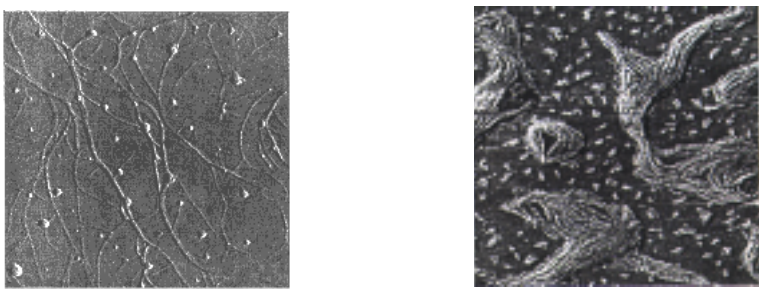

Figure 2.6: AFM images of thin films of PPE-*b*-PDMS (left) and of PPP-*b*-PS (right) cast from toluene solution on mica.

Another example of the formation of cylindrical object is reported by Massey and co-workers[32]. They report the synthesis of poly(ferrocenyldimethylsilane)(PFS)-b-poly(dimethyslsiloxane) with a block ratio 1:6 and their aggregation into rod-like micelles in hexane solution, a specific solvent for the PDMS block and a precipitant for PFS. The micellar structures consist of a cylindrical iron-rich PFS core surrounded by a swollen corona of PDMS chains. Upon drying, the PDMS chains collapse to form a solid continuos insulating sheath (Figure 2.7).

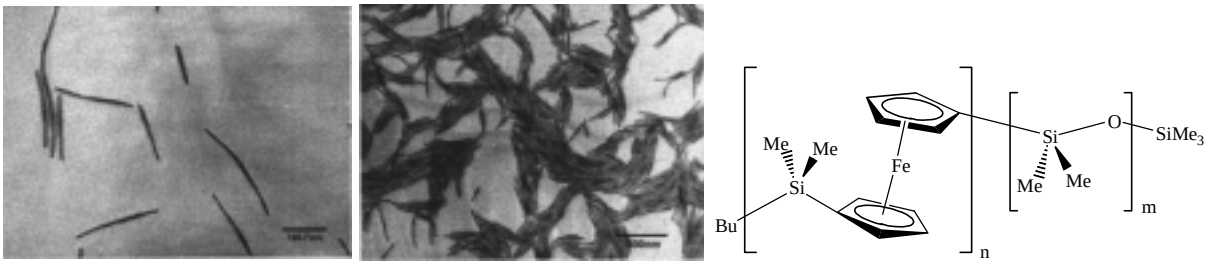

Figure 2.7: TEM of PFS-*b*-PDMS which self-assembles in hot hexane to form wormlike micelles.

Opposite to that, above the T_m of PFS (120-145°C), spherical aggregates are formed, which suggested that crystallization of the core polymer is the driving force for the formation of the wormlike micelles below T_m. This was confirmed by the fact that amorphous polyferrocene blocks like poly(ferrocenylmethylphenylsilane) (instead of PFS) form spherical micelles in hexane at room temperature[33].

Recently, it has been reported that PFS-*b*-PDMS block copolymers with a block ratio of 1:13 form also nanotubes[34]. Moreover, encapsulation of *n*-butylferrocene showed the ability of the micelles interior to insert small molecules (Figure 2.8).

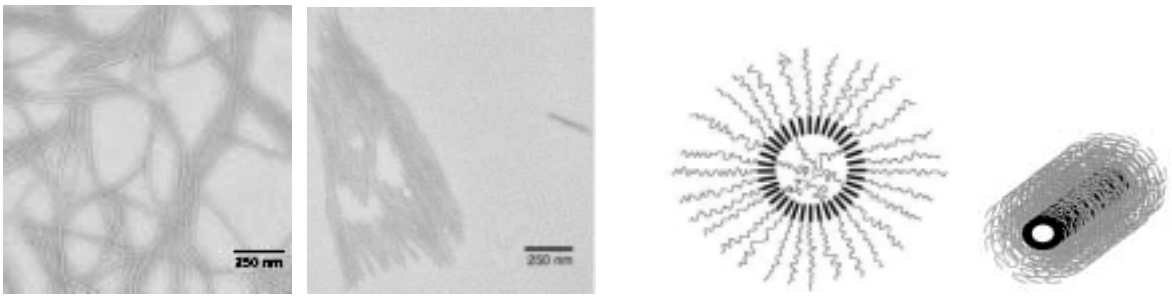

Figure 2.8: TEM micrographs of PFS-*b*-PDMS micelles in hexane (left) and tubules with *n*-butylferrocene encapsulated within the cavities (middle). On the right side the schematic representation of a tubule.

To conclude, beside their interesting morphology, rod-coil block copolymers can also be used for the formations of individual nanometer scale objects such as spheres or cylinders. The next steps are investigations towards the functionalization of the objects interior.

3 Synthesis of oligomer-substituted shape-persistent macrocycles (coil-ring-coil block copolymers)

3.1 Introduction

As it was already mentioned, coil-ring-coil block copolymers are formed by nanometer sized shape persistent macrocycles based on the phenyl-ethynyl backbone as rigid block and flexible oligomers like polystyrene or polydimethylsiloxane (Scheme 3.1).

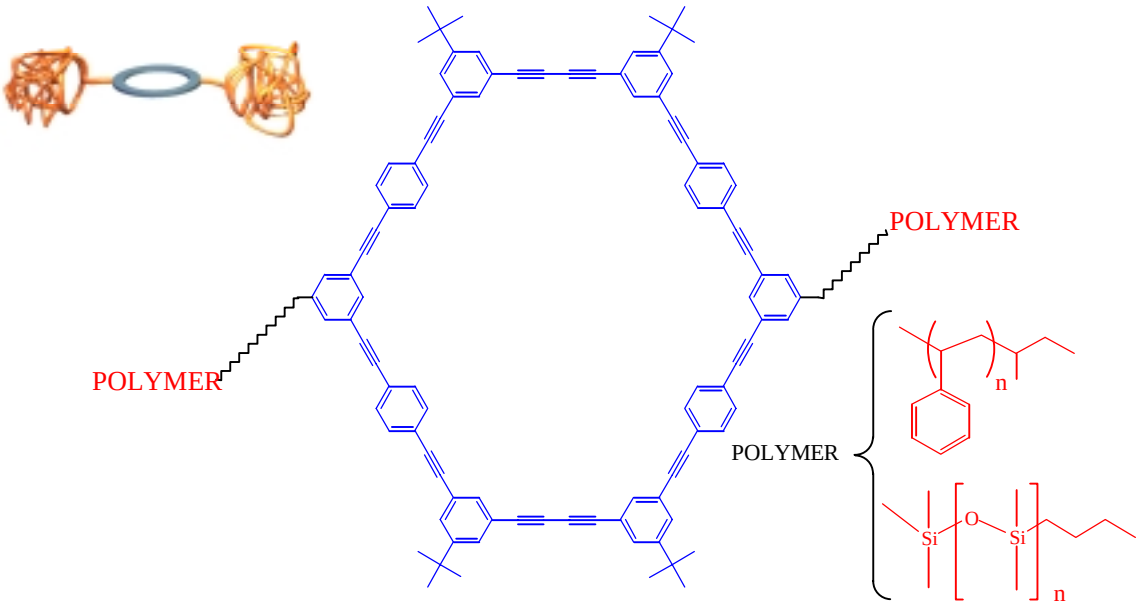

Scheme 3.1 Schematic structure of the coil-rod-coil block copolymers.

Two different strategies can be used to synthesize the copolymers. The macrocycle and the polymer can be synthesized independently and then bound together (Scheme 3.2 (a)) or a polymer substituted half-ring can be dimerized (Scheme 3.2 (b)).

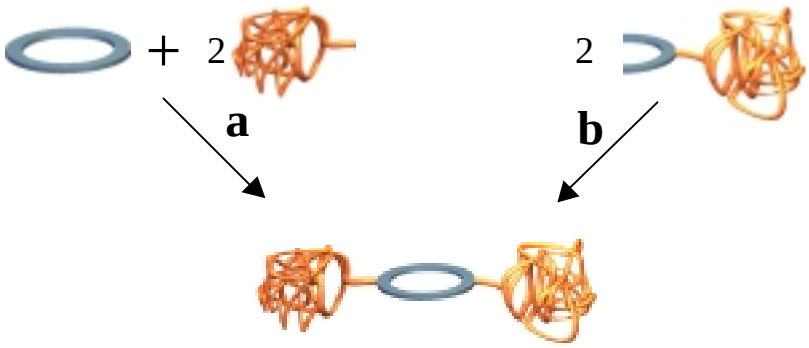

Scheme 3.2 Possible strategies to synthesize the copolymers.

The first strategy (a) is more convenient for two reasons. First, it opens the possibility to attach different polymers at the final ring and therefore to prepare different copolymers in only one step starting from the same macrocyclic building block. And second, the separation of oligomer substituted cyclic dimers from higher oligomers formed in the cyclization according to the strategy (b) might be difficult. Another point that has to be discussed is the way in which the polymer and the macrocycle can be connected. A reasonable possibility is to use an aliphatic ester group, because it is stable and relatively easy to form. In addition, is convenient to prepare macrocycles with an alcoholic functionality and a polymer with a carboxyl end group.

The experimental work can be divided in three main parts. The first contains the synthesis of the functionalized macrocycle, then the synthesis of functionalized polystyrene and polydimethylsiloxane is described, and finally the attachment of the two blocks will be discussed.

3.2 Synthesis and purification of functionalized macrocycles

The synthesis of the shape persistent macrocycles is based on two separate steps. In the first step the buildings blocks of the macrocycles are connected to form a precursor of defined length and then in the second step this precursor undergoes a ring-closure reaction together with the formation of oligomeric and polymeric side products. Two different strategies are found in the literature to perform this task.

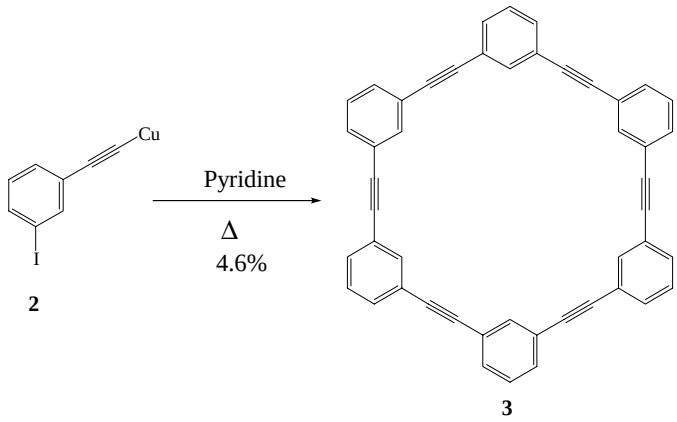

2 **3**

Scheme 3.3 Synthesis of the macrocycle: Staab's approach.

In Staab's[35] approach both steps are performed in a one-pot procedure (Scheme 3.3). A very simple starting material was used in the condensation and a very broad mixture of cyclic and noncyclic oligomers and polymers of different molecular weight were obtained as expected from a purely statistical reaction. Nevertheless, the cyclic hexameric macrocycle **3** was isolated in 4.6 % yield. However, the loss of most of the educt in this approach can be problematic if valuable starting materials are used and the purification of the product may not always be easy.

A completely different approach was investigated by Moore and co-workers[36]. First the precursor **4** was prepared via a repetitive stepwise reaction and then cyclized in the final step via an intramolecular palladium-catalyzed Hagihara-coupling under pseudo-high-dilution conditions (Scheme 3.4).

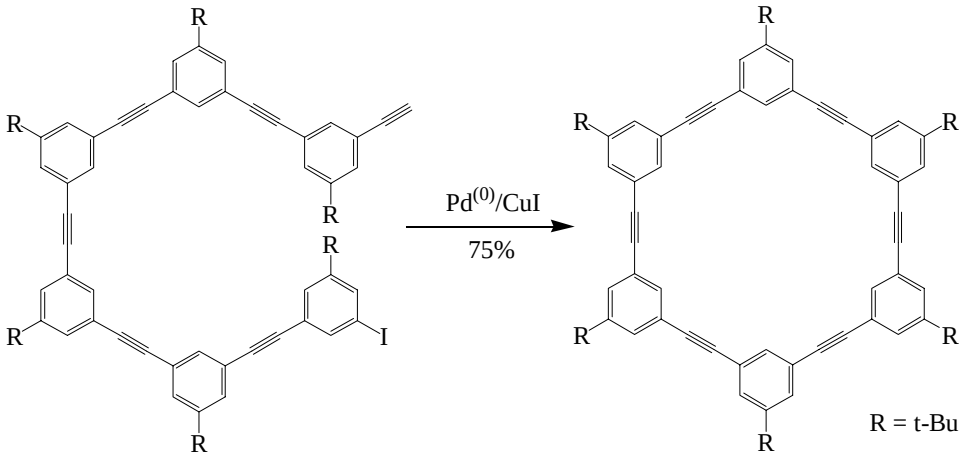

4 **5**

Scheme 3.4 Synthesis of the macrocycle: Moore's approach.

The macrocycle **5** was isolated in 75 % yield as the only product. The high yield and the non-problematic purification have to be compared with the complexity of the precursor **4** that was prepared by several repetitive reactions. In any case, the stepwise formation of the precursor opens the possibility to synthesize rings with different components.

Between those two different approaches is the strategy used in Höger's group. It can be viewed as a compromise between the high yield and the facility of purification of the products in the cyclization reaction and the easy precursor preparation. The main idea is to synthesized an "half-ring" as precursor for the macrocycle, that contains two free acetylenes. Then, the half-ring is cyclized by forming two *sp*-*sp* bonds via a copper-catalyzed Glaser coupling under pseudo-high-dilution conditions. In this reaction all the statistical products are formed, the dimeric ring together with trimeric, tetrameric and polymeric material. Nevertheless, by using pseudo-high-dilution conditions the macrocycle can be obtained in 50-60 % yield and the purification is in general not problematic because of the low solubility of the dimeric ring with respect to the more flexible oligomers. To clarify the concept, a schematic retro synthesis is presented in Scheme 3.5.

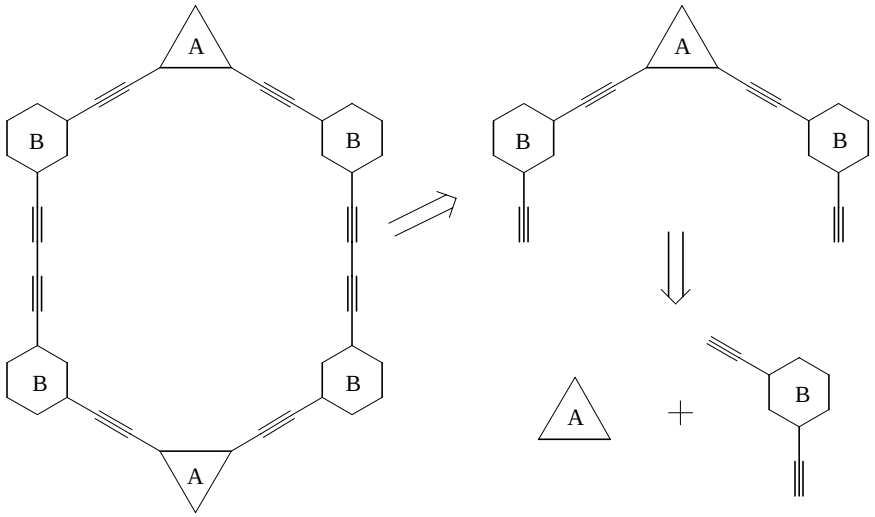

Scheme 3.5 Retro-synthesis of the macrocycle.

The macrocycle is symmetric with respect to the plane between the *sp*-*sp* bond, and a line between the pieces **A**. The half ring is built by assembling blocks of type **A** and block of type **B**. The blocks **A** can be termed "central corner pieces" while the **B** can be defined as "side corner pieces". The latter need to be mono protected bis-acethylenes in order to avoid polymerization reactions. The side piece **B'** (Scheme 3.6) has been used before in the group, and it is already described. Differently, the "side pieces" **B"** and the "central corner pieces" **A** are new building blocks and their synthesis will be described in detail. They carry protected functional groups at which the polymers can be attached. The different types of corner pieces **A'**, **A"**, **B'** and **B"** that have been prepared and used are listed in Scheme 3.6.

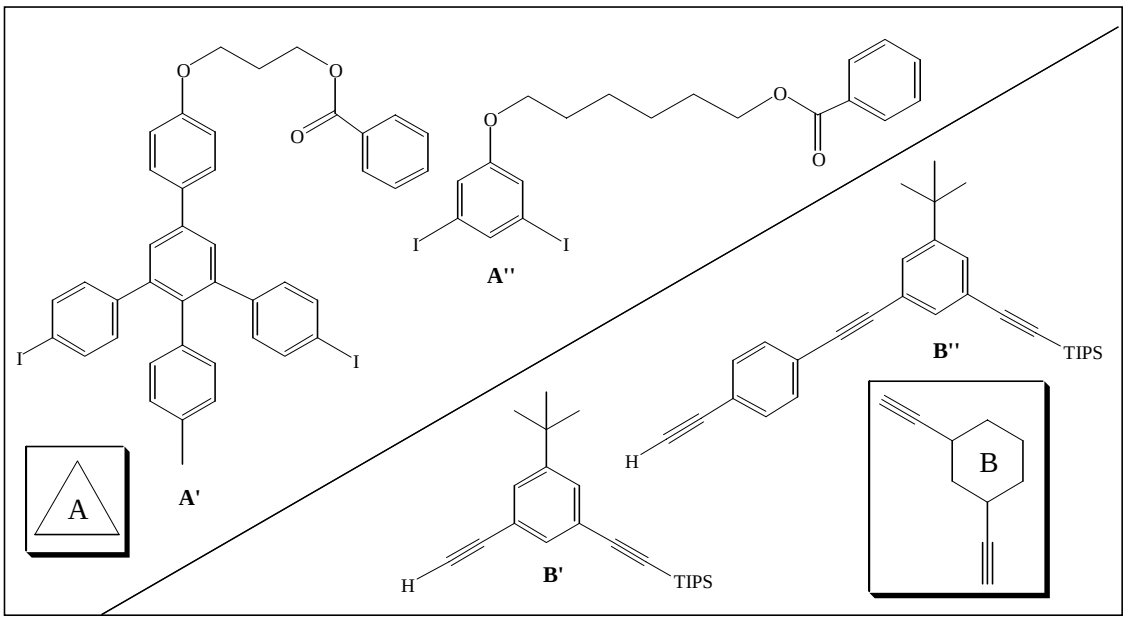

Scheme 3.6 Building blocks of the macrocycle.

3.2.1 Synthesis of the building blocks

The synthesis of the block **A'** is based on the transformation of 2,4,6-triaryl pyrylium salts (**6**) to the 2',6'-diaryl *p*-terphenyls (**7**) described by Zimmerman[37] (Scheme 3.7).

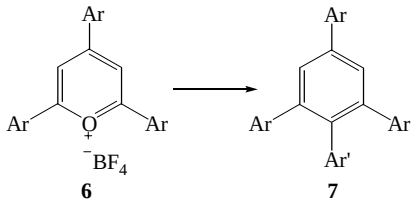

Scheme 3.7 Transformation of 2,4,6-triaryl pyrylium salts to the 2',6'-diaryl *p*-terphenyls

Condensation of one equivalent of 4-methoxy-benzaldehyde (**8**) with two equivalents of 4-iodo-acetophenone (**9**) in the presence of $BF_3 \bullet Et_2O$ at 100 °C for 2 h gives the 2,6-di-(4-iodo-phenyl)-4-(4-methoxy-phenyl)-pyrylium-tetrafluoroborate (**10**) in 48 % yield (Scheme 3.8)**.**

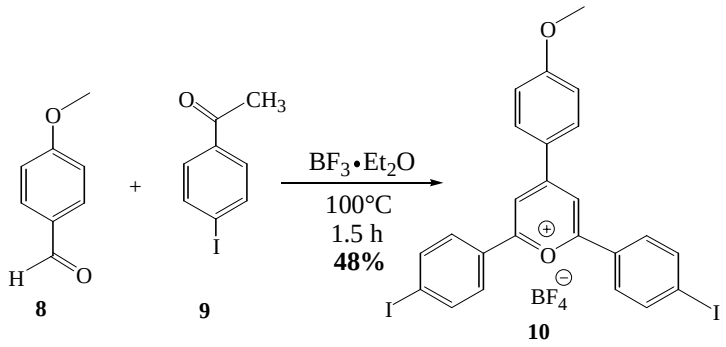

Scheme 3.8 Synthesis of pyrilium salt **10**.

The mechanism of this reaction can be divided in three steps (Scheme 3.9).

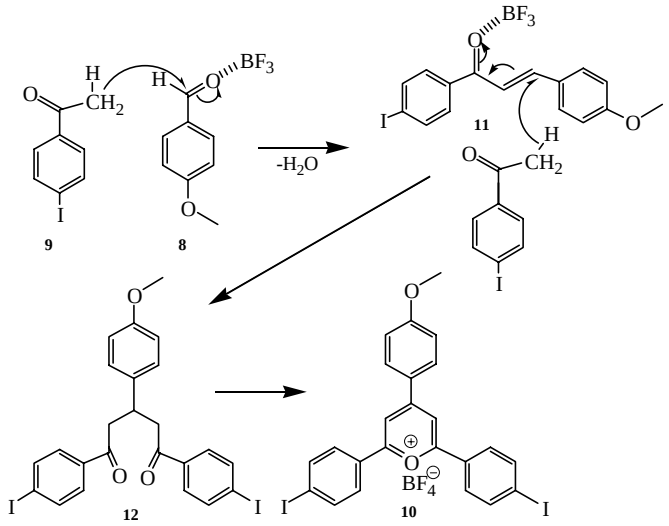

Scheme 3.9 Mechanism of the formation of the pyrilium salt **10**.

In the first step 4-iodo-acetophenone (**9**) reacts with 4-methoxy-benzaldehyde (**8**) to form the α-β unsaturated benzalacetophenone (**11**) as in a normal aldol condensation. In the further step the condensation between **11** and another molecule of 4-iodo-acetophenone (**9**) leads to a δ-diketone **12** that in the presence of acid is transformed into the pyrylium salt **10** in the last step.

10 was refluxed in acetic anhydride with sodium 4-methyl phenylacetic acetate (**13**) for 1.5 h to give **14**. After chromatographic purification, **14** was obtained in 9-15 % yield. As side product 1-methyl-2',6'-di-(4-iodo-phenyl)-4''-iodo-p-terphenyl (**15**) was also isolated (Scheme 3.10).

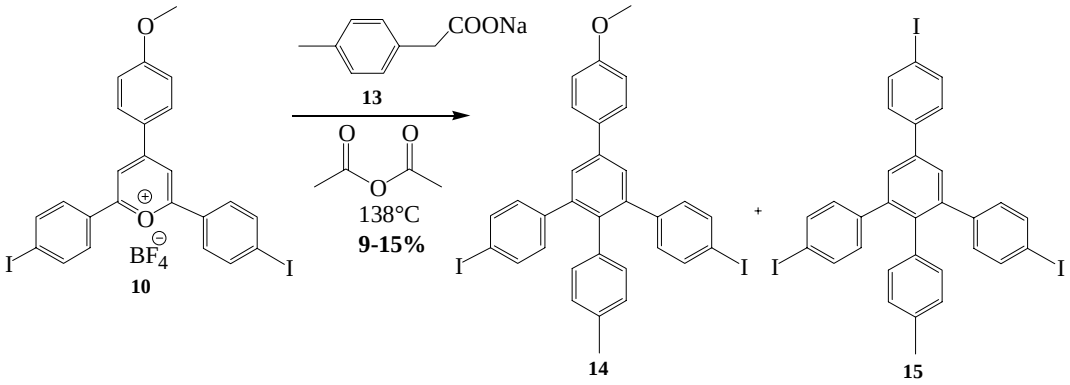

Scheme 3.10 Transformation of pyrylium salt **10** to the *p*-terphenyls **14** and **15**.

By recristallization in acetic acid, crystals of **14** were obtained. The details of the crystallographic structure are reported in Appendix A.

The mechanism of the latter transformation is proposed as following. In the initial step, acetic anhydride reacts with sodium 4-methyl phenylacetic acetate (**13**) to form sodium acetate and the mixed anhydride **16** which is under the reaction condition in equilibrium with its deprotonated form **16'** (Scheme 3.11).

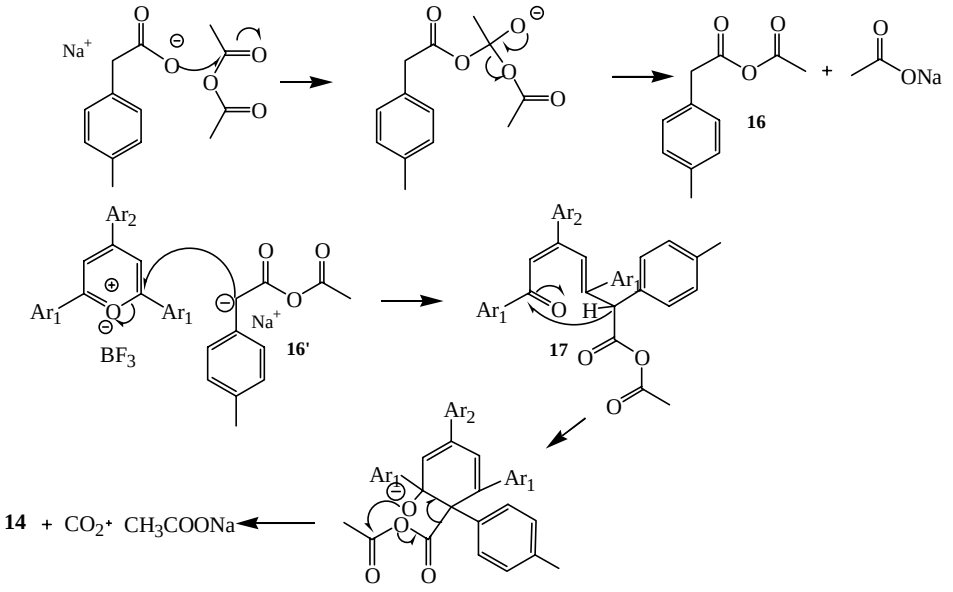

Scheme 3.11 Mechanism of the formation of the p-terphenyl **14**.

In the further step **16'** attacks the pyrylium salt **10** which ring opens. Condensation, rearrangement and elimination gives the p-terphenyl **14**.

The yield of this reaction is in our case unexpected low, which is caused by the fact that the pyrylium salt **10** can not be purified in a proper way. The presence of inorganic iodo species results in the formation of the side product 1-methyl-2',6'-di(4-iodo-phenyl)-4''-iodo-p-terphenyl (**15**), where the methoxy group is substituted by an iodide. This nucleophilic substitution on the aromatic ring is possible because the pyrylium ring has a strong electron withdrawing effect on the methoxy containing phenyl ring (Scheme 3.12).

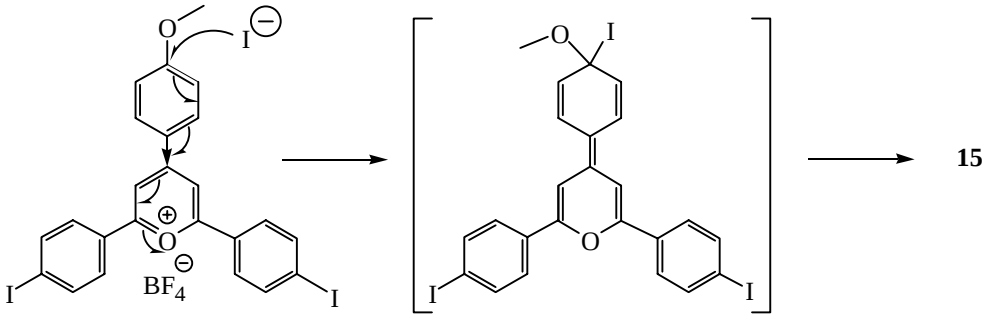

Scheme 3.12 : Proposed mechanism of the formation of **15**

Attempts to recrystallize the pyrylium salt **10** from acetone, ethanol, chloroform, acetonitrile or acetic acid were not successful. In order to eliminate iodo species, the salt was washed with sodium thiosulfate solution and then with water, but in this case the product decomposed.

Alternative reaction conditions were used as well. The 4-methoxy benzaldehyde (**8**) and the 4-iodo-acophenone (**9**) were dissolved in acetic acid in the present of $BF_3 \bullet 2CH_3COOH$ and stirred at room temperature for 90 h, but no pyrylium salt was formed (Scheme 3.13).

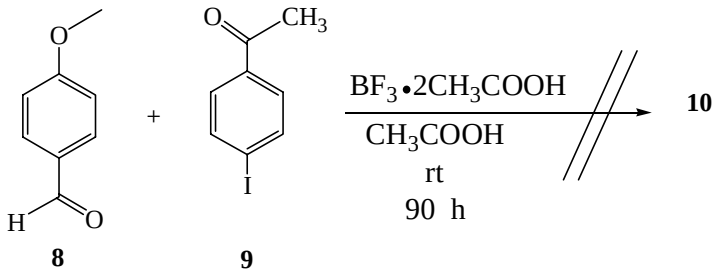

Scheme 3.13 Synthesis of pyrilium salt **10** using other reaction conditions.

Another idea was to prepare the terphenyl **14** in a few more steps, using diazonium salt chemistry (Scheme 3.14).

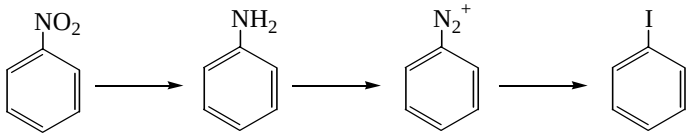

Scheme 3.14 Transformation of nitro compound, via the diazonium salt, to an iodo compound.

A nitro compound can be reduced to an aniline derivate that can be transformed via the diazonium salt in an iodo compound. Normally nitro compounds are quite easy to purify because of their ability to crystallize. However, if 4-nitro-acetophenone (**18**) was used instead of the 4-iodo-acetophenone in the synthesis of the pyrilium salt, the desired product was not obtained (Scheme 3.15).

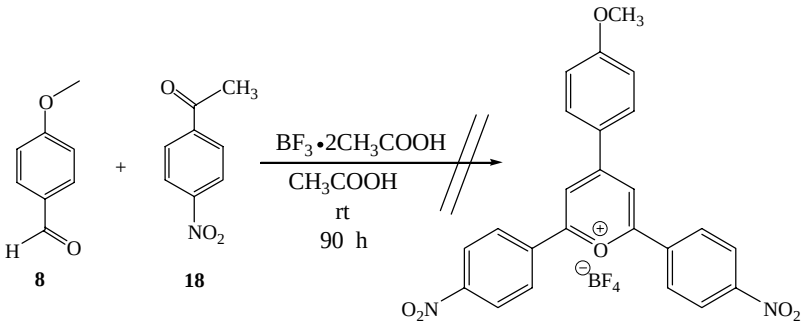

Scheme 3.15 Reaction between 4-nitro-acetophenone (**18**) and 4-methoxy-benzaldehyde (**8**).

More successful was the synthesis of the pyrylium salt **19** that contains bromide instead of iodide. The reaction conditions were exactly the same as used for the syntheses of **10**. The main idea was that even though it is not possible to purify the salt, bromide is less nucleophilic than iodide and so the nucleophilic aromatic substitution as side reaction during the synthesis of the *p*-terphenyl should not take place. Unfortunately, this was not true and although the yield of the reaction for the formation of **20** was slightly higher than for **10**, 1-methyl-2',6'-di(4-brom-phenyl)-4''-brom-p-terphenyl (**21**) was also isolated as side product (Scheme 3.16).

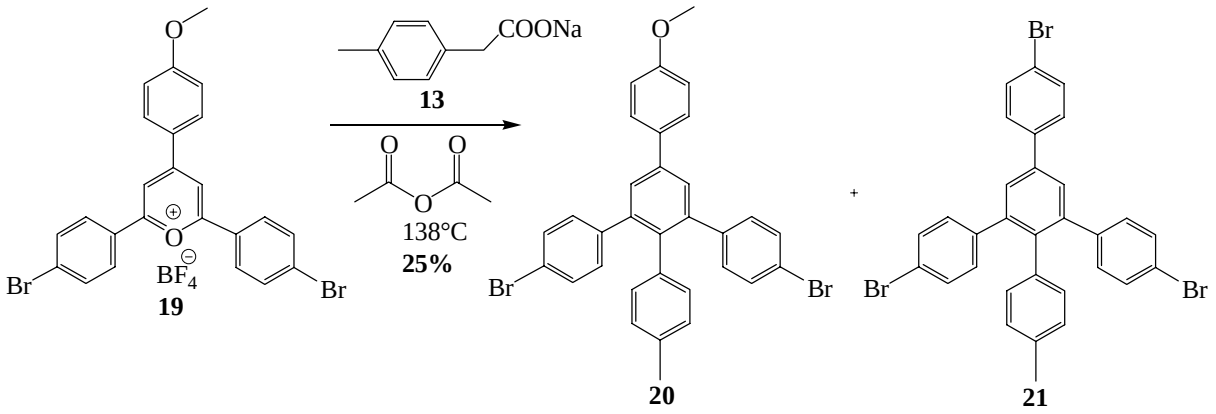

Scheme 3.16 Transformation of pyrylium salt **19** to the *p*-terphenyls **20** and **21**.

Since **10** could neither be obtained by alternative ways nor properly purified, it was investigated if addition of an iodide scavenger improves the yield of **14**. Reacting **10** and **13** in the presence of one equivalent silver tetrafluoroborate ($AgBF_4$) increased the yield up to 20 %. The use of an excess of $AgBF_4$ (two equivalents) lead to a complete decomposition of the products.

Since it was our attempt to connect the oligomeric carboxylic acid to the macrocycle by means of an alcoholic ester group and not by a phenolic ester group, **22** was transformed to **23** as shown in the scheme 3.17.

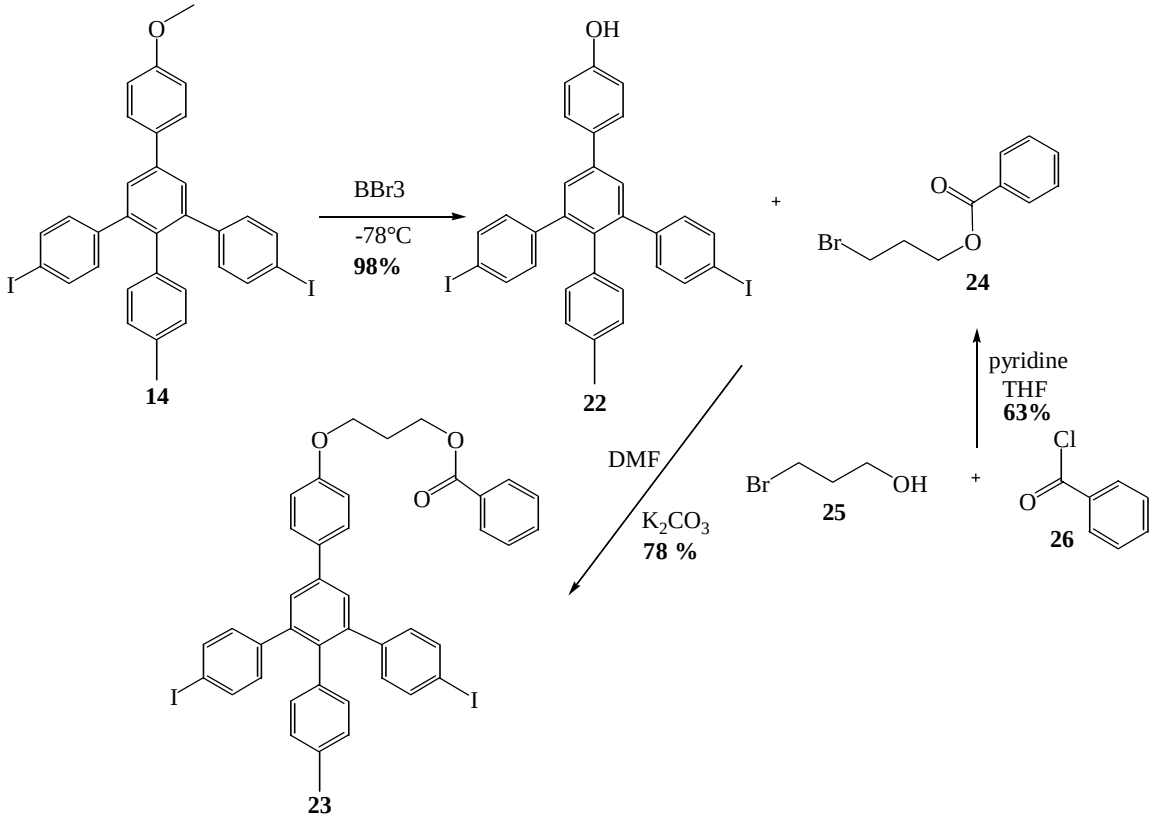

Scheme 3.17 Transformation of *p*-terphenyl **14** to the *p*-terphenyl **23**.

After cleaving the methoxy group of **14** by BBr_3 at –78° C 4-methyl-2',6'-di-(4-iodo-phenyl)-4"-hydroxy-p-terphenyl (**22**) was obtained in 98 % yield as a white solid. The phenol was alkylated by 3-bromo-propylbenzoate (**23**) in DMF at 60° C in presence of potassium carbonate. After purification, 2',6'-di(4-iodo-phenyl)-4"-propylbenzoate-p-terphenyl (**24**) was obtained in 78 % yield. The 3-bromo-propyl benzoate (**23**) was prepared from 3-bromo-1-propanol (**25**) and benzoyl chlorid (**26**) in the presence of pyridine.

The synthesis of the corner pieces **23** from **14** is straight forward because all reactions run with high yield and the products are easy to purify. However, because of the low yield in the first two steps it was not possible to prepare larger amounts of **14**. For this reason another type of corner piece, **A"**, was prepared. The synthesis started from the 3,5-diiodphenol (**27**), a compound already synthesized

in the group[38]. **27** was reacted with one equivalent of 6-bromo-1-hexanol (**28**) in DMF in the presence of potassium carbonate. After purification, (6-hydroxy-hexyloxy)-3,5-diiodbenzene (**29**) was obtained in 79 % yield. In order to protect the alcohol as an ester, it was treated with benzyl chloride (**26**) in the presence of pyridine and gave the corner piece **30** (**A''**) (88 % yield) (Scheme 3.18).

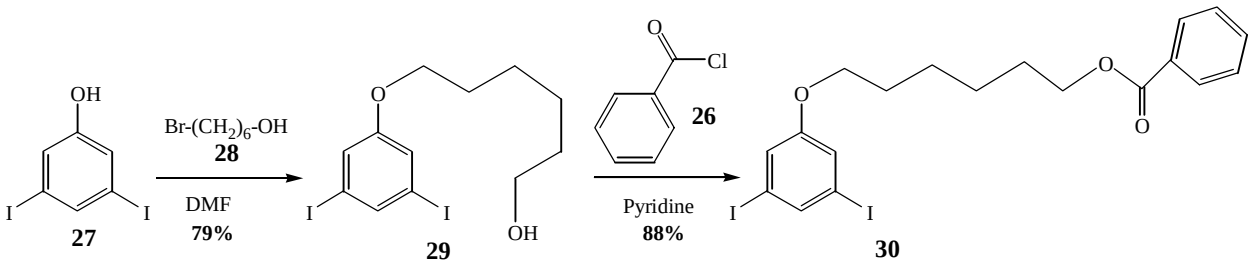

Scheme 3.18 Transformation of 3,5-diiodphenol (**27**) to the corner piece **30** (**A''**).

The side piece **B', 31** was already synthesized and used in the group[39] and is the starting material for the synthesis of **B''**.

In the first step, 4-bromo-iodobenzene (**32**) was reacted with 2-triethylsilylacetylene (TES-acetylene) (**33**) in piperidine using $PdCl_2(PPh_3)_2$ and CuI as catalyst in the presence of triphenyl posphine. After reacting overnight, 1-ethinyl-3-(2-triisopropylsilylethinyl)-5-tert-butyl-benzene (**31**) was added and the solution stirred for additional 4 days. After purification by column chromatography, **34** was obtained in 91 % yield (Scheme 3.19).

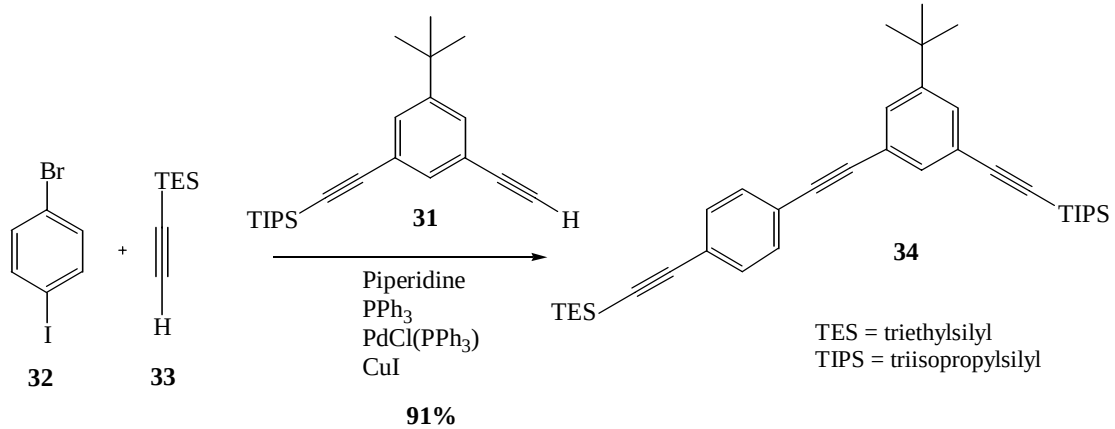

Scheme 3.19 Synthesis of the protected side piece **34** (**B''**).

34 contains two acetylenes, protected with two different groups: the TIPS group and the TES group. The use of this two protecting groups in the same molecule allows the selective deprotection of one the two acetylenes. In fact, in the presence of potassium carbonate the TES group is cleaved while the TIPS group is not affected. According to this, **34** was treated with K_2CO_3 and gave compound **35** (83 % yield) (Scheme 3.20).

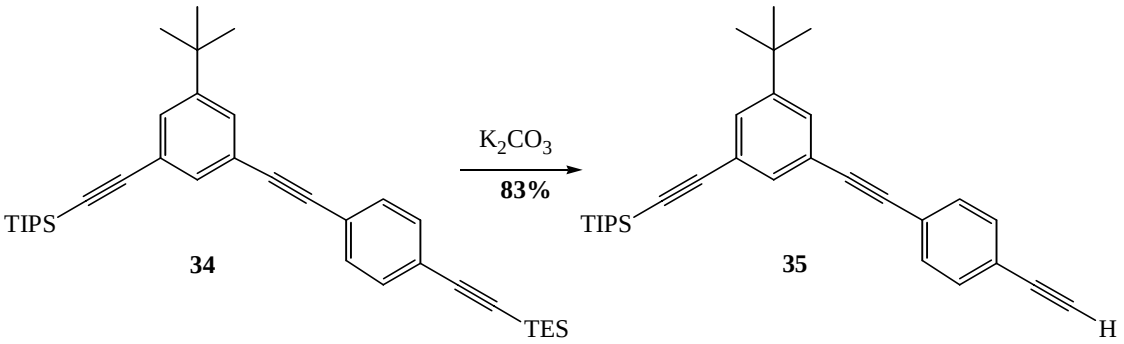

Scheme 3.20 Deprotection of corner piece **34**.

3.2.2 Synthesis of the macrocycles

By using the four different building blocks **23**, **30**, **31** and **35**, three different half rings were synthesized.

Corner piece **A'** (**23**) was reacted with both types of side pieces **B'** (**31**) and **B''** (**35**). Palladium-catalyzed coupling of the two different building blocks in the presence of CuI and PPh_3 provided the two half rings in their TIPS-protected form (**36** and **37**). After chromatographic purification, the half rings were obtained in high yields (80 %) (Scheme 3.21).

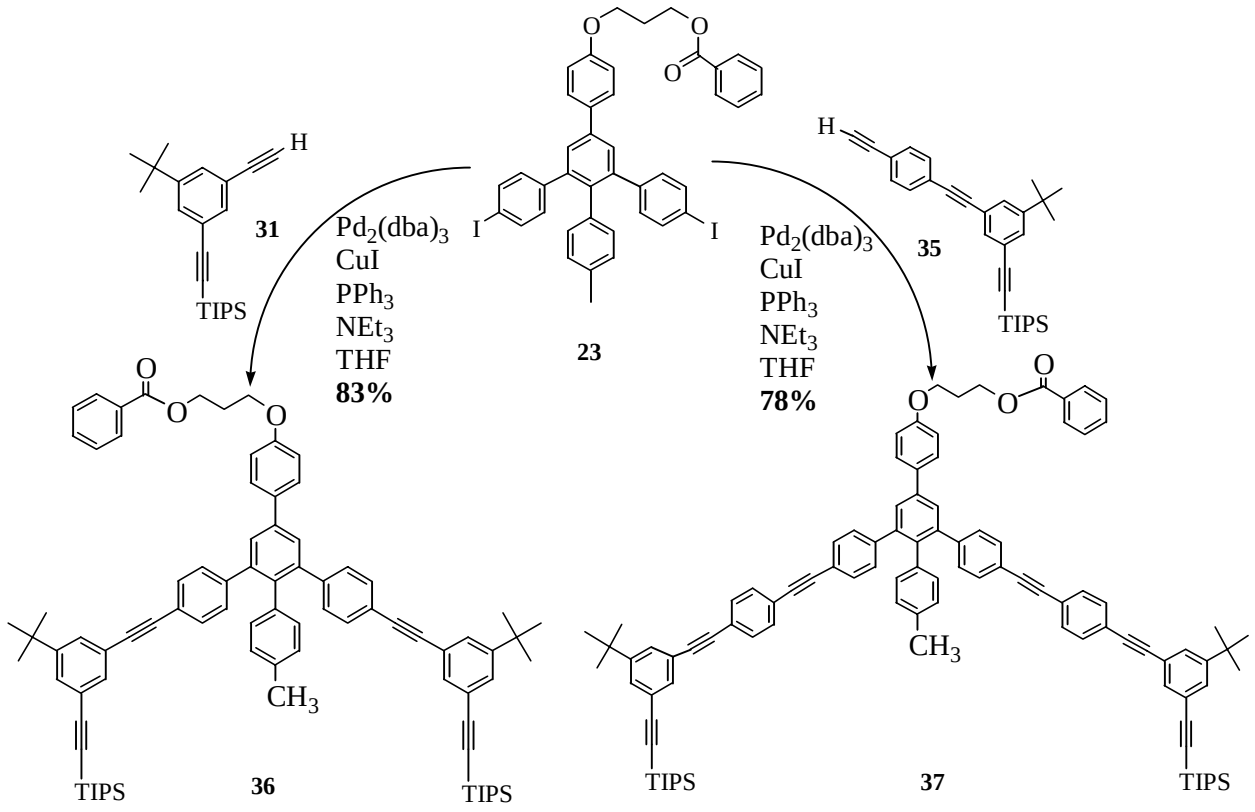

Scheme 3.21 Synthesis of the protected half rings**36** and **37**.

The reaction is known as Hagiara-Sogonaschira coupling, and has already been used in the synthesis of **34**. It is a palladium-catalyzed coupling reaction between an aromatic halide and a terminal acetylene to form a sp^2-sp bond. The proposed mechanism of this reaction is illustrated in the Scheme 3.22.

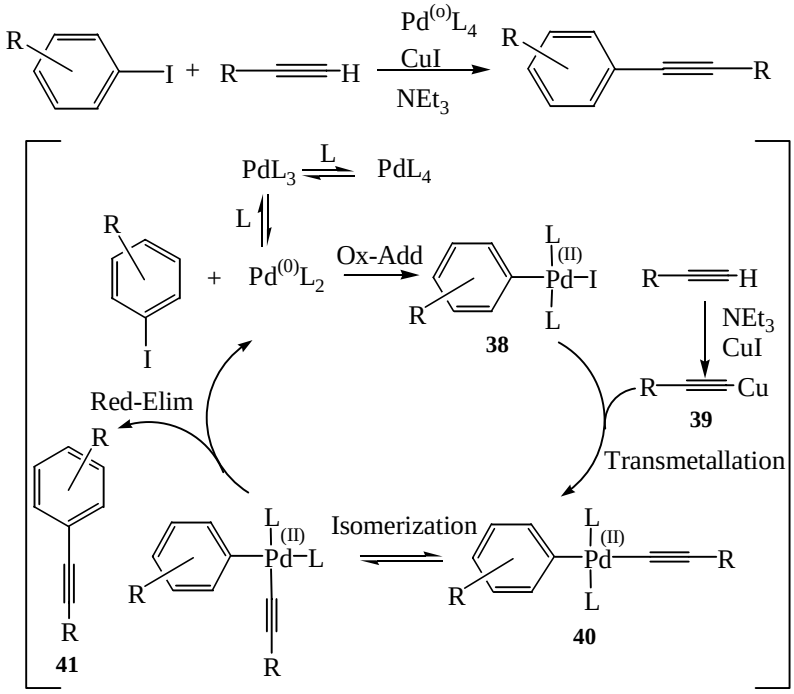

Scheme 3.22: Proposed mechanism of the Hagiara-Sogonaschira coupling.

The coordinatively unsaturated $Pd(0)L_2$ oxidatively adds to the aromatic halide to form **38.** In the presence of CuI, the acetylene is converted to the copperacetylide **39** which reacts with **38** to give the complex **40**. After isomerization of the *trans* to the *cis* form, the complex reductive elimination gives the product **41** and regenerates the catalyst $Pd(0)L_2$.

Subsequent deprotection of **36** and **37** using tetra-butyl ammonium fluoride in THF gave the bisacetylenes **42** and **43** (90 % yield). In this step it was not necessary to add about 5 % water to the THF in order to prevent ester cleavage by the fluoride, as it was seen in other cases. The reaction was complete in 12 h and no cleavage of the ester group was detected (Scheme 3.23).

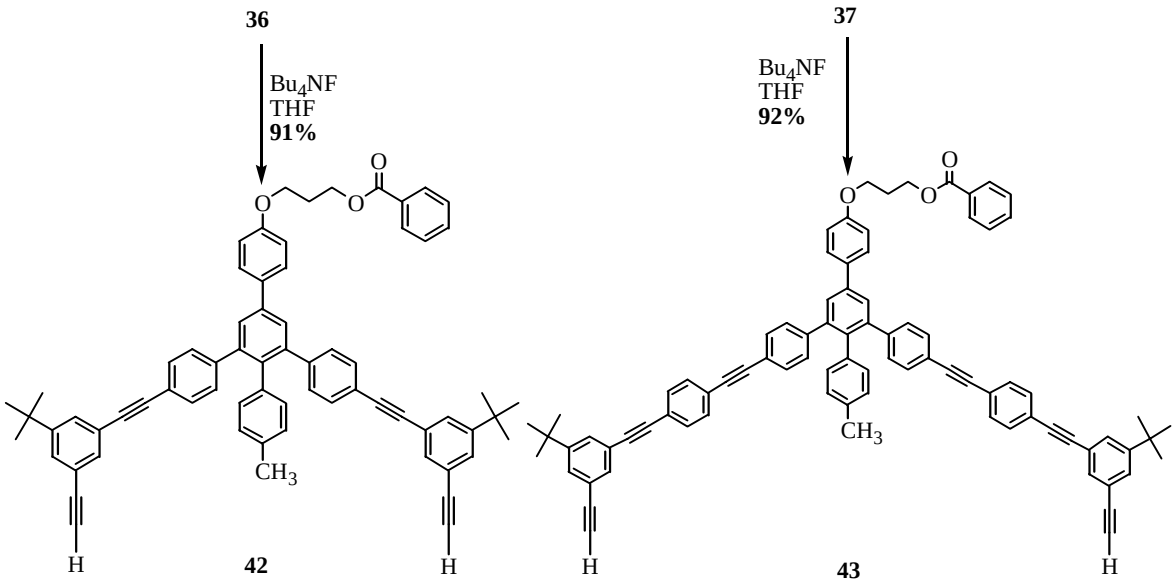

Scheme 3.23 Deprotection of the half rings**36** and **37**.

The cyclization of **42** and **43** under pseudo high-dilution conditions was carried out by adding a solution of deprotected half ring in pyridine in 96 h to a slurry of $CuCl/CuCl_2$ in the same solvent at 55 °C (Scheme 3.24).

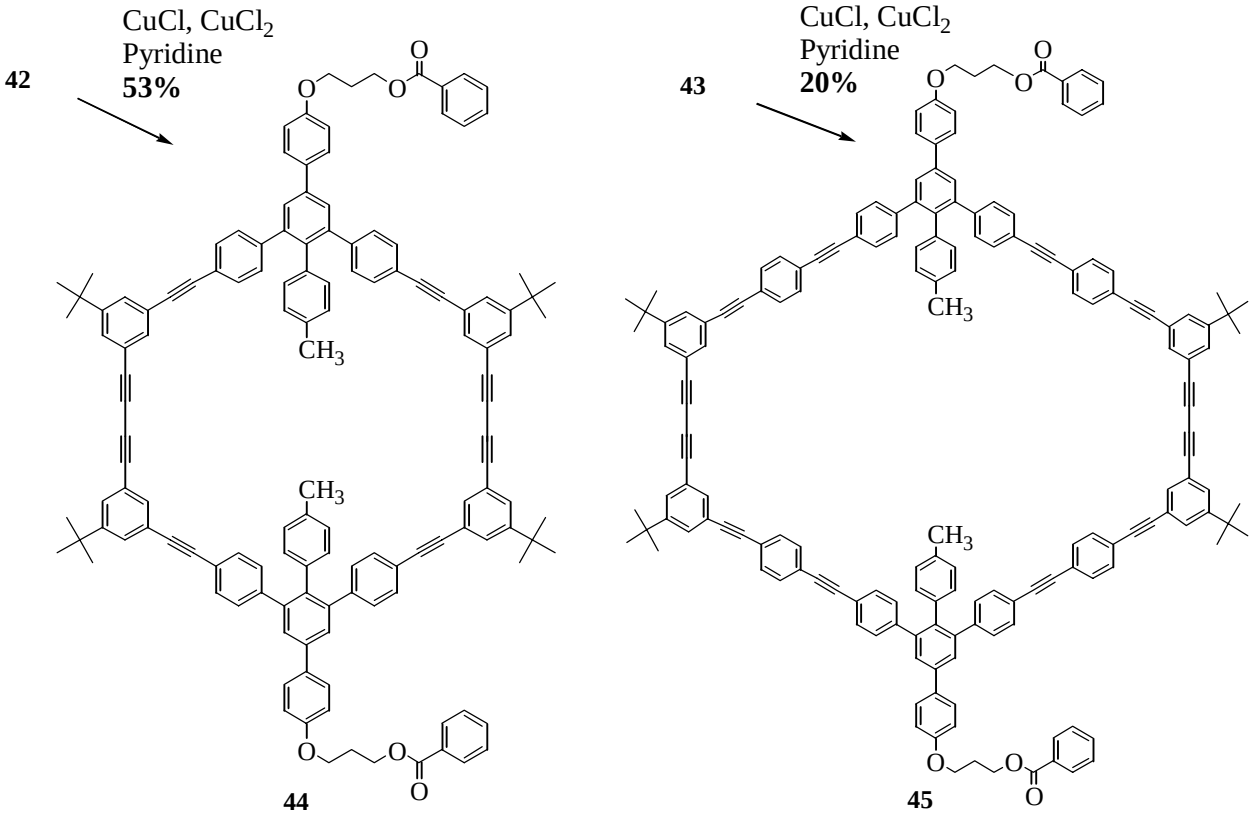

Scheme 3.24 Formation of the macrocycles **44** and **45**.

After complete addition, the mixture was stirred for an additional day at room temperature and then worked up to give the crude reaction products as white-yellow powders.

The cyclization reaction we used is known as Glaser coupling[40]. It is the formation of a *sp-sp* bond between two terminal acetylenes. The proposed mechanism[41] of this reaction can been divided in three main steps (scheme 3.25).

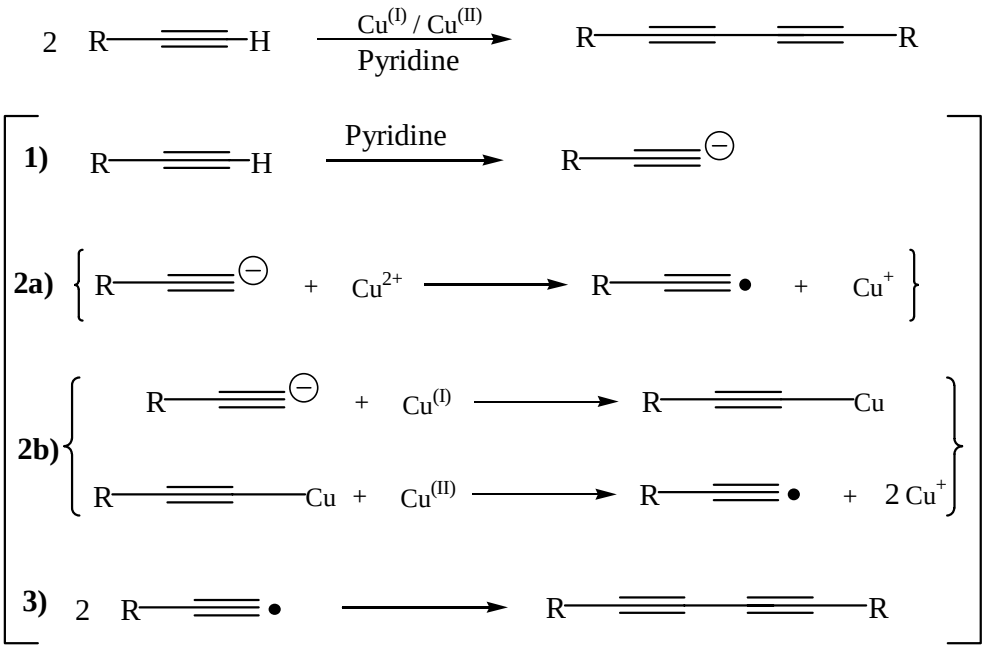

Scheme 3.25 Proposed mechanism of the Glaser coupling.

In the first one, the acetylene looses its acidic hydrogen and forms the anion by means of pyridine. The second step is still controversially discussed and has been not fully understood. Some authors suggest the transformation of the anion into the radical by means of Cu^{2+} (**2a**), others suggest first the formation of the organo-copper(I)-complex and subsequent oxidation by means of Cu(II) (**2b**). In any case the last step is the dimerization of two radicals and the formation of a diacetylene.

The cyclization reaction is a statistical reaction so that dimers, trimers, tetramers and polymers are formed. In the first step, two half rings are bound together and then the molecule can react intramolecularly to form the ring, or it can react with another half ring and form a longer oligomer. The use of high-dilution conditions increases the yield of cyclic dimer for the following reason. The intramolecular ring-closure reaction is of first order, its rate is proportional to the concentration. The intermolecular condensation reactions is of second order, its rate is proportional to the square of the concentration. Therefore, high dilution should favor the intramolecular reaction. Because high-dilution conditions require large amounts of solvents (high dilution condition means concentration < 1mM), it is common to use pseudo-high-dilution conditions in which the reagent is added slowly to

the reaction vessel. It is necessary that the rate of addition of the reactants is lower than their consumption in order to keep their stationary concentration low.

From the Gel Permeation Chromatography (GPC) data of the crude cyclization product it is possible to estimate the amount of the cyclic dimer in the crude product (Figure 3.1).

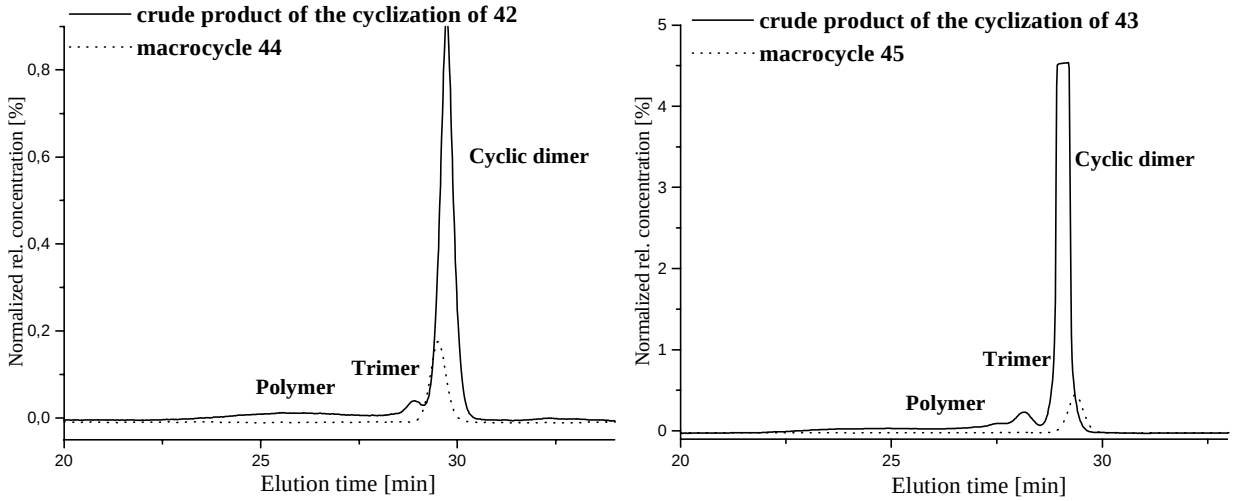

Figure 3.1 GPC data of the crude cyclization products and the purified macrocycles **44** and **45**.

In particular, the crude product of the cyclization of **42** contained about the 80 % of **44**. It could be easily purified by column chromatography and gave **44** in an isolated yield of 53 %. Ring **45** was obtained in a lower yield. It is present in 65 % in the crude cyclization mixture and its purification was not possible by column chromatography. Pure **45** was obtained by recrystallization from 1,2-dichloroethene in only 20 %.

Deprotection of the macrocycles **44** and **45** was performed using a mixture NaOH/LiOH in THF/water.

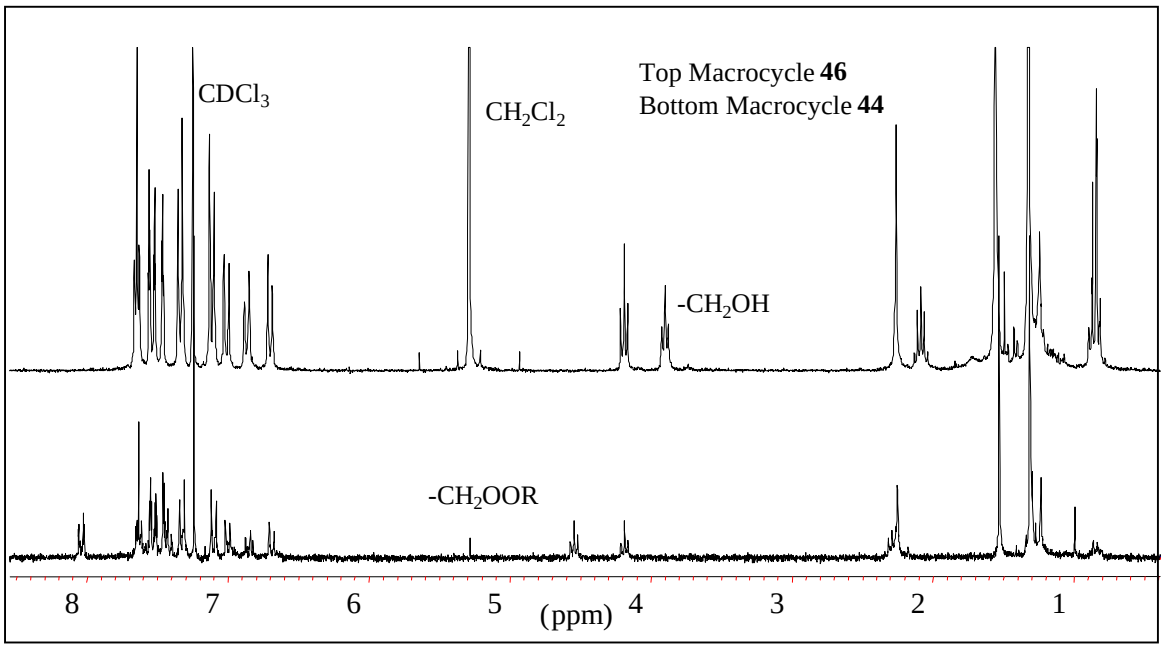

Figure 3.2 ^{1}H NMR spectra of the macrocycle **46** (top) and macrocycle **44** (bottom).

After refluxing overnight, complete deprotection of the alcoholic group was confirmed in the NMR spectra and the rings **46** and **47** were obtained in about 90 % yield (Figure 3.2) (Scheme 3.26).

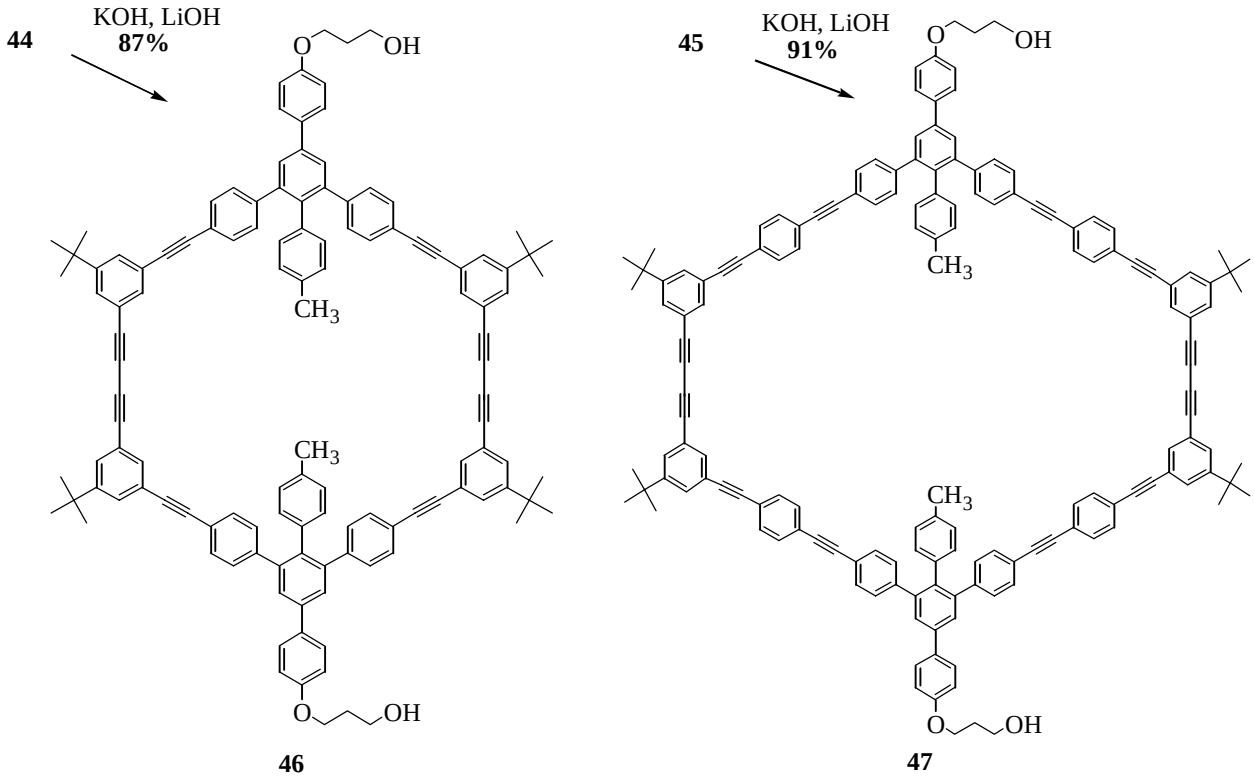

Scheme 3.26 Saponification of the macrocycles **44** and **45**.

The corner piece **A''** (**30**) was reacted only with the larger side piece **B''** (**35**). The reaction sequence was exactly the same as described before (Scheme 3.27).

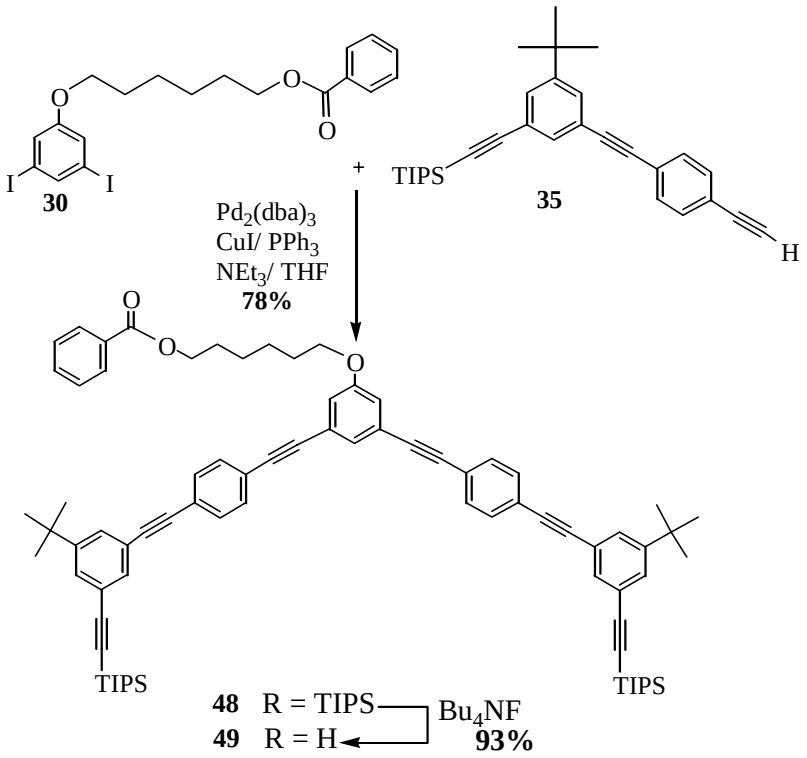

Scheme 3.27 Synthesis of the half rings **49**.

Palladium-catalyzed coupling lead to **48** in which the acetylenes are protected with the TIPS groups (78 % yield). After reaction with tetra-butyl ammonium fluoride the deprotected half ring **49** was isolated in 93 % yield.

Cyclization of the half ring was performed by a Glaser coupling using the same conditions as described before (pseudo-high-dilution conditions with a mixture of CuCl/$CuCl_2$ as catalyst) (Scheme 3.28).

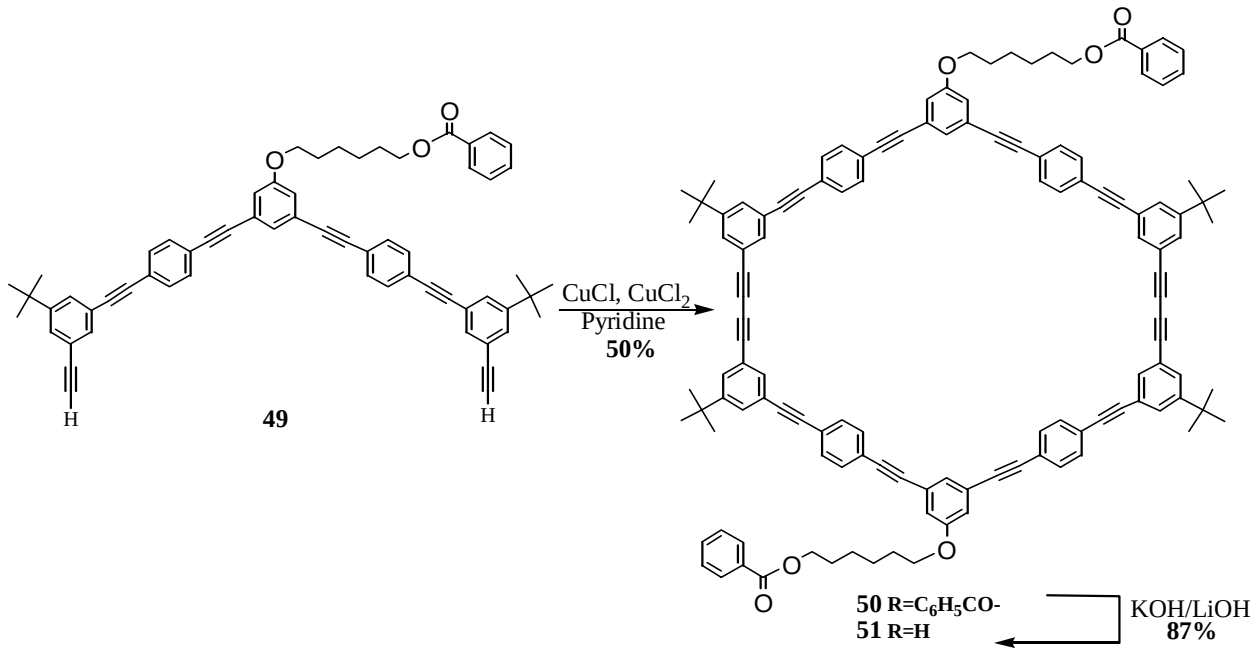

Scheme 3.28 Formation of the macrocycles **51**

The macrocycle **50** was purified by column chromatography (50 % yield) and the purity determinated by GPC (Figure 3.3).

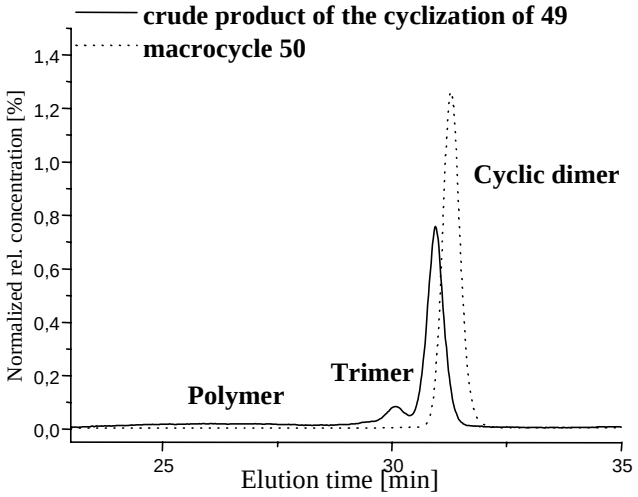

Figure 3.3 GPC data of the crude cyclization product and the purified macrocycle **50**.

Saponification with potassium hydroxide and lithium hydroxide in THF/water (as for **46** and **47**) lead to the macrocycle **51** with the free alcohol groups in 87 % yield.

The NMR spectra of the macrocycle 50 e 51 are reported in Figure 3.4.

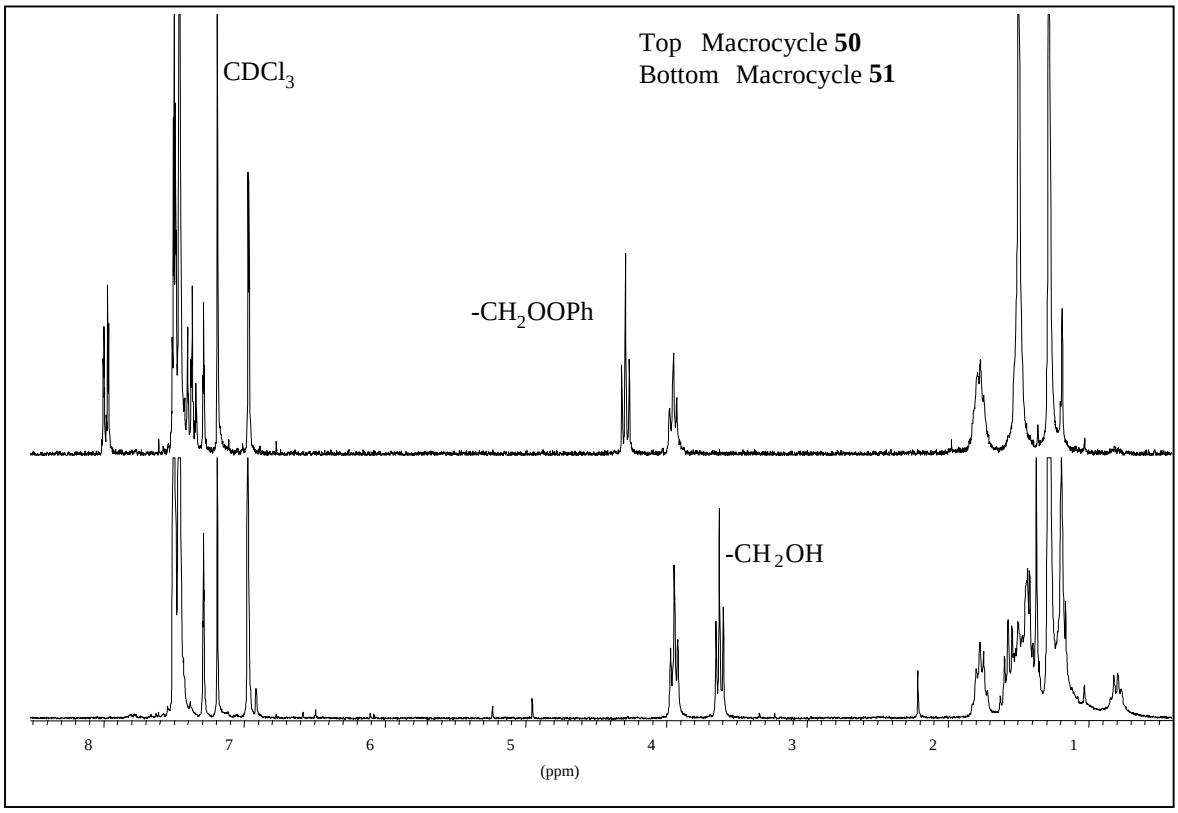

Scheme 3.4 ^{1}H NMR spectra of the macrocycle **50** (top) and macrocycle **51** (bottom).

3.3 Synthesis and purification of functionalized polystyrene

The best way to prepare carboxyl terminated polystyrene is the use of living anionic polymerization. Living anionic polymers are very suitable precursors of functionalized polymers with nearly ideal structures, since they have controlled molecular weights with a narrow molecular weight distribution as well as highly reactive carbanionic chain ends which allow reactions with electrophilic compounds. Polymers with terminal carboxyl groups are obtained by carboxylation of the living chain end with carbon dioxide. However, significant amounts of side products are obtained. In the reaction mixture are also the corresponding ketone (dimer) and tertiary alcohol (trimer) formed:

$$\mathbf{PS\text{-}Li} \xrightarrow[(2)\ H^+]{(1)\ CO_2} \mathbf{PS\text{-}COOH + (PS)_2C{=}O + (PS)_3COH} \quad \mathbf{PS = polystyrene}$$

In order to improve the yield of carboxyl-terminated polymer it was first tried to use the procedure described by Hirao and co-workers[42]. They reported an alternative synthesis of well-defined polystyrenes with terminal carboxy groups by the reaction of polystyryl anions with 4-bromo-1,1,1-trimethoxybutane. The orthoester function is a protected base-stable form of the carboxyl group.

After acidification and cleavage of the methyl group the polystyrene carboxylic acid can be obtained with a spacer of three carbons between the polymer chain and the carboxylic acid.

Unfortunately the mayor product of this reaction was a polystyrene ketone with a bromo end group, PS-CO-CH_2-CH_2-CH_2-Br. It is the result of the attachment of the anionic chain at the end of ester H_3C-O-CO-CH_2-CH_2-CH_2-Br present as an impurity in the reagent (used as received).

The method by J.C.M. van Hest[43] was more successful. It is a modification of the end-capping procedure with CO_2. The author found that siphoning the anionic polymer chain into a THF solution, saturated with CO_2, made it possible to obtain > 95 % of polystyrene carboxylic acid. Using the reported procedure it was possible to synthesize polystyrene carboxyl acid lithium salt that after acidification lead to the free acid (Scheme 3.29).

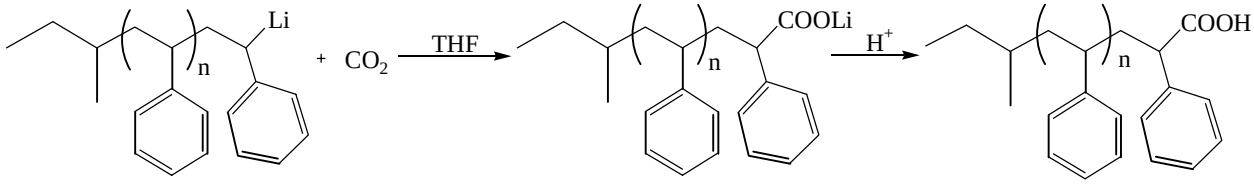

Scheme 3.29 Synthesis of the polystyrene carboxylic acid.

The polymer was purified by column chromatography, using toluene as eluent. All the side products that have less polar groups than the polystyrene carboxylic acid were eluted (PS, PS-ketone). The product has with toluene a R_f value of nearly 0 and was eluted by changing the eluent to THF. By this way polystyrene carboxylic acids with molecular weights of 1000, 1500, 2500, 3500 and 5000 were obtained in yields of 60 – 80 %. The materials were characterized by NMR and MALDI-TOF spectroscopy (Figure 3.5).

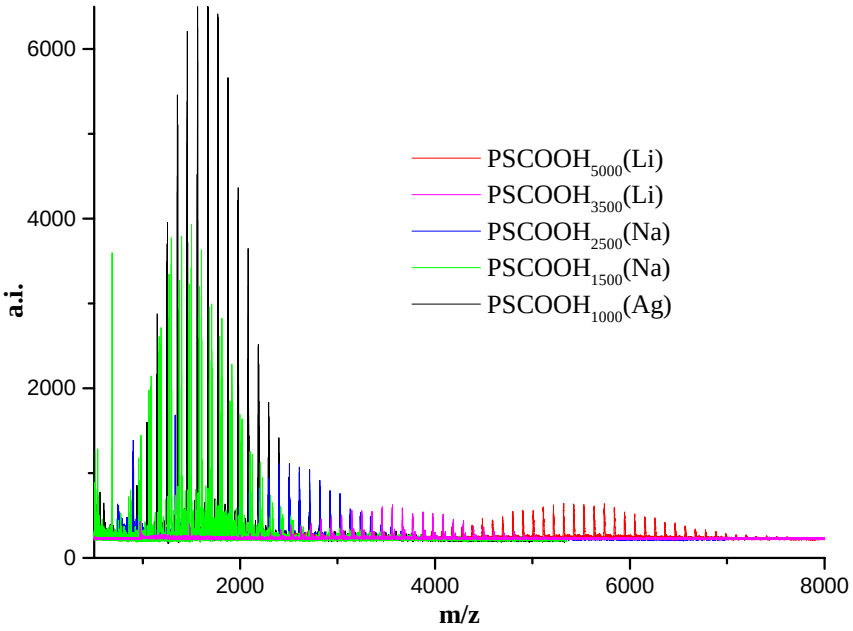

Figure 3.5 MALDI-TOF spectra of different molecular weights polystyrene carboxylic acids.

3.4 Synthesis and purification of functionalized polydimethylsiloxane

Poly(dimethylsiloxane) (PDMS) was also used as coiled block in our polymer structure. It exhibits some interesting features such as: high surface tension, large permeability to gases and high hydrophobicity. Most important, the glass transition temperature of PDMS is very low (< -120 °C) and the chain flexibility at room temperature is very high. In this sense it is quite different from polystyrene and should give different results in terms of the physical proprieties of the copolymers.

The synthetic strategy we used towards PDMS carboxylic acid is based on one of the most common reactions in organosilicon chemistry, hydrosilylation (Scheme 3.30).

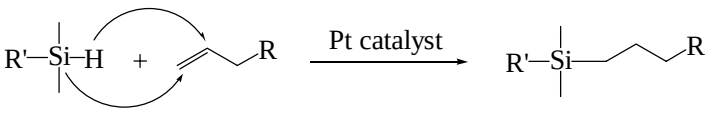

Scheme 3.30 Hydrosilylation reaction.

Polydimethylsiloxane was synthesised by ring-opening polymerization of the corresponding hexamethylcyclotrisiloxane . The living anionic chain was quenched with dimethyl chloro silane (Scheme 3.31).

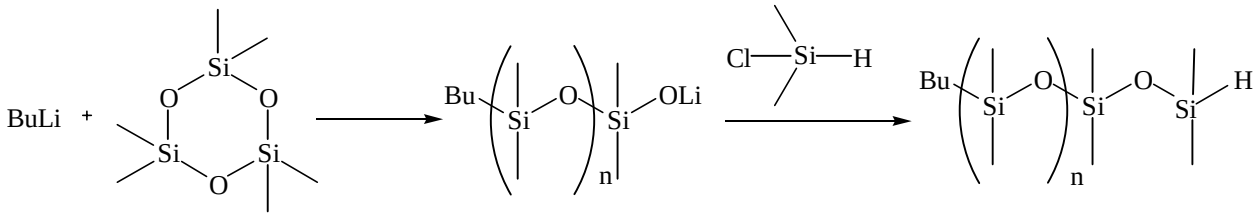

Scheme 3.31 Formation of the polydimethylsiloxane.

Polymers of three different molecular weights (1500, 3000 and 5000) were synthesized and analyzed by GPC in THF (Figure 3.6).

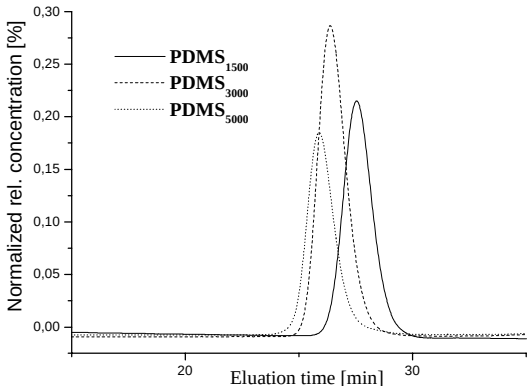

Figure 3.6 GPC data of the different molecular weights polydimethylsiloxane.

The PDMS containing Si-H end groups were then reacted with benzyl-4-pentenoate (**52**), (synthesized by reaction of 4-pentenoic acid chloride (**53**) and benzyl alcohol (**54**)) in toluene at 100 °C to give the desired polymers in form of the benzyl esters in 70-80 % yield. The reaction was catalyzed by H_2PtCl_6, a common hydrosililation catalyst, and the progress of the reaction was monitored by infrared spectroscopy. The disappearance of the 2120 cm^{-1} absorption band indicated that all Si-H groups reacted with **52** (Scheme 3.32).

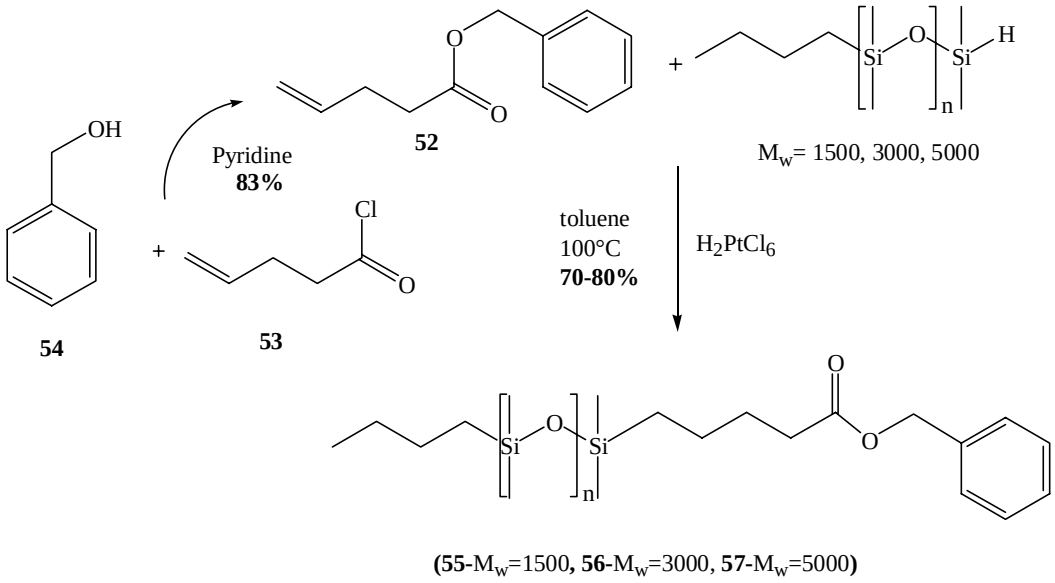

Scheme 3.32 Synthesis of the protected polydimethylsiloxane carboxylic acids **55**, **56** and **57**.

The benzyl ester were then cleaved by palladium catalyzed hydrogenation and the PDMS carboxylic acids were obtained in 85-90 % yield (Scheme 3.33).

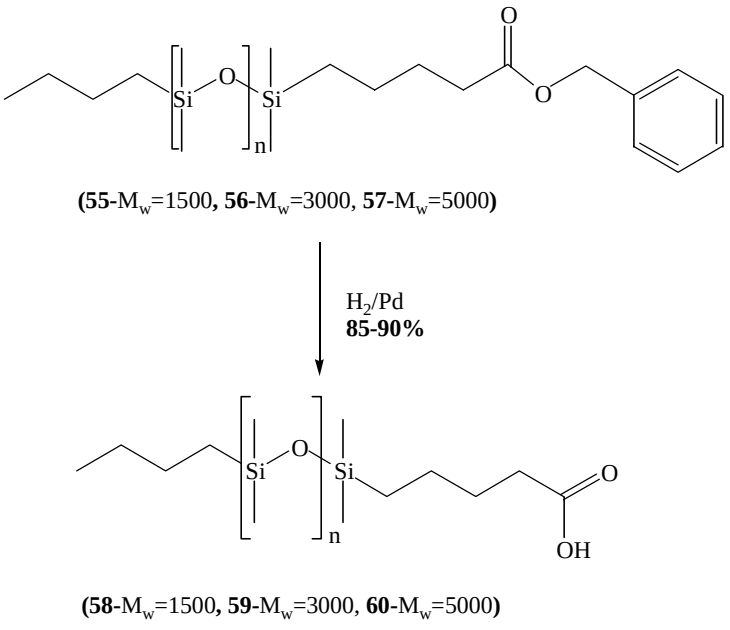

Scheme 3.33 Synthesis of the polydimethylsiloxane carboxylic acids **58**, **59** and **60**.

Opposite to the polystyrene carboxylic acids these specific PDMS carboxylic acids have not been reported in the literature before.

3.5 Synthesis of coil-ring-coil block copolymers

The easiest way to form an ester bond is to react an acid chloride with an alcohol. In order to follow this procedure, polystyrene carboxylic acid (M_w = 3500) was first treated with an excess of oxalylchloride (**61**) to give to the corresponding acid chloride. After removing the volatile side products and the excess of oxalylchloride, **62** was stirred with the macrocycle **43** in the presence of pyridine in THF for three days. After quenching with water (to transform the unreacted polymer **62** in polymer carboxylic acid) the crude reaction mixture was analyzed by GPC (Scheme 3.30).

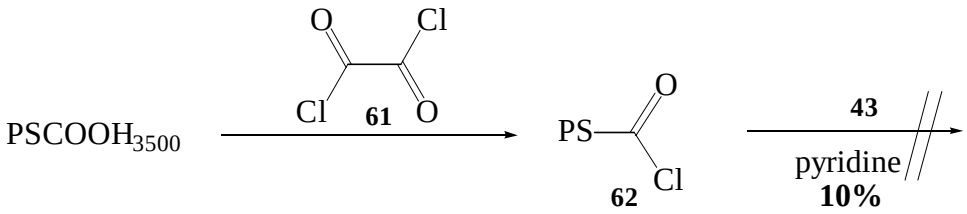

Scheme 3.34 Reaction of the polystyrene carboxylic acid chloride(M_w=3500) with the ring **43**.

The product was obtained in very low yield (10 %) and it was not possible to purify it by simple column chromatography. It was possible to detect small peaks which are probably related to the desired copolymer, peaks related to the unreacted macrocycle and peaks related to the unreacted polymer (Figure 3.7).

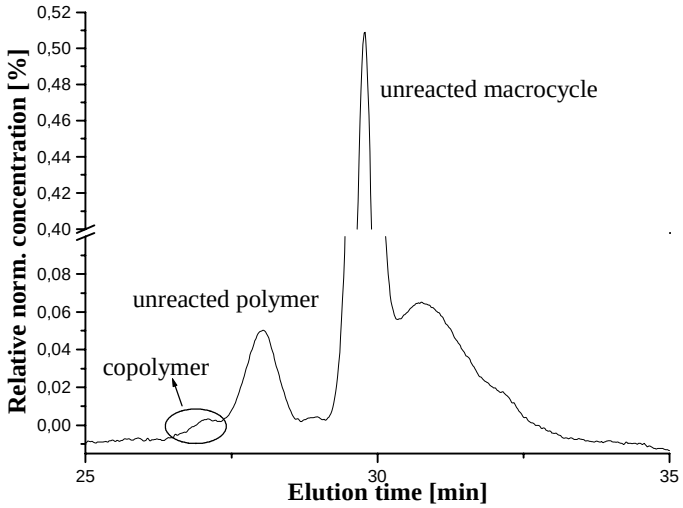

Figure 3.7 GPC data of the crude product.

It was expected that the different polarity of the reagents and the product (the macrocycle has two alcohol groups, the polymer a carboxyl group, and the copolymer has two less polar ester groups), allows their easy purification by column chromatography. Using moderately polar methylene chloride as eluent, the two unreacted reagents stay on the top of the column, while the copolymer migrates

with the front of the solvent. Unfortunately, significant amounts of polymer can not be separated from the copolymer. That means that during the quenching procedure not all of the excess of acid chloride (**62**) was transformed to the carboxylic acid.

In order to avoid this problem, a reaction that allows to work directly with the polymer carboxylic acid was used, the Mitsunobu-reaction.

In this reaction an ester bond is formed starting from an acid and an alcohol. The macrocycle **43**, the polystyrene carboxylic acid (M_w=3500) and triphenylphospine were dissolved in THF, and then diethylazodicarboxylate (DEAD) was slowly added. After reacting overnight, the product was obtained in good yield and purified by column chromatography (Scheme 3.35).

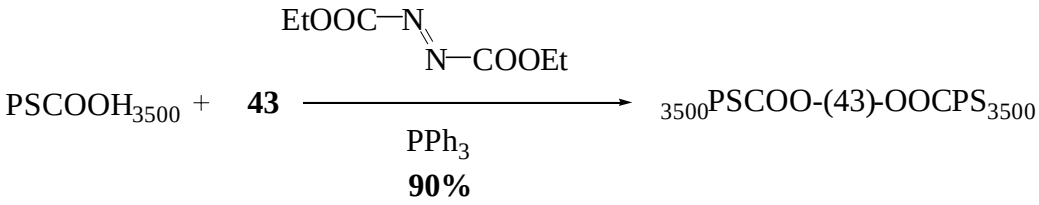

Scheme 3.35 Mitsunobu reaction between the polystyrene carboxylic acid (M_w=3500) and **43**.

The proposed mechanism of this reaction is illustrated in Scheme 3.36.

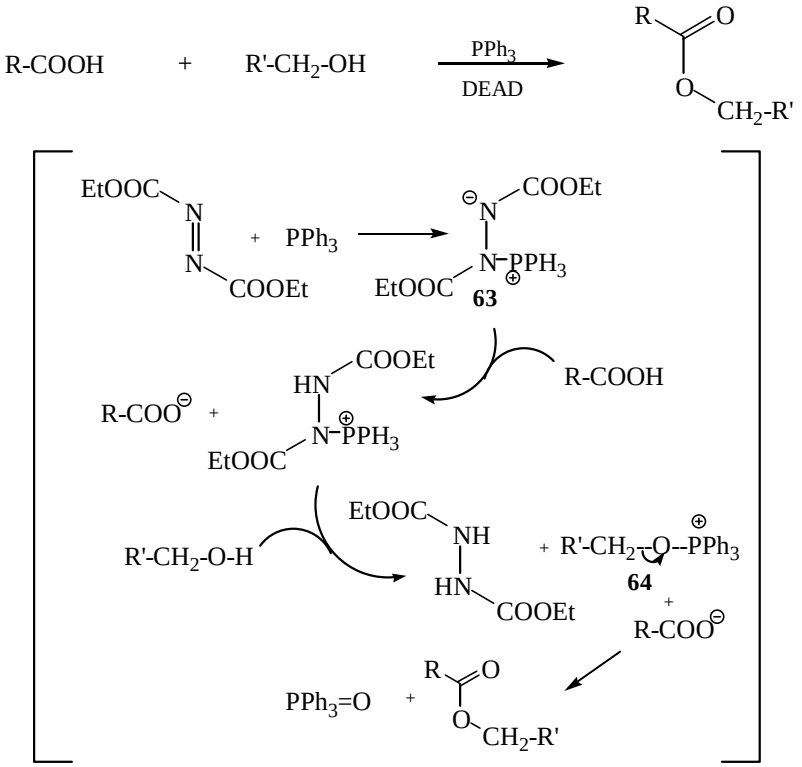

Scheme 3.36 Proposed mechanism of the Mitsunobu reaction.

The triphenyl phosphine attacks the DEAD to form the ionic species **63**, which reacts first with the acid to form the carboxylate and then with the alcohol to form the activated alcohol **64**. In the last step the activated alcohol **64** reacts with the carboxylate to form the ester and triphenylphospine oxide.

In this case it was possible to obtain the copolymer in high yield. However, even the purified product contained, according to the GPC analysis, a small but significant amount of a polymeric byproduct that could not be separated by column chromatography (Figure 3.8).

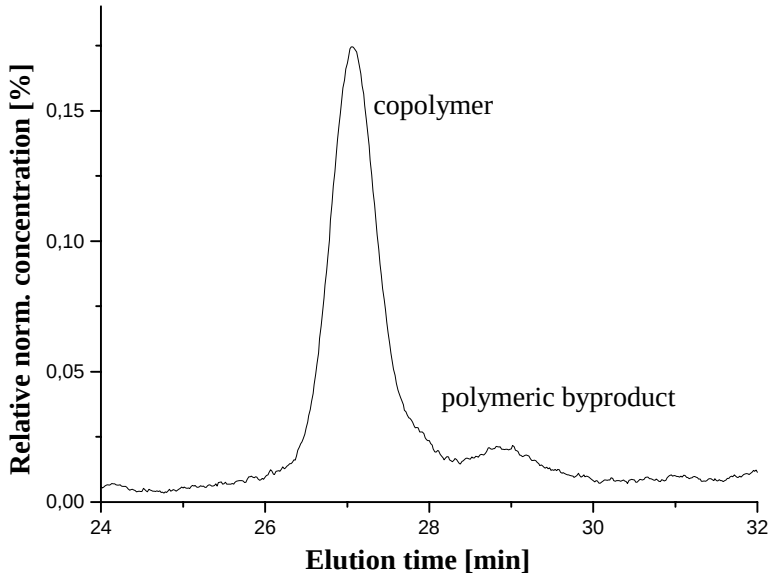

Figure 3.8 GPC data of the crude product.

The same reaction was also tried using the same macrocycle **43** and the macrocycle **51** and polystyrene carboxylic acid of a different molecular weight (M_w = 5000), but the results didn't change and the corresponding copolymers couldn't be purified properly (Scheme 3.37).

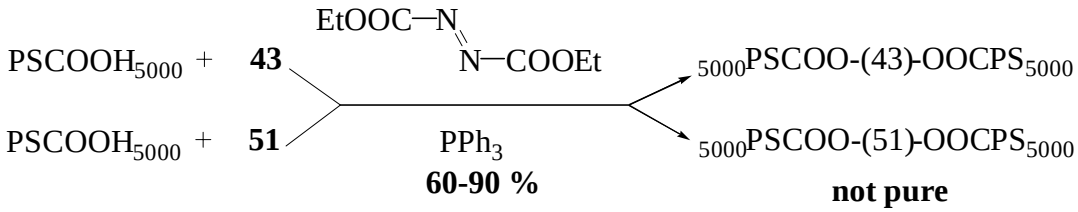

Scheme 3.37 Mitsunobu reaction between the polystyrene carboxylic acid (M_w=5000) and **43** and **51**.

Good results were obtained using a different type of reaction, the carbodiimide condensation[44]. The general scheme of the reaction is illustrated in the scheme 3.38.

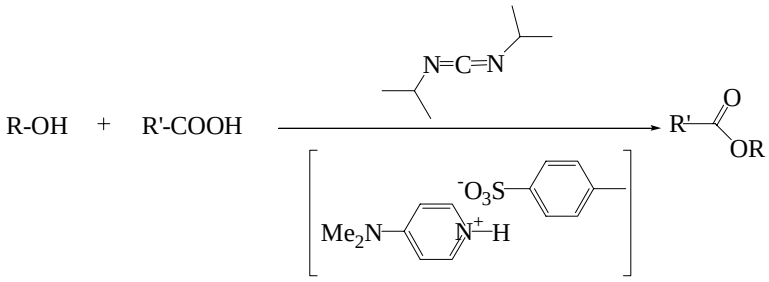

Scheme 3.38 General scheme of the carbodiimide condensation.

As in the Mitsunobu reaction, the ester bond it is formed directly from carboxylic acid and alcohol, but in this case the carboxylic acid is activated instead of the alcohol as it is in the Mitsunobu reaction. The first attempt was performed using the macrocycle **43** and the polystyrene carboxylic acid (Mw= 5000) (Scheme 3.39).

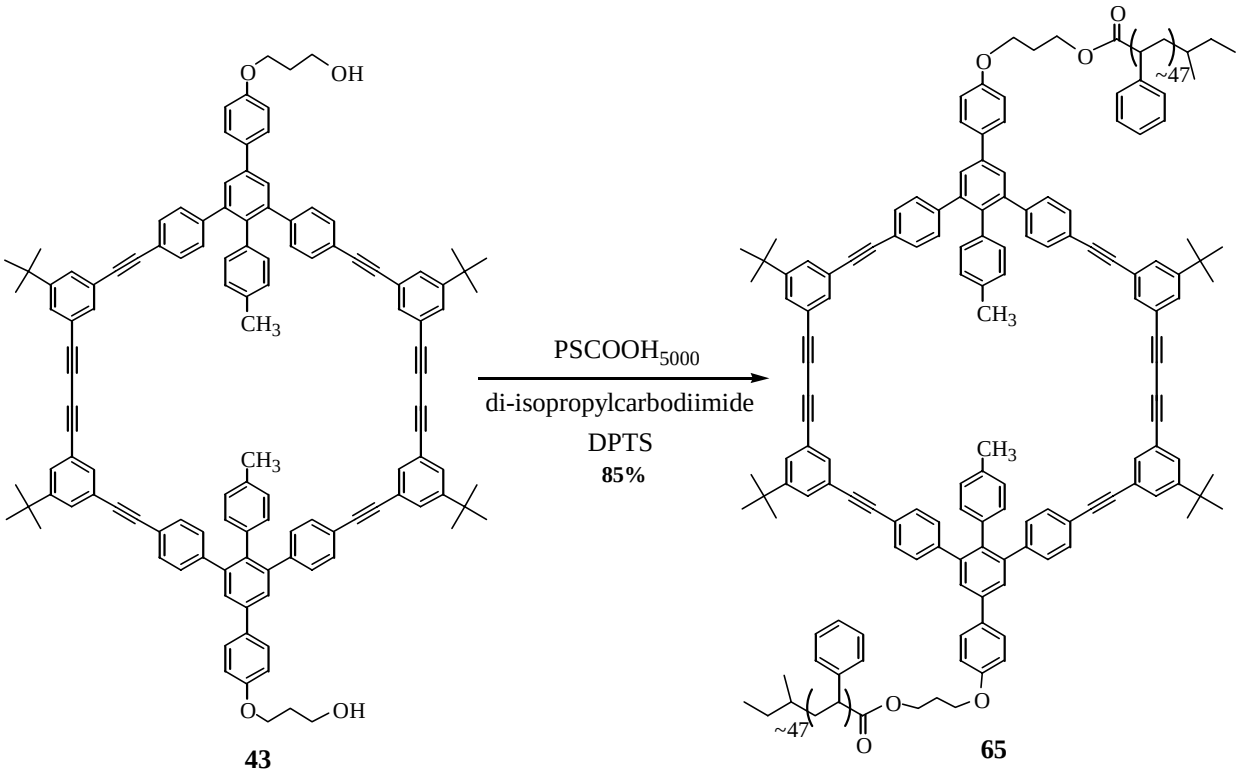

Scheme 3.39 Synthesis of the copolymer **65**.

One equivalent of the macrocycle and two equivalents of polymer were dissolved in dry methylene chloride with two equivalents of 4-(dimethylamino)pyridinium 4-toluensulfonate (DPTS). After solubilizing the starting materials, diisopropyl carbodiimide was added and the mixture stirred overnight. The work up has high impact on the product purification. If the reaction mixture is worked up by adding distilled water, the product contained in most cases a small amount (3-5 %) of an impurity with slightly higher molecular weight, which could not be separated from the block

copolymers by simple column chromatography. If, on the other end, the solvent is removed under vacuum and the crude product immediately purified by column chromatography, **65** was obtained in pure form in 85 % yield.

The mechanism of the carbodiimide condensation reactions is believed to involve the O-acylisourea intermediate **a** shown in scheme 3.40. This intermediate can follow two different reaction pathways. Bimolecular reaction between **a** and a second carboxylic acid leads to the formation of the acid anhydride and urea (path A). Alternatively it is possible to postulate that DPTS is effective at capturing the O-acylisourea as the active N-acylpyridinium intermediate **b** (path B). Formation of **b** from **a** involves a series of proton-transfer steps and is accompanied by the generation of urea. Reaction of b with a nucleophile such as phenol produces the ester and DPTS, ready again for another catalytic cycle (scheme 3.40).

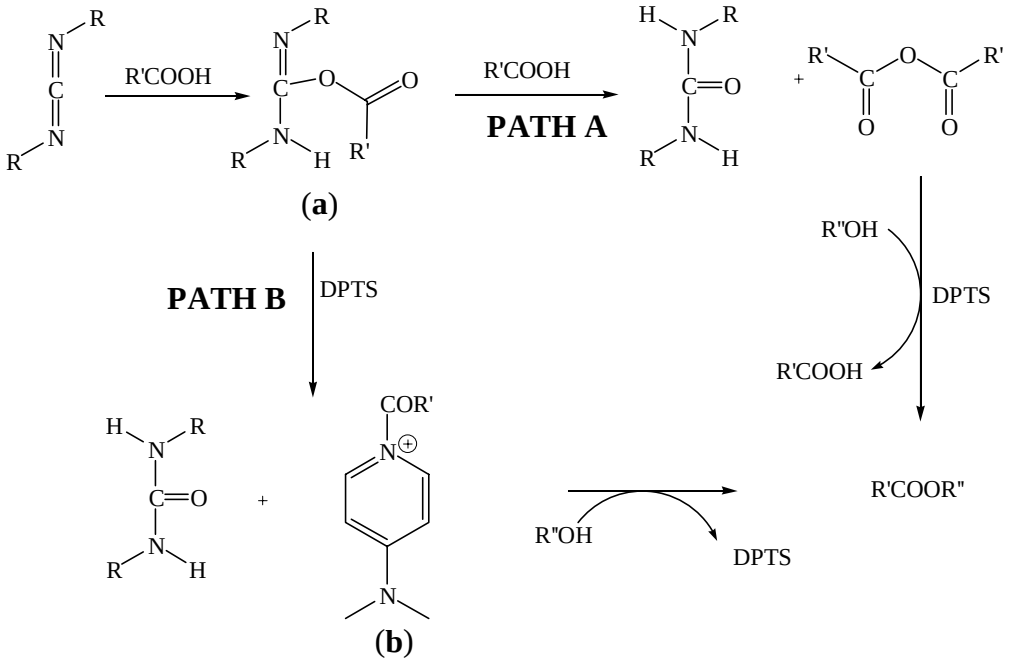

Scheme 3.40 Proposed mechanism of the carbodiimide condensation.

The copolymer was analyzed by GPC and no trace of impurities were found. In order to characterize the molecular weight of the material in more detail, a MALDI-TOF spectrum was recorded and the measured molecular weight of circa 12000 is in perfect agreement with the expected molecular weight (Figure 3.9).

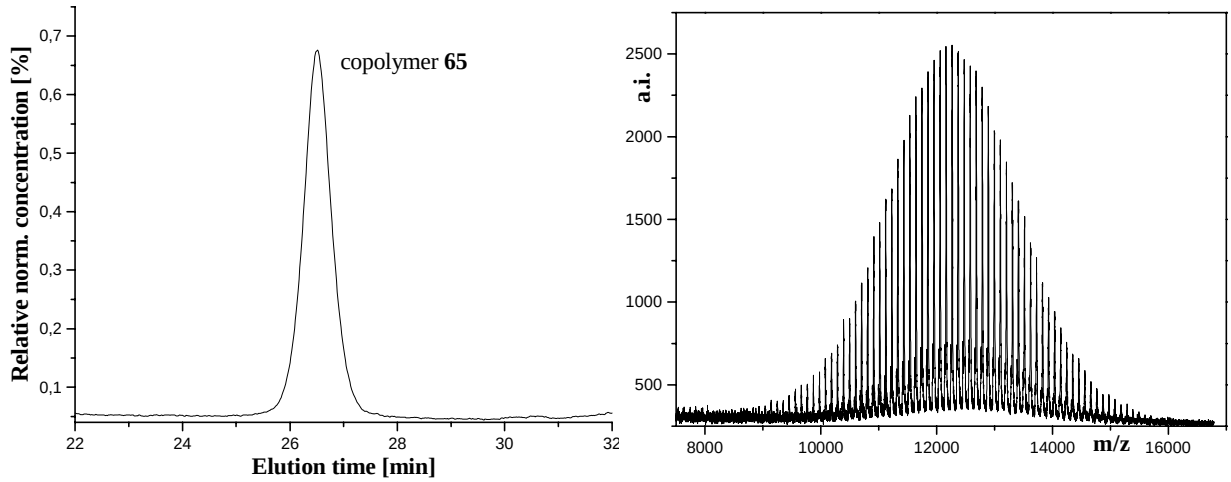

Figure 3.9 GPC data (left) and MALDI-TOF spectrum (right) of copolymer **65**.

In the ^{1}H NMR spectra of the copolymer the signals of the polystyrene cover partially the signals of the macrocycle.

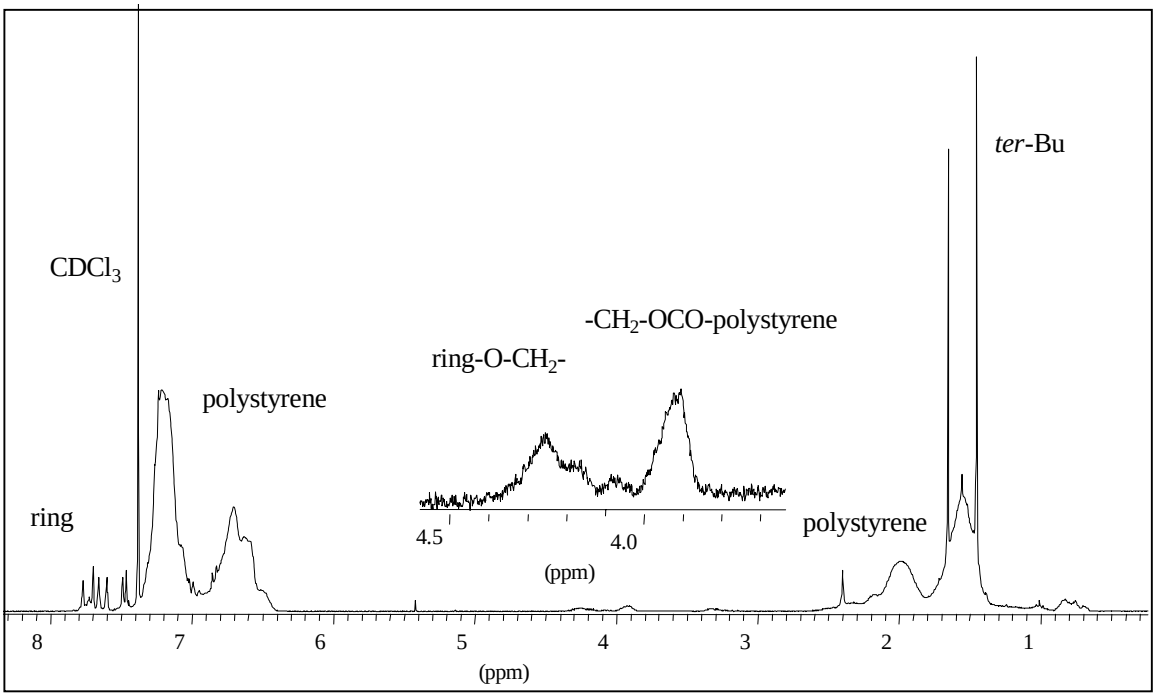

Figure 3.10 ^{1}H NMR spectrum of the copolymer **65**.

However, it is possible to detect the ring peaks in the range from 7.5-8 ppm and as a broad singlett between 3.5 and 4 ppm the signal of the protons of the CH_2 group adjacent to the ester bond between macrocycle and polymer. The protected CH_2 group adjacent to the ether bond is also visible as broad singlett in the range 4 – 4.5 ppm (Figure 3.10).

The same type of reaction was performed using the macrocycle **51** and polystyrene carboxylic acids of different molecular weight. The general structure of the resulting copolymers is shows in scheme 3.41. Table 3.1 summarizes some data of the different copolymers.

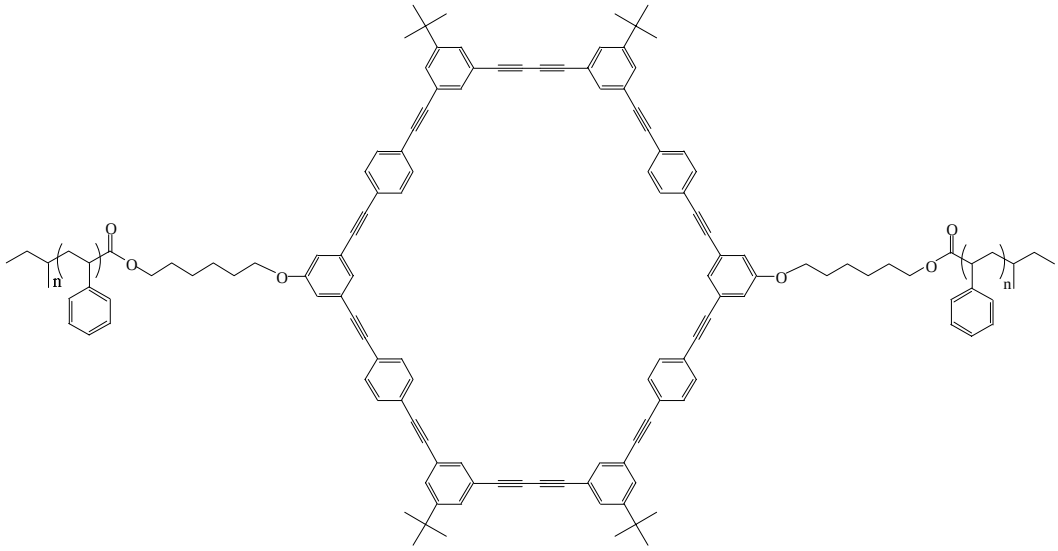

Scheme 3.41 General structure of the copolymers polystyrene-ring(**51**)-polystyrene.

Tabelle 3.1 Data of the different copolymers.

Macrocycle	M_w of Polystyrene	Copolymer	M_w of Copolymer	Yield
51	5000	**66**	11500	39 %
51	3500	**67**	8500	64 %
51	2500	**68**	6500	84 %
51	1500	**69**	4500	86 %
51	1000	**70**	3500	32 %

In all cases the copolymers were obtained in good yield and easily purified. The characterization of the copolymer **68** is reported here in more detail as an example for all compounds in table 3.1. The GPC analysis using THF as eluent shows that the compound is pure and has a monodisperse molecular weight distribution. In the MALDI-TOF spectra the molecular weight of circa 6600 is in perfect agreement with the expected molecular weight of the copolymer **68** (Figure 3.11).

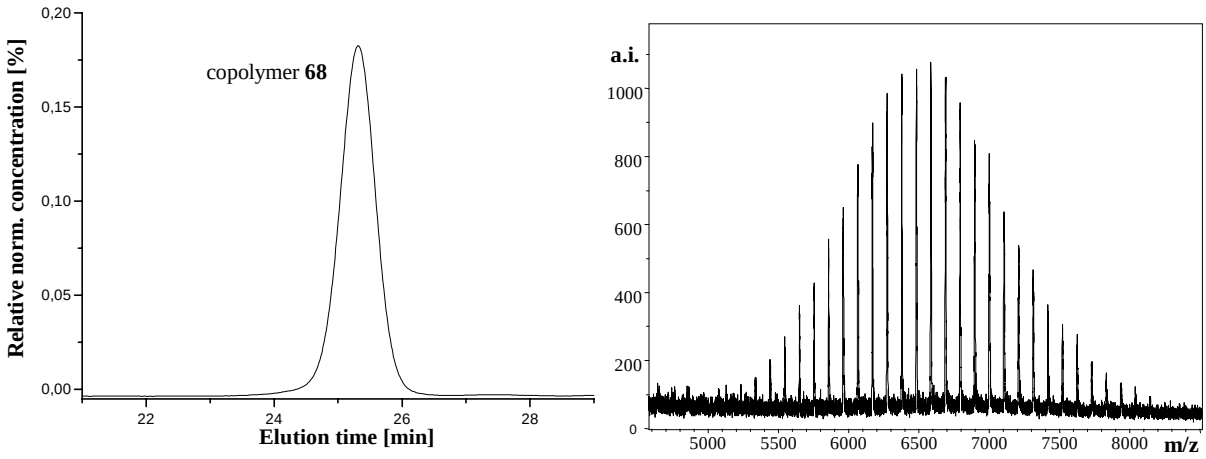

Figure 3.11: GPC data (left) and MALDI-TOF spectrum (right) of **68**.

The ^{1}H NMR spectrum is shown in figure 3.12. As in the case of copolymer **65**, the signals of the polystyrene cover most of the signals of the macrocycle. In any case, distinct signals of the ring are present in the range between 7.3 and 7.6 ppm. The protons of the CH_2 groups, one adjacent to the ether group and the other one adjacent to the ester group, give a broad multiplett between 3.5 and 4 ppm.

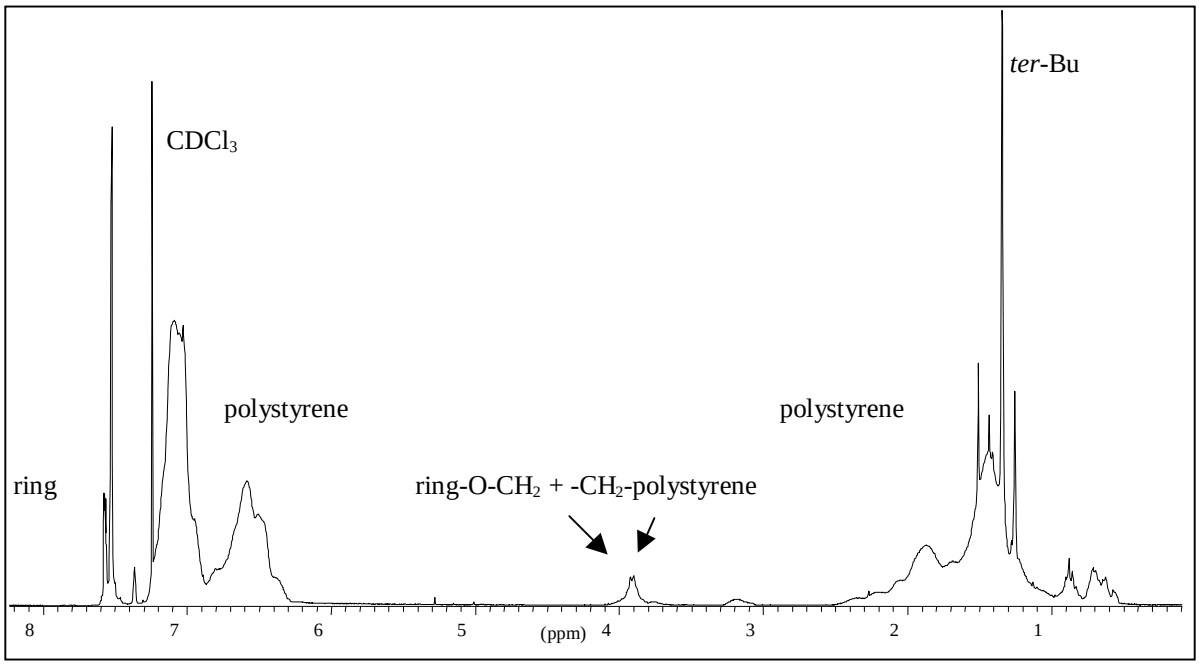

Figure 3.12 ^{1}H NMR spectrum of copolymer **68**.

The carbodiimide condensation has been also used to couple the macrocycle **51** with the three polydimethylsiloxane carboxylic acid (**59**, **60** and **61)**. The general structure of the corresponding copolymer is shown in the scheme 3.42.

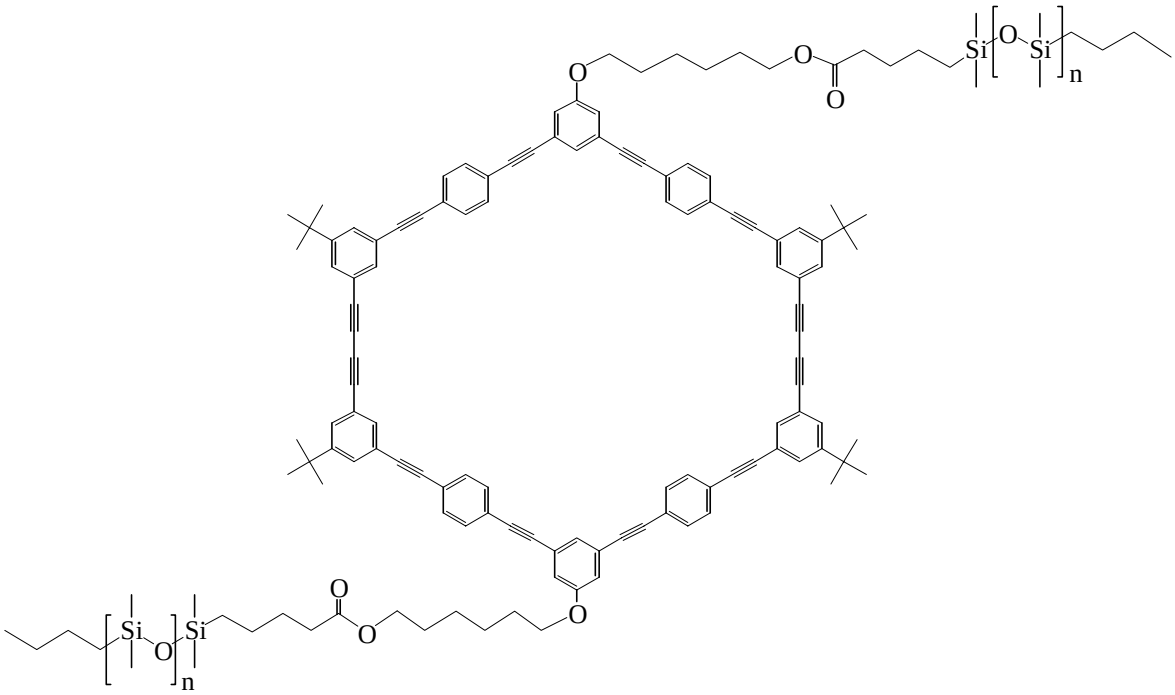

Scheme 3.42 General structure of the copolymers polydimethylsiloxane-ring(**51**)-polydimethylsiloxane.

Table 3.2 are summarizes the different molecular weights of the copolymers that have been synthesized.

Table 3.2 Data of the different copolymers.

Macrocycle	Polydimethylsiloxane	Copolymer	M_w of Copolymer	Yield
51	**59** (M_w = 1500)	**71**	4500	96 %
51	**60** (M_w = 3000)	**72**	7500	50 %
51	**61** (M_w = 5000)	**73**	11500	61 %

The three copolymers have been analyzed by GPC using toluene as eluent and the refractive index detector in order to determine their purity (Figure 3.13).

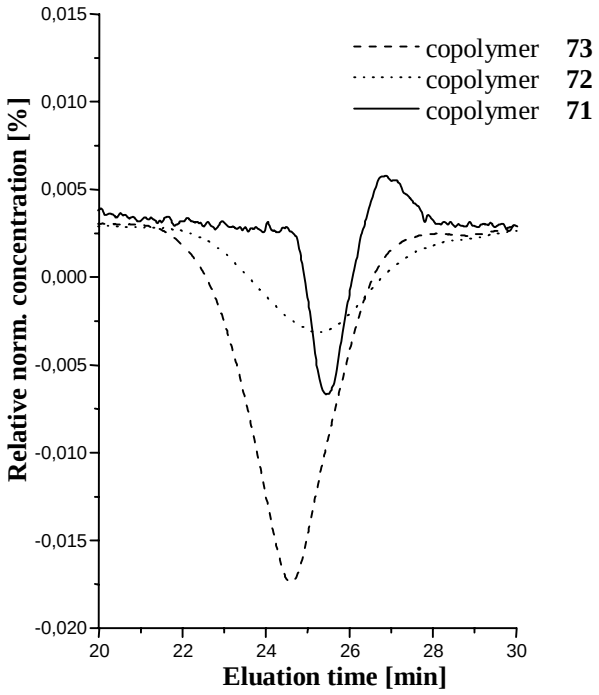

Figure 3.13 GPC data of the copolymers **71**, **72** and **73**.

PDMS has a lower refractive index than toluene and therefore the peaks are negative. In the case of copolymer **71** the GPC curve changes from positive to negative values. This is due to the fact that the weight fraction of macrocycle (that has a higher refractive index than toluene) in the copolymer on average is 0.3 and a change in the refractive index between the two different component of the copolymer can be detected. With increasing the molecular weight of the PDMS in the copolymer (**72** and **73**) the influence of the macrocycle is reduced and only negative peaks are detected.

Differently from the polystyrene copolymers, the ^{1}H NMR spectrum in this case show very clearly the signals of the ring that are mostly at low field and the signal of the polydimethylsiloxane that are exclusively at high field (Figure 3.14).

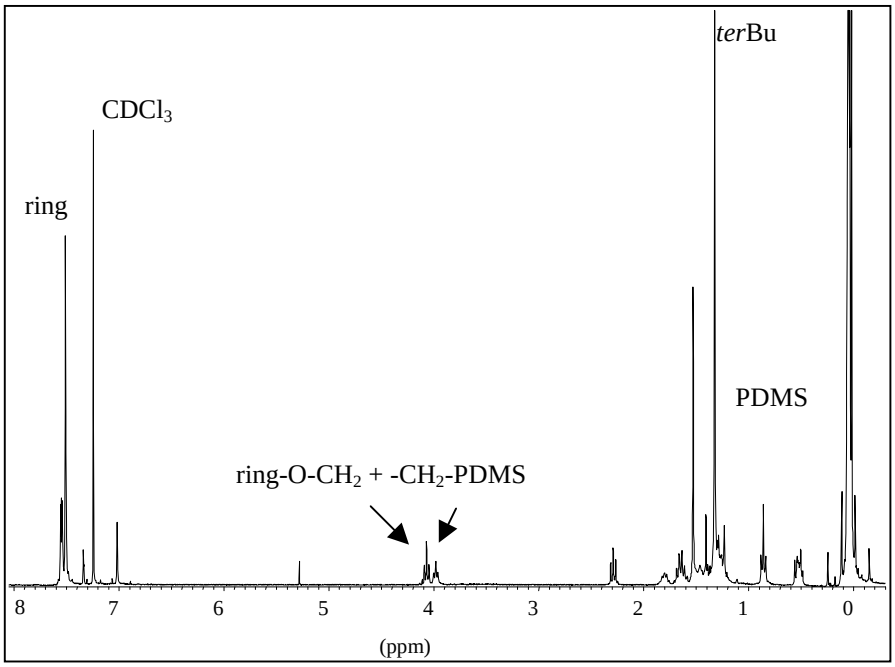

Figure 3.14 ^{1}H NMR spectrum of copolymers **71**.

Distinct signals of the ring are present in the range between 7 and 7.6 ppm and the four t-butyl groups lead to a sharp singlett at 1.31 ppm. The two protons of the CH_2 group, one adjacent to the ether group and the other one adjacent to the ester group, give two tripletts at 3.9 and 4 ppm respectively. The signals of the PDMS are in the range between 0 and 2.3 ppm.

4 Properties of polystyrene-ring-polystyrene block copolymers

4.1 Investigation in solution

All polystyrene-ring-polystyrene copolymers are readily soluble at room temperature in chloroform, dichlohoromethane, THF and toluene. In order to enforce aggregation due to the incompatibility of the oligomeric chains and the macrocycle, the use of a selective solvent for the polystyrene was tried. As first attempt cyclohexane was used. This is a non-solvent for the macrocycle and a theta solvent for polystyrene. The tetha state is defined as that state of a polymer solution at which the excess chemical potential, and correspondingly, the excess Gibbs energy of dilution is zero. For a given polymer-solvent system, this state is obtained at a certain characteristic temperature, the theta temperature (θ). A solvent at this temperature is called a theta solvent. The theta temperature for polystyrene in cyclohexane is 34 °C. The copolymers **66**, **67**, **68**, **69** were dissolved in warm cyclohexane. Upon cooling, **66** forms a gel at concentrations above 0.5 wt %, **68** forms a very viscous solution rapidly, similar as **67** does after some days. Exceptions are solutions of **69**, which exhibit no unusual viscosity and **70** that forms only a suspension under the same condition (but dissolves it in warm cyclohexane) (table 4.1).

Table 4.1 Behavior of the cyclohexane solutions of PS-ring-PS block copolymers.

Copolymer	$M_{w\ polystyrene}$	Aggregation behaviour
62, 66	PS-$COOH_{5000}$	Solution
67	PS-$COOH_{3500}$	Viscous solution after two weeks
68	PS-$COOH_{2500}$	Viscous solution
69	PS-$COOH_{1500}$	Gel
70	PS-$COOH_{1000}$	Suspension

The formation of a viscous solution and even more of gels is the first indication of aggregation. These observations can be explained by the different solubility of the rigid cyclic block and the flexible polystyrene block of the copolymer. The attachment of the polymeric side group, even of relatively low molecular weight, is sufficient enough to solubilize the block copolymer in cyclohexane at elevated temperatures. However, upon cooling, the rigid parts of the block copolymer aggregate if the size of the coiled block is below a certain level. As expected, extension of the solubility and aggregation kinetics strongly depend on the block size of the polystyrene.

Other solvents were used to solubilize the copolymer in order to observe the same type of behavior. Therefore, solvents having a similar Hildebrand solubility parameter δ (a measure of the cohesive energy density) as cyclohexane were investigated (table 4.2).

Table 4.2 Behavior of PS-ring-PS block copolymers solutions in different solvents.

Solvent	Solubility parameter δ (MPa) ^{½} *	Behavior
diethylamine	16.4	suspension
diisopropyl ketone	16.4	solution
dihexylether	16.4	suspension
2,2-dichloropropan	16.8	solution
butyl metacrylate	16.8	solution
cyclohexane	**16.8**	**viscous solution**
ethyl benzoate	16.8	solution
bicyclohexyl	17.4	solution
decalin	18.0	solution
toluene	18.2	solution
chloroform	19.0	solution

* Data from E. A. Grukle "*Polymer Handbook*", 4th Edition, pag VII/675.

As shown in the table, cyclohexane is the only solvent in which aggregation behavior was observed (what has to be mentioned is that the solubility parameter δ describes the entalphy change by mixing nonpolar solvents well, but does not give uniform results when extended to polar systems. In this case polar and hydrogen bonding terms should be taken into account).

Due to the topology of the block copolymers, the aggregation should lead to the formation of rod-shaped aggregates with large aggregate numbers, reducing the contact of the rigid cyclic unit with the solvent. In order to support this assumption, the aggregation behavior of the copolymers in solution was investigated in more detail using light microscopy (LM), static and dynamic light scattering (SLS and DLS), ultra small and small angle x-ray scattering (USAX and SAXS), transmission electron microscopy (TEM), and atomic force microscopy (AFM).

4.1.1 Light microscopy: lyotropic liquid crystalline phases

4.1.1.1 General consideration

In a plane-polarized beam, the oscillations of the electromagnetic wave are confined to a single plane perpendicular to the direction of propagation.

The electric FIELD associated with light distorts the electronic configurations of atoms and molecules in matter through which the light passes. When the electronic configuration of the medium is preferentially oriented, vibrations polarized in certain directions interact preferentially, experiencing direction-dependent variations in absorption or refractive index. Media that exhibit these effects are said to be anisotropic, whereas media that transmit or absorb polarized light uniformly in all directions are isotropic. Materials, including certain biological structures and most crystals, exhibit birefringence (a variation of refractive index with respect to direction). The phenomenon of birefringence reveals the presence of ordered structures (for example oriented chemical bonds) within a specimen. Birefringence can be measured, providing information from which the orientation of macromolecules in the specimen can be deduced by means of polarizing microscopy. In particular between crossed-polarizers (two perpendicular oriented polarizers), isotropic specimens appear dark at all orientations. When a birefringent specimen is placed between crossed polarizers, it resolves the incident plane-polarized light (from the polarizer) into two components polarized in mutually perpendicular directions leading to the appearance of a so called texture

4.1.1.2 Light microscopy

The viscous solutions of **67**, **68** and **69** in cyclohexane were investigated under the light microscope using crossed polarizers revealing for all samples birefringence (Figure 4.1).

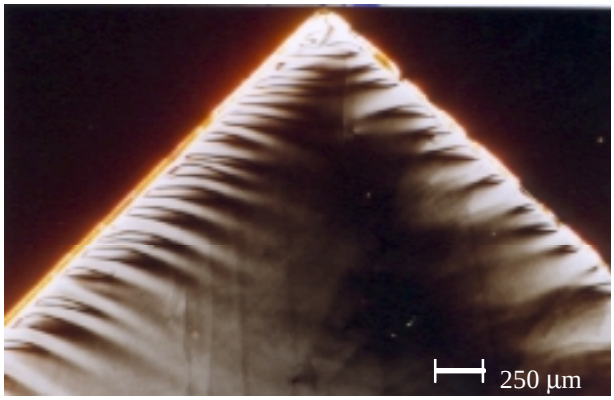

Figure 4.1: Texture of **68** in cyclohexane between crossed polarizers (2 wt %; at the edges of the cover glass).

These copolymers in cyclohexane are lyotropic liquid crystals. The liquid crystallinity can be proved by shearing the sample between the object glass and the cover glass. The texture change and ribbons are formed in the direction perpendicular to the shearing direction (Figure 4.2)

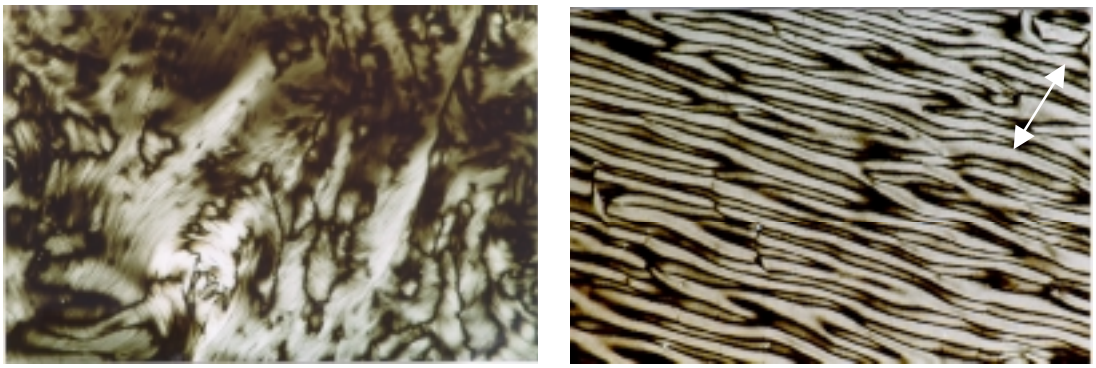

Figure 4.2: Optical micrograph between crossed polarizers of a 2 wt % solution of **68** in cyclohexane before and after shearing (the white arrows indicate the shearing direction).

Interesting, the dried lyotropic samples maintained the birefringence indicating that once the anisotopy of the material is enforced by the solvent, the anisotropy is maintained also in the dry state, when the solvent is evaporated (Figure 4.3 and 4.4).

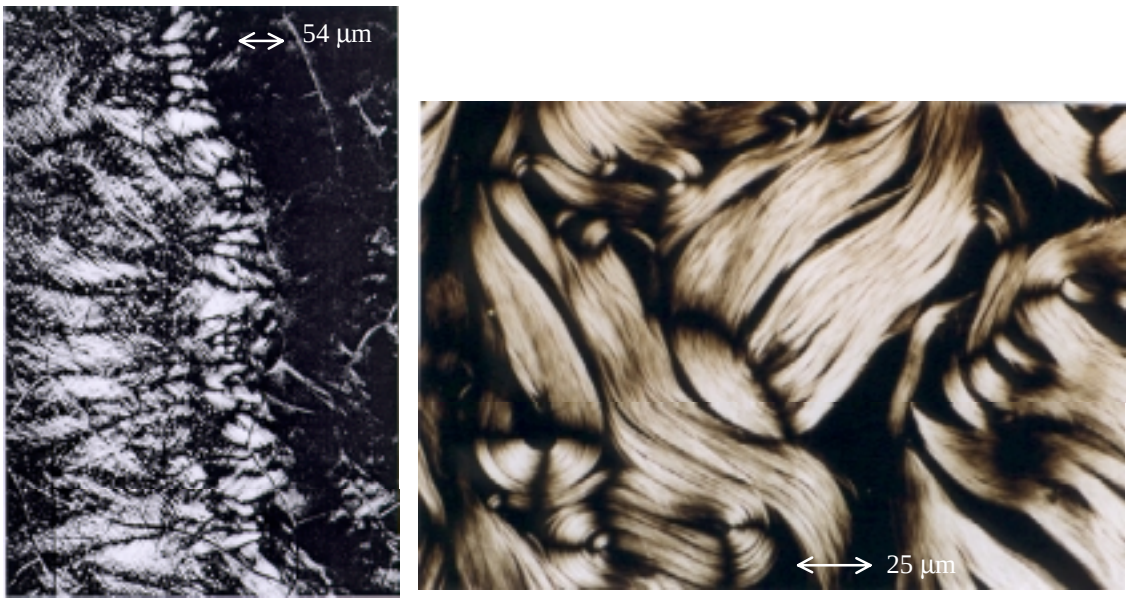

Figure 4.3: Film of **67** (left) and **68** (right) obtained by drying cyclohexane solutions.

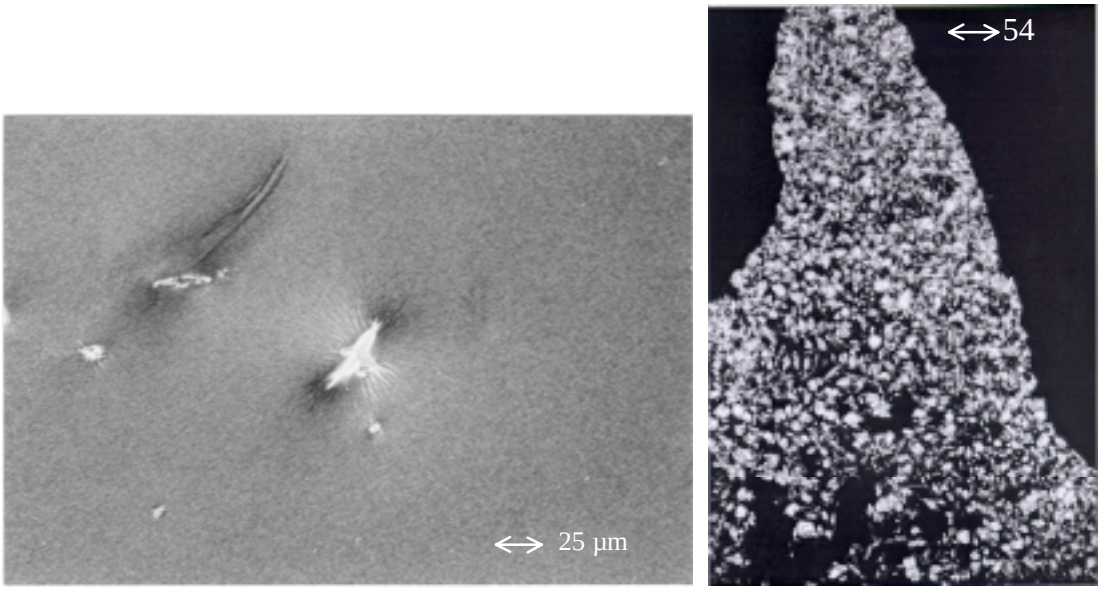

Figure 4.4: Film of **69** (left) and **70** (right) obtained by drying cyclohexane solutions.

Contrary, this anisotropy cannot be obtained by cooling an isotropic melt of the materials.
From the light microscope images it appears that the copolymer solutions form a lyotropic smectic phase. This means that the molecules, or aggregates of the molecules, are parallel to one another and are arranged in layers. Because of the complexity of the textures and because textures of oligomers and polymers are not as easy to interpret as for low molecular weight compounds, it was not possible to obtain more information by the light microscopical investigations.

4.1.2 Static and dynamic light scattering

4.1.2.1 General consideration

Light is scattered by macromolecules or particles like colloids in solution. Static light scattering (SLS) involves measuring the amount of light scattered by a solution at some angle relative to the incident laser beam. The intensity of the scattered light is a function of the nature of the molecules, their size, molecular weight, shape, their concentration and additional parameters.
When the molecules are larger than approximately 1/20 of the wavelength of the incident light, the scattered intensity becomes also a function of the scattering angle, the angle between the incident and the scattered light, due to intramolecular interference of the scattered light. Altogether the reciprocal of the relative intensity of the scattered light can be expressed by the ZIMM-equation:

$$\frac{Kc}{R_\theta} = \frac{1}{M_w}\left(1+\frac{1}{3}q^2R_g{}^2\right)+2A_2c$$

where K is an optical constant, depending on the refractive index *n* of the solvent, the refractive index increment $\partial n/\partial c$, the wavelength λ of the incident light in the vacuum, and the concentration *c*. R_θ, the relative intensity of the scattered light (or Rayleigh ratio), is define for vertically polarized light as $R_\theta = \frac{i_\theta}{I_0} r^2$ with i_θ and I_0, the intensity of scattered light at angle θ, and of the primary light respectively, and *r* the distance of the detector from the center of scatter. Finally, $q = \left(\frac{4\pi n}{\lambda} \sin\frac{\theta}{2}\right)$ is the absolute value of the scattering vector, depending on the scattering angle θ.

A corresponding plot yields by appropriate extrapolation the weight-average of the molecular weight M_w, the sphere-equivalent radius of gyration R_g and the second virial coefficient A_2, a parameter which describes the interaction between the polymer and the solvent.

In the static light scattering the angle dependence of the time-averaged scattered light intensity from a certain particle dimension (larger than l/20 of the wavelength, in other words larger than 15 nm) gives information about the particle form (form factor). If several processes are present (and this can be seen using dynamic light scattering (DLS) analysis) the contributions of the respective processes to the total scattered light intensity can be calculated, and then used to get information about the shape of the particle.

In contrast to the static light scattering, where the time averaged scattered intensity is analyzed, the relation of interest in dynamic light scattering is the fluctuation of the intensity of the scattered light with the time t. In other words, DLS is concerned with the investigation of correlation of photons. A typical way to describe a scattered signal is by the way of its 'autocorrelation'. The autocorrelation function of the signal from the scattered intensity is the convolution of the intensity signal as a function of time with itself. In more abstract terms, if the detected intensity is described as a function I(t), then the autocorrelation function of this signal is given by the following expression, where t is the shift time.

$$G(\tau) = \int_0^\infty I(t) \cdot I(t+\tau) dt$$

The above function is also called the intensity correlation function, and it is used to describe the correlation between the scattering intensities measured at t = 0 and some later time (t+τ). For light scattered from diffusing molecules, the intensity correlation curve exhibits an exponential decay and it has the form of 1 plus an exponential decay function:

$$G(\tau) = 1 + (g^{(1)}(q,t))^2$$

$g^{(1)}(q,t)$ is the field autocorrelation function of the scattered amplitude and can be describe as an exponential decay:

$$g^{(1)}(q,t) = S\ (qL)\exp(-q^2 Dt)$$

If two types of molecules with different molecular weight contribute to the scattering, $g^{(1)}(q,t)$ can be described by a double exponential decay:

$$g^{(1)}(q,t) = S_0(qL)\exp(-q^2 D_1 t) + S_1(qL)\exp(-q^2 D_2 t)$$

Evaluation of $g^{(1)}(q,t)$ leads to the particle diffusion coefficient D, which in turn is used to calculate the hydrodynamic radius R_h via the Stokes Einstein equation:

$$R_h = \frac{k_B T}{6\pi\eta D}$$

where k_B is the Boltzmann constant, T is the absolute temperature and η the dynamic viscosity of the solvent. In other words, the analysis of the autocorrelation functions give information about the number of processes (different particle sizes) and the appropriate hydrodynamic radii of the species can be estimated. For this purpose different fit programs were used:

A) Linux CONTIN fit by Provencher[45] (inverse Laplace transformation): the number of processes must not be given, the program calculates different smoothing factors rate distribution functions and gives the solution with the smallest deviation from the measured data as "choosen solution" (csl). The other solutions (res) can also be used if necessary. The fit programme has a limitation. If the smoothing is too strong it is possible to see instead of two processes only one, very broad process. In this case it is possible to loose information. If the smoothing is too weak, broad molecular weight distributions can split into several processes, which are not really based on distinct different particles. In order to check the validity of the "choosen solution" the results obtained at several scattering angle are compared and additionally studied with other information about the sample and the system.

B) double exponential fit (dexpf): if there are two processes, the field autocorrelation function can be described as:

$$y = P_1 \cdot \exp^{-\left(\frac{x}{P_2}\right)} + P_3 \exp^{-\left(\frac{x}{P_4}\right)} + P_5$$

Where P_1 and P_3 are the amplitudes of the 1st and 2nd process and P_2 and P_4 are the time constants of the 1st and 2nd process. Finally P_5 is the baseline.

4.1.2.2 Static and dynamic light scattering of copolymer 68

4.1.2.2.1 Copolymer 68 in toluene

Solutions of **68** in toluene (0.062 wt % and 0.109 wt %) showed two weight fraction, also after storing the solutions for 8 days, only relatively low scattering intensities. Linux CONTIN fits at different angles result in one process with a R_h of approximately 2.5 nm for both samples (Figure 4.5).

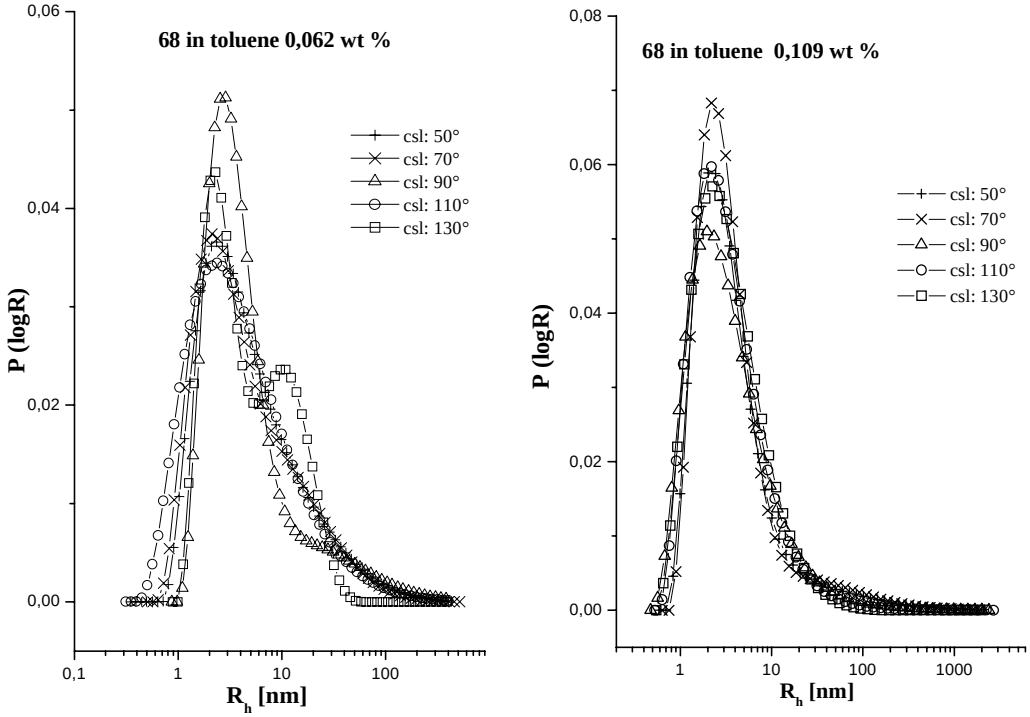

Figure 4.5 CONTIN analysis of **68** in toluene (0.062 wt % and 0.109 wt %).

The fit curves show in the high R_h range a tail or, for high angles, a shoulder and this is probably due to the fact that the field autocorrelation curves are quite noise (Figure 4.6).

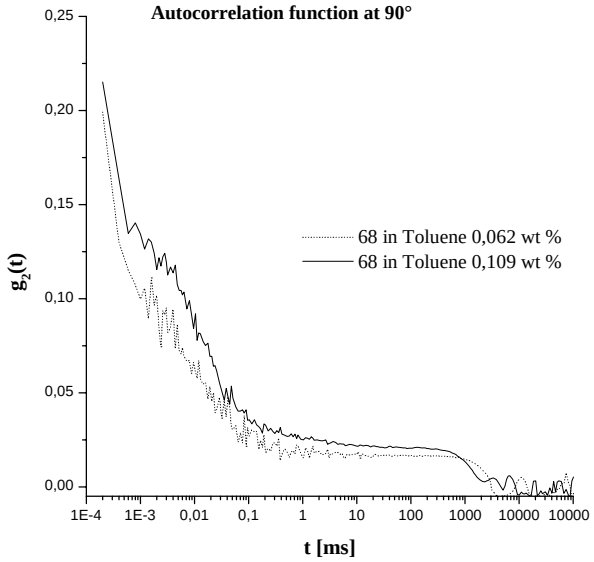

Figure 4.6 Field autocorrelation curves are of **68** in toluene (0.062 wt % and 0.109 wt %).

From the fact that toluene is a good solvent for the macrocycle and for polystyrene, the particle with R_h of approximately 2.5 nm can be associated with the copolymer molecules. The next step is the analysis of cyclohexane solutions of **68**.

4.1.2.2.2 Copolymer 68 in cyclohexane

Since preliminary tests showed that solutions of **68** in cyclohexane at concentrations above approximately 0.1 wt % can be filtered only with difficulty, the sample were prepared using the following methodology. The appropriate amount of solid was dissolved in cyclohexane in order to obtain solutions with a concentration of approximately 0.05 wt %. These were filtered through a Teflon filter with a pore diameter of 0.45 μm. Higher concentrations were obtained by evaporation of parts of the solvent at room temperature in the fume hood. The new concentrations were determined gravimetrically (weighting the cuvettes). The scattering behavior of the samples strongly changed within the first 4 days after filtering. Further changes were also detected in similar sample cuvettes but were not in all cases reproducible.

Two ranges of concentrations were investigated, a low concentration, around 0.05 wt %, and a high concentration, around 0.15 wt %. The measurements were performed at different times and at different scattering angles. The different samples and the conditions of the measurements are summarized in table 4.3

Table 4.3 Different samples and the conditions of the measurements.

Sample	Concentration	Storing time	Scattering angles	Type of measure
2.1a; 2.1b	circa 0.06 wt %	1, 4 and 8 days	SA1	DLS
2.3a; 2.3b	circa 0.07 wt %	1, 4 and 8 days	SA1	DLS
2.2a	0.15 wt %	1, 4 and 8 days	SA1	DLS
2.2b	0.138 wt %	1, 4 and 8 days	SA1	DLS
3.1; 3.2	circa 0.05 wt %	after 5 days	SA2	SLS and DLS
4.1	0.085 wt %	after 5 days	SA2	SLS and DLS
4.2	0.093 wt %	after 5 days	SA2	SLS and DLS
4.3	0.113 wt %	after 5 days	SA2	SLS and DLS

SA1: 50°, 70°, 90°, 110°, 130°

SA2: 30°, 35°, 40°, 45°, 50°, 55°, 60°, 70°, 80°, 90°, 100°, 110°, 120°, 130°, 140°, 150°

The analysis of samples 3.1 and 3.2 is shown here in detail. The linux CONTIN fit results in two reproducibly processes, a fast mode with a R_h = 2.4 nm and a slow mode with a R_h = 68 nm (figure 4.7).

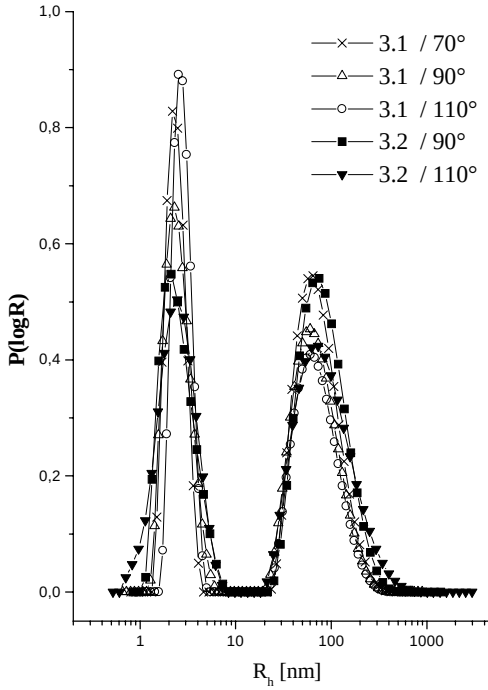

Figure 4.7 CONTIN analysis of samples 3.1 and 3.2.

Using the two hydrodynamic radius of the CONTIN as initial values, a double exponential process (dexp) was also fitted (table 4.4).

Table 4.4

Sample	CONTIN fit		Dexp fit	
	$\varnothing R_{h1}$	$\varnothing R_{h2}$	$\varnothing R_{h1}$	$\varnothing R_{h2}$
3.1	2,3 nm	59 nm	2,4 nm	72 nm
3.2	2,2 nm	69 nm	2,6 nm	90 nm

Both fitting methods give values for the two R_h of 2.5 nm and 70 nm respectively. This means that in cyclohexane solution together with the single copolymer molecules (R_h = 2.5 nm) (fast mode) other objects of R_h = 70 nm (slow mode) contribute to the scattering intensity. This objects can only be aggregates of the copolymer.

To get an idea of the aggregates structure and shape, in other words to discriminate between a Gaussian coil, a wormlike chain or a rod, two types of plots can be used. The Kratky plot, shows the intensity $I \cdot q^2$ versus q, suitable for Gaussian coils and chains with little deviation from the random coil and the Holzer plot, $I \cdot q$ versus q, useful for semiflexible chains close to rod behavior[46]. The scattering behavior of polymers of different flexibility are shown in figure 4.8.

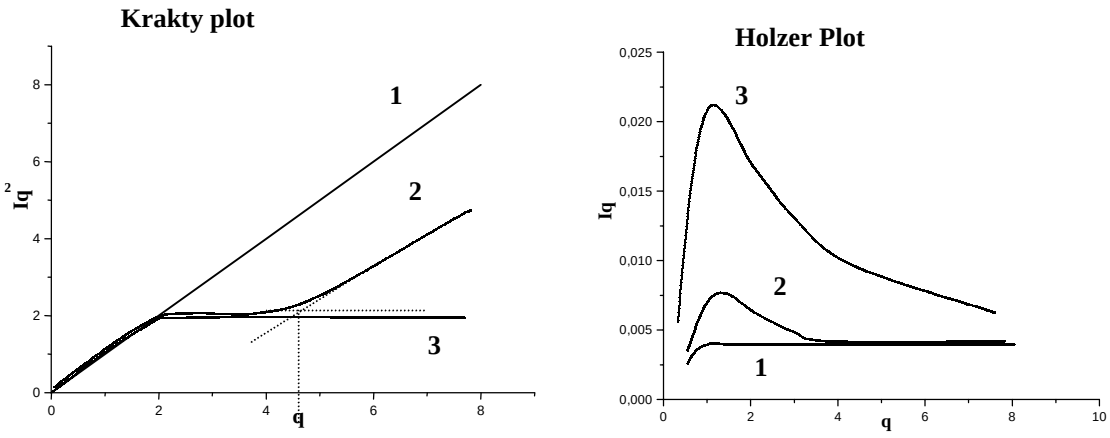

Figure 4.8 Coils (3), rigid rods (1), and wormlike chains (2) in a Kratky plot (left) and in a Holzer plot (right).

In the Krakty plot the Gaussian coil develops a q-independent plateau whereas rods show a linear increase with q. Wormlike chain are in between and the transition from coil-like to rod-like behavior

is expected to occur around a value q = q*. q* is determined by extrapolation the coil plateau to larger q values and the asymptotic straight line of the rod toward smaller q values until the asymptotes intersect. q* is a measure of the stiffness of the polymer. $(q^*)^{-1}$ gives the persistent length of the polymer. It has long been known that the coil plateau is often not well developed in experimental curves, which makes the determination of q* sometimes questionable or even not possible. In such cases it makes sense to choose a plot which tends to rod rather than to coil-like behavior, the Holzer plot. In a Holzer plot a rod shows a horizontal asymptote. The value of the plateau does not depend on chain length polydispersity. At lower q values, the curve bends downward continuously and approaches the origin at q = 0. This happens also for semiflexible chains, but here the curve passes through a maximum at smaller q value before the rod plateau is reached. The occurrence of the maximum is typical for coiled chains. The height of the maximum is affected from the polydispersity.

The Krakty plots displaying the $I \cdot q^2$ versus q behavior of the slow mode in 3.1 and 3.2 are shown in figure 4.9. From the shape of the curves it is possible to conclude that the aggregates are wormlike object. The data are in agreement with the linear fit in both case at least until q = 0.014 nm^{-1}, that means that those rod object have a persistent length of at least 70 nm.

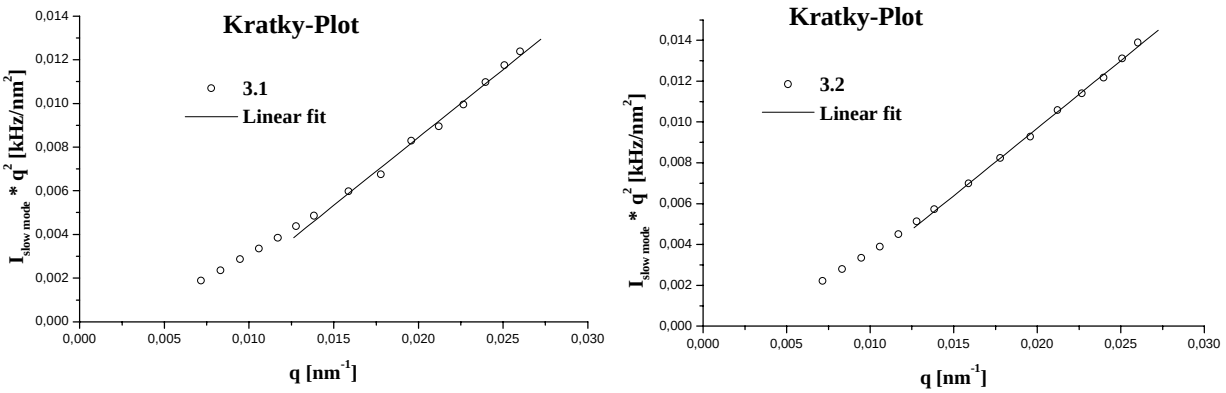

Figure 4.9 Krakty plots displaying the $I \cdot q^2$ versus q behavior of the slow mode in 3.1 and 3.2.

The Holzer plots show neither a plateau at high q values nor a maximum at low q values. This type of behavior is found in cases of rod-like objects with an high polydispersity in the length[46] (Figure 4.10).

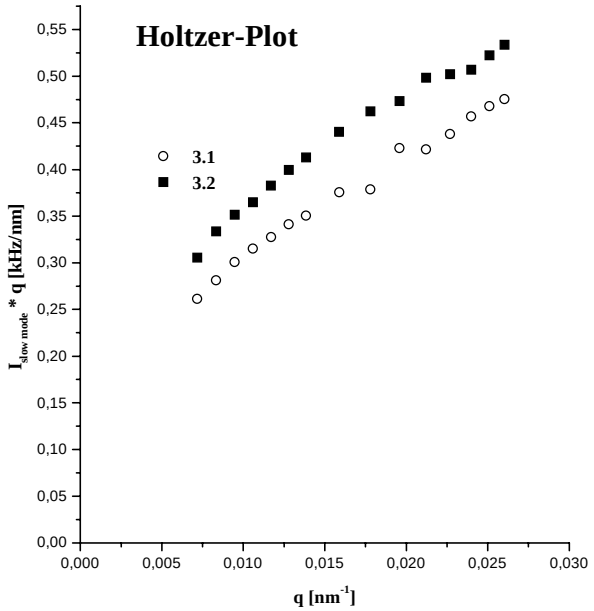

Figure 4.10 Holzer plots displaying the I·q versus q behavior of the slow mode in 3.1 and 3.2.

In order to get more information about the shape of those aggregates, the angle dependent intensity of the slow modes is fitted using different form factors: a rod of a certain length L and an infinitely small diameter, and a sphere of the radius R[47,48,49] (see Appendix B). The data and the form factor fits are shown in figure 4.11.

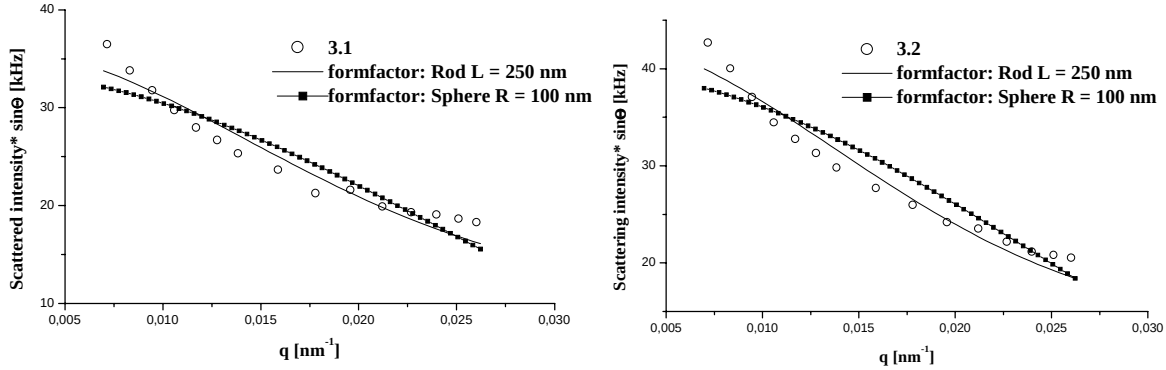

Figure 4.11 Angle dependent intensity of the slow modes in 3.1 and 3.2.

The agreement between the fit function and the data is not very good which is probably due to the simplicity of the fitting function, which does not cover a distribution of shapes. Moreover the intensity contributions were not determined directly but by separating two processes by the analysis of the dynamic data by CONTIN-Analysis. In any case the χ^2 is better for rods than for spheres. Attempts to fit the data with a form factor of a cylinders gives no better agreement with the experimental data. The reason can be due to the fact that the solution contains a distribution of

aggregates of different shapes, in the sense that some aggregates are short and compared with the diameter (estimated of circa 10 nm) they look like sphere or ellipses, while other are longer and have a shape of cylinders and rods. To test this hypothesis the data were fitted with a distribution of polydisperse rods (see Appendix B) and as it shows in the figure 4.12, the agreement between the data and the fit curve is quite good.

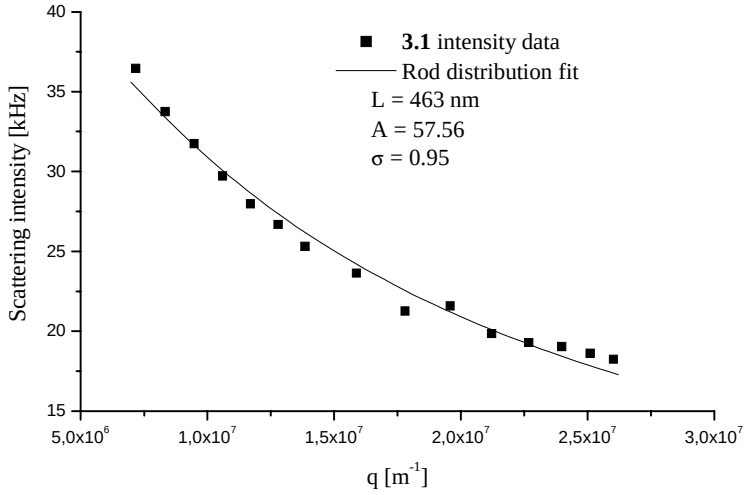

Figure 4.12 Data of 3.1 fitted with a distribution of polydisperse rods.

With increasing concentration (sample 4.2-4.3), the linux CONTIN fit does not give a uniform picture over different angles, like it did in the case of lower concentrated samples (sample 3.1-3.2) (Figure 4.13).

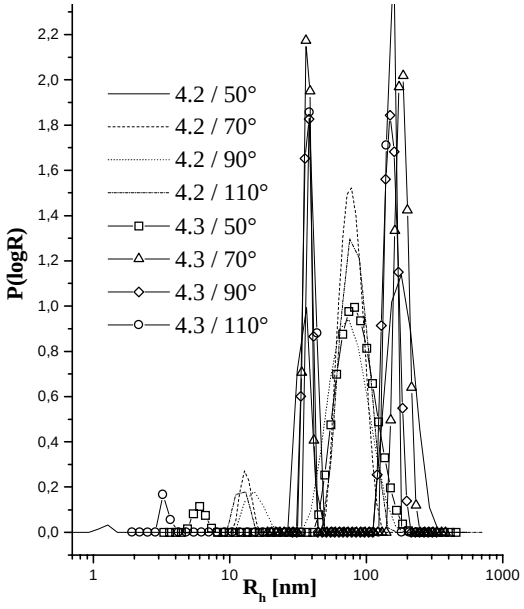

Figure 4.13 CONTIN analysis of samples 4.2 and 4.3.

It is not possible to obtain reproducible peaks at small R_h, and at larger R_h are usually two processes detected. By a dexp fit the fast processes (small values of R_h) cannot be detected. This happens because the intensity is proportional to R_h^6, therefore a particle 10 times larger than the other scatters 10^6 times more than the small particles. This means, that although the small particles are present even at high concentration, their contributions to the scattering intensity is so small that they can not be detect. Only two slower processes (large values of R_h) are calculated (Table 4.5).

Table 4.5

Sample	CONTIN fit		Dexp fit	
	$\varnothing R_{h1}$	$\varnothing R_{h2}$	$\varnothing R_{h1}$	$\varnothing R_{h2}$
4.2	20 ± 5 nm	90 ± 10 nm	38 nm	166 nm
4.3	30 ± 15 nm	160 ± 20 nm	31 nm	160 nm

The data analysis suggests that two types of large particles (two type of aggregates) are present in solution. One with an R_h ~ 36 nm and another with an R_h ~ 160 nm. The data for these processes show relatively large fluctuations.

The CONTIN analysis varies strongly, as describe before, with the scattering angle. Nevertheless, the Kratky plot for both processes show high noise (no systematic deviations) from the linear fit (Figure 4.14; same for 4.3).

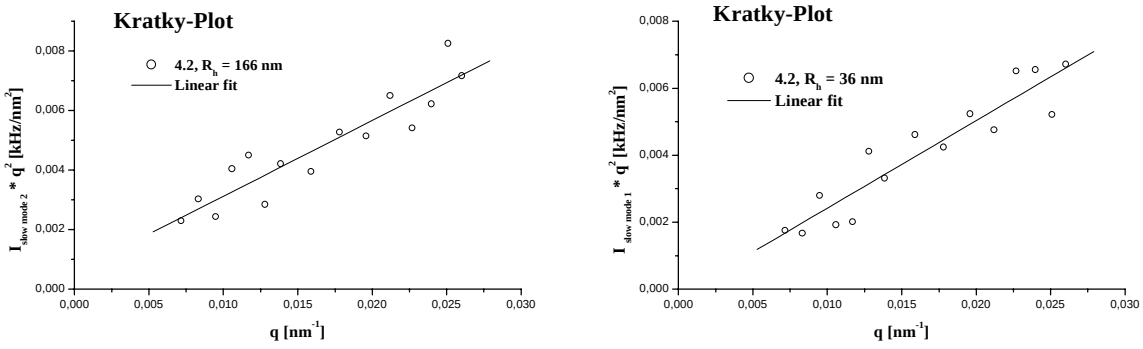

Figure 4.14 Krakty plots displaying the $I \cdot q^2$ versus q behavior of the slow modes in 4.2.

Moreover, the scattering intensities show a similar q-dependency for both modes and this is unusual for particles having so different values of hydrodynamic radius (Figure 4.15; same for 4.3).

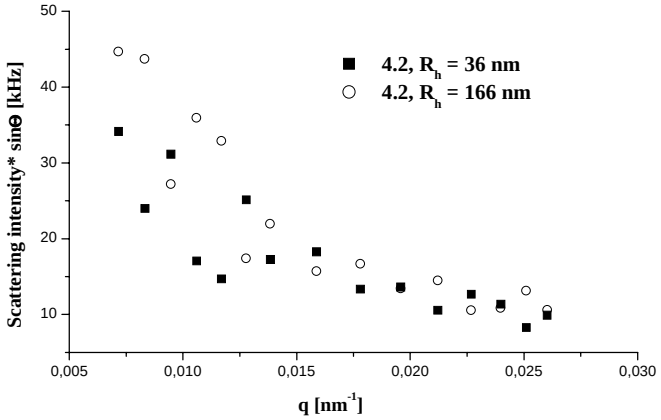

Figure 4.15 Angle dependent intensity of the slow modes in 4.2.

From the physical point of view there are no reasons for an aggregation of our block copolymers to form two types of aggregates of distinct lengths. Therefore the scattering data were analyzed with a model of a single type of aggregates. The fact that the CONTIN analysis and the dexp fit resulted in two processes can be explained by the fact that very broad distributions of particle sizes are present in the solution. In this case it seems that the fitting programs splits a very broad distribution of R_h in two different R_h values (at the side of the range). If the two processes are analyzed together, the Krakty-plot shows a linear behavior, typical for rod, at least until q = 0.0071 nm^{-1} (Figure 4.16).

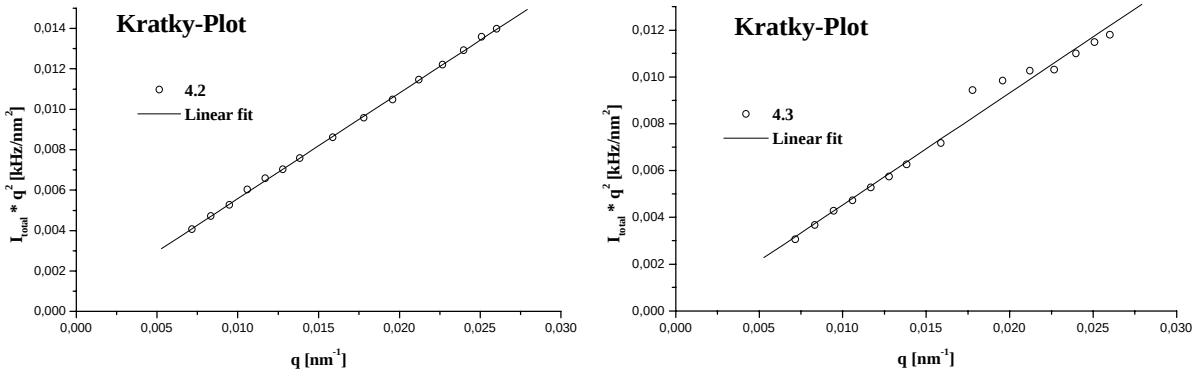

Figure 4.16 Krakty plots of the slow modes analyzed together in 4.2 and 4.3.

This corresponds to a persistent length of at least 140 nm, higher than the value for DNA (about 100 nm). The total scattering intensity versus q, has a smooth behavior that fits well with a form factor of a rod having a length of around 500-700 nm (Figure 4.17).

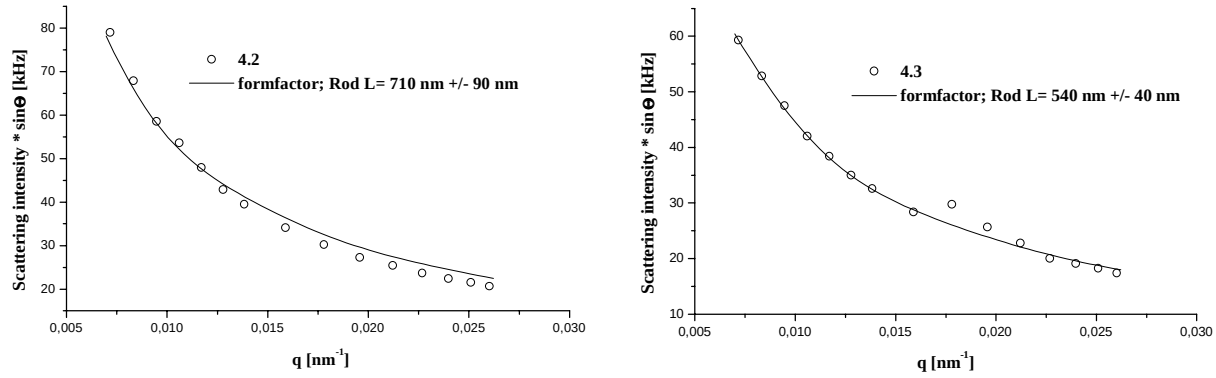

Figure 4.17 Angle dependent intensity of the slow modes in 4.2 and 4.3.

The rod behavior is also confirmed from the Holtzer plot (Figure 4.18). The data tend in fact to a plateau for high q values.

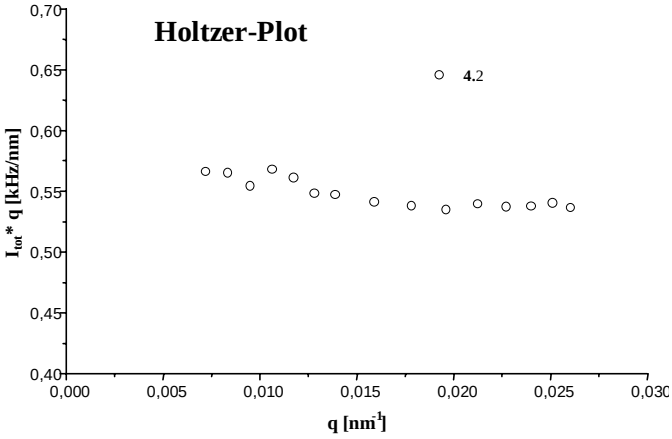

Figure 4.18 Holzer plots displaying the I·q versus q behavior of the slow mode in 4.2.

It seems reasonable that at low concentrations (samples 3) the copolymer molecules start to aggregate and form supramolecular objects that are quite stiff ("virtual persistance length" of 70 nm) but do not have the shape of monodisperse infinitive thin simple rods or spheres. At higher concentration (samples 4), the aggregates grow and seem to become even more stiff ("virtual persistent length" of at least 140 nm). Their shape can now be approximated by an infinitely small rod of around 600 nm. The calculated increase of the "virtual persistent length" may come from the fact that at high concentration, smaller aggregates with L >>*d*, do not contribute to the scattering anymore. Therefore, due to the fact that the scattering intensity is proportional to R_h^6, only the scattering of the "pure" rods can be detected.

R_h can be used to estimate the length of the aggregates[50].. For rod-like objects of the length L and diameter d exists the following relation between the hydrodynamic radius R_h and the radius of gyration R_g: $R_g/R_h = 1/\sqrt{3}\cdot(\ln(L/d)+0.38)$. In our case the diameter d (around 10 nm) is small

compared to L because of the large extension of the aggregation. If the ratio L/d is circa 60, the ratio between the hydrodynamic radius and the radius of gyration R_g/R_h is 2.58. With $R_g^2 = L^2/12$ follows $L = [12\ (2.58R_h)^2]^{1/2}$ Because the values of R_h are in the range between 40 and 200 nm, this means that the length of the rods is in the range of 350 to 1800 nm, which is in good agreement of the static analysis which give values around 700 nm.

With a high smoothing factor it is possible to find similar behavior in the CONTIN fit between the sample 3 and the sample 4.2 (at least at a similar scattering angle; 110° and 130°) (figure 4.19).

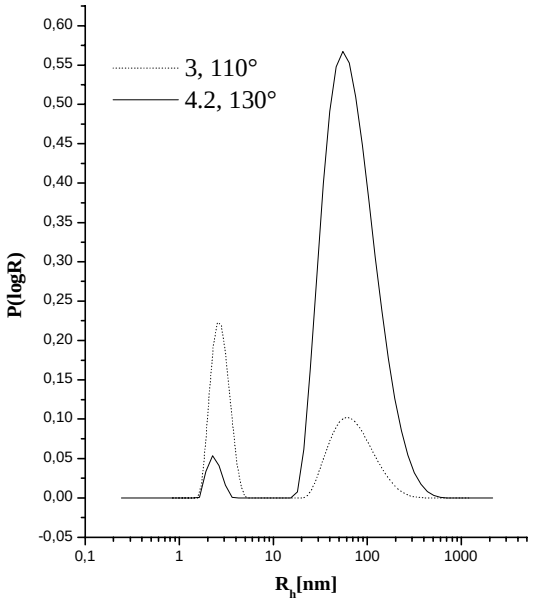

Figure 4.19 CONTIN analysis at two different concentrations.

When the concentration increases, the intensity due to the small particles decreases and the intensity due to the aggregates increases.

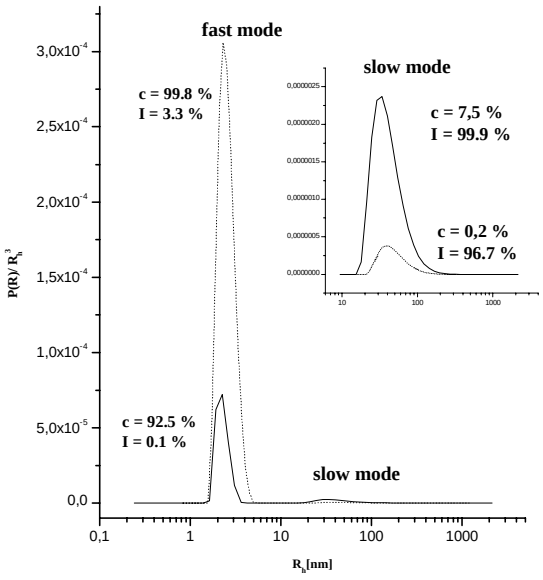

Figure 4.20 Plot of $P(logR)/R_h^3$ against R_h

If the intensity is divided by the volume (R_h^3) it is possible to get a rough estimation of the concentration of the species in solution. This can be done by plotting $P(\log R)/R_h^3$ against R_h (Figure 4.21). In the low concentrated sample (3, 0.05 wt %) 99.8 % of the block copolymers are monomeric particles (about 2.5 nm: single copolymer molecules) which contribute, however, only for 3.3 % to the total scattering intensity. There are only a few large particles (0.3 %) (about 70 nm: aggregates) which scatter much more and which are responsible for 96.7 % of the total scattering intensity. At the higher concentrations (4.2, 0.093 wt %) the amount of aggregates strongly increases, and even though the single copolymer molecules are still the majority of objects in the solution (92.5 % of the total concentration), their scattering intensity is nearly negligible.

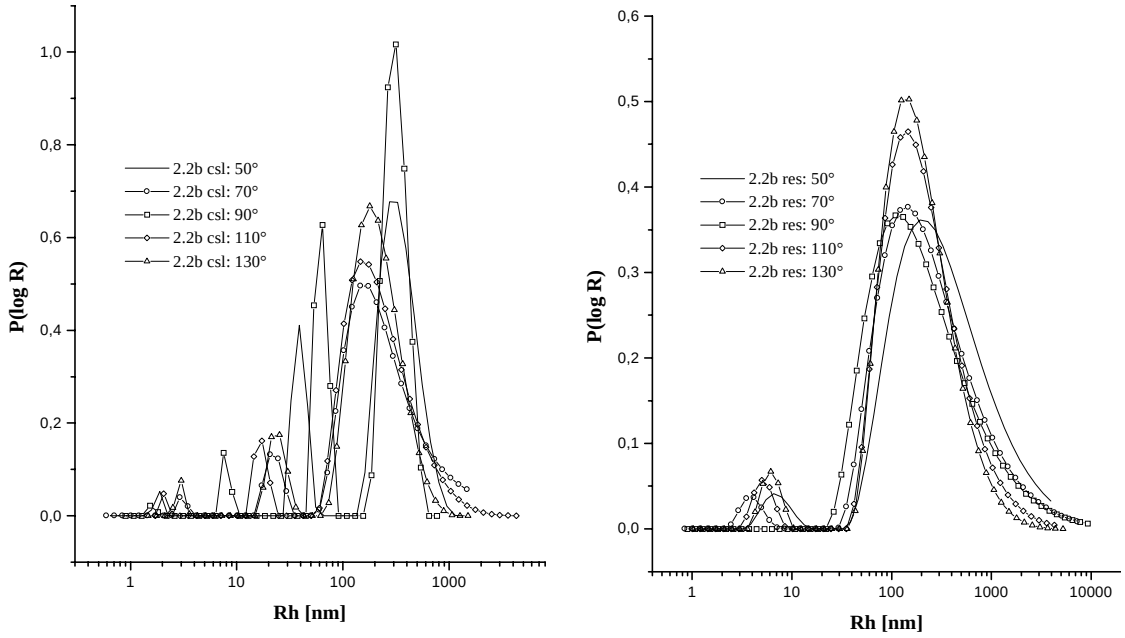

(a) **(b)**

Figure 4.21 CONTIN analysis of 2.2b with two different smoothing factors.

Analysis of the samples 2.2b (circa 0.14 wt %) and 2.a (0.15 wt %) (even higher concentrations) give similar CONTIN fit results. It was not possible to obtain reproducible peaks in the low R_h range (1-3 nm) and at the high R_h range (10-1000 nm) (Figure 4.21a). As described before, it was only possible to achieve for all scattering angles a uniform picture by increasing the smoothing factor. This leads to two process with broad distributions of the hydrodynamic radii. The R_{h1} varies between 3 nm and 11 nm, while R_{h2} ranges from 35 nm to 1300 nm (figure 4.21b).

The difficulty in the detection of only two types of processes is due to the fact that the aggregates have a very broad distribution in length and that the intensity of the small particles with increasing

concentration is becoming very small. This can be clearly detected in the field autocorrelation function curves (Figure 4.22).

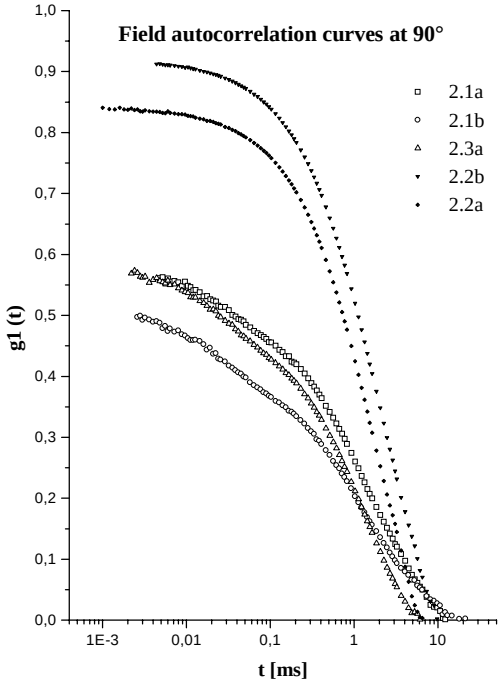

Figure 4. 22 Field autocorrelation function curves of 2.1, 2.2 and 2.3a.

For small concentrations the autocorrelation curves show clearly a double exponential decay (Figure 4.22, sample 2.1a/b and 2.3a), but at higher concentration (Figure 4.22, sample 2.2a/b), it is nearly impossible to distinguish them without the information of the scattering data at low concentrations.

4.1.2.3 Static and dynamic light scattering of copolymer 67

Cyclohexane solutions of copolymer **67** are also viscous and they show birefringence if observed under optical microscope with crossed-polarizers. However, contrary to **68**, these phenomena are not observed immediately after cooling the solution, but only after storing them at room temperature for one or more weeks (0.5 wt % solution). This slower kinetics of the aggregate formation can be used to the study of the time dependence of the aggregation.

Therefore, solutions of **67** in cyclohexane were prepared and the changes of their scattering behavior during a larger time period (about 2 months) was investigated. The changes in the concentration of the solutions by evaporation of cyclohexane from the LS cells was prevented on one hand by keeping the cuvettes in a vacuum desiccator saturated with cyclohexane vapor, and on the other hand by refilling the quantity of evaporated solvent. In order to check whether the occasional refilling up and stirring of the solution could influence the aggregate formation, samples were parallel prepared and kept in the essiccator but not refilled with solvent. In the latter case an

increase in the concentration was expected, but at maximum it was only in the order of about 6 % for the higher concentrated samples and 10 % for the lower concentrated samples. Two samples were prepared, for each concentration and procedure. (Table 4.5).

Table 4.5

Concentration	**c_1 = 0,065 wt %**	**c_2 = 0,151 wt %**
Sample	293 refill and stir	297 refill and stir
	294 refill and stir	298 refill and stir
	295	299
	296	300

The samples were measured (DLS) in each case after certain fixed times at 5 scattering angles (30°, 60°, 90°, 120°, 150°) and the data were analyzed by the CONTIN fit analysis (csl). When aggregates were detected, also static measurements were performed and the data were fitted was with form factors to investigate the shape of the aggregates. The measurements and the results are summarized in the Figure 4.23.

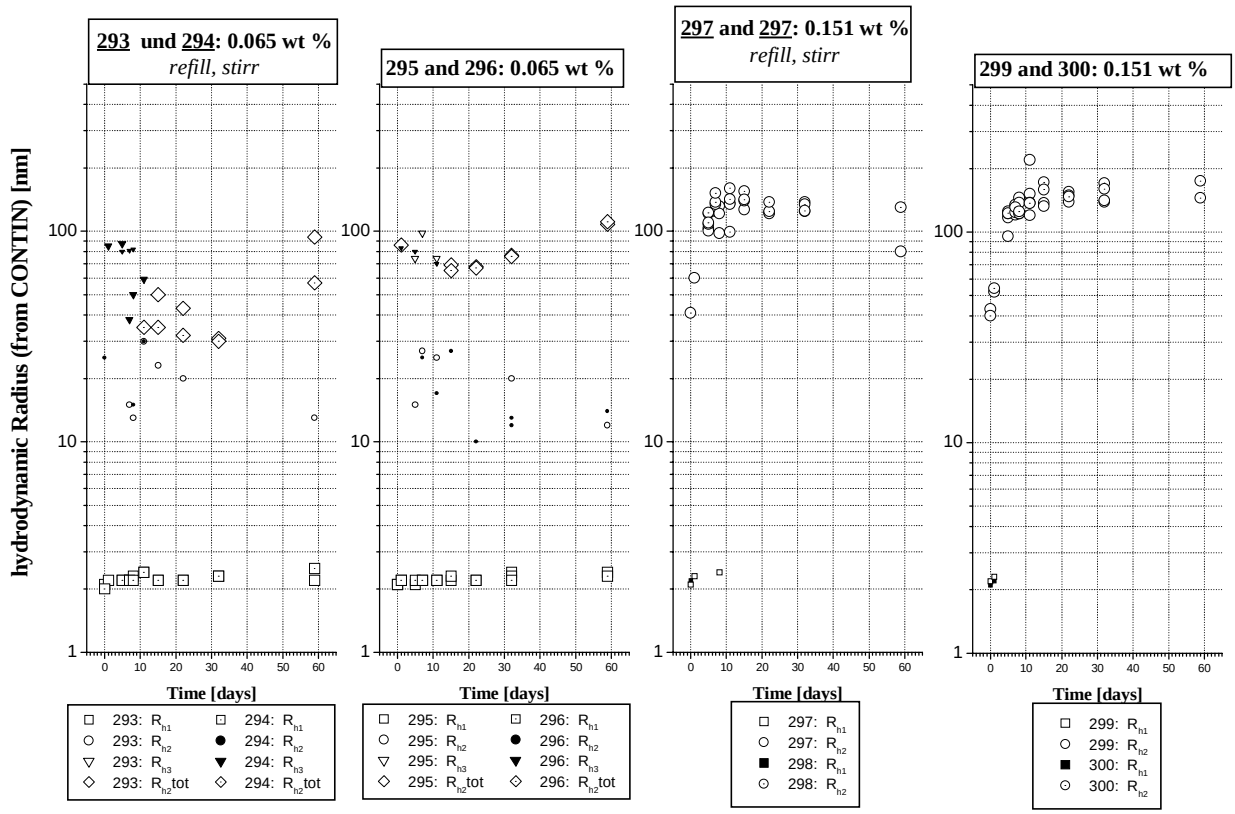

Figure 4.23 CONTIN analysis of copolymer **67**.

The hydrodynamic radius of the particles in the solution, which resulted from the CONTIN analysis in the dynamic measurements, is plotted against the time. Larger symbols mark a "CONTIN peaks" that was clearly detected and reproducible by measurements at several different angles, and smaller symbols mark "CONTIN peaks" which were not clear or not reproducible.

At smaller concentration it was in almost all measurements possible to detect the small particles with R_{h1} ~2.3 nm (□), that are the copolymer molecules. The aggregates were clearly detected in both series of samples after 15 days. The R_{h2} (◊) values are in the case of samples 295-296 around 70 nm, while in the case of sample 293-294 some what smaller, circa 30 nm. This discrepancy can be attributed to the slight increase of the concentration of the sample 295-296 that can have an influence on the size of the aggregates. Additionally, the perturbation of the equilibrium due to the refilling and the stirring of the samples as probably an affection on the aggregate size. At higher concentrations the two series of samples (refill and stir, and unmodified) give nearly the same results. The signal due to the copolymer molecules (R_{h1}) is not detectable (except rarely in the first 8 days), while the value of R_{h2}, that in the first days is around 40-50 nm, reaches in that time a constant value of circa 150 nm. This means that the aggregates grow at the beginning and then reach an equilibrium size. Of course, these aggregates are rather polydisperse and only an average over all aggregate sizes is measured. The aggregates are stable in solution and do not fall out as it was observed in copolymer **68**.

The CONTIN analysis for the sample 293 (0.065 wt %) at different times but at the same scattering angle (90°) is reported in figure 4.24.

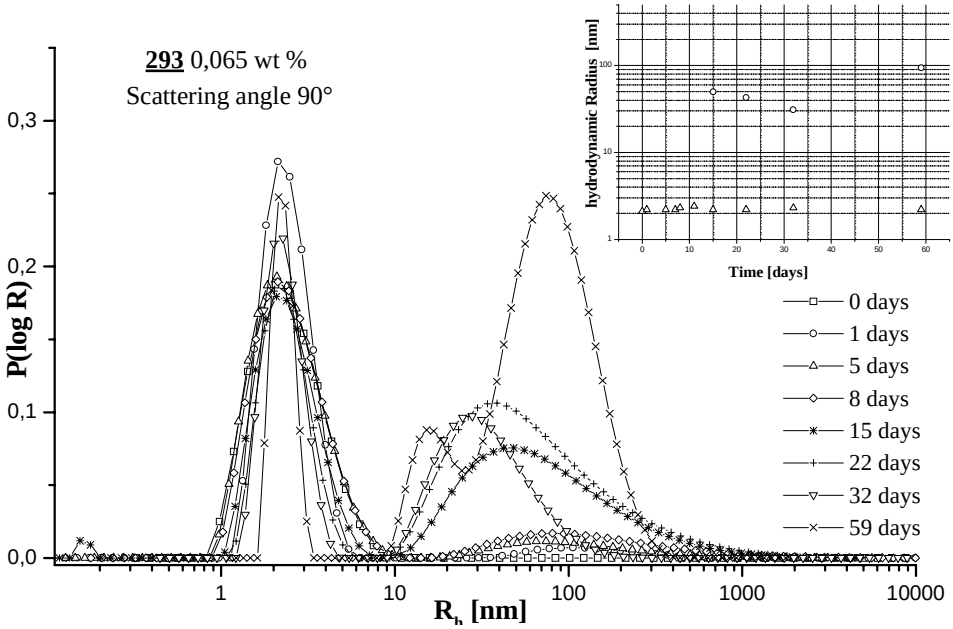

Figure 4.24 CONTIN analysis for the sample 293.

The CONTIN analysis is clear and reproducible at all different concentration, even though after longer storing times the peaks for R_{h2} get broad and split in same cases into two peaks. As in the case of **68**, the analysis of the angle dependent intensity of the scattered light for the slow mode can not be well fitted, neither with a rod nor with a sphere model.

The CONTIN analysis of the higher concentrated sample 298 (0.151 wt %) gave even more complex results (Figure 4.25).

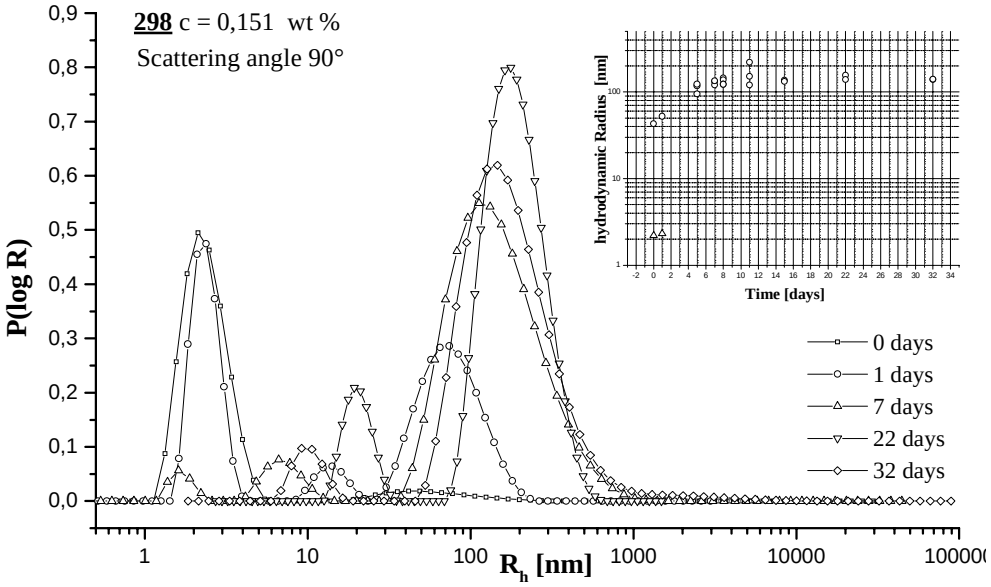

Figure 4.25 CONTIN analysis for the sample 298

In this case, as in the case of the cyclohexane solution of **68**, the CONTIN analysis devides sometimes the broad distribution of the species with the high hydrodynamic radius in two process.
In order to see if the aggregate has the same rod shape as for copolymer **68**, SLS measurement were done. As example the Kratky-Plot and the q-dependent intensity of the scattered light of the sample 297 after 32 days is reported (Figure 4.26).

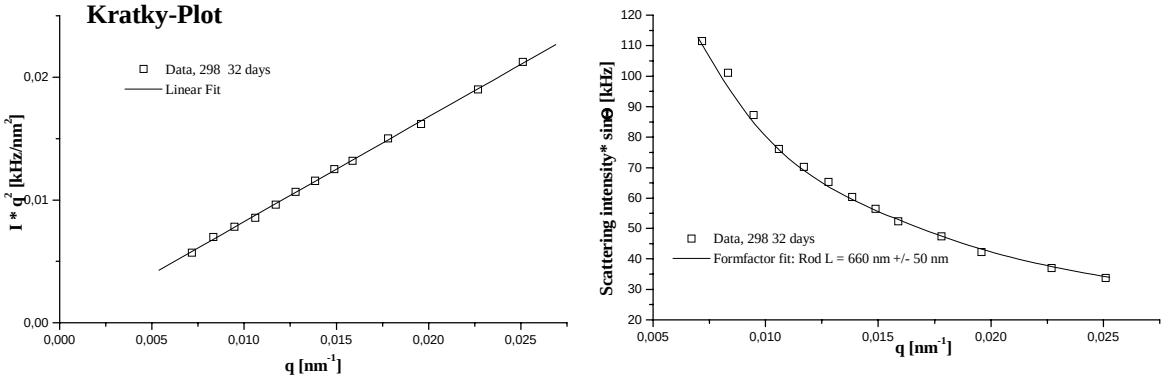

Figure 4.26 Kratky-Plot and the q-dependent intensity of the scattered light of the sample 297.

In the Kratky plot, data linearly increase at least until the last data point (q = 0.0071 nm^{-1}). That means that the aggregates have a "virtual persistent length" of at least 140 nm. The angle dependent scattering intensity fits well with the rod form factor having a length L = 660 nm ± 50 nm. The lengths obtain from the fitting of all high concentrated samples at different times are summarized in the figure 4.27.

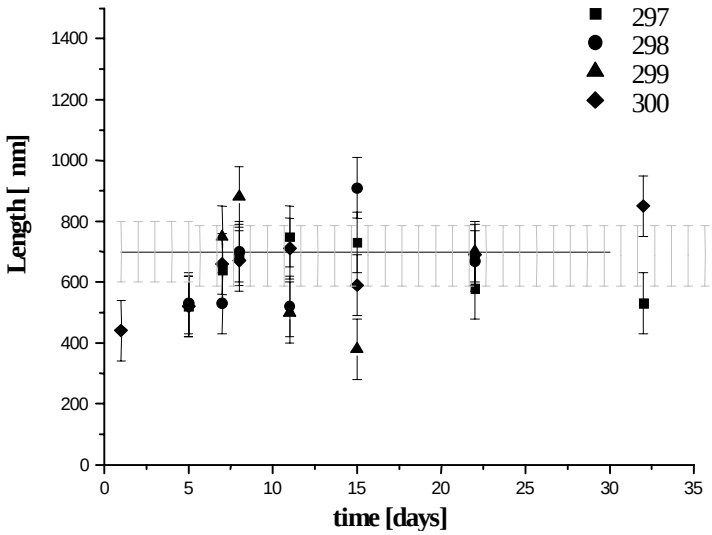

Figure 4.27 Lengths obtain from the fitting of all high concentrated samples at different times.

In all cases the length reaches a maximum of around 700 nm ± 100 nm after 7 days.

The model that can be developed from all these data is the following. In the presence of a good solvent (like toluene), the copolymer molecules are well solubilized and do not aggregate. In cyclohexane the copolymer molecules aggregate to rod-shape units. The unsubstituted macrocycle is not soluble in cyclohexane and wants to avoid the contact with the solvent. As result, the rings aggregate and the polystyrene acts as a coat around the stacks of rings. The resulting structure can be described as supramolecular cylindrical brush with high rigidity (and polydispersity) (figure 4.28).

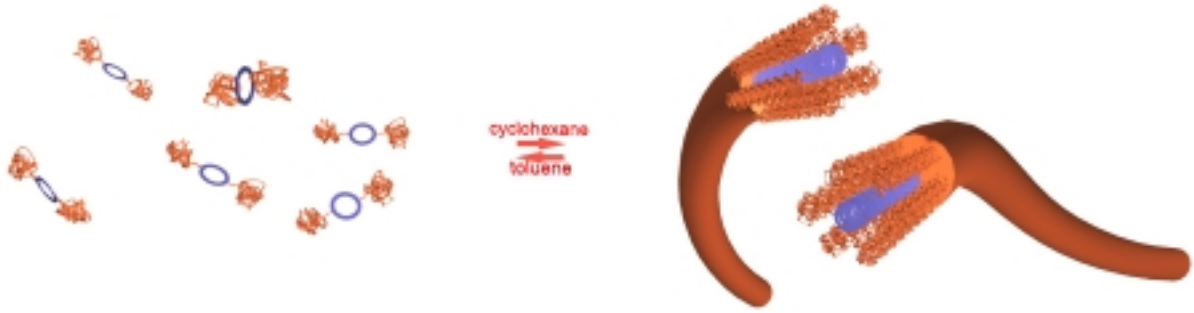

Figure 4.28 Schematization of the aggregation phenomena.

4.1.3 Ultra small and small angle x-ray scattering

4.1.3.1 General consideration

When X-rays interact with matter, coherent scattering can occur. That is, the photons are deviated from their course without any energy loss. As it is shown in the figure 4.29, the waves are scattered in phase and constructive interference occurs only when the path difference (AB + BC) is λ (or an integer multiple of λ). This results in the well known Bragg law.

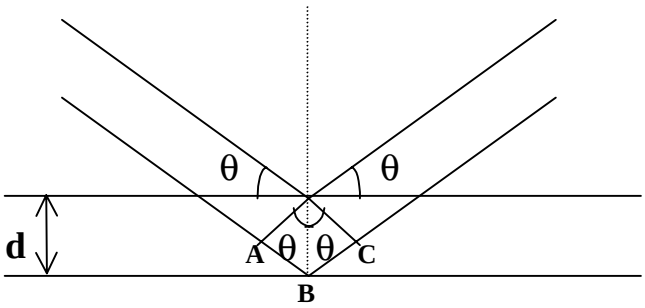

$$AB + BC = 2d \sin\theta = n\lambda$$

Figure 4.29 Geometry in the x-ray scattering.

Depending on the scattering angle that can be detected, different distances d can be calculated. In particular, using Ultra Small and Small X-ray Scattering (USAXS and SAXS) the measured angle range of is from 0.1°-1° (USAXS) and 0.7°-5° (SAXS) respectively, that means distances from 40 to 1 nm for CuK_α radiation. This methods give the possibility to observe distances within the range of a few nanometer, which is in the size of the macrocycle. By this methods information about the diameter and the inside of the brushes could be obtained.

4.1.3.2 USAX and SAXS of copolymer 68 in cyclohexane

At 2 wt % solution of **68** in cyclohexane (that it is strongly birefringent) was filled in a glass capillary of 0.7 mm diameter and then the capillary was sealed in order to prevent evaporation of the solvent. The same capillary was used for USAXS and SAXS measurements. The theoretical description of the measured data was not possible by using a simple massive cylinder model (showing an abrupt radial electron density change) of any length or thickness. In that case the scattering curve should show pronounced oscillations. Therefore, a model was used that describes the electron density profile at the outside of the cylinder more accurately (Figure 4.30).

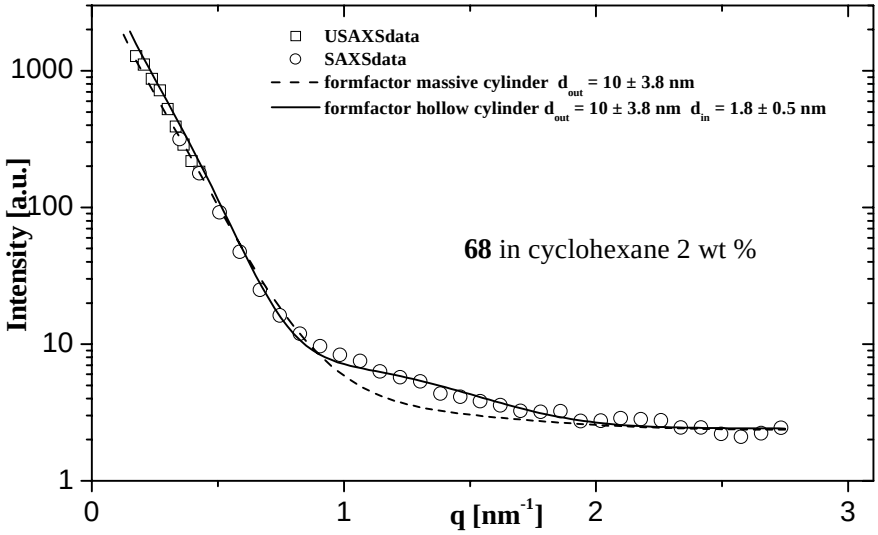

Figure 4.29 USAXS and SAXS data.

The different length of the oligomeric polystyrene chains and the radial decrease of the cylinder density was taken into account by giving the cylinder a polydispersity in the diameter. The calculated form factor of a massive cylinder 10 nm in diameter having a polydispersity at the outside (d_{out} = 10 nm, polydispersity: 3.8 nm, half width half maximum of a Gaussian distribution) agrees with the observed data at low q-values (see Appendix B). However, the observed scattering intensity is remarkably higher than the theoretical prediction in the q- range between 1 nm^{-1} and 2 nm^{-1}. Only the use of a radial density profile with a reduced electron density inside the cylinder resolved this discrepancy. The calculated form factor of a cylinder with the same electron density profile at the outside as described before and with an additional reduced electron density at the inside (hollow size d_{in} = 1.8 nm, polydispersity: 0.5 nm, half width half maximum of a Gaussian distribution) fits with the observed data over the whole q-range. The scattering data undoubtedly show that the coil-ring-coil block copolymers **68** aggregate in solution into hollow cylinder-shaped objects with a diameter of circa 10-15 nm.

4.1.4 Imaging methods: transmission electon microscopy (TEM) and atomic force microscopy (AFM)

4.1.4.1 General consideration

The transmission electron microscopy (TEM) is a well-known technique and often used in the investigation of polymeric materials, while the atomic force microscopy (AFM) is was invented in 1981 by Gerd Binnig and Heinrich Rohrer at IBM Zürich. The atomic force microscope probes the surface of a sample with a sharp tip, a couple of microns long and often less than 100 Å in diameter. The tip is located at the free end of a cantilever that is 100 to 200 μm long. Forces between the tip

and the sample surface cause the cantilever to bend, or deflect. A detector measures the cantilever deflection as the tip is scanned over the sample, or the sample is scanned under the tip. The measured cantilever deflections allows the generation of a map of the surface topography.

Tapping mode is a key advance in AFM. This potent technique allows high resolution topographic imaging of sample surfaces that are easily damaged, loosely hold to their substrate, or difficult to image by other AFM techniques. Tapping mode imaging is performed in air by oscillating the cantilever at or near the cantilever's resonant frequency using a piezoelectric crystal. The piezo motion causes the cantilever to oscillate with a high amplitude (typically greater than 20 nm) when the tip is not in contact with the surface. The oscillating tip is then moved toward the surface until it begins lightly to touch, or tap the surface. During the scanning process, the vertically oscillating tip alternately contacts the surface and lifts off, generally at a frequency of 50,000 to 500,000 Hertz. As the oscillating cantilever begins to intermittently contact the surface, the cantilever oscillation is necessarily reduced due to energy loss caused by the tip contacting the surface. The reduction in oscillation amplitude is used to identify and measure surface features. Tapping mode overcomes problems associated with friction, adhesion, electrostatic forces, and other difficulties that may take place by using conventional AFM scanning methods. It places alternately the tip in contact with the surface to provide high resolution, and then lifts the tip off the surface to avoid dragging the tip across the surface. Since the contact with the sample is intermittent, the probe exerts negligible frictional forces on the sample resulting in a high resolution image.

Both methods were used here and give further evidence for the existence of the supramolecular cylinders.

4.1.4.2 Experiments on cyclohexane solution of copolymer 68

A 0.15 wt % cyclohexane solution of **68** (15 mg of **68** in 10 ml of cyclohexane) was stored for one day and then two different types of experiments were performed.

5 ml of the solution was frozen in at liquid nitrogen temperature and then freeze-dried to form a fine white powder. The powder was shed on a glass slide and then the slide was shacked in order to eliminate the excess of material that did not stick on it. By vacuum deposition of carbon and successive platinum shadowing an uniform coating over the sample surface was performed. The thin supporting film (replica) was floated off in water with hydrofluoric acid and placed on a copper gride. The transmission electron micrograph (TEM) of the material is shown in figure 4.31.

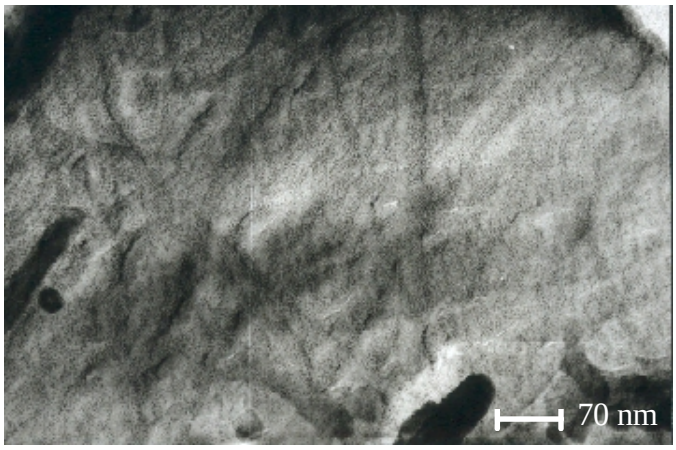

Figure 4.31 TEM picture; C/Pt shadowed replica of the sample surface obtained by freeze drying a 0.15 wt % cyclohexane solution of **68**

It is possible to see clearly several ribbons of different width at the sample surface. In particular, the narrowest are in the range of approximately 15 nm. The idea behind freeze-drying the sample was to investigate which type of objects are really present in cyclohexane solution. In other words, the solid material was obtained under non equilibrium condition, and this should let to a solid state structure that is similar to the solution structure.

Following the same idea, a piece of mica was dipped into the 0.15 wt % solution of **68** for a few seconds and the dried surface scanned with the AFM. The tapping mode and the amplitude mode pictures are shown in figure 4.32.

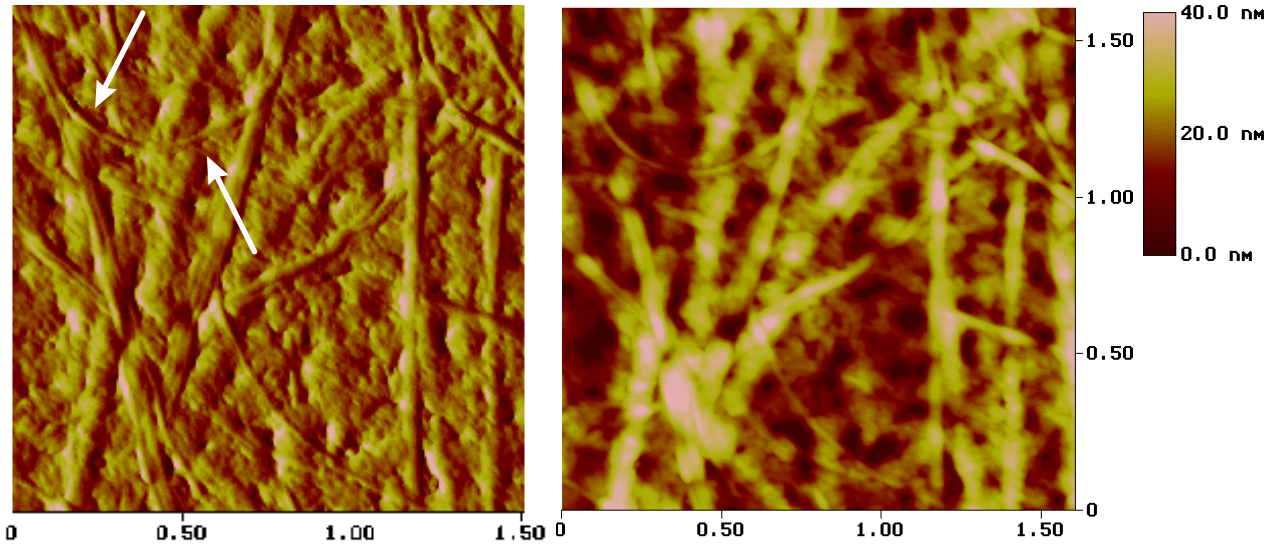

Figure 4.32 AFM image, amplitude picture (left) and tapping mode picture (right).

The images show a thick copolymer film on the mica surface, on which long bundles of two or three cylindrical aggregates, as well as individual aggregates are deposited. Surveying the most curved

cylindrical object found in the AFM images (Figure 4.31, indicated by white arrows) and treating it as worm-like chain gives a persistent length of approximately 350 nm for the cylindrical aggregate.
In order to obtain the dimensions of those cylindrical aggregates, the measured widths needed to be corrected for a broadening effect, which is related to the radius of the tip apex. By using a simple model based on a spherical tip apex with a radius R and a rectangular cross-section of the ribbon of height *h*, the broadening D is given by $2[h(2R-h)]^{1/2}$. Assuming a tip radius of 10 nm (data gives by the tip supplier) and a measure width of the aggregates of 19 nm gives an actual diameter of the cylinder of 13 nm (Figure 4.33).

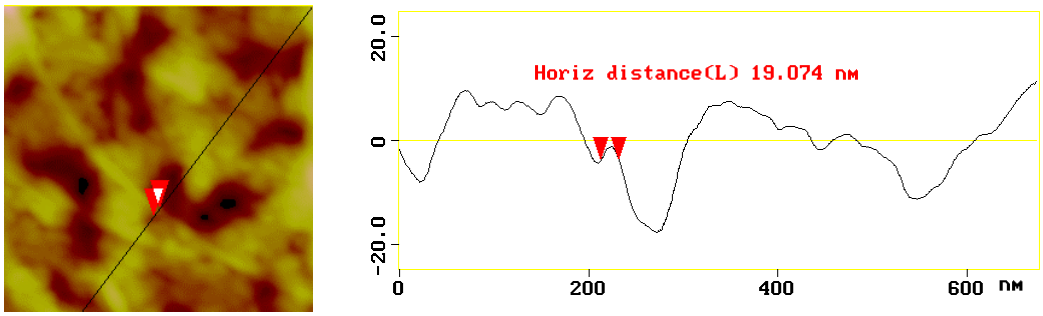

Figure 4.33 Section analysis of the AFM image in Figure 4.32.

The dimensions obtained by TEM and AFM correspond well with the molecular dimensions obtained by the scattering methods and are in accordance with the molecular dimensions of the molecular building blocks[51]. The correspondence of our structures with covalently linked polymer brushes[52] suggests to describe them as hollow supramolecular cylindrical brushes.
In order to see isolated aggregates, the same type of experiment was performed using a less concentrated solution (0.05 wt % in cyclohexane).

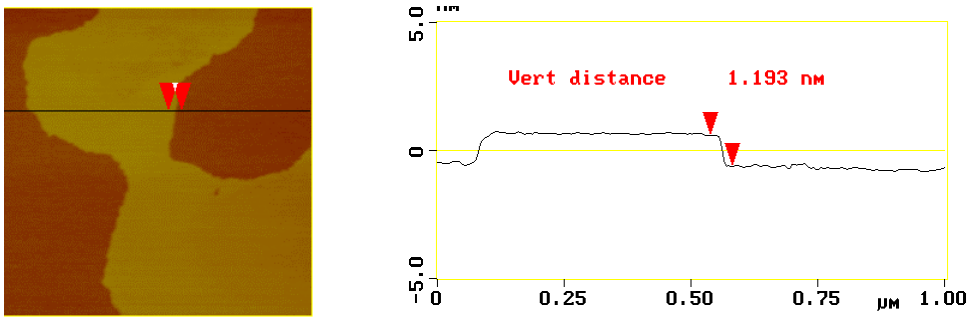

Figure 4.34 Section analysis of an AFM image of a 0.05 wt % cyclohexane solution of **68**.

Again a piece of mica was dipped for a few seconds into the polymer solution. Surprisingly, instead of individual aggregates, it was only possible to observed the formation of a very smooth film with a high of about 1.2 nm (Figure 4.34).

Because it was not possible to see the macrocycles structure, it seemed reasonable that the ring sticks on the mica surface and the polystyrene chains cover them completely. If this is true, increasing the molecular weight of the polystyrene of the block copolymer, should increase the height of the film. In order to prove that, a piece of mica was dipped into a 0.05 wt % solution of copolymer **65** in cyclohexane, the copolymer with polystyrene substituents of M_w = 5000. Again in this case a smooth film was detected with a height of around 3 nm, however not as smooth as in the case of **68** (Figure 4.35).

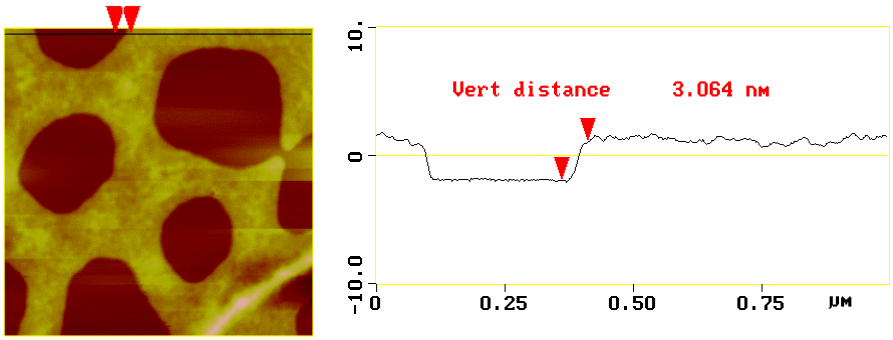

Figure 4.35 Section analysis of an AFM image of a 0.05 wt % cyclohexane solution of **65**.

To prove that the formation of the monolayer it is a peculiarity of the copolymer in cyclohexane, mica was dipped in a 0.05 wt % solution of n-propyl polystyrene carboxylate of M_w = 2500 in cyclohexane and in this case a film of about 10 nm height was formed (Figure 4.36). The polymer did under this conditions not form a monolayer.

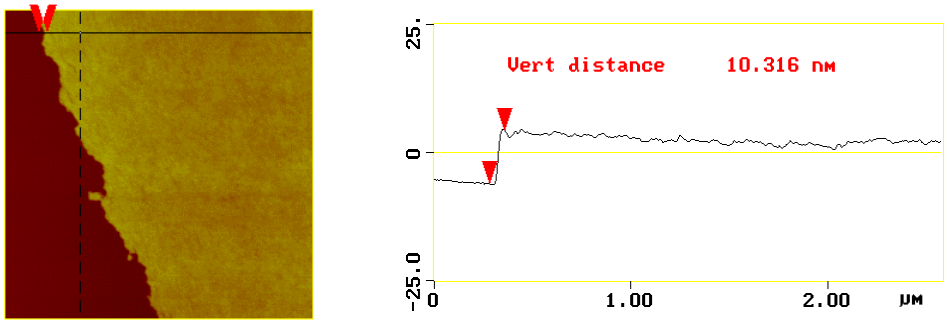

Figure 4.36 Section analysis of an AFM image of a 0.05 wt % cyclohexane solution of n-propyl polystyrene carboxylate of M_w = 2500.

It is also interesting that no aggregates were detected by dipping mica into a 0.2 % solution of **68** in methylene chloride (Figure 4.37).

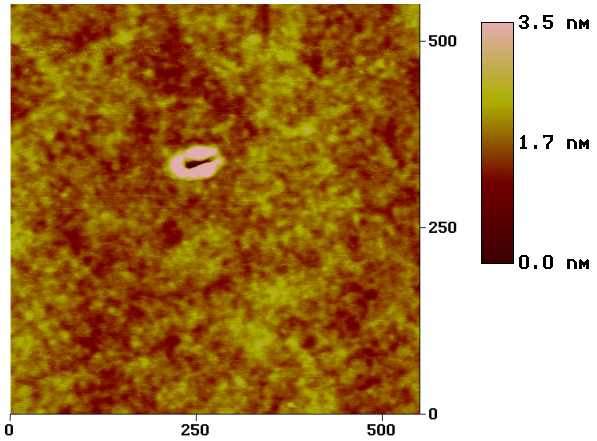

Figure 4.37 Section analysis of an AFM image of a 0.05 wt % methylene chloride solution of **68**.

4.1.5 Langmuir-Blodgett technique (LB)

4.1.5.1 General consideration

1917 demonstrated Langmuir that by applying pressure, monolayers of fatty acids can be ordered on the water surface. They undergo phase changes from a disperse state in which the available area is larger than the molecules areas to a "solid" state where the molecules form a rigid film. Langmuir and Blodgett realized the transfer of such monolayers from the water surface to a solid substrate by slowly passing an appropriately treated substrate through the air/water interface. Films may be picked up on passing from air into water and vice versa. In practice, molecules are spread on an ultra clean water subphase in a Teflon trough in a clean room. The trough has a moveable Teflon barrier straddling the air water interface. This is controlled mechanically and allows to compress the film under servo-control. As the surface area of the film is thus reduced the surface pressure of the film increases. The pressure-area isotherm is monitored continuously and as the area/molecule decreases, suddenly the pressure will rapidly increase as the solid phase is reached (while the area per molecule remains approximately constant). If the pressure increases further, the film will collapse. At some predetermined pressure in the solid phase, the film pressure is held constant and a substrate can be passed through the air/water interface. Monolayers are transferred to the substrate and the film area is reduced. The pressure is held constant by a feedback from the pressure monitor and the reduction of area is monitored to determine the transfer ratio (area of slide covered/loss of area from film on trough).

In order to see if it is possible to organize the copolymer molecules on the air/water interface, the following experiments were performed.

4.1.5.2 Experiments on cyclohexane solution of copolymer 68

A 0.05 wt % solution of copolymer **68** in chloroform (good solvent for macrocycle and polystyrene) and a 0.05 wt % solution of **68** in cyclohexane were stored for one day and then spread on the water bath of the LB apparatus. The pressure-area isotherms are shown in figure 4.38.

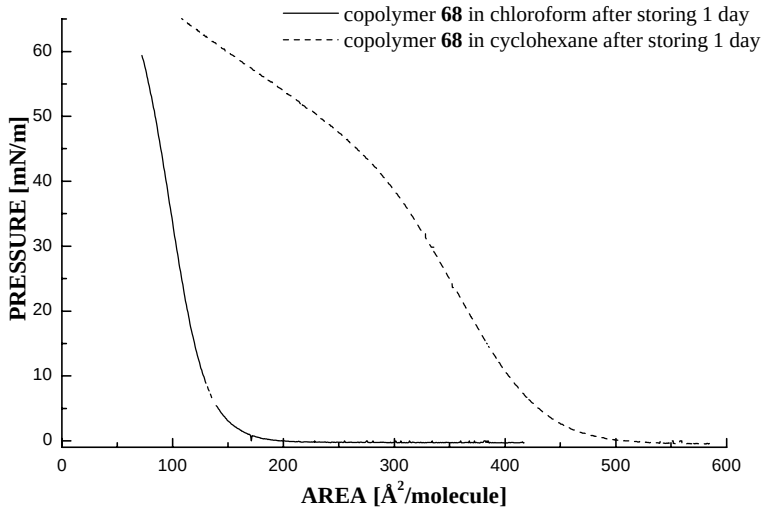

Figure 4.38 Pressure-area isotherms of **68** in chloroform and cyclohexane.

In the case of the chloroform solution in it appears that the copolymer molecules are compressed at constant pressure until around 200 Å^2, then the pressure rapidly increases. The molecules form a so call "solid film"[53] of a low compressibility nearly equal to that for bulk material. From these, the extrapolated area at zero pressure can be calculated as 135 Å^2. Although pure speculation, this can be associated with an arrangement in which the macrocycles lay perpendicular to the water surface with the polymer chains stretched in the air and the water. Such an arrangement of low molecular weight phenylacetylene macrocycle has been proposed by others[54]. However, so far it is unclear what the actual organization of our copolymers at the air/water interface really is.

In the case of the cyclohexane solution, the shape of the isotherm differs completely. Such a shape of the isotherm is described for "liquid expanded films" that have a rather high compressibility, meaning that on average the intermolecular distance is much larger than for bulk liquids and in which usually a single phase is present. At around 250 Å^2 a change to a film of much higher compressibility is visible. The area extrapolated at zero pressure is around 435 Å^2. This can be associated with an arrangement of the copolymer molecules in such a way that the rigid cyclic part of the copolymer lays perpendicular to the water surface and the polymer chains are also deposited on the air/water interphase.

Cyclohexane is a non solvent for the macrocycle and a theta solvent for the polystyrene. In cyclohexane the copolymer **68** shows a lyotropic liquid crystalline phase, that means that the

macrocyclic part tends to aggregate in order to minimize the contact with the solvent. In this sense it seems reasonable that the copolymer molecules show on the water surface a similar organization behavior. The model that can describe this behavior is a series of domains in which the macrocycle are packet as in a lamella fashion with the ring perpendicular to the surface and the polymer chains at the side (Figure 4.39).

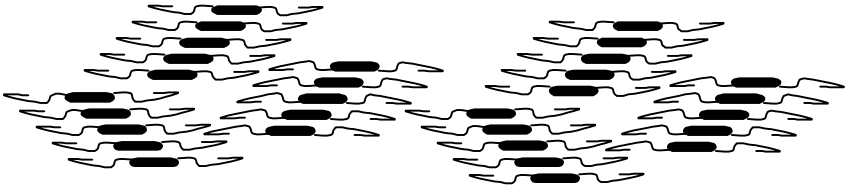

Figure 4.39 Top view of the arrangement in the air / water interface from cyclohexane.

If the measurement is performed at low temperature (6 °C), the area extrapolated at zero pressure is increased from 435 to 475 Å^2 but the shape of the isotherm remains the same (Figure 4.40).

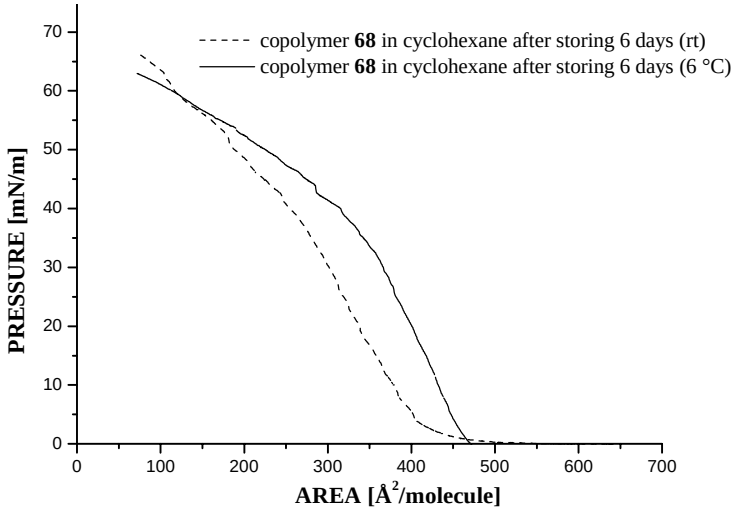

Figure 4.40 Pressure-area isotherms of **68** in and cyclohexane after 6 days at different temperatures.

If the measurement is repeated after storing the solution 6 days, the area extrapolated at zero pressure is decreasing from 435 to 410 Å^2 that is in agreement with the fact, that aggregation process increases with the time. In other words, if the film is more ordered, the area for molecule decreases (Figure 4.41).

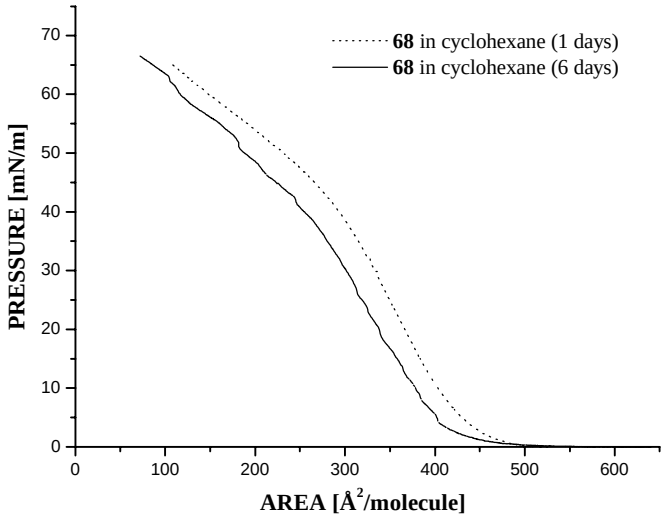

Figure 4.41 Pressure-area isotherms of **68** in cyclohexane after 1 and 6 days.

4.2 Investigation in the solid state

As already mentioned, once that lyotropic solutions of the copolymers in cyclohexane are dried, they remain birefringent and this means that the solid state has an ordered structure. Because of the fact that the copolymer **68** has shown the most interesting solution properties, it was also investigated in detail in the solid state.

4.2.1 Light microscopy, transmission electron microscopy (TEM) and scanning electron miscoscopy (SEM)

When cyclohexane solutions of **68** were dried very slowly in equilibrium with an excess of solvent, it is possible to detect in the solid film fiber-like bundles, that in same cases can be also very well oriented.

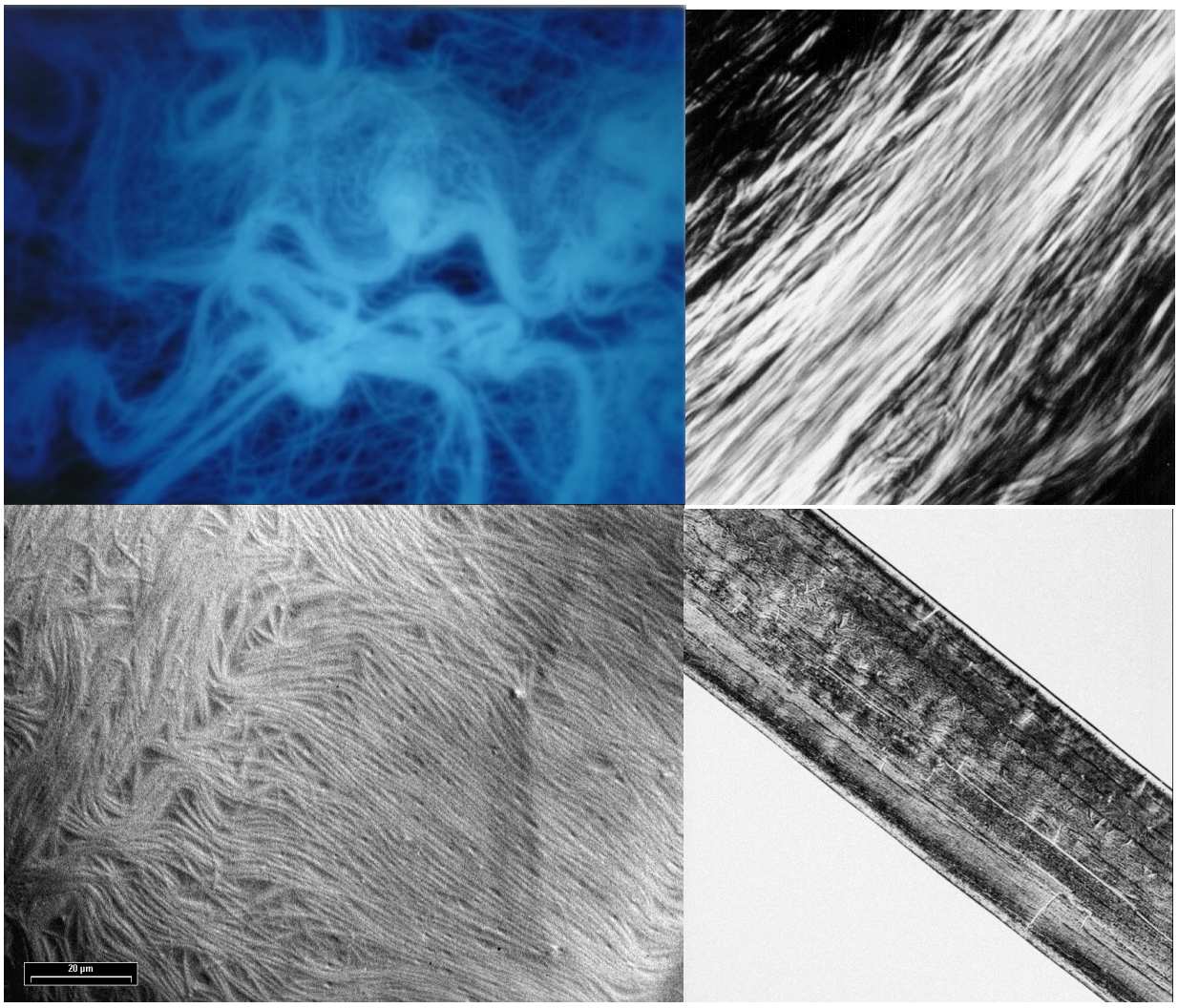

Figure 4.42: Films of copolymer **68** with fluorescence (top-left), crossed-polarized (top-right) and DIC reflection (bottom) light microscope.

These bundles can be observed with the light microscope using different techniques like crossed-polarized microscopy, fluorescence microscopy or differential interference contrast (DIC) reflection microscopy (Figure 4.42). In all cases it appears clear that these bundles are formed by aggregation of smaller bundles like in a rope.

In order to understand which type of inner structure those bundels have, electron microscopic investigations were performed, but surprisely no change in the type of structure can be observed. In other words, by increasing the magnification, it can be seen that the bundles are made of bundle-like subunits (Figure 4.43, left).

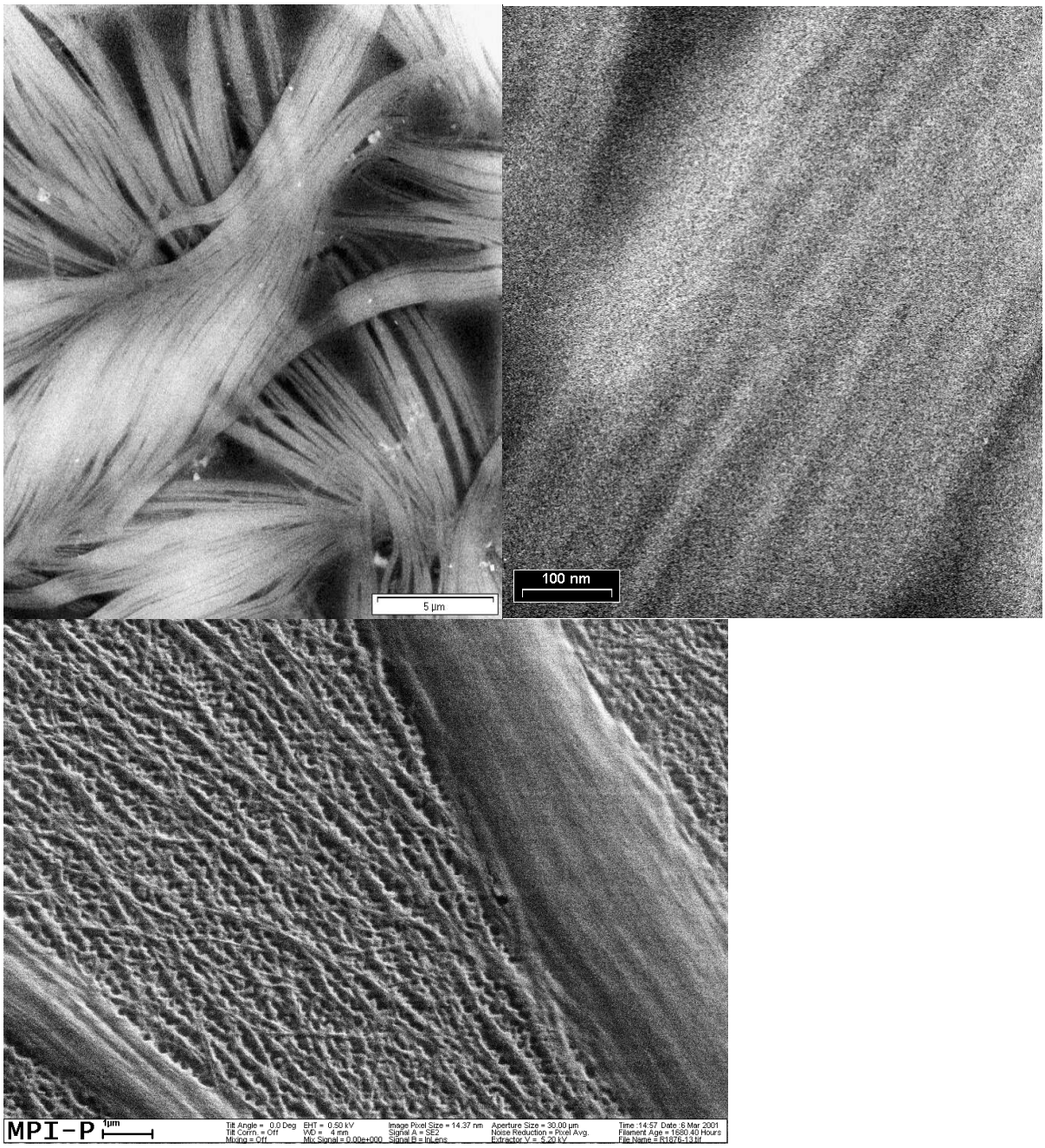

Figure 4.43: TEM (top) (left, inelastic image), and SEM (bottom) pictures.

If the magnification is increased even more, rows of bright and dark regions alternate, having an medium distance of about 70 nm (Figure 4.43, top right). In the SEM picture (Figure 4.43, bottom) it appears clearly how small fiber-like bundles enter and depart from the bigger bundles.

4.2.2 Electron diffraction and wide angle x-ray scattering (WAXS)

4.2.2.1 General consideration

The principles of electron diffraction technique are essentially the same as for the x-ray scattering technique that have been already discussed previously. The strong interaction of electrons with matter results in a low penetration depth, and electron diffraction is done in a reflection geometry to study surfaces or thin films or in a transmission mode, like in our experiments, for films or particles that are sufficiently thin. With electron beams is possible to investigate small sample, which is a major advantage compared to X-ray diffraction.

Electrons scatter from gases and electron diffraction must be performed under vacuum, usually in an electron microscope. For sufficiently thin samples, electron diffraction is performed in a transmission electron microscope (TEM) and the diffraction pattern can be viewed on a phosphor screen or recorded on film.

4.2.2.2 Solid state structure of copolymer 68

A number of electron diffraction patterns of samples cast from cyclohexane could be obtained. As a common feature they exhibit orientation, i.e. they resemble fibre diagrams. The orientation in the diffraction patterns could in all cases be attributed to oriented strands of material as morphological features seen in the corresponding electron micrographs. In general, the electron diffraction patterns consist of an equator and a first layer line. In some cases a reflection on the meridian of the second layer is also observed.

The proper preparation of the samples used for electron diffraction turned out to be an essential task. Reproducible results were obtained only when the samples which had been directly cast on carbon films were put into the high vacuum of the electron microscope at temperatures below 0 °C. The electron microscopic investigation was then carried out at temperatures below -50 °C.

Two typical electron diffraction patterns are shown in Figure 4.44.

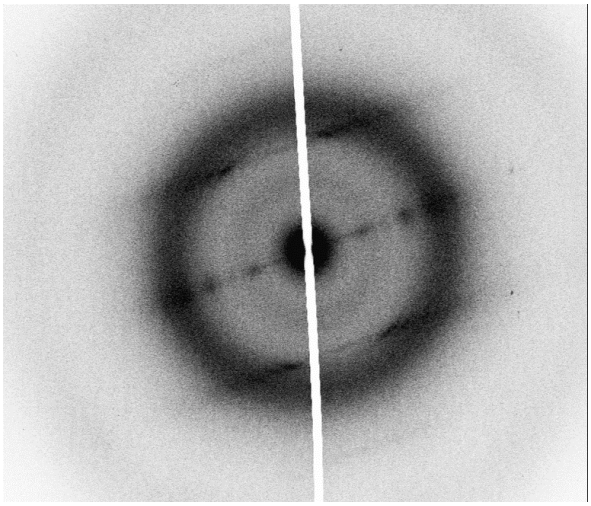

Figure 4.44 Electron diffraction patterns of copolymer **68** (dry sample cast from of a cyclohexane solution).

They can be interpreted as the superposition of a diffuse, isotropic halo which is attributed to the scattering of the polystyrene and the oriented diffraction which has been described above. Complimentary to the electron diffraction X-ray scattering experiments were carried out with samples which were prepared in a similar fashion but which were much thicker than those used for the electron microscopic investigation. A diffractogram is shown in Figure 4.45.

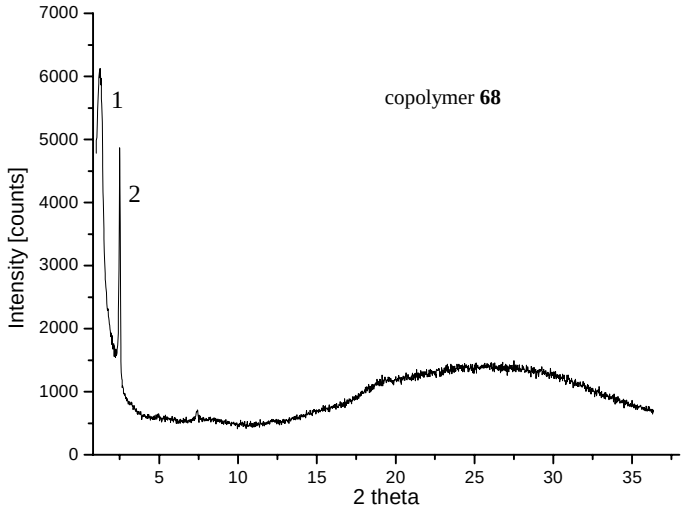

Figure 4.45 WAXS data copolymer **68** (dry sample cast from of a cyclohexane solution).

Here in addition to the amorphous halo three sharp reflections are visible with d spacings which have the ratio 1 : 2 and even higher reflections. This is an indication that we deal here with a lamellar structure with a spacing for the first order of 71 Å. The results from X-ray scattering and electron diffraction are complimentary since the orientation of the primary beam is nearly parallel to the

sample in the case of X-ray scattering and perpendicular in the electron microscopic investigation. The combination of both techniques offers the possibility to obtain a three dimensional model for the crystalline order in the samples. The complete set of data are reported in Appendix C. The electron diffraction pattern will be indexed so that the reciprocal lattice vector a* is oriented along the equator and c* (equivalent to the repeat along the oriented strands) along the meridian. The predominant electron diffraction pattern therefore contains the h0l reflections. Owing to small fills of the strands with respect to the substrate, additional reflections are observed in various diffraction pattern with index k≠0. The three reflections in the X-ray diffraction can thus be indexed as 010, 020 and 030. Close inspection of the electron diffraction patterns shows that both on the equator and the first layer a number of reflections can be identified. The periodicity suggests that the a parameter is in the range of 40 Å .On the equator the reflections are often smeared out to a certain degree so that it is not easy to determine exact d-spacings. However, some of the reflections on the first layer lines are well resolved and could be used in the determination of the cell parameters. It is assumed that the smearing of the reflections on the equator comes from the fact that owing to the very short distance in reciprocal space reflections in the neighbouring reciprocal plane, i.e the h10 and h20 reflections line are also nearly in reflecting position so that the recorded intensity maxima are in reality the superposition of several reflections.

The position of the first layer line is also somewhat sample dependent and varied between 5.9 and 6.2 Å . The d-spacings from the X-ray diffractogram and from the reflections on the first layer in electron diffraction patterns were used in a least-squares analysis to refine the lattice parameters of an orthorhombic cell. The values obtained from the data were:

a = 46.2 Å, b = 71.6 Å, c = 6.19 Å, V = 20490 $Å^3$.

Under the assumption that the molecule has a molecular weight of 13500 Dalton and that 6 molecules cyclohexane are included in the structure a density of 1.09 g/cm^3 can be calculated if two molecules are present in the unit cell.

In all electron diffraction patterns high intensity is observed near reflections 3k1, 4k1 and 5k1. This intensity pattern suggests that we deal here with a herringbone-like packing of the macrocycles. A model for the state of order in the investigated samples is shown in Figure 4.46. The macrocycles are arranged in a layer in columns with an intercolumnar spacing of 6.2 Å. Neighboring stacks are tilted with respect to each other so that a herringbone packing results. These crystalline layers are separated by amorphous layers which contain the polystyrene substituents. The thickness of one double layer consisting of one crystalline layer and one amorphous layer is 71 Å.

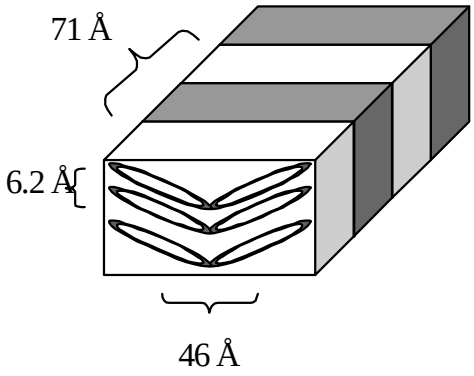

Figure 4.46 Proposed solid state model for copolymer **68**.

The observation that upon evaporation of the cyclohexane the periodicity of the columnar stacking is lost points to the assumption that the included cyclohexane molecules are located in the crystalline layers. This is in close analogy to the crystal structures of various alkyl-substituted rings which also crystallize as solvates in which the solvent molecules are built into the array of stacked rings.
Independently the presence of cyclohexane in the dried film was determined by 1H NMR spectroscopy.

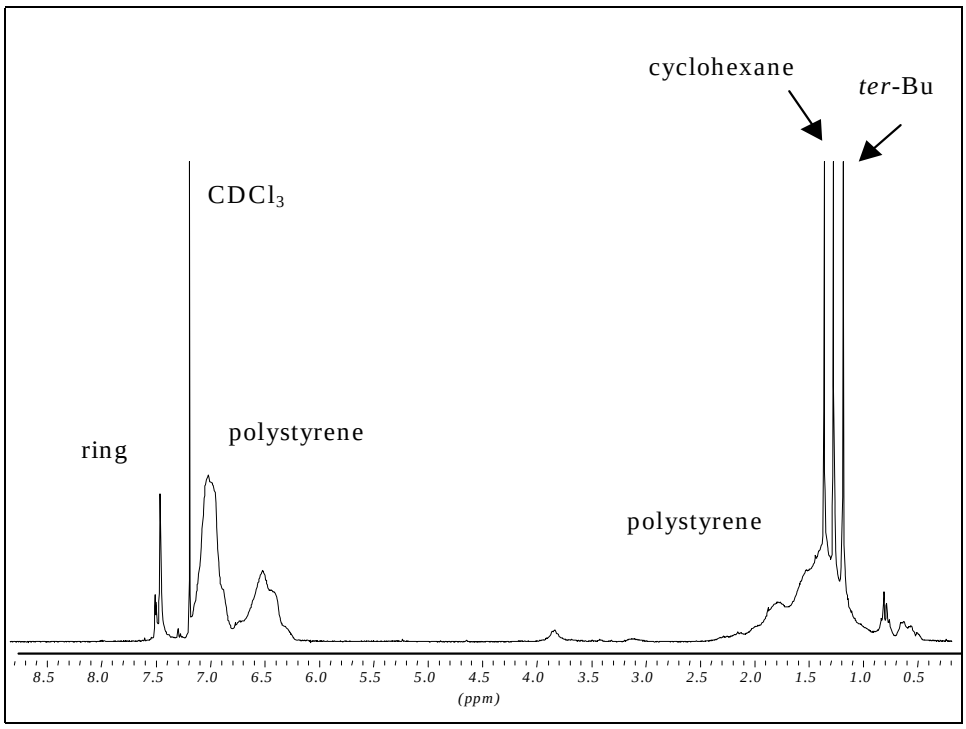

Figure 4.47: ^{1}H NMR of a dried film after 1 week.

5 Properties of polydimethylsiloxane-ring-polydimethylsiloxane block copolymers

5.1. Investigation in the solid state

Polydimethylsiloxane is a viscous liquid at room temperature (T_g < -120 °C) and therefore the ring-coil block copolymers were also expected to be more or less fluid at room temperature. Indeed, all polydimethylsiloxane-ring-polydimethylsiloxane block copolymers (**71**, **72**, **73**) have a waxy consistence. They are all birefringent at room temperature what can be easily seen under the cross-polarized microscope (figure 5.1).

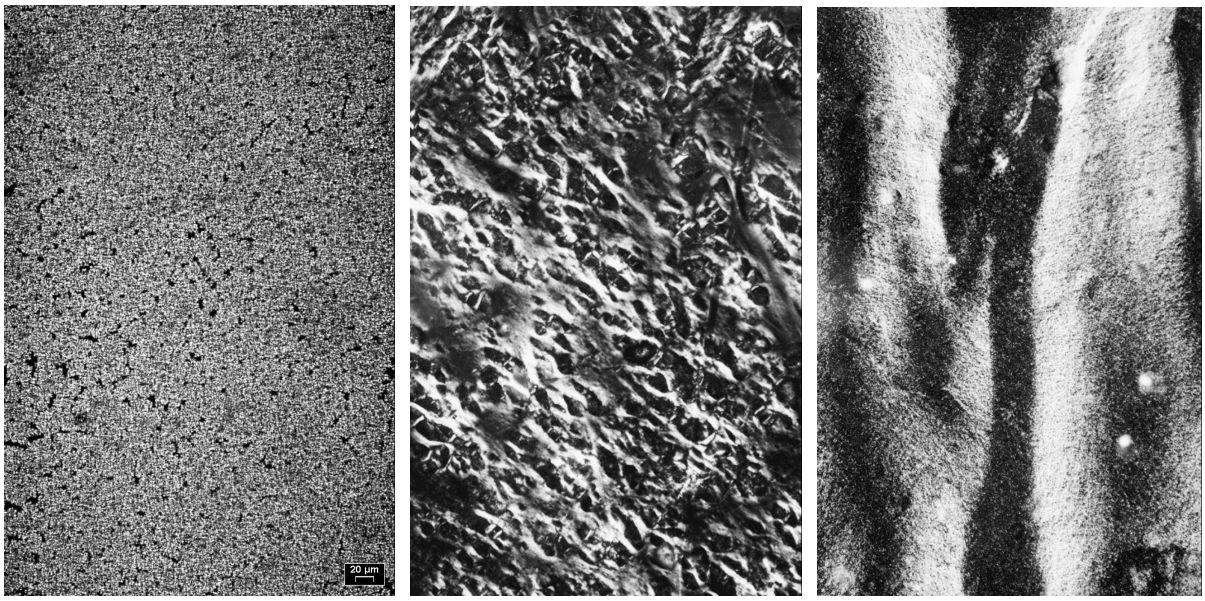

Figure 5.1: Texture of copolymer **71** (left), **72** (center) and **73** (right) under cross-polarized microscope.

This is a prove that the copolymers are ordered in the fluid state. Again, origin of that is the incompatibility of the macrocycle and the polydimethylsiloxane chains. The polymer chains are very mobile and this allows the copolymers to phase segregate in order to minimize the contact surface between the two blocks. All copolymers are thermotropic liquid crystals, within a large temperature interval. The anisotropy is reached at a temperature that decreases with increasing the molecular weight of the polydimethylsiloxane chains. Specifically, **73** becomes at 120 °C isotropic, **71** at 158 °C and **72** above 200 °C, a temperature at which also slow decomposition is expected.
The TGA data and the DSC (second heating curves) are reported in figure 5.2.

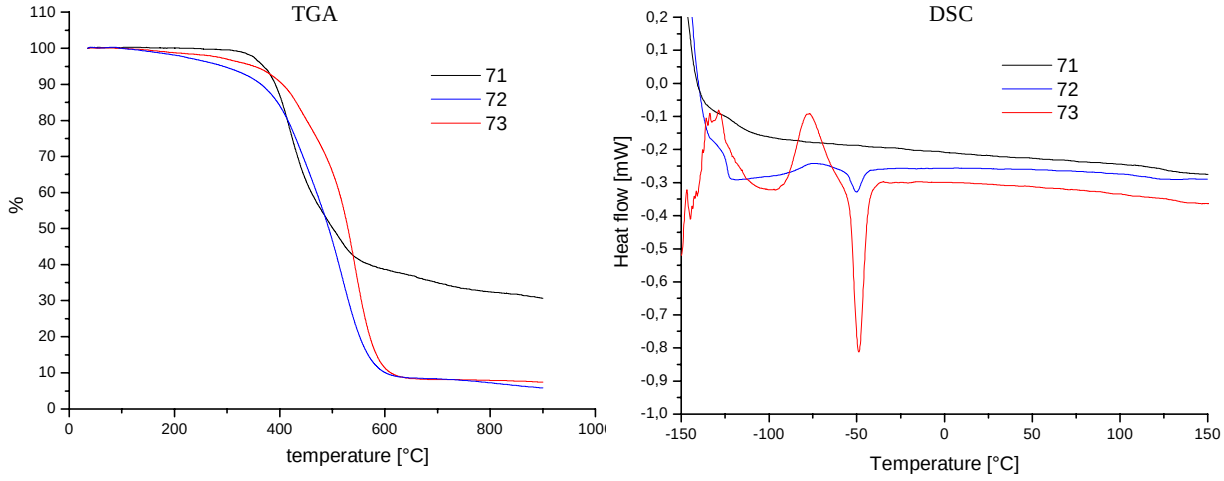

Figure 5.2 TGA and DSC data of copolymer **71**, **72** and **73**.

The DSC decomposition temperature is increasing with the molecular weight of the polydimethylsiloxane chains from around 400 °C for copolymer **71** to 500 °C for copolymer **73**. However, even at lower temperatures (above 200 °C) a crosslinking of the phenyl-acetylene structures might occur, which is not accompanied with a weight-loss. The DSC of the copolymer **71** shows a glass transition (T_g) at -116.33 °C. In the case of copolymer **69** and **70** crystallization occurs. Clearly an exothermic peak can be seen at –75.72 °C (ΔH_{cryst} = 45.29 mJ) for copolymer **72**, followed from an endothermic melting peak at –50.52 °C (ΔH_{melt} = -33.78 mJ). In the case of copolymer **73** the exothermic peak due to the crystallization is at –76.94 °C (ΔH_{cryst} = 266.63 mJ), and the melting occurs at –49.76 °C (ΔH_{melt} = -242.31 mJ). This can be explained considering that by increasing the molecular weight of the polydimethylsiloxane, the siloxane chains have the possibility to crystallize[55].

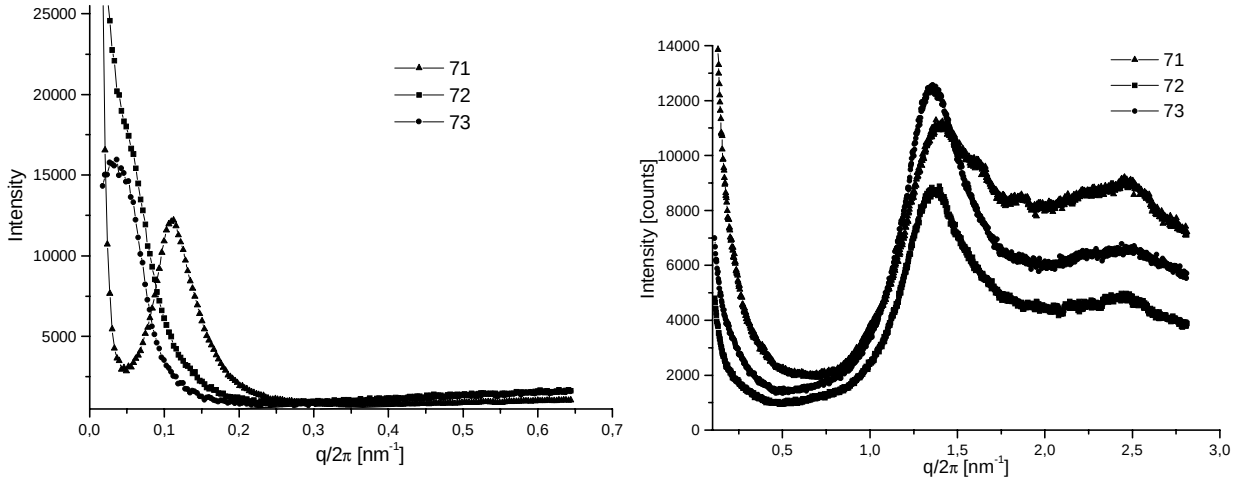

Figure 5.3 SAXS (left) and WAXS (right) of copolymer **71**, **72** and **73**.

In order to determinate the solid state structure of the block copolymers, SAXS and WAXS measurements were performed (Figure 5.3).

The distances that can be determinate from the measurements are summarized in table 5.1

Table 5.1

Copolymer	Distances [Å]
71	89, 7.1, 6.13, 5.34
72	143, 7.3
73	176, 7.3

These values are in agreement with the model of a lamella structure similar to the suggest model for the polystyrene-ring-polystyrene block copolymer (Figure 5.4).

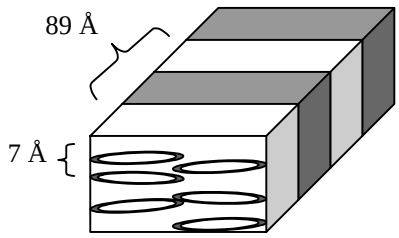

Figure 5.4: Proposed model for copolymer **71**.

However the order within the lamellae is not as good as in the polystyrene-ring-polystyrene block copolymers.

The longer distance corresponds to the layer spacing and increases with increasing the molecular weight of the polydimethylsiloxane. The 7.3 Å distance can be attributed to the ring-ring distance (it is very similar to the 6.2 Å found in the case of polystyrene-ring-polystyrene copolymer) that also in this case should be arranged in stacks. In the case of block copolymers with the short side chains this distance is slightly smaller (7.1 Å).

Since no information about the relation between two neighboring stacks has been detected, a model similar to Lee's hockey puck model can be suggested[56]. A limited number of ring (about 6-10, more or less) arrange into stacks, which are not correlated. There might be also a higher degree of order, but this has to date not been detected. However, due to the appearance of the 7 Å peak a purely nematic ordered arrangement of the ring within the lamellae can be excluded.

6 Summary

This work describes the synthesis of a new class of rod-coil block copolymers, oligosubstituted shape persistent macrocycles, (coil-ring-coil block copolymers), and their behavior in solution and in the solid state.

6.1 Synthesis of the block copolymers

The coil-ring-coil block copolymers are formed by nanometer sized shape persistent macrocycles based on the phenyl-ethynyl backbone as rigid block and oligomers of polystyrene or polydimethylsiloxane as flexible blocks. The strategy that has been followed is to synthesize the macrocycles with an alcoholic functionality and the polymer carboxylic acids independently, and then bind them together by esterification. The ester bond is stable and relatively easy to form.

The synthesis of the shape persistent macrocycles is based on two separate steps. In the first step the building blocks of the macrocycles are connected by Hagiara-Sogonaschira coupling to form an "half-ring" as precursor, that contains two free acetylenes. In the second step the half-ring is cyclized by forming two *sp*-*sp* bonds via a copper-catalyzed Glaser coupling under pseudo-high-dilution conditions. In this reaction all statistical products are formed, the dimeric ring together with trimeric, tetrameric and polymeric material. Nevertheless, by using pseudo-high-dilution conditions the macrocycle can be obtained in 50-60 % yield and the purification is in general not problematic because of the low solubility of the dimeric ring with respect to the more flexible oligomers.

The polystyrene carboxylic acid was prepared directly by siphoning the living anionic polymer chain into a THF solution, saturated with CO_2, while the polydimethylsiloxane carboxylic acid was obtained by hydrosilylating an unsaturated benzylester with an Si-H terminated polydimethylsiloxane, and cleavage of the ester.

The carbodiimide coupling was found to be the best way to connect macrocycles and polymers in high yield and high purity. Of special importance is the nonaqueous work up of the reaction which allows a simple product purification. By this method five different molecular weight of polystyrene carboxylic acids and three different molecular weight of polydimethylsiloxane carboxylic acids were attached at the ring.

6.2 Properties in solution

The polystyrene-ring-polystyrene block copolymers are well soluble in solvents like toluene or THF. However they aggregate in cyclohexane that is a non-solvent for the macrocycle and a theta solvent for polystyrene. The copolymer are, depending on the molecular weight of the polystyrene, lyotropic liquid crystals due to the incompatibility of the macrocycle and the cyclohexane. The extension of the aggregation and aggregation kinetics strongly depend on the block size of the polystyrene.

The aggregation behavior of the copolymers in solution was investigated in more detail using light microscopy (LM), static and dynamic light scattering (SLS and DLS), ultra small and small angle x-ray scattering (USAX and SAXS), transmission electron microscopy (TEM), and atomic force microscopy (AFM).

As a result it can be concluded that the polystyrene-ring-polystyrene block copolymers can aggregate into hollow cylinder-like objects with an average length of 700 nm by a combination of shape complementary and demixing of rigid and flexible polymer parts. The resulting structure can be described as supramolecular hollow cylindrical brush.

6.3 Properties in the solid state

If the lyotropic solution of the polystyrene-ring-polystyrene block copolymers are dried, they remain birefringent indicating that the solid state has an ordered structure. By a careful investigation using electron diffraction and wide-angle X-ray scattering, it has been possible to derive a model for the 3D-order of the copolymer. The macrocycles are arranged in a layer of columns with an intracolumnar spacing of about 6 Å. Rings within neighboring stacks are tilted so that a herringbone packing results. These crystalline layers are separated by amorphous layers which contain the polystyrene substituents. The thickness of the double layer consisting of one crystalline layer and one amorphous layer is about 70 Å.

The polydimethylsiloxane-ring-polydimethylsiloxane block copolymers are more or less fluid at room temperature, and are all birefringent (termotropic liquid crystals). This is a prove that the copolymers are ordered in the fluid state. Again, origin of that is the incompatibility of the macrocycle and the polydimethylsiloxane chains. The polymer chains are very mobile and this allows the copolymers to phase segregate in order to minimize the contact surface between the two blocks. All copolymers are thermotropic liquid crystals within a large temperature interval. The isotropic phase is reached at a temperature that decreases with increasing the molecular weight of the polydimethylsiloxane chains.

In order to determinate the solid state structure of the block copolymers, SAXS and WAXS measurements were performed. The data indicate a lamella structure similar to the suggested model for the polystyrene-ring-polystyrene block copolymer. However, the order within the lamellae is not as good as in the polystyrene-ring-polystyrene block copolymers (modified hockey puck model).

7 Experimental part

7.1 Devices and Methods

***NMR spectroscopy*:** ^{1}H and ^{13}C NMR spectra were recorded on a BRUKER AMX 250 (250 MHz for the proton and 62.90 MHz for the carbon) or AMX 300 (300 MHz for the proton and 75.48 MHz for the carbon), at room temperature unless stated otherwise. Chemical shifts are given in parts per million (ppm) relative to tetramethylsilane (TMS). The specific solvent signal is used as standard: (^{13}C signals is in parenthesis) dimethyl-d_6 sulphoxide [DMSO] 2.49 (39.7); chloroform-d [$CDCl_3$] 7.24 (77.0); cyclohexane-d_{12} [C_6D_{12}] 1.38 (26.43); methylene chloride-d_2 [CD_2Cl_2] 5.32 (53.50); tetrahydrofuran-d_8 [THF] 1.73, 3.58 (25.2, 67.4). The carbon multiplicity was determinated by SPINECO experiments. The follow abbreviations are used for the spin coupling multiplicity: **s** = singlet, **br s** = broad singlet, **d** = doublet, **dd** = doublet of doublet, **t** = triplet, **td** = triplet of doublet, **tt** = triplet of triplet, **q** = quartet, **m** = multiplet.

***Mass spectrometry*:** Electron-impact (EI) mass spectra were recorded on a VG TRIO 2000, field-desorption (FD) mass spectra were recorded on a ZAB 2-SE-FPD. MALDI TOF (Matrix Assisted Laser Desorption Ionization Time Of Flight) spectroscopy measurements were carried out on a Bruker reflex spectrometer (Brucker, Bremen), which incorporates a 337 nm nitrogen laser with a 3 ns pulse duration (10^6-10^7 wcm^{-1}, 100 µm spot diameter). The instrument was operated in a linear mode with an accelerating potential of 33.65 kV. The mass scale was calibrated using polystyrene (M_w = 2300), using a number of resolved oligomers. As matrix dithranol (1,8,9-trihydroxyantracene) served in all cases. Addition of salts is indicated case by case.

***FT-IR spectroscopy*:** FT-IR spectra were measured between two KBr plates without spacer against air on a Perkin Elmer Paragon 1000.

***Chromatography*:** For the preparative column chromatography silica gel 60 (grain size 230 - 400 mesh of the company Merck) as stationary phase served. The columns were filled with the stationary phase suspended in the respective solvent. Analytic thin-layer chromatography was performed on aluminum plates pre-coated with Merck 5735 silica gel 60 F_{254}. The detection of the different substances took place either via fluorescence deletion at 254 nm or on the basis of self-fluorescence after irradiation at 366 nm.

Elemental analysis: Elemental analyses (EA) were performed at the analytical laboratory of the Institute of Organic Chemistry of the Johannes Gutenberg University in Mainz.

Gel permeation chromatography: Analytic gel permeation chromatography (GPC) was performed on a Waters system. A combination of three styragel columns of the company PSS was used, which were with styrene divinyl benzene (SDV) gel particles of the size of 10 □ m and in each case had a dimension of 0.8 x 30 cm. Porosity was 10^3, 10^4 and 10^6 Å respectively. The flow rate was 1 ml/min. The measurements were executed at ambient temperature, and as eluent THF were used. Detection was performed UV spectroscopically at a wavelength of 254 nm or by means of the refractive index. The molecular weight was obtained from polystyrene calibrated SEC columns. In the case of polydimethylsiloxane and its derivatives toluene was used as eluent and the molecular weight was obtained from polydimethylsiloxane calibrated SEC columns.

***DSC*:** The DSC investigations were performed on a Perkin Elmer DSC 7 calorimeter. The heating and cooling rate was 1.5 or 10 K/min.

***TGA*:** The thermogravimetric analyses were performed at a TG 5000-apparatus (Mettler) with a heating rate of 10 K/min.

***Melting points*:** The melting points determined with a melting point microscope Thermovar of the company Renriches with heating desk.

***Light microscopy*:** Morphology and textures of liquid crystal were performed at a light microscope Axiophot (Zeiss). For the investigation of the thermal behavior a heating desk of the company Linkham, model TMS 600 was used.

***Transmission Electron microscopy*:** Electron microscopy images and the electron diffraction spectra were recorded on a LEO 912 ω microscope (Zeiss).

***Atomic Force Microscopy*:** All AFM pictures were recorded using a Nanoscope IIIa Multimode (Digital Instruments, Santa Barbara , CA). The instrument was operated in the tapping mode in air. Commercially available silicon cantilevers NSC12/200 (Silicon-MDT) were used. The spring constant was around 14 N/m and the resonant frequency was around 300 kHz. According to the specifications of the supplies curvature radius was less than 10 nm.

***Light Scattering*:** Light scattering experiments were performed using as equipment a Krypton-Ion-Laser with a wavelength of 647,1 nm, a goniometer ALV-SP81 and ALV-5000/E Multiple Tau Digital Correlator. The detector was a avalanche photo diode module and the data were elaborated

using as software ALV-5000/E for WINDOWS and CONTIN-Version 2DP (MAR1984) (PCS-1 PACK).

X-ray Scattering- Ultra-Small-Angle-X-ray Scattering measurements were performed by means of a X-ray diffractometer in the HASYLAB (A2) in Hamburg. X-ray radiation was produced by a bending magnet, operating at 4.5 GeV and with a beam size 0.7 x 5.4 mm FWHM. The wavelength was fixed to 0.15 nm, $E/E = 10^{-3}$. The distance sample-detector was ca. 3.0 m and the range of scattering angles was 0.22° - 0.9° depending on distance sample-detector. Small-Angle-X-ray Scattering measurements were performed by means of a Kratky camera (Kratky Compact, A. Paar, Austria). X-ray radiation was produced by a generator (Siemens, Kristalloflex 710H) operating at 35 kV and 10-30 mA. The primary beam was filtered and collimated, resulting in a cross section of 1 mm x 50 µm at the sample position and a wavelength of 1.54 Å (CuK_α). The distance between the sample and the detector was set to 240 mm. We used a one-dimensional position-sensitive detector (N. Braun) with a spatial resolution of 117 µm. The data were first corrected for solvent and background scattering. Because of the large horizontal beam width the main correction process consisted of desmearing the raw data. Therefore, we used a program based on the Strobl algorithm. Absolute intensities were determined by means of the moving slit method. Wide-Angle-X-ray Scattering measurements were performed by means of diffractometer (Siemens, D500/501 or Philips, PW 1820). The wavelength was 1.54 Å (CuK_α). The range of angles that could be measured was between 5° and 150°. Small-&-Wide-Angle-X-ray Scattering were performed also with a Rigaku RU-300 rotating anode. The primary beam was filtered and collimated, resulting in a point of 0.2 mm at the sample position and a wavelength of 1.54 Å (CuK_α). The distance between the sample and the detector was set to 140 cm for measuring Small-Angle, and to 10 cm for measuring the Wide-Angle range.

7.2 Chemicals

If not otherwise indicated, commercially available chemicals were used as received. They were supplied by different companies (Aldrich, Deutero, Fluka, Merck, Riedel-de Haën and Sigma). All solvents used were at least "p.a." quality. Water-free solvents were distilled according to literature procedures and handled under argon. THF was distilled from potassium and stored under argon. Pyridine, piperidine and triethylamine were distilled over calcium hydride and stored under argon. Argon of the quality 4.8 was used directly from the gas cylinder. For filtering of the macrocycle PTFE filters (Sartorius) with a pore size of 0.45 or 0.5 µm were used.

7.3 Synthesis of macrocycles

7.3.1 Synthesis of 2,6-bis(4-iodo-phenyl)-4-(4-methoxy-phenyl) pyrylium tetrafluoro borate (10)

Under an argon atmosphere, 10 ml (79 mmol) of BF_3•OEt_2 were added to a mixture of 2.76 g (20 mmol) of anysaldehyde and 10 g (40 mmol) of iodoacetophenone without the use of further solvent. The mixture was stirred at 100 °C for 2 h. After cooling to room temperature, the viscous brown oil was dissolved in 250 ml of acetone and the dark solution was poured in 1 l Et_2O. The brown precipitate was filtered and washed with Et_2O. The brown powder was purified by refluxing in THF for 2 h. After filtration and drying under vacuum, 6.5 g (48 %) of the pyrylium salt were obtained as a brown powder and used as received.

Mp: 185 °C (decomp.)

^{1}H NMR (DMSO-d_6): 3.98 (s, 3 H), 7.31 (d, *J* = 8.77 Hz, 2 H), 8.15 (d, *J* = 8.47 Hz, 4 H), 8.27 (d, *J* = 8.47 Hz, 4 H), 8.69 (d, *J* = 9.11 Hz, 2 H), 9.05 (s, 2 H).

^{13}C NMR (DMSO-d_6): 56.26, 103.88, 104.64, 113.45, 115.64, 124.29, 128.46, 128.67, 129.76, 130.01, 133.14, 138.76, 163.56, 166.08, 168.26, 169.61.

7.3.2 Synthesis of 4-methyl-2',6'-di-(4-iodo-phenyl)-4''-methoxy-p-terphenyl (14)

In a round flask, 3.08 g (4.54 mmol) of **10** and 1.56 g (9.09 mmol) of sodium 4-methylphenylacetate were dissolved in 20 ml of acetic anydride and reflux at 138 °C for 1.5 h. After cooling to room temperature, the mixture was stirred over the weekend. After that, the precipitate was filtrate and washed with water and methanol. The powder was purified by column chromatography using as eluent a mixture dichloromethane/petrolether (1:2) (R_f = 0.42). After evaporation of the solvent and drying under vacuum, 0.52 g (17 %) of the product were obtained in form of a white powder. As a side product compound **15** could be isolated.

Mp: 128 °C

^{1}H NMR ($CDCl_3$): 2.22 (s, 3 H), 6.67 (d, *J* = 8.2 Hz, 2 H), 6.82 (d, *J* = 7.8 Hz, 2 H), 6.83 (d, *J* = 8.4 Hz, 4 H), 6.84 (s, 3 H), 6.97 (d, *J* = 9.1 Hz, 2 H), 7.48 (d, *J* = 8.4 Hz, 4 H), 7.54 (s, 2 H), 7.57 (d, *J* = 9.1Hz, 2 H).

^{13}C NMR ($CDCl_3$): 21.14, 55.38, 92.17, 114.41, 127.93, 128.15, 128.40, 131.33, 131.78, 132.64, 135.48, 135.92, 136.78, 137.27, 139.90, 141.48, 141.59, 159.55.

MS (FD): m/z = 677.6 [M^+]

$C_{32}H_{24}I_2O$ (678.34): **calc.**, C. 56.66, H. 3.57
found: C. 56.91, H. 3.38

Compound 15: R_f = 0.68; **^{1}H NMR** ($CDCl_3$): 2.08 (s, 3 H), 6.67 (d, J = 8.2 Hz, 2 H), 6.82 (dd, J_1 = 6.6 Hz, J_2 = 1.87 Hz, 6 H), 7.37 (d, J = 8.47 Hz, 2 H), 7.48 (d, J = 8.4 Hz, 4 H), 7.53 (s, 2 H), 7.75 (d, J = 8.77 Hz, 2 H); **MS (FD)**: m/z = 774.1 [M^+]

7.3.3 Synthesis of 4-methyl-2',6'-di-(4-iodo-phenyl)-4''-hydroxy-p-terphenyl (22)

Under an argon atmosphere, 3.93 g (5.34 mmol) of **14** were dissolved in 20 ml dry dichloromethane. The solution was cooled to -78 °C and 1.54 ml (16 mmol) of BBr_3 were added in one portion. The color of the solution changed immediately to black. The solution was allowed to obtain room temperature overnight and then quenched with a few drops of water and stirred for 1 h. Diethyl ether and water were added, the organic phase was separated and washed with water, saturated NaCl solution and dried over $MgSO_4$. After filtration and evaporation of the solvent 3.48 g (98 %) of p-terphenyl were obtained as white powder.

Mp: 214 °C
^{1}H NMR ($CDCl_3$): 2.22 (s, 3 H), 4.97 (s, 1 H), 6.67 (dd, J_1 = 6.26 Hz, J_2 = 1.58 Hz, 2 H), 6.82 (d, J = 8.5 Hz, 2 H), 6.83 (d, J = 8.47 Hz, 4 H), 6.89 (dd, J_1 = 6.2 Hz, J_2 = 2.2 Hz, 2 H), 7.48 (dd, J_1 = 8.47 Hz, J_2 = 2.2 Hz, 4 H), 7.50 (s, 2 H), 7.53 (d, J = 8.77Hz, 2 H).
^{13}C NMR ($CDCl_3$): 21.14, 92.18 115.83, 127.92, 128.40, 131.32, 131.77, 132.62, 135.45, 135.94, 136.78, 137.33, 139.81, 141.49, 141.56, 155.47.
MS (FD): m/z = 663.6 [M^+]
$C_{31}H_{22}I_2O$ (664.3): **calc.**: C. 56.05, H. 3.34
found: C. 55.91, H. 3.38

7.3.4 Synthesis of 3-bromo-propylbenzoate (24)

In a round flask 4.17 g (3 mmol) of 3-bromo-1-propanol and 5 g (3.5 mmol) of benzoyl chloride were dissolved in 10 ml of THF. The solution was cooled to 0 °C and 3.23 ml (4 mmol) of pyridine were added dropwise. After stirring overnight at room temperature, diethyl ether and water were added and the organic phase was separated and washed with water, 10 % acetic acid, 10 % sodium hydroxide, and saturated NaCl solution. The organic phase was dried over $MgSO_4$. After filtration and evaporation of the solvent 4.6 g (63 %) of a colorless liquid were obtained.

^{1}H NMR ($CDCl_3$): 2.29 (m, J = 6.32 Hz, 4 H), 3.52 (t, J = 6.47 Hz, 2 H), 4.44 (t, J = 6 Hz, 2 H), 7.41 (t, J = 7.27 Hz, 2 H), 7.49-7.57 (m, 1 H), 7.99-8.04 (m, 2 H).

^{13}C NMR ($CDCl_3$): 29.25, 31.50 61.35, 128.09, 129.23, 130.20, 132.74, 165.94.

MS (FD): m/z = 242.9 [M^+], 245.0 [$(M+2)^+$]

$C_{10}H_{11}BrO_2$ (241.99): **calc.**: C. 49.41, H. 4.56

found: C. 49.03, H. 4.81

7.3.5 Synthesis of 4-methyl-2',6'-di-(4-iodo-phenyl)-4''-propylbenzoate-p-terphenyl (23)

Under an argon atmosphere, 3.47 g (5.23 mmol) of **22**, 1.96 g (7.85 mmol) of 3-bromo-propilbenzoate (**24**) and 2.17 g (15.7 mmol) of potassium carbonate were dissolved in 20 ml of DMF. The mixture was refluxed at 60 °C overnight. After cooling to room temperature, diethyl ether and water were added to the solution and the organic phase was separated and washed with water, saturated NaCl solution and dried over $MgSO_4$. After filtration and evaporation of the solvent the crude product was purified by column chromatography using a mixture dichloromethane/petrolether as eluent (1:1) (R_f = 0.49). After evaporation of the solvent and drying under vacuum, 3.38 g (78 %) of **23** were obtained in form of a white powder.

Mp: 84 °C

^{1}H NMR ($CDCl_3$): 2.22 (s, 3 H), 2.28 (q, J = 5.97 Hz, 2 H), 4.17 (t, J = 5.97 Hz, 2 H), 4.53 (t, J = 5.97 Hz, 2 H), 6.67 (d, J = 7.85 Hz, 2 H), 6.81 (t, J = 2.2 Hz, 4 H), 6.83-6.86 (m, 2 H), 6.96 (d, J = 8.77 Hz, 2 H), 7.39-7.53 (m, 11 H), 8.04 (dd, J_1 = 8.48 Hz, J_2 = 1.25 Hz, 2 H).

^{13}C NMR ($CDCl_3$): 21.16, 28.81, 61.80, 64.59, 92.20, 114.92, 127.93, 128.16, 128.37, 128.40, 129.56, 131.29, 131.75, 132.97, 135.89, 136.74, 139.81, 140.40, 141.51, 165.94.

MS (FD): m/z = 825.6 [M^+]

$C_{41}H_{32}I_2O_3$ (825.8): **calc.**: C. 59.58, H. 3.90

found: C. 58.88, H. 4.44

7.3.6 Synthesis of (6-hydroxy-hexyloxy) 3,5-diiodbenzene (29)

In a round flask 5.28 g (15 mmol) of 3,5-diiodophenol[57], 2.78 g (15 mmol) of 6-bromo-1-hexanol and 4.26 g (30 mmol) of potassium carbonate were dissolved in 30 ml of DMF. The mixture was heated to 60 °C overnight and then cooled to room temperature. Diethyl ether and water were added to the brown suspension and the organic phase was separated and washed four times with water, saturated NaCl solution and dried over $MgSO_4$. After filtration and evaporation of the

solvent, the crude product was purified by column chromatography using as eluent a mixture of diethyl ether/petrol ether (3:1) (R_f = 0.48). After evaporation of the solvent and drying under vacuum, 6.49 g (79 %) of (1-hydroxy-hesoxy) 3,5-diiodbenzene were obtained as a white powder.

Mp: 46 °C

^{1}H NMR ($CDCl_3$): 1.36-1.45 (m, 4 H), 1.57 (m, *J* = 7.27 Hz, 2 H), 1.74 (m, *J* = 7.27 Hz, 2 H), 3.63 (t, *J* = 6.65 Hz, 2 H), 3.86 (t, *J* = 6.65 Hz, 2 H), 7.16 (d, *J* = 1.27 Hz, 2 H), 7.57 (t, *J* = 1.27 Hz, 1 H).

^{13}C NMR ($CDCl_3$): 25.42, 25.72, 28.95, 32.57, 62.79, 68.29, 94.54, 123.40, 137.30, 159.84.

MS (FD): m/z = 445.6 [M^+]

$C_{12}H_{16}I_2O_2$ (446.06): **calc.**, C. 32.31, H. 3.62

found: C. 32.41, H. 3.73

7.3.7 Synthesis of 6-(3,5-diiodbenzene)-hexylbenzoate (30)

In a round flask 6.49 g (14,5 mmol) of **29** and 2.1 g (14.9 mmol) of benzoyl chloride were dissolved in 20 ml of THF. The mixture was cooled to0 °C and 1.5 g (18,9 mmol) of pyridine were slowly added. In the meanwhile the formation of a white precipitate could be observed. After stirring overnight at room temperature, diethyl ether and water were added and the organic phase was separated and washed with water, 10 % acetic acid, 10 % sodium hydroxide, and saturated NaCl solution. The organic phase was dried over $MgSO_4$ and after filtration and evaporation of the solvent, the crude product was purified by column chromatography using as eluent a mixture of methylene chloride/petrol ether (1:1) (R_f = 0.36). After evaporation of the solvent and drying under vacuum, 7 g (88 %) of **7** were obtained as a white powder.

Mp: 56 °C

^{1}H NMR ($CDCl_3$): 1.49 (m, *J* = 3.47 Hz, 4 H), 1.76 (m, *J* = 6.47 Hz, 4 H), 3.87 (t, *J* = 6.32 Hz, 2 H), 4.31 (t, *J* = 6.32 Hz, 2 H), 7.16 (d, *J* = 1.25 Hz, 2 H), 7.41 (tt, J_1 = 8.05 Hz, J_2 = 1.9 Hz, 2 H), 7.50-7.58 (m, 2 H), 8.02 (td, J_1 = 6.95 Hz, J_2 = 1.42 Hz, 2 H).

^{13}C NMR ($CDCl_3$): 25.62, 25.75, 28.60, 28.88, 64.82, 68.20, 94.56, 123.35, 128.31, 129.48, 130.38, 132.81, 137.29, 159.79, 166.59.

MS (FD): m/z = 549.6 [M^+]

$C_{19}H_{20}I_2O_3$ (549.8): **calc.**, C. 41.48, H. 3.66

found: C. 41.32, H. 3.83

7.3.8 Synthesis of 1-{-2-[3-tert-butyl-5-(2-triisopropylsilylethinyl)-phenyl]-ethinyl}-4-{2-triethylsilylethinyl}-benzene (34)

Under an argon atmosphere, 10 g (35.3 mmol) of 4-bromo-iodobenzene and 0.38 g (1.45 mmol) of triphenyl posphine were dissolved in 245 ml of piperidine. The solution was cooled down at 0 °C by an ice bath and 5.44 g (38.7 mmol) of 2-triisopropylsilylacetylene and 0.38 mg (0.54 mmol) of $PdCl_2(PPh_3)_2$ were added The mixture was stirred overnight at room temperature. Then, the solution was heat to 50 °C for 1 h and then 14.13 g (41.72 mmol) of 1-ethinyl-3-(2-triisopropylsilylethinyl)-5-tert-butyl-benzene (**31**)[58] were added and the solution stirred at this temperature for 4 days. After cooling down, diethyl ether and water were added to the solution and the organic phase was separated and washed with water, 10 % acetic acid, 10 % sodium hydroxide, and saturated NaCl solution. The organic phase was dried over $MgSO_4$ and after filtration and evaporation of the solvent, the crude product was purified by column chromatography using as eluent pure petrol ether (R_f = 0.38). After evaporation of the solvent and drying under vacuum, 17.5 g (91 %) of **9** were obtained as a white powder.

^{1}H NMR ($CDCl_3$): 0.66 (q, *J* = 7.99 Hz, 6 H), 1.03 (t, *J* = 7.62 Hz, 9 H), 1.12 (s, 21 H), 1.31 (s, 9 H), 7.42-7.44 (m, 5 H), 7.45-7.48 (m, 5 H).

^{13}C NMR ($CDCl_3$): 4.43, 7.47, 11.36, 31.10, 34.68, 88.96, 90.64, 90.97, 93.87, 105.92, 106.72, 122.82, 123.11, 123.25, 123.54, 128.79, 129.04, 131.40, 131.98, 132.39, 151.53.

MS (FD): m/z = 552.7 [M^+], 1105.1 [$2M^+$].

$C_{37}H_{52}Si_2$ (552.98): **calc.**, C. 80.36, H. 9.48

found: C. 80.31, H. 9.59

7.3.9 Synthesis of 5-ethinyl-2-{-2-[3-tert-butyl-5-(2-triisopropylsilylethinyl)-phenyl]}-benzene (35)

In a round flask, 17.55 g (32.26 mmol) of **34** and 18.6 g (134 mmol) of K_2CO_3 were dissolved in 250 ml of a mixture THF/methanol (2:1). The solution was stirred for 4 days at room temperature, then diethyl ether and water were added and the organic phase was separated and washed with water and saturated NaCl solution. The organic phase was dried over $MgSO_4$ and after filtration and evaporation of the solvent, the crude product was purified by recrystallization using a mixture of methanol/ethanol (3:1). After filtration and drying under vacuum, 11.77 g (83 %) of pure **35** were obtained as a white powder.

Mp: 75 °C

^{1}H NMR ($CDCl_3$): 1.12 (s, 21 H), 1.31 (s, 9 H), 3.15 (s, 1 H), 7.43 (t, J = 1.53 Hz, 5 H), 7.46-7.48 (m, 5 H).

^{13}C NMR ($CDCl_3$): 11.36, 18.69, 31.10, 34.68, 78.92, 88.71, 90.64, 90.70, 91.12, 106.69, 121.99, 122.74, 123.56, 123.65, 128.79, 129.12, 131.50, 132.08, 132.39, 151.56.

MS (FD): m/z = 438.2 [M^+], 879.3 [$2M^+$], 1318.3 [$3M^+$].

$C_{31}H_{38}Si$ (438.72): **calc.**, C. 84.87, H. 8.73

found: C. 84.88, H. 8.69

7.3.10 Synthesis of the half macrocycle 36

Under an argon atmosphere, 0.56 g (0.67 mmol) of **23**, 0.57 g (1.69 mmol) of **31** and 17 mg of triphenyl phosphine were dissolved in 5 ml of THF and 2 ml of triethyl amine. To the solution 8.5 mg of copper iodide and 17 mg of $Pd_2(dba)_3$ were added and the mixture was stirred overnight at room temperature. The next day the solution heated to 50 °C for 1 h. After cooling to room temperature diethyl ether and water were added to the solution and the organic phase was separated and washed with water, 10 %acetic acid, 10 % sodium hydroxide, and saturated NaCl solution. The organic phase was dried over $MgSO_4$ and after filtration and evaporation of the solvent, the crude product was purified by column chromatography using as eluent a mixture of petrol ether/methylene chloride (1:1) (R_f = 0.53). After evaporation of the solvent and drying under vacuum, 0.69 g (83 %) of **36** were obtained as a white powder and used as received.

Mp: 118 °C

^{1}H NMR ($CDCl_3$): 1.12 (s, 42 H), 1.30 (s, 18 H), 2.2 (s, 3 H), 2.28 (t, J = 6.27 Hz, 2 H), 4.17 (t, J = 5.95 Hz, 2 H), 4.54 (t, J = 6.27 Hz, 2 H), 6.69 (d, J = 8.17 Hz, 2 H), 6.79 (d, J = 7.85 Hz, 2 H), 6.98 (d, J = 7.88 Hz, 2 H), 7.09 (dt, J_1 = 8.45 Hz, J_2 = 1.87 Hz, 4 H),7.34 (dt, J_1 = 8.45 Hz, J_2 = 1.87 Hz, 4 H), 7.40 (t, J = 1.72 Hz, 2 H), 7.42-7.46 (m, 6 H), 7.55-7.63 (m, 5 H), 8.04 (dd, J_1 = 8.15 Hz, J_2 = 1.57 Hz, 2 H).

^{13}C NMR ($CDCl_3$): 11.37, 18.69, 21.12, 28.89, 31.11, 34.67, 61.85, 64.68, 89.31, 90.55, 114.98, 120.94, 123.11, 123.49, 127.97, 128.24, 128.32, 128.38, 128.76, 129.60, 129.94, 130.99, 131.42, 132.35, 132.96, 135.66, 135.79, 137.52, 139.75, 141.92, 142.29, 151.48, 158.68.

MS (FD): m/z = 1246.2 [M^+], 623.6 [M^{2+}].

7.3.11 Synthesis of the half macrocycle 37

Under an argon atmosphere, 1.60 g (1.94 mmol) of **23**, 2.12 g (4.84 mmol) of **35** and 48.5 mg of triphenyl phosphine were dissolved in 10 ml of THF and 5 ml of triethyl amine. To the solution 24 mg of copper iodide and 48 mg of $Pd_2(dba)_3$ were added and the mixture was stirred overnight at room temperature. The next day the solution was heated to 50 °C for 1 hour and then cooled to room temperature. Diethyl ether and water were added and the organic phase was separated and washed with water, 10 % acetic acid, 10 %sodium hydroxide, and saturated NaCl solution. The organic phase was dried over $MgSO_4$ and after filtration and evaporation of the solvent, the crude product was purified by column chromatography using as eluent a mixture of petrol ether/ methylene chloride (1:1) (R_f = 0.63). After evaporation of the solvent and drying under vacuum, 2.58 g (92 %) of **37** were obtained as a white powder and used as received.

Mp: 128 °C

^{1}H NMR ($CDCl_3$): 1.12 (s, 42 H), 1.31 (s, 18 H), 2.20 (s, 3 H), 2.28 (t, *J* = 5.97 Hz, 2 H), 4.18 (t, *J* = 5.97 Hz, 2 H), 4.54 (t, *J* = 6.27 Hz, 2 H), 6.70 (d, *J* = 8.17 Hz, 2 H), 6.81 (d, *J* = 8.17 Hz, 2 H), 6.98 (d, *J* = 8.47 Hz, 2 H), 7.09 (d, *J* = 8.15 Hz, 4 H), 7.34 (d, *J* = 8.47 Hz, 4 H), 7.39-7.47 (m, 16 H), 7.51-7.63 (m, 5 H), 8.03 (dd, J_1 = 6.9 Hz, J_2 = 1.57 Hz, 2 H).

^{13}C NMR ($CDCl_3$): 11.37, 18.69, 21.14, 28.88, 31.11, 34.69, 61.85, 64.67, 89.01, 89.34, 91.00, 91.47, 106.73, 114.98, 120.87, 122.92, 123.26, 128.00, 128.23, 128.79, 129.07, 129.60, 129.98, 130.99, 131.43, 131.49, 131.57, 132.39, 132.97, 135.65, 135.84, 137.50, 139.79, 141.89, 151.55, 158.70, 166.55.

MS (FD): m/z = 1447.9 [M^+], 722.7 [M^{2+}].

7.3.12 Synthesis of the half macrocycle 42

In a round flask, 2.05 g (1.64 mmol) of **36** were dissolved in 5 ml of THF and then 3.3 ml (3.3 mmol) of tetra-butyl ammonium fluoride (1 M in THF) were added. The mixture was stirred overnight at room temperature, then diethyl ether and water were added to the solution and the organic phase was separated and washed with water and saturated NaCl solution. The organic phase was dried over $MgSO_4$ and after filtration and evaporation of the solvent an yellow oil was obtained. In order to remove the triisopropyl silyl alcohol the oil was dissolved in a small amount of petrol ether and stored overnight. After decantation the resulting powder was purified by column chromatography using as eluent a mixture of petrol ether/methylene chloride (1:1) (R_f = 0.37). After evaporation of the solvent and drying under vacuum, 1.2 g (78 %) of **42** were obtained as a white powder and used as received.

^{1}H NMR ($CDCl_3$): 1.30 (s, 18 H), 2.21 (s, 3 H), 2.28 (t, J = 6.27 Hz, 2 H), 3.05 (s, 2 H), 4.18 (t, J = 6.27 Hz, 2 H), 4.54 (t, J = 6.27 Hz, 2 H), 6.72 (d, J = 8.15 Hz, 2 H), 6.82 (d, J = 8.15 Hz, 2 H), 6.99 (d, J = 8.77 Hz, 2 H), 7.11 (dt, J_1 = 8.77 Hz, J_2 = 1.87 Hz, 4 H),7.35 (dt, J_1 = 8.47 Hz, J_2 = 1.9 Hz, 4 H), 7.39 (t, J = 1.25 Hz, 1 H), 7.42-7.47 (m, 6 H), 7.51 (m, 2 H), 7.60-7.64 (m, 4 H), 8.05 (dd, J_1 = 8.15 Hz, J_2 = 1.57 Hz, 2 H).

^{13}C NMR ($CDCl_3$): 21.12, 28.89, 31.07, 34.68, 61.85, 64.67, 89.11, 89.56, 114.98, 120.87, 122.05, 123.29, 127.98, 128.23, 128.32, 128.37, 128.76, 129.59, 129.95, 130.99, 131.41, 132.21, 132.95, 135.65, 135.81, 137.50, 139.77, 141.90, 142.35, 151.63, 158.69.

7.3.13 Synthesis of the half macrocycle 43

In a round flask, 2.57 g (1.77 mmol) of **37** were dissolved in 20 ml of THF and then 3.55 ml (3.55 mmol) of tetra-butyl ammonium fluoride (1 M in THF) were added. The mixture was stirred overnight at room temperature, then diethyl ether and water were added to the solution and the organic phase was separated and washed with water and saturated NaCl solution. The organic phase was dried over $MgSO_4$ and after filtration and evaporation of the solvent an yellow oil was obtained. In order to remove the triisopropyl silyl alcohol the oil was dissolved in a small amount of petrol ether and stored overnight. After decantation the resulting powder was purified by column chromatography using as eluent a mixture of petrol ether/methylene chloride (1:1) (R_f = 0.46). After evaporation of the solvent and drying under vacuum, 1.84 g (91 %) of **43** were obtained as a white powder and used as received.

Mp: 103 °C

^{1}H NMR ($CDCl_3$): 1.31 (s, 18 H), 2.20 (s, 3 H), 2.28 (t, J = 6 Hz, 2 H), 3.06 (s, 2 H), 4.18 (t, J = 6 Hz, 2 H), 4.54 (t, J = 6.15 Hz, 2 H), 6.71 (d, J = 8.05 Hz, 2 H), 6.81 (d, J = 8.05 Hz, 2 H), 6.99 (d, J = 8.85 Hz, 2 H), 7.10 (d, J = 8.53 Hz, 4 H), 7.34 (d, J = 8.53 Hz, 4 H), 7.39-7.47 (m, 16 H), 7.51-7.63 (m, 5 H), 8.03 (dt, J_1 = 6.95 Hz, J_2 = 1.43 Hz, 2 H).

^{13}C NMR ($CDCl_3$): 13.43, 28.87, 31.11, 34.70, 61.84, 64.67, 89.16, 89.31, 91.00, 91.47, 114.98, 120.85, 122.14, 122.83, 123.03, 123.34, 128.00, 128.23, 128.36, 129.26, 129.43, 129.60, 129.98, 130.99, 131.43, 131.50, 131.58, 132.27, 132.94, 135.65, 135.84, 137.49, 139.79, 141.89, 142.43, 151.71, 2, 158.69, 166.54.

MS (FD): m/z = 1134.0 [M^+], 567.9 [M^{2+}].

7.3.14 Synthesis of the macrocycle 44

Under an argon atmosphere, 3.55 g of copper (I) chloride and 0.71 g of copper (II) dichloride were suspended in 120 ml of pyridine. The suspension was heated to 55 °C and 0.58 g (0.62 mmol) of **42** dissolved in 15 ml of pyridine, were added in 96 h (high dilution condition). After complete addition that 200 ml of methylene chloride and 200 ml of water were added to the solution and the organic phase was separated and washed with water, 25 % aqueous NH_3 solution (until the aqueous phase stayed nearly colorless), 10 % acetic acid, 10 % sodium hydroxide, and saturated NaCl solution. The organic phase was dried over $MgSO_4$ and after filtration the solution was concentrated to 20 ml. A precipitate was formed after the addition of about 100 ml of methanol. After filtration, the crude product was purified by column chromatography using as eluent a mixture petrol ether/methylene chloride (1:3) (R_f = 0.59). After evaporation of the solvent and drying under vacuum, 0.61 g (53 %) of **44** were obtained as white powder.

Mp: > 277 °C (decomposition)

^{1}H NMR ($CDCl_3$): 1.31 (s, 36 H), 2.25 (s, 6 H), 2.28 (t, J = 6.27 Hz, 4 H), 4.18 (t, J = 5.97 Hz, 4 H), 4.54 (t, J = 8,2 Hz, 4 H), 6.68 (d, J = 8.15 Hz, 4 H), 6.85 (d, J = 8.15 Hz, 4 H), 6.99 (d, J = 9,1 Hz, 4 H), 7.09 (d, J = 8.45 Hz, 8 H), 7.32 (d, J = 8.47 Hz, 8 H), 7.42-7.65 (m, 36 H), 8.03 (dd, J_1 = 8.47 Hz, J_2 = 1.25 Hz, 4 H).

^{13}C NMR ($CDCl_3$): 21.09, 28.89, 31.07, 34.78, 61.84, 64.67, 73.91, 81.39, 88.80, 89.83, 114.97, 120.80, 121.75, 123.52, 128.25, 128.38, 128.76, 129.59, 129.99, 130.94, 131.43, 132.96, 133.89, 135.65, 135.81, 137.50, 139.82, 141.88, 142.28, 151.85, 158.69.

GPC (THF) Single peak M_w= 2300

MS (MALDI-TOF): m/z = 1973.3 [$(M+Ag)^+$]

$C_{138}H_{112}O_6$ (1866.36): **calc.**, C. 88.81, H. 6.05

found: C. 88.44, H. 5.86

7.3.15 Synthesis of the macrocycle 45

Under an argon atmosphere, 10.86 g of copper (I) chloride and 2.17 g of copper (II) dichloride were suspended in 300 ml of pyridine. The suspension was heated to 55 °C and 1.81 g (1.60 mmol) of compound **43** dissolved in 50 ml of pyridine, were added in 96 h (high dilution condition). After complete addition that 200 ml of methylene chloride and 200 ml of water were added to the solution and the organic phase was separated and washed with water, 25 % aqueous NH_3 solution (until the aqueous phase stayed nearly colorless), 10 % acetic acid, 10 % sodium hydroxide, and saturated NaCl solution. The organic phase was dried over $MgSO_4$ and after filtration the solution was

concentrated to 20 ml. A precipitate was formed after the addition of about 100 ml of methanol. After filtration, the crude product was purified by column chromatography using as eluent a mixture petrol ether/methylene chloride (1:3) (R_f = 0.40). After evaporation of the solvent and drying under vacuum, 0.57 g (20 %) of **45** were obtained as a white powder and used as received.

Mp: > 250 °C (decomposition)

^{1}H NMR ($CDCl_3$): 1.31 (s, 36 H), 2.21 (s, 6 H), 2.28 (t, *J* = 6.57 Hz, 4 H), 4.18 (t, *J* = 6.6 Hz, 4 H), 4.54 (t, *J* = 6.6 Hz, 4 H), 6.68 (d, *J* = 7.85 Hz, 4 H), 6.81 (d, *J* = 6.9 Hz, 4 H), 6.99 (d, *J* = 8.4 Hz, 4 H), 7.09 (d, *J* = 7.82 Hz, 8 H), 7.33 (d, *J* = 7.52 Hz, 8 H), 7.42-7.62 (m, 42 H), 8.03 (d, *J* = 9.1 Hz, 4 H).

^{13}C NMR ($CDCl_3$): 21.14, 28.89, 31.07, 34.80, 61.85, 64.68, 73.95, 81.38, 89.27, 89.42, 90.56, 91.58, 114.98, 120.84, 121.82, 122.74, 123.28, 123.42, 127.81, 128.23, 128.37, 129.31, 129.59, 129.98, 130.96, 131.41, 131.52, 131.60, 132.95, 135.69, 135.81, 137.68, 139.81 141.90, 142.37, 151.92, 158.69.

GPC (THF) Single peak M_w= 3354

MS (MALDI-TOF): m/z = 2289 $[(M+Na)^+]$

7.3.16 Synthesis of the macrocycle 46

In a round flask, 0.61 g (0.33 mmol) of **44** were dissolved in 40 ml of THF. 3 ml of 10 % methanolic NaOH solution and 6 ml of 10 % aq. LiOH solution were added. The mixture was refluxed at 66 °C overnight. After cooling to room temperature methylene chloride and water were added. The organic phase was separated and washed with water, 10 %sodium hydroxide, and saturated NaCl solution. The organic phase was dried over $MgSO_4$ and after filtration, the crude product was purified by column chromatography using as eluent a mixture of methylene chloride/THF (100:1) (R_f = 0.81). After evaporation of the solvent and drying under vacuum, 0.48 g (87 %) of **46** were obtained as a white powder.

Mp: > 250 °C (decomposition)

^{1}H NMR ($CDCl_3$): 1.31 (s, 36 H), 2.07 (m, *J* = 5.67 Hz, 4 H), 2.25 (s, 6 H), 3.88 (t, *J* = 5.67 Hz, 4 H), 4.17 (t, *J* = 6 Hz, 4 H), 6.68 (d, *J* = 7.87 Hz, 4 H), 6.85 (d, *J* = 7.9 Hz, 4 H), 6.99 (d, *J* = 8.85 Hz, 4 H), 7.10 (d, *J* = 8.2 Hz, 8 H), 7.32 (d, *J* = 8.22 Hz, 8 H), 7.45 (t, *J* = 1.57 Hz, 4 H), 7.52 (dt, J_1 =8.82 Hz, J_2 = 1.57 Hz, 8 H), 7.63 (t, *J* = 4.1 Hz, 8 H).

^{13}C NMR ($CDCl_3$): 21.08, 31.08, 32,08, 34.78, 60.49, 65.88, 73.92, 81.40, 88.81, 89.83, 114.96, 120.82, 121.76, 123.52, 128.25, 128.38, 128.65, 129.04, 129.99, 130.94, 131.43, 133.03, 133.89, 135.71, 135.82, 137.77, 139.80, 141.89, 142.28, 151.85, 158.69.

GPC (THF) Single peak M_w= 2287

MS (MALDI-TOF): m/z = 1657.4 [M^+]

$C_{124}H_{104}O_4$ (1658.15): **calc.**, C. 89.82, H. 6.32

found: C. 86.5, H. 6.5

7.3.17 Synthesis of the macrocycle 47

In a round flask, 0.3 g (0.13 mmol) of **45** were dissolved in 20 ml of THF. 2 ml of 10 % methanolic NaOH solution and 3 ml of 10 % aq. LiOH solution were added. The mixture was refluxed at 66 °C overnight. After cooling to room temperature methylene chloride and water were added. The organic phase was separated and washed with water, 10 %sodium hydroxide, and saturated NaCl solution. The organic phase was dried over $MgSO_4$ and after filtration, evaporation of the solvent and drying under vacuum, 0.25 g (91 %) of **45** were obtained as a white powder.

Mp: > 250 °C (decomposition)

^{1}H NMR ($CDCl_3$): 1.31 (s, 36 H), 2.07 (t, *J* = 6.0 Hz, 4 H), 2.21 (s, 6 H), 3.88 (t, *J* = 4.57 Hz, 4 H), 4.17 (t, *J* = 5.85 Hz, 4 H), 6.68 (d, *J* = 8.05 Hz, 4 H), 6.81 (d, *J* = 8.22 Hz, 4 H), 7.00 (d, *J* = 8.67 Hz, 4 H), 7.09 (d, *J* = 8.45 Hz, 8 H), 7.33 (d, *J* = 8.37 Hz, 8 H), 7.48-7.55 (m, 28 H), 7.62 (t, *J* = 3.65 Hz, 8 H).

^{13}C NMR ($CDCl_3$): 21.16, 29.47, 31.07, 32.07, 60.49, 65.87, 73.95, 81.38, 89.27, 89.42, 90.56, 91.57, 114.97, 120.84, 121.82, 122.75, 123.27, 123.42, 127.81, 128.23, 128.34, 129.31, 129.99, 130.97, 131.41, 131.52, 131.60, 135.69, 135.81, 141.90, 142.37, 151.92, 158.69.

GPC (THF) Single peak M_w= 2690, PD = 1.1

MS (MALDI-TOF): m/z = 2057.44 [M^+]

$C_{156}H_{120}O_4$ (2058.62): **calc.**, C 91.02, H 5.88

found: C 89.90 H 5.45

7.3.18 Synthesis of the half macrocycle 48

Under an argon atmosphere, 1.82 g (3.3 mmol) of **30**, 2.9 g (6.6 mmol) of **35** and 85 mg of triphenyl phosphine were dissolved in 20 ml of triethyl amine. To the solution 43 mg of copper iodide and 85 mg of $Pd_2(dba)_3$ were added and the mixture was stirred for three days at room temperature. Diethyl ether and water were added and the organic phase was separated and washed with water, 10 % acetic acid, 10 % sodium hydroxide, and saturated NaCl solution. The organic phase was dried over $MgSO_4$. After filtration and evaporation of the solvent, the crude product was purified by column chromatography using as eluent a mixture of petrol ether/methylene chloride (2:1) (R_f = 0.43). After

evaporation of the solvent and drying under vacuum, 3 g (78 %) of **48** were obtained as a white powder.

Mp: 72 °C

^{1}H NMR ($CDCl_3$): 1.12 (s, 42 H), 1.31 (s, 18 H), 1.54 (m, 4 H), 1.81 (m, 4 H), 3.99 (t, J = 6.32 Hz, 2 H), 4.33 (t, J = 6.62 Hz, 2 H), 7.02 (d, J = 1.27 Hz, 2 H), 7.29 (t, J = 1.25 Hz, 2 H), 7.42-7.50 (m, 16 H), 8.03 (dt, J_1 = 6.95 Hz, J_2 = 1.57 Hz, 2 H).

^{13}C NMR ($CDCl_3$): 11.32, 18.67, 25.75, 25.84, 28.68, 29.04, 31.08, 34.67, 64.90, 68.09, 88.91, 89.42, 90.42, 91.10, 106.65, 117.90, 122.74, 122.82, 123.18, 123.50, 124.29, 128.33, 128.79, 129.08, 129.52, 129.98, 131.59, 132.38, 132.83, 151.52, 152.29.

MS (FD): m/z = 1169.8 [M^+]

$C_{81}H_{94}O_3Si_2$ (1171.78): **calc.**, C. 83.02, H. 8.09

found: C. 82.81, H. 8.13

7.3.19 Synthesis of the half macrocycle 49

In a round flask, 3 g (2.57 mmol) of **48** were dissolved in 10 ml of THF and then 5.5 ml (5.15 mmol) of tetra-butyl ammonium fluoride (1 M in THF) were added. The mixture was stirred overnight at room temperature, then diethyl ether and water were added to the solution and the organic phase was separated and washed with water and saturated NaCl solution. The organic phase was dried over $MgSO_4$ and after filtration and evaporation of the solvent, the crude product was purified by column chromatography using as eluent a mixture of petrol ether/methylene chloride (1:1) (R_f = 0.55). After evaporation of the solvent and drying under vacuum, 2.03 g (93 %) of **49** were obtained as a white powder.

Mp: 52 °C

^{1}H NMR ($CDCl_3$): 1.31 (s, 18 H), 1.53 (m, 4 H), 1.81 (m, 4 H), 3.06 (s.2 H), 3.99 (t, J = 6.15 Hz, 2 H), 4.33 (t, J = 6.47 Hz, 2 H), 7.02 (d, J = 1.42 Hz, 2 H), 7.29 (t, J = 1.42 Hz, 2 H), 7.43 (dd, J_1 = 6 Hz, J_2 = 1.27 Hz, 2 H), 7.47 (d, J = 1.72 Hz, 4 H), 7.49 (s, 8 H), 7.52 (t, J = 1.72 Hz, 2 H), 8.03 (dt, J_1 = 7.1 Hz, J_2 = 1.27 Hz, 2 H).

^{13}C NMR ($CDCl_3$): 25.76, 25.84, 28.68, 29.04, 31.05, 34.69, 64.90, 68.09, 76.49, 88.91, 89.40, 90.42, 90.89, 117.90, 122.09, 122.91, 123.10, 124.28, 128.33, 129.26, 129.45, 129.52, 131.60, 132.25, 132.83, 151.52, 158.79.

MS (FD): m/z = 858.0 [M^+]

$C_{63}H_{54}O_3$ (859.10): **calc.**, C. 88.08, H.6.34

found: C. 88.06, H. 6.28

7.3.20 Synthesis of the macrocycle 50

Under an argon atmosphere, 3.82 g of copper (I) chloride and 0.75 g of copper (II) dichloride were suspended in 120 ml of pyridine. The suspension was heated to 55 °C and 0.60 g (0.64 mmol) of **49** dissolved in 15 ml of pyridine, were added in 96 h (high dilution condition). After complete addition that 200 ml of methylene chloride and 200 ml of water were added to the solution and the organic phase was separated and washed with water, 25 % aqueous NH_3 solution (until the aqueous phase stayed nearly colorless), 10 % acetic acid, 10 % sodium hydroxide, and saturated NaCl solution. The organic phase was dried over $MgSO_4$ and after filtration the solution was concentrated to 20 ml. A precipitate was formed after the addition of about 100 ml of methanol. After filtration, the crude product was purified by column chromatography. Two chromatographic purification were necessary. The first one using as eluent a of mixture petrol ether/methylene chloride (1:3) (R_f = 0.30), the second one using as eluent a mixture of petrol ether/methylene chloride (1:2) (R_f = 0.57). After evaporation of the solvent and drying under vacuum, 0.30 g (50 %) of **50** were obtained as a white powder.

Mp: > 250 °C (decomposition)

^{1}H NMR ($CDCl_3$): 1.32 (s, 36 H), 1.53 (m, 8 H), 1.81 (m, 8 H), 3.99 (t, J = 6.15 Hz, 4 H), 4.33 (t, J = 6.47 Hz, 4 H), 7.01 (d, J = 1.40 Hz, 4 H), 7.33 (t, J = 1.25 Hz, 4 H), 7.39-7.55 (m, 32 H), 8.03 (dt, J_1 = 6.95 Hz, J_2 = 1.43 Hz, 4 H).

^{13}C NMR ($CDCl_3$): 25.78, 25.86, 28.71, 29.07, 31.07, 34.80, 64.92, 68.09, 73.93, 81.32, 89.39, 89.46, 90.53, 90.75, 117.71, 121.84, 123.07, 123.25, 124.34, 128.35, 129.55, 131.65, 132.83, 133.13, 151.92, 158.89.

GPC (THF) Single peak M_w= 2500

MS (FD): m/z = 1713.9 [M^+]

$C_{126}H_{104}O_6$ (1714.17): **calc.**, C. 88.28, H. 6.12

found: C. 88.29, H. 6.19

7.3.21 Synthesis of the macrocycle 51

In a round flask, 0.4 g (0.23 mmol) of **50** were dissolved in 20 ml of THF. 2 ml of 10 % NaOH methanolic solution and 3 ml of 10 % aq. LiOH solution were added. The mixture was refluxed at 66 °C overnight. After cooling to room temperature, the solvent volume ml was reduced to about 5

and the macrocycle was precipitated with methanol. After filtration and drying under vacuum, 0.3 g (87 %) of **51** were obtained as a white powder.

Mp: > 250 °C

^{1}H NMR ($CDCl_3$): 1.32 (s, 36 H), 1.38-1.63 (m, 12 H), 1.81 (t, J = 6.9 Hz, 4 H), 3.66 (t, J = 6.3 Hz, 4 H), 3.98 (t, J = 6.57 Hz, 4 H), 7.01 (d, J = 1.25 Hz, 4 H), 7.33 (t, J = 1.27 Hz, 2 H), 7.51 (s, 20 H), 7.54 (t, J = 1.25 Hz, 8 H).

^{13}C NMR ($CDCl_3$): 25.57, 25.90, 29.20, 31.10, 32.76, 34.82, 62.92, 68.37, 74.03, 81.40, 89.46, 90.59, 90.81, 117.85, 121.97, 123.14, 123.39, 124.45, 127.97, 129.45, 131.68, 133.19, 152.01, 159.03.

GPC (THF) Single peak M_w= 2142

MS (FD): m/z = 1504.4 [M^+]

$C_{112}H_{96}O_4$ (1505.96): **calc.**, C. 89.33, H. 6.43

found: C. 88.78, H. 6.37

7.4 Synthesis of polystyrene carboxylic acids

7.4.1 General synthesis

Anionic polymerizations were carried out under nitrogen atmosphere. The polymerization system was dried by heating under vacuum and was purged several times with nitrogen. Cyclohexane previously distilled over butyl lithium and diphenylethane, was used as solvent. Styrene was dried with a suspension of 9-fluorenyllithium for some minutes and then distilled under vacuum.

100 ml of cyclohexane and 10 ml of styrene were mixed in a large ampoule, then the appropriate amount of 1.3 M sec-butyl lithium in hexane was added in the dry box. After 3 h more than 99 % of polystyrene has been formed. Before quenching the anionic chain 1 ml of solution was taken, quenched with methanol and investigated by GPC.

After that the cyclohexane solution of the polystyrene anion was added drop wise to THF saturated with CO_2 that was bobble inside the flask for circa 20 minutes in order to use a volume of circa 20 l. The reaction was complete when the red color of the typical of the anionic chain disappeared. In order to acidify the lithium salt hydrochloric acid in methanol was added until the solution was acid against the pH paper.

After evaporation of the solvent the polystyrene carboxylic acid was purified by column chromatography. Using toluene as eluent all impurities were easily removed (R_f = 0.92), while the polystryrene carboxylic acid stayed at the starting line. Further elution with THF and evaporation of the solvent gave the polymer as white powder.

7.4.1.1 Characterization of Polystyrene carboxylic acid M_w = 5000

^{1}H NMR ($CDCl_3$): 0.57-0.91 (m, $\underline{Bu^{sec}}$-$(CH_2$-$CHPh)_n$, 9 H), 1.24-1.50 (m, $(C\underline{H}_2$-$CHPh)_n$), 1.70-2.35 (m, $(CH_2$-$C\underline{H}Ph)_n$), 3.19 (br s, $(C\underline{H}_2$-$CHPh)_{n-1}$-$C\underline{H}_2$-CHPh-COOH), 6.30-7.25(m, $(C\underline{H}_2$-$CH\underline{Ph})_n$).

^{13}C NMR ($CDCl_3$): 17.2, 31.08, 31.55, 34.79, 40.60-41.58, 43.74-45.58, 49.5, 125.59-126.19, 127.57-131.13, 145.25-146.74, 178.8-179.8.

TGA: 410 °C

DSC: T_g = 88.38 °C

MS (MALDI-TOF): m/z = 5319.52 [M-Li^+], PD<1.1

$C_{405}H_{410}O_2$ (5302): **calc.**, C. 91.66, H. 7.73

found: C. 91.24, H. 7.94

7.4.1.2 Characterization of Polystyrene carboxylic acid M_w = 3500

^{1}H NMR ($CDCl_3$): 0.57-0.91 (m, $\underline{Bu^{sec}}$-$(CH_2$-$CHPh)_n$, 9 H), 1.24-1.51 (m, $(C\underline{H}_2$-$CHPh)_n$), 1.52-2.34 (m, $(CH_2$-$C\underline{H}Ph)_n$), 3.19 (br s, $(C\underline{H}_2$-$CHPh)_{n-1}$-$C\underline{H}_2$-CHPh-COOH), 6.38-7.24(m, $(C\underline{H}_2$-$CH\underline{Ph})_n$).

^{13}C NMR ($CDCl_3$): 17.2, 31.08, 31.55, 34.79, 40.60-41.58, 43.74-45.58, 49.5, 125.59-126.19, 127.57-131.13, 145.25-146.74, 178.8-179.8.

TGA: 420 °C

DSC: T_g = 77.03 °C

MS (MALDI-TOF): m/z = 3456.02 [M-Na^+], PD<1.1

$C_{261}H_{266}O_2$ (3430): **calc.**, C. 91.31, H. 7.55

found: C. 91.30, H. 7.45

7.4.1.3 Characterization of Polystyrene carboxylic acid M_w = 2500

^{1}H NMR ($CDCl_3$): 0.57-0.90 (m, $\underline{Bu^{sec}}$-$(CH_2$-$CHPh)_n$, 9 H), 1.30-1.51 (m, $(C\underline{H}_2$-$CHPh)_n$), 1.75-2.35 (m, $(CH_2$-$C\underline{H}Ph)_n$), 3.19 (br s, $(C\underline{H}_2$-$CHPh)_{n-1}$-$C\underline{H}_2$-CHPh-COOH), 6.30-7.25(m, $(C\underline{H}_2$-$CH\underline{Ph})_n$).

^{13}C NMR ($CDCl_3$): 17.2, 31.08, 31.55, 34.79, 40.60-41.58, 43.74-45.58, 49.5, 125.59-126.19, 127.57-131.13, 145.25-146.74, 178.8-179.8.

TGA: 410 °C

DSC: T_g = 82.53 °C

MS (MALDI-TOF): m/z = 2710.49 [M-Ag^+], PD<1.1

$C_{197}H_{202}O_2$ (2598): **calc.**, C. 90.99, H. 7.77

found: C. 90.74, H. 7.72

7.4.1.4 Characterization of Polystyrene carboxylic acid M_w = 1500

^{1}H NMR ($CDCl_3$): 0.56-1.05 (m, $\underline{Bu^{sec}}$-(CH_2-CHPh)$_n$, 9 H), 1.30-1.60 (m, ($C\underline{H_2}$-CHPh)$_n$), 1.75-2.34 (m, (CH_2-C$\underline{H}$Ph)$_n$), 3.18 (br s, ($C\underline{H_2}$-CHPh)$_{n-1}$-$C\underline{H_2}$-CHPh-COOH), 6.30-7.25(m, ($C\underline{H_2}$-CH$\underline{Ph}$)$_n$).

^{13}C NMR ($CDCl_3$): 17.2, 31.08, 31.55, 34.79, 40.60-41.58, 43.74-45.58, 49.5, 125.59-126.19, 127.57-131.13, 145.25-146.74, 178.8-179.8.

TGA: 410 °C

DSC: T_g = 56.79 °C

MS (MALDI-TOF): m/z = 1665.38 [M-Ag^+], PD<1.1

$C_{117}H_{122}O_2$ (1558): **calc.**, C. 90.11, H. 7.83

found: C. 88.96, H. 8.19

7.4.1.5 Characterization of Polystyrene carboxylic acid M_w = 1000

^{1}H NMR ($CDCl_3$): 0.56-0.90 (m, $\underline{Bu^{sec}}$-(CH_2-CHPh)$_n$, 9 H), 1.42-1.73 (m, ($C\underline{H_2}$-CHPh)$_n$), 1.84-2.29 (m, (CH_2-C$\underline{H}$Ph)$_n$), 3.18 (br s, ($C\underline{H_2}$-CHPh)$_{n-1}$-$C\underline{H_2}$-CHPh-COOH), 6.40-7.25(m, ($C\underline{H_2}$-CH$\underline{Ph}$)$_n$).

^{13}C NMR ($CDCl_3$): 17.2, 31.08 ,31.55, 34.79, 40.60-41.58, 43.74-45.58, 49.5, 125.59-126.19, 127.57-131.13, 145.25-146.74, 178.8-179.8.

TGA: 410 °C

DSC: T_g = 29.03 °C

MS (MALDI-TOF): m/z = 1249.28 [M-Ag^+], PD<1.1

$C_{85}H_{90}O_2$ (1142): **calc.**, C. 89.31, H. 7.88

found: C. 88.95, H. 8.06

7.5 Synthesis of polydimethylsiloxane carboxylic acids

7.5.1 General synthesis of polydimethylsiloxane

The polymerization system was dried by heating under vacuum and was purged several times with nitrogen. Cyclohexane was distilled over butyllithium and diphenylethane, and THF was distilled over potassium and then over butyllithium and diphenylethane. The ratio of the solvent was 40:60. Dimethylsiloxane was dried with a suspension of calcium hydride and then distilled. The reaction was performed under vapor pressure of the solvent.

In a large ampoule 10 % of hexamethylcyclotrisilane in cyclohexane solution was mixed with the appropriate amount of butyllithium (1.3 M in hexane) in the dry box. After 12 h, 90 % of the mixture was composed of Bu-Si$(CH_3)_2O^-$ anion. The rest of the monomer was added in such a

mixture of THF and cyclohexane solution that the final solvent system contained THF and cyclohexane in the ratio of 60:40. After 4 h the reaction was quenched with dimethyl chloro silane [$Si(CH_3)_2ClH$].

After evaporation of the solvent the polydimethylsiloxane was purified from the unreacted monomer by heating under vacuum at 80 °C overnight.

7.5.1.1 Characterization of Polydimethylsiloxane M_w = 1500

^{1}H NMR ($CDCl_3$): 0.00-0.10 (br s, $(Si(C\underline{H}_3)_2\text{-}O)_n$, 125.5 H), 0.16 (d, $\text{-}(Si(CH_3)_2\text{-}O)_{n-1}\text{-}Si(C\underline{H}_3)_2\text{-}H$, J = 2.67 Hz, 6 H), 0.52 (t, $CH_3\text{-}CH_2\text{-}CH_2\text{-}C\underline{H}_2\text{-}(Si(CH_3)_2\text{-}O)_n$, J = 7.87 Hz, 2 H), 0.86 (t, $C\underline{H}_3\text{-}CH_2\text{-}CH_2\text{-}CH_2\text{-}(Si(CH_3)_2\text{-}O)_n$, J = 6.62 Hz, 3 H), 1.20-1.35 (m, $CH_3\text{-}C\underline{H}_2\text{-}C\underline{H}_2\text{-}CH_2\text{-}(Si(CH_3)_2\text{-}O)_n$, 4 H), 4.68 (m, $\text{-}Si(CH_3)_2\text{-}\underline{H}$, J = 2.7 Hz, 1 H).

^{13}C NMR ($CDCl_3$): 0.19, 0.55, 0.69, 0.84, 1.05, 1.16, 1.54, 13.78, 18.01, 25.51, 26.38.

IR (neat):661.4, 703.1, 800.0, 913.1, 1023.9, 1093.7, 1260.9, 1412.6, 2127.9, 2962.5.

GPC: Single peak at 2167 g/mol, PD=1.35

MS (MALDI-TOF): m/z = 1545.3 [$M\text{-}Na^+$]

$C_{42}H_{124}O_{18}Si_{19}$ (1448): **calc.**: C. 34.80, H. 8.56

found: C. 34.45, H. 8.68

7.5.1.2 Characterization of Polydimethylsiloxane M_w = 3000

^{1}H NMR ($CDCl_3$): 0.00-0.10 (br s, $(Si(C\underline{H}_3)_2\text{-}O)_n$, 264 H), 0.16 (d, $\text{-}(Si(CH_3)_2\text{-}O)_{n-1}\text{-}Si(C\underline{H}_3)_2\text{-}H$, J = 1.70 Hz, 6 H), 0.52 (t, $CH_3\text{-}CH_2\text{-}CH_2\text{-}C\underline{H}_2\text{-}(Si(CH_3)_2\text{-}O)_n$, J = 8.01 Hz, 2 H), 0.86 (t, $C\underline{H}_3\text{-}CH_2\text{-}CH_2\text{-}CH_2\text{-}(Si(CH_3)_2\text{-}O)_n$, J = 6.87 Hz, 3 H), 1.22-1.34 (m, $CH_3\text{-}C\underline{H}_2\text{-}C\underline{H}_2\text{-}CH_2\text{-}(Si(CH_3)_2\text{-}O)_n$, 4 H), 4.68 (m, $\text{-}Si(CH_3)_2\text{-}\underline{H}$, J = 3.05 Hz, 1 H).

^{13}C NMR ($CDCl_3$): 0.17, 0.54, 0.68, 0.83, 1.03, 1.16, 1.53, 13.77, 17.98, 25.46, 26.35.

IR (neat):661.4, 703.1, 800.0, 913.1, 1023.9, 1093.7, 1260.9, 1412.6, 2127.9, 2962.5.

GPC: Single peak at 2132 g/mol, PD=1.42

MS (MALDI-TOF): m/z = 2438 [$M\text{-}Na^+$]

$C_{68}H_{202}O_{31}Si_{32}$ (2410): **calc.**: C. 33.85, H. 8.38

found: C. 33.57, H. 8.32

7.5.1.3 Characterization of Polydimethylsiloxane M_w = 5000

^{1}H NMR ($CDCl_3$): 0.00-0.10 (br s, $(Si(C\underline{H}_3)_2\text{-}O)_n$, 324 H), 0.16 (d, $\text{-}(Si(CH_3)_2\text{-}O)_{n-1}\text{-}Si(C\underline{H}_3)_2\text{-}H$, J = 2.67 Hz, 6 H), 0.51 (t, $CH_3\text{-}CH_2\text{-}CH_2\text{-}C\underline{H}_2\text{-}(Si(CH_3)_2\text{-}O)_n$, J = 8.01 Hz, 2 H), 0.86 (t, $C\underline{H}_3\text{-}CH_2\text{-}CH_2\text{-}$

CH_2-($Si(CH_3)_2$-O)$_n$, J = 6.87 Hz, 3 H), 1.23-1.32 (m, CH_3-C<u>H</u>$_2$-C<u>H</u>$_2$-CH_2-($Si(CH_3)_2$-O)$_n$, 4 H), 4.68 (m, -$Si(CH_3)_2$-<u>H</u>, J = 2.67 Hz, 1 H).

^{13}C NMR ($CDCl_3$): 0.17, 0.54, 0.68, 0.83, 1.03, 1.14, 1.53, 13.77, 17.98, 25.46, 26.34.

IR (neat):661.4, 703.1, 800.0, 913.1, 1023.9, 1093.7, 1260.9, 1412.6, 2127.9, 2962.5.

GPC: Single peak at 3155 g/mol, PD=1.39

MS (MALDI-TOF): m/z = 3772 [M-Na^+]

$C_{104}H_{310}O_{49}Si_{50}$ (3742): **calc.**: C. 33.35, H. 8.28

found: C. 33.15, H. 8.27

7.5.2 Synthesis of Benzenyl-4-pentenoate (52)

In a round flask 2.14 g (18 mmol) of 4-penteneacylchloride and 1.95 g (18 mmol) of benzyl chloride were dissolved in 30 ml of methylene chloride. To this solution 1.42 g (18 mmol) of pyridine were slowly added and the mixture was stirred overnight. The solvent was evaporated and diethyl ether and water were added. The organic phase was separated and washed with water, 10 % acetic acid, 10 % sodium hydroxide, and saturated NaCl solution. After drying over $MgSO_4$, filtration and evaporation of the solvent, 2.83 g (83 %) of **52** were obtained as a yellow oil.

^{1}H NMR ($CDCl_3$): 2.27-2.43 (m, CH_2=CH-C<u>H</u>$_2$-C<u>H</u>$_2$-, 4 H), 4.93 (dd, C<u>H</u>$_A$H$_B$=CH-CH_2, J_1 = 10.12 Hz, J_2 = 1.27 Hz, 1 H), 5.03 (dd, CH_A<u>H</u>$_B$=CH-CH_2, J_1 = 10.12 Hz, J_2 = 1.27 Hz, 1 H), 5.05 (s, -COO-C<u>H</u>$_2$-Ph , 2 H), 5.67-5.83 (m, CH_2=C<u>H</u>-CH_2-CH_2, 1 H), 7.23-7.28 (m, -COO-CH_2-<u>Ph</u> , 5 H).

^{13}C NMR ($CDCl_3$): 28.97, 33.65, 66.28, 115.66, 127.01, 127.54, 128.31, 128.56, 128.64, 136.21, 136.72, 172.85.

IR (neat):697.9, 750.7, 916.1, 1002.6, 1165.9, 1258.6, 1350.7, 1382.6, 1417.9, 1455.2, 1497.8, 1641.7, 1737.4, 2341.3, 2360.2, 2950.5, 3067.2.

MS (EI): m/z = 189.9 [M^+].

$C_{12}H_{14}O_2$(190.1): **calc.**: C. 75.76, H. 7.42

found: C. 75.32, H. 7.23

7.5.3 General synthesis of Polydimethylsiloxane-$(CH_2)_4$-COO-CH_2-Ph

Under an argon atmosphere, polydimethylsiloxane and two equivalent of benzyl-4-pentenoate (**52**) were mixed in 40 ml of freshly distilled toluene and then 0.5 mg of H_2PtCl_6 were added. The mixture was refluxed at 100 °C and the reaction was followed by IR: The disappearance of the absorption band at 2120 cm^{-1} indicates that all Si-H groups have reacted. When the reaction was complete (12

h), the mixture was cooled down and the solution filtered through two filter most of to try to eliminate the catalyst. After evaporation of the solvent the product was filtered over a short column of silica gel using methylene chloride as eluent (R_f =0.43).

7.5.3.1 Characterization of Polydimethylsiloxane-$(CH_2)_4$-COO-CH_2-Ph (55) (M_w = 1500)

^{1}H NMR ($CDCl_3$): 0.00-0.10 (br s, $(Si(C\underline{H}_3)_2\text{-}O)_n$, 136 H), 0.50-0.56 (m, -$Si(CH_3)_2O\text{-}CH_2\text{-}C\underline{H}_2\text{-}C\underline{H}_2\text{-}CH_2\text{-}COOCH_2Ph$, 4 H), 0.87 (t, $C\underline{H}_3\text{-}CH_2\text{-}CH_2\text{-}CH_2\text{-}(Si(CH_3)_2\text{-}O)_n$, J = 6.85 Hz, 3 H), 1.22-1.33 (m, 6 H), 1.63 (m, -$Si(CH_3)_2O\text{-}CH_2\text{-}CH_2\text{-}C\underline{H}_2\text{-}CH_2\text{-}COOCH_2Ph$, J = 7.27 Hz, 2 H), 2.35 (t, -$Si(CH_3)_2O\text{-}CH_2\text{-}CH_2\text{-}CH_2\text{-}C\underline{H}_2\text{-}COOCH_2Ph$, J = 7.42 Hz, 2 H), 5.10 (s,-$COOC\underline{H}_2Ph$, 2 H), 7.06-7.33 (m, ,-$COOCH_2\underline{Ph}$, 5 H).

^{13}C NMR ($CDCl_3$): 0.18, 0.23, 0.59, 1.09, 1.20, 1.58, 13.82, 18.00, 22.97, 25.52, 26.40, 28,60, 34.16, 66.09, 128.19, 128.59, 136.29,173.62.

Yield: 70 %

GPC: Single peak at 1752 g/mol, PD=1.19

IR (neat): 726.8, 805.0, 1029.6, 1094.6, 1260.6, 1495.8, 1604.4, 1739.6, 2961.1, 3027.5.

MS (MALDI-TOF): m/z = 1739.26 [M-Na^+].

$C_{54}H_{140}O_{20}Si_{19}$ (1640): **calc.**: C. 39.51, H. 8.53

found: C. 39.64, H. 8.54

7.5.3.2 Characterization of Polydimethylsiloxane-$(CH_2)_4$-COO-CH_2-Ph (56) (M_w = 3000)

^{1}H NMR ($CDCl_3$): 0.00-0.10 (br s, $(Si(C\underline{H}_3)_2\text{-}O)_n$, 205 H), 0.48-0.55 (m, -$Si(CH_3)_2O\text{-}CH_2\text{-}C\underline{H}_2\text{-}C\underline{H}_2\text{-}CH_2\text{-}COOCH_2Ph$, 4 H), 0.86 (t, $C\underline{H}_3\text{-}CH_2\text{-}CH_2\text{-}CH_2\text{-}(Si(CH_3)_2\text{-}O)_n$, J = 6.62 Hz, 3 H), 1.23-1.37 (m, 6 H), 1.65 (m, -$Si(CH_3)_2O\text{-}CH_2\text{-}CH_2\text{-}C\underline{H}_2\text{-}CH_2\text{-}COOCH_2Ph$, J = 7.57 Hz, 2 H), 2.34 (t, -$Si(CH_3)_2O\text{-}CH_2\text{-}CH_2\text{-}CH_2\text{-}C\underline{H}_2\text{-}COOCH_2Ph$, J = 7.42 Hz, 2 H), 5.09 (s,-$COOC\underline{H}_2Ph$, 2 H), 7.06-7.33 (m, ,-$COOCH_2\underline{Ph}$, 5 H).

^{13}C NMR ($CDCl_3$): 0.15, 0.23, 0.43, 1.02, 1.14, 1.60, 13.78, 17.90, 22.88, 25.43, 26.35, 28,53, 34.08, 66.03, 128.13, 128.52, 128.72,173.62.

Yield: 70 %

GPC: Single peak at 2596 g/mol, PD=2.45

IR (neat): 726.8, 805.0, 1029.6, 1094.6, 1260.6, 1495.8, 1604.4, 1739.6, 2961.1, 3027.5.

MS (MALDI-TOF): m/z = 2404 [M-Na^+].

$C_{80}H_{216}O_{33}Si_{32}$ (2600): **calc.**: C. 36.92, H. 8.30

found: C. 36.93, H. 8.53

7.5.3.3 Characterization of Polydimethylsiloxane-$(CH_2)_4$-COO-CH_2-Ph (57) (M_w = 5000)

^{1}H NMR ($CDCl_3$): 0.00-0.10 (br s, $(Si(C\underline{H}_3)_2\text{-}O)_n$, 289 H), 0.48-0.55 (m, $\text{-}Si(CH_3)_2O\text{-}CH_2\text{-}C\underline{H}_2\text{-}C\underline{H}_2\text{-}CH_2\text{-}COOCH_2Ph$, 4 H), 0.86 (t, $C\underline{H}_3\text{-}CH_2\text{-}CH_2\text{-}CH_2\text{-}(Si(CH_3)_2\text{-}O)_n$, J = 6.95 Hz, 3 H), 1.23-1.37 (m, 6 H), 1.65 (m, $\text{-}Si(CH_3)_2O\text{-}CH_2\text{-}CH_2\text{-}C\underline{H}_2\text{-}CH_2\text{-}COOCH_2Ph$, J = 7.57 Hz, 2 H), 2.34 (t, $\text{-}Si(CH_3)_2O\text{-}CH_2\text{-}CH_2\text{-}CH_2\text{-}C\underline{H}_2\text{-}COOCH_2Ph$, J = 7.42 Hz, 2 H), 5.09 (s,$\text{-}COOC\underline{H}_2Ph$, 2 H), 7.06-7.33 (m, ,$\text{-}COOCH_2\underline{Ph}$, 5 H).

^{13}C NMR ($CDCl_3$): 0.11, 0.16, 0.43, 1.14, 1.61, 13.79, 17.91, 22.89, 25.44, 26.36, 28,53, 34.09, 66.04, 128.14, 128.53, 128.72,173.92.

Yield: 80 %

GPC: Single peak at 4195 g/mol, PD=1.65

IR (neat): 726.8, 805.0, 1029.6, 1094.6, 1260.6, 1495.8, 1604.4, 1739.6, 2961.1, 3027.5.

MS (MALDI-TOF): m/z = 3960 [M-Na^+].

$C_{116}H_{324}O_{51}Si_{50}$ (3932): **calc.**: C. 35.40, H. 8.24

found: C. 35.35, H. 8.11

7.5.4 General synthesis of Polydimethylsiloxane-$(CH_2)_4$-COOH

180 mg of Palladium on carbon were added to a solution of polydimethylsiloxan-$(CH_2)_4$-$COOCH_2Ph$ in 40 ml of freshly distilled toluene in a two necks flask under an argon atmosphere. The flux of argon was replaced by hydrogen that was bubbled by a needle through the solution for 20 minutes. The mixture was stirred vigorously for 2 days. When the reaction was complete (TLC control), THF was added and the mixture was filtered to eliminate part of the catalyst. After evaporation of the solvent the product was purified over a short column of silica gel using as eluent toluene.

7.5.4.1 Characterization of Polydimethylsiloxane-$(CH_2)_4$-COOH (58) (M_w = 1500)

^{1}H NMR ($CDCl_3$): 0.00-0.10 (br s, $(Si(C\underline{H}_3)_2\text{-}O)_n$, 136 H), 0.48-0.56 (m, $\text{-}Si(CH_3)_2O\text{-}CH_2\text{-}C\underline{H}_2\text{-}C\underline{H}_2\text{-}CH_2\text{-}COOH$, 4 H), 0.85 (t, $C\underline{H}_3\text{-}CH_2\text{-}CH_2\text{-}CH_2\text{-}(Si(CH_3)_2\text{-}O)_n$, J = 6.85 Hz, 3 H), 1.21-1.40 (m, 8 H),1.63 (m, $\text{-}Si(CH_3)_2O\text{-}CH_2\text{-}CH_2\text{-}C\underline{H}_2\text{-}CH_2\text{-}COOH$, J = 7.33 Hz, 2 H), 2.30 (q, $\text{-}Si(CH_3)_2O\text{-}CH_2\text{-}CH_2\text{-}CH_2\text{-}C\underline{H}_2\text{-}COOH$, J = 7.33 Hz, 2 H).

^{13}C NMR ($CDCl_3$): 0.18, 0.21, 0.57, 1.07, 1.17, 1.56, 13.80, 18.02, 25.51, 26.39, 28,29, 29.49, 30.39, 33.80, 179.76.

Yield: 83 %

MS (MALDI-TOF): m/z = 1645.41 [M-Na^+]

IR (neat): 703.1, 800.0, 1022.8, 1093.7, 1260.8, 1412.8, 1713.4, 2962.5.

$C_{47}H_{133}O_{20}Si_{19}$ (1549): **calc.**: C. 36.41, H. 8.58

found: C. 36.62, H. 8.75

7.5.4.2 Characterization of Polydimethylsiloxane-$(CH_2)_4$-COOH (59) (M_w = 3000)

^{1}H NMR ($CDCl_3$): 0.00-0.10 (br s, $(Si(C\underline{H}_3)_2\text{-}O)_n$, 210 H), 0.48-0.56 (m, $\text{-}Si(CH_3)_2O\text{-}CH_2\text{-}C\underline{H}_2\text{-}C\underline{H}_2\text{-}CH_2\text{-}COOH$, 4 H), 0.86 (t, $C\underline{H}_3\text{-}CH_2\text{-}CH_2\text{-}CH_2\text{-}(Si(CH_3)_2\text{-}O)_n$, J = 6.85 Hz, 3 H), 1.21-1.41 (m, 8 H),1.64 (m, $\text{-}Si(CH_3)_2O\text{-}CH_2\text{-}CH_2\text{-}C\underline{H}_2\text{-}CH_2\text{-}COOH$, J = 7.33 Hz, 2 H), 2.33 (q, $\text{-}Si(CH_3)_2O\text{-}CH_2\text{-}CH_2\text{-}CH_2\text{-}C\underline{H}_2\text{-}COOH$, J = 7.33 Hz, 2 H).

^{13}C NMR ($CDCl_3$): 0.16, 0.21, 0.43, 1.03, 1.14, 1.61, 13.06, 17.94, 22.82, 25.43, 26,36, 28.03, 27.25, 33.80, 179.76.

Yield: 85 %

MS (MALDI-TOF): not detectable.

IR (neat): 703.1, 800.0, 1022.8, 1093.7, 1260.8, 1412.8, 1713.4, 2962.5.

$C_{73}H_{210}O_{33}Si_{32}$ (2510): **calc.**: C. 34.90, H. 8.36

found: C. 34.29, H. 8.71

7.5.4.3 Characterization of Polydimethylsiloxane-$(CH_2)_4$-COOH (60) (M_w = 5000)

^{1}H NMR ($CDCl_3$): 0.00-0.10 (br s, $(Si(C\underline{H}_3)_2\text{-}O)_n$, 276 H), 0.48-0.56 (m, $\text{-}Si(CH_3)_2O\text{-}CH_2\text{-}C\underline{H}_2\text{-}C\underline{H}_2\text{-}CH_2\text{-}COOH$, 4 H), 0.86 (t, $C\underline{H}_3\text{-}CH_2\text{-}CH_2\text{-}CH_2\text{-}(Si(CH_3)_2\text{-}O)_n$, J = 6.12 Hz, 3 H), 1.21-1.41 (m, 8 H),1.57-1.66 (m, $\text{-}Si(CH_3)_2O\text{-}CH_2\text{-}CH_2\text{-}C\underline{H}_2\text{-}CH_2\text{-}COOH$, 2 H), 2.29-2.35 (m, $\text{-}Si(CH_3)_2O\text{-}CH_2\text{-}CH_2\text{-}CH_2\text{-}C\underline{H}_2\text{-}COOH$, 2 H).

^{13}C NMR ($CDCl_3$): 0.16, 0.52, 1.01, 1.13, 1.51, 13.64, 13.75, 17.93, 17.97, 22.21, 22.87, 25.46, 26.33, 26.87, 28.34, 29.45, 30.36, 33.60, 34.24, 41.56, 125.51, 125.91, 125.97, 128.23, 128.28, 128.38, 128.42, 128.74, 128.82, 128.88, 128.93, 129.04, 129.14, 135.87, 149.29.

Yield: 88 %

MS (MALDI-TOF): no detectable

IR (neat): 703.1, 800.0, 1022.8, 1093.7, 1260.8, 1412.8, 1713.4, 2962.5.

$C_{109}H_{318}O_{51}Si_{50}$ (3852): **calc.**: C. 33.95, H. 8.27

found: C. 33.45, H. 8.27

7.6 Synthesis of polystyrene-macrocycle-polystyrene block copolymers

7.6.1 General synthesis

In all cases the synthesis was performed using the same procedure and the same conditions. As example here it's reported the synthesis of the block copolymer at the macrocycle **51** and polystyrene carboxylic acid of M_w = 2500.

Under an argon atmosphere, 50 mg ($3.32\ 10^{-5}$ mol) of macrocycle **51**, 182 mg ($7.31\ 10^{-5}$ mol) of polystyrene carboxylic acid of M_w = 2500 and 43 mg of 4-(dimethylamino)pyridinium 4-toluenesulfonate (DPTS) ($1.46\ 10^{-4}$ mol) were dissolved in 10-15 ml of water free methylene chloride. In order to improve the solubilization of the compounds, the mixture was gently warmed and then cooled to room temperature. To the solution 18 mg ($1.46\ 10^{-4}$ mol) of diisopropyl carbodiimide were added and the mixture was stirred for three days at room temperature. The solvent was evaporated and the crude product was purified by column chromatography using as eluent methylene chloride (R_f = 0.93). After evaporation of the solvent and drying under vacuum, 180 mg (94 %) of **68** were obtained as a white powder.

It is strongly advised not to perform an aqueous work-up.

7.6.1.1 Characterization of Block Copolymer 65

^{1}H NMR ($CDCl_3$): 0.56-0.68 (m, 12 H), 0.84-0.89 (m, 6 H), 1.31 (s, 36 H), 1.20-2.22 (m, 346 H), 2.26 (s, 6 H), 3.76 (m, 4 H), 4.11 (m, 4 H), 6.30-7.20 (m, 520 H), 7.33 (d, *J* = 8.37 Hz, 8 H), 7.48-7.55 (m, 28 H), 7.62 (m, 8 H).

^{13}C NMR ($CDCl_3$): 17.2, 31.08, 31.54, 34.78, 40.42-42.10, 42.51-46.07, 64.23, 73.63, 81.40, 88.82, 89.84, 114.91, 120.82, 121.77, 123.53, 125.30-126.00, 127.32-128.15, 130.0, 130.96, 131.44, 141.89, 142.29, 145.23-146.15, 151.85.

Yield: 85 %

TGA: 420 °C

DSC: Tg = 103.10 °C

GPC: Single peak at 14150 g/mol, PD = 1.02.

MS (MALDI-TOF): m/z = 11850.9 [M-Na^+].

$C_{966}H_{938}O_6$ (12626): **calc.**, C. 91.81, H. 7.42

found: C. 90.75, H. 7.87

7.6.1.2 Characterization of Block Copolymer 66

^{1}H NMR ($CDCl_3$): 0.55-0.68 (m, 12 H), 0.86 (t, *J* = 6.48 Hz, 6 H), 1.01-2.20 (m, 270 H), 3.72 (t, *J* = 6.48 Hz, 4 H), 3.88 (m, 4 H), 6.41-7.06 (m, 388 H), 7.45-7.48 (m, 28 H).

^{13}C NMR ($CDCl_3$): 25.54, 28.36, 28.98, 29.69, 31.07, 31.57, 34.79, 40.45, 43.71, 43.93, 44.26, , 45.97, 64.41, 68.12, 73.95, 81.33, 89.40, 89.48, 90.53, 90.77, 117.70, 121.85, 123.02, 123.07, 123.26, 124.34, 125.48-125.64, 126.76-128.63, 131.65, 133.12, 145.23, 145.32, 145.65, 146.11, 151.92, 158.87.

Yield: 39 %

TGA: 420 °C

DSC: T_g = 99.83 °C

GPC: Single peak at 12540 g/mol, PD = 1.06

MS (MALDI-TOF): m/z = 12190.3 [M-Ag^+].

$C_{922}H_{912}O_6$ (12072): **calc.**, C. 91.65, H. 7.55

found: C. 91.32, H. 7.88

7.6.1.3 Characterization of Block Copolymer 67

^{1}H NMR ($CDCl_3$): 0.57-0.72 (m, 12 H), 0.84-0.89 (m, 6 H), 1.09-2.05 (m, 305 H), 1.35 (s, 36 H), 3.70-3.40 (m, 8 H), 6.40-7.09 (m, 366 H), 7.53 (br s, 20 H), 7.58 (m, *J* = 1.5 Hz, 28 H).

^{13}C NMR ($CDCl_3$): 25.53, 28.36, 28.98, 29.68, 31.07, 31.54, 34.78, 40.44, 41.88, 42.85, 44.26, 44.86, 45.88, 64.46, 68.10, 73.95, 81.32, 89.40, 89.48, 90.53, 90.76, 117.70, 121.85, 123.02, 123.07, 123.26, 124.34, 125.47, 125.64, 127.31-129.44, 131.65, 133.12, 145.23, 145.32, 145.65, 146.11, 151.92, 158.87.

Yield: 64 %

TGA: 410 °C

DSC: Tg = 94.50 °C

GPC: Single peak at 10010 g/mol, PD = 1.04

MS (MALDI-TOF): m/z = 8463.8 [M-Na^+]

$C_{634}H_{624}O_6$ (8328): **calc.**, C. 91.35, H. 7.49

found: C. 90.59, H. 7.99

7.6.1.4 Characterization of block copolymer 68

^{1}H NMR ($CDCl_3$): 0.57-0.71 (m, 12 H), 0.85-0.90 (m, 6 H), 1.09-2.05 (m, 198 H), 3.76-3.92 (m, 8 H), 6.40-7.08 (m, 283 H), 7.52 (br s, 20 H), 7.57 (m, *J* = 1.5 Hz, 28 H).

^{13}C NMR ($CDCl_3$): 25.54, 29.00, 29.68, 30.34, 31.06, 31.54, 34.79, 40.33-40.84, 42.64-45.97, 54.86, 64.42, 68.09, 73.94, 81.32, 89.39, 89.47, 90.53, 90.75, 117.69, 121.84, 123.02, 123.07, 123.26, 124.34, 125.47, 125.63, 127.32-128.39, 129.47, 131.65, 133.12, 144.77-146.11, 151.92, 158.87.

Yield: 84 %

TGA: 420 °C

DSC: Tg = 91.25 °C

GPC: Single peak at 8171 g/mol, PD=1.04

MS (MALDI-TOF): m/z = 6587.0 [M-Na^+]

$C_{490}H_{482}O_6$ (6458): **calc.**, C. 91.04, H. 7.46

found: C. 90.11, H. 8.17

7.6.1.5 Characterization of block copolymer 69

^{1}H NMR ($CDCl_3$): 0.46-0.65 (m, 12 H), 0.73-0.90 (m, 6 H), 1.01-2.33 (m, 200 H), 3.70-3.90 (m, 8 H), 6.41-7.05 (m, 140 H), 7.41-7.48 (m, 28 H).

^{13}C NMR ($CDCl_3$): 25.54, 28.31, 28.99, 29.48, 29.69, 30.35, 31.07, 31.45, 31.56, 34.22, 34.80, 40.33-40.84, 44.03-45.90, 54.86, 64.42, 68.09, 73.95, 81.32, 89.40, 89.47, 90.54, 90.77, 117.69, 121.86, 123.02, 123.09, 123.27, 124.35, 125.50, 125.65, 125.77, 127.14-128.80, 129.45, 131.66, 133.13, 135.83, 144.94-146.59, 151.93, 158.89.

Yield: 86 %

TGA: 410 °C

DSC: Tg = 58.96 °C

GPC: Single peak at 5169 g/mol, PD = 1.08.

MS (MALDI-TOF): m/z = 4194 [M-Na^+].

$C_{346}H_{336}O_6$ (4586): **calc.**, C. 90.53, H. 7.38

found: C. 87.69, H. 8.01

7.6.1.6 Characteristics of block copolymer 70

^{1}H NMR ($CDCl_3$): 0.50-0.71 (m, 12 H), 0.83-0.95 (m, 6 H), 1.03-2.27 (m, 108 H), 3.76-3.92 (m, 8 H), 6.43-7.30 (m, 98 H), 7.52 (br s, 20 H), 7.57 (m, J = 1.5 Hz, 28 H).

^{13}C NMR ($CDCl_3$): 18.53, 19.85, 25.47, 25.55, 28.36, 28.99, 29.47, 29.68, 30.34, 31.06, 31.45, 31.55, 34.22, 34.78, 40.33-40.84, 44.03-45.90, 49.16, 49.28, 49.33, 49.52, 64.42, 68.09, 74.03, 81.40, 89.39, 89.48, 90.53, 90.75, 117.69, 121.84, 123.02, 123.07, 123.26, 124.34, 125.50, 125.64, 125.77, 126.16, 127.04, 127.34, 127.67-128.50, 129.43, 131.65, 133.12, 135.83, 144.77-146.23, 151.91, 158.86.

Yield: 32 %

GPC: Single peak at 4735 g/mol, PD = 1.05

MS (MALDI-TOF): m/z = 3464 [M-Na^+]

7.7 Synthesis of polydimethylsiloxane-macrocycle-polydimethylsiloxane block copolymers

7.7.1 General synthesis

In all cases the synthesis was performed using the same procedure and the same conditions. As example the synthesis of the block copolymer of the macrocycle **51** and the polydimethylsiloxane carboxylic acid of **58** (M_w = 1500).

Under an argon atmosphere, 51.5 mg (3.42 10^{-5} mol) of macrocycle **51**, 143 mg (7.53 10^{-5} mol) of polydimethylsiloxane carboxylic acid **58** and 44 mg of 4-(dimethylamino)pyridinium 4-toluenesulfonate (DPTS) (1.5 10^{-4} mol) were dissolved in 10-15 ml of water free methylene chloride. In order to improve the solubilization of the compounds, the mixture was gently warmed and then cooled to room temperature. To the solution 19 mg (1.5 10^{-4} mol) of diisopropyl carbodiimide were added and the mixture was stirred for four days at room temperature. After that the solvent was evaporated and the crude product was purified by column chromatography using as eluent methylene chloride (R_f = 0.87). After evaporation of the solvent and drying under vacuum, 150 mg (96 %) of compound **71** were obtained.

7.7.1.1 Characterization of Block Copolymer 71

^{1}H NMR ($CDCl_3$): 0.00-0.10 (br s, $(Si(C\underline{H}_3)_2\text{-}O)_n$, 348 H), 0.48-0.56 (m, $\text{-}Si(CH_3)_2O\text{-}CH_2\text{-}C\underline{H}_2\text{-}C\underline{H}_2\text{-}CH_2\text{-}COOH$, 8 H), 0.85 (t, $C\underline{H}_3\text{-}CH_2\text{-}CH_2\text{-}CH_2\text{-}(Si(CH_3)_2\text{-}O)_n$, *J* = 6.87 Hz, 6 H), 1.21-1.41 (m, 16 H), 1.32(s, Bu^{ter}, 36 H), 1.64 (m, $\text{-}Si(CH_3)_2O\text{-}CH_2\text{-}CH_2\text{-}C\underline{H}_2\text{-}CH_2\text{-}COOH$, *J* = 7.33 Hz, 4 H), 2.28 (t, $\text{-}Si(CH_3)_2O\text{-}CH_2\text{-}CH_2\text{-}CH_2\text{-}C\underline{H}_2\text{-}COOH$, *J* = 7.23 Hz, 4 H), 3.98 (t, J = 6.09 Hz, 4 H), 4.06 (t, J = 6.84 Hz, 4 H), 7.01 (d, J = 1.14 Hz, 4 H), 7.33 (t, J = 1.14 Hz, 2 H), 7.49-7.51 (br s, 18 H), 7.54 (m, J = 2.28 Hz, 2 H).

^{13}C NMR ($CDCl_3$):0.13, 0.15, 0.43, 1.02, 1.14, 1.61, 13.78, 17.92, 22.91, 25.42, 25.73, 26.34, 28.59, 29.07, 31.05, 34.13, 34.78, 64.18, 68.13, 73.87, 81.27, 89.35, 89.42, 90.48, 90.70, 117,67, 121.76, 122.97, 123.01, 123.19, 124.28, 129.45, 131.63, 133.07, 149.29, 151.87, 158.84.

Yield: 96 %

TGA: 440 °C

DSC: Tg = -116.75 °C

GPC: Two peaks between 1100 and 6300 g/mol, PD = 1.51.

MS (MALDI-TOF): m/z = 4742.12 [M-Na^+].

$C_{206}H_{358}O_{42}Si_{38}$ (4566): **calc.**, C. 54.13, H. 7.84

found: C. 50.34, H. 7.22

7.7.1.2 Characterization of Block Copolymer 72

^{1}H NMR ($CDCl_3$): 0.00-0.10 (br s, $(Si(C\underline{H}_3)_2\text{-}O)_n$), 0.48-0.53 (m, $\text{-}Si(CH_3)_2O\text{-}CH_2\text{-}C\underline{H}_2\text{-}C\underline{H}_2\text{-}CH_2\text{-}COOH$, 8 H), 0.85 (t, $C\underline{H}_3\text{-}CH_2\text{-}CH_2\text{-}CH_2\text{-}(Si(CH_3)_2\text{-}O)_n$, *J* = 6.87 Hz, 6 H), 1.22-1.41 (m, 16 H), 1.32 (s, Bu^{ter}, 36 H), 1.64 (m, $\text{-}Si(CH_3)_2O\text{-}CH_2\text{-}CH_2\text{-}C\underline{H}_2\text{-}CH_2\text{-}COOH$, *J* = 7.33 Hz, 4 H), 2.29 (t, $\text{-}Si(CH_3)_2O\text{-}CH_2\text{-}CH_2\text{-}CH_2\text{-}C\underline{H}_2\text{-}COOH$, *J* = 8.4 Hz, 4 H), 3.96 (t, J = 6.09 Hz, 4 H), 4.07 (t, J = 6.48 Hz, 4 H), 7.01 (d, J = 1.14 Hz, 4 H), 7.32 (m, 2 H), 7.49-7.51 (br s, 18 H), 7.54 (m, J = 2.28 Hz, 2 H).

^{13}C NMR ($CDCl_3$): 0.16, 0.43, 1.02, 1.14, 1.61, 13.78, 17.92, 22.91, 25.42, 25.73, 26.34, 28.59, 29.07, 31.05, 34.13, 34.78, 64.18, 68.13, 73.87, 81.27, 89.35, 89.42, 90.48, 90.70, 117,67, 121.76, 122.97, 123.01, 123.19, 124.28, 129.45, 131.63, 133.07, 149.29, 151.87, 158.84.

Yield: 50 %

TGA: 490 °C

DSC: T_g = -123.65, T_{cryst} = -75,72 °C, T_m = -50,52 °C

GPC: Single peak at 3812 g/mol, PD = 2.22

MS (MALDI-TOF): No peaks could be detected.

$C_{258}H_{512}O_{68}Si_{64}$ (6488): **calc.**, C. 47.71, H. 7.89

found: C. 39.14, H. 7.49

7.7.1.3 Characterization of Block Copolymer 73

^{1}H NMR ($CDCl_3$): 0.00-0.10 (br s, $(Si(C\underline{H}_3)_2\text{-}O)_n$), 0.48-0.55 (m, $\text{-}Si(CH_3)_2O\text{-}CH_2\text{-}C\underline{H}_2\text{-}C\underline{H}_2\text{-}CH_2\text{-}COOH$, 8 H), 0.86 (t, $C\underline{H}_3\text{-}CH_2\text{-}CH_2\text{-}CH_2\text{-}(Si(CH_3)_2\text{-}O)_n$, *J* = 6.87 Hz, 6 H), 1.22-1.41 (m, 16 H), 1.32 (s, Bu^{ter}, 36 H), 1.65 (m, $\text{-}Si(CH_3)_2O\text{-}CH_2\text{-}CH_2\text{-}C\underline{H}_2\text{-}CH_2\text{-}COOH$, *J* = 7.33 Hz, 4 H), 2.29 (t, $\text{-}Si(CH_3)_2O\text{-}CH_2\text{-}CH_2\text{-}CH_2\text{-}C\underline{H}_2\text{-}COOH$, *J* = 6.87 Hz, 4 H), 3.98 (t, J = 6.48 Hz, 4 H), 4.07 (t, J = 6.48 Hz, 4 H), 7.01 (d, J = 1.14 Hz, 4 H), 7.33 (m, 2 H), 7.49-7.51 (br s, 18 H), 7.54 (m, J = 2.28 Hz, 2 H).

^{13}C NMR ($CDCl_3$): 0.16, 0.52, 1.02, 1.14, 1.50, 13.75, 17.96, 18.66, 25.45, 26.32, 28.59, 30.34, 31.07, 34.10, 34.80, 64.18, 68.13, 73.87, 81.27, 89.35, 89.42, 90.48, 90.70, 117,67, 121.76, 122.97, 123.01, 123.19, 124.28, 129.45, 131.63, 133.07, 149.29, 151.87, 158.84.

Yield: 50 %

TGA: 520 °C

DSC: T_{cryst} = -76,94 °C, T_m = -49,76 °C

GPC: Single peak at 8510 g/mol, PD = 1.45.

MS (MALDI-TOF): No peaks could be detected.

$C_{330}H_{728}O_{104}Si_{100}$ (9152): **calc.**, C. 43.26, H. 7.95

found: C. 38.20, H. 8.28

APPENDIX A

Data of the single c rystal structure of compound 14**.**

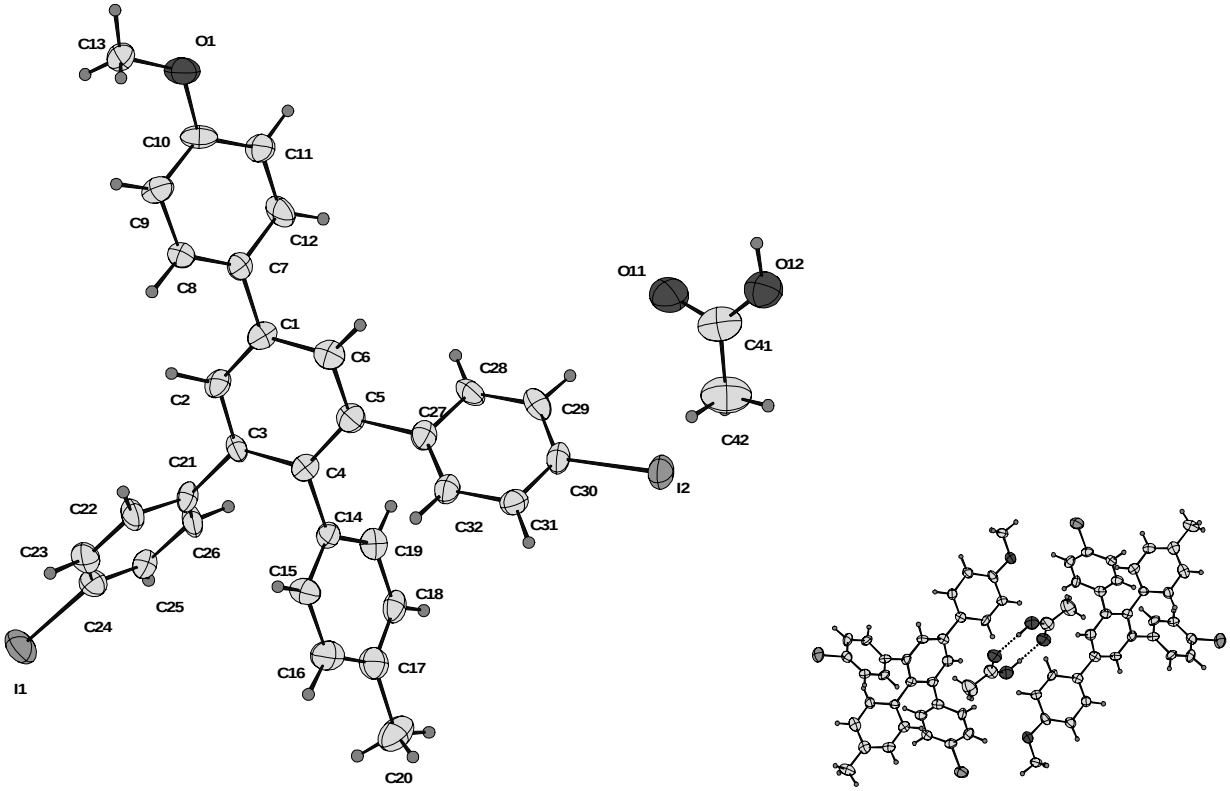

Table 1: Atomic coordinates, isotropic temperature factor and occupancy for the single crystal structure of compound **14**

Atom	x/a	y/b	z/c	U(iso)	Occ
I(1)	-0.27409(6)	0.37410(14)	-0.45853(4)	0.0738	
I(2)	0.22955(5)	-0.90936(15)	-0.24984(4)	0.0749	
O(1)	-0.2385(5)	-0.3408(14)	0.0675(3)	0.0673	
O(11)	-0.0151(6)	0.138(2)	-0.0632(5)	0.0959	
C(1)	-0.1321(6)	-0.3157(17)	-0.1621(5)	0.0443	
C(3)	-0.1344(6)	-0.1884(17)	-0.2646(5)	0.0427	
C(4)	-0.0714(5)	-0.2864(16)	-0.2757(5)	0.0368	
C(5)	-0.0402(6)	-0.3990(19)	-0.2276(5)	0.0515	
C(7)	-0.1619(6)	-0.3227(16)	-0.1020(5)	0.0404	
C(10)	-0.2174(7)	-0.3407(19)	0.0095(5)	0.0530	
C(14)	-0.0382(6)	-0.2692(17)	-0.3340(5)	0.0424	
C(17)	0.0264(7)	-0.237(2)	-0.4436(6)	0.0594	
C(21)	-0.1666(5)	-0.0621(16)	-0.3120(5)	0.0383	
C(24)	-0.2274(7)	0.1851(18)	-0.3961(5)	0.0489	
C(27)	0.0247(6)	-0.5137(18)	-0.2370(5)	0.0470	
C(30)	0.1423(6)	-0.7324(18)	-0.2459(5)	0.0498	
C(41)	0.019(1)	0.011(3)	-0.0864(7)	0.0801	
O(12)	0.0440(6)	-0.1171(18)	-0.0528(5)	0.0861	
C(2)	-0.1619(6)	-0.2041(18)	-0.2086(5)	0.0457	

C(6)	-0.0705(6)	-0.4135(19)	-0.1732(5)	0.0518
C(8)	-0.2325(6)	-0.3100(18)	-0.0989(5)	0.0468
C(9)	-0.2635(7)	-0.3152(19)	-0.0431(5)	0.0543
C(11)	-0.1436(6)	-0.3543(19)	0.0068(5)	0.0546
C(12)	-0.1174(6)	-0.350(2)	-0.0482(5)	0.0581
C(15)	-0.0779(6)	-0.3141(19)	-0.3887(5)	0.0517
C(16)	-0.0456(9)	-0.296(2)	-0.4436(6)	0.0624
C(18)	0.0618(6)	-0.1982(19)	-0.3886(5)	0.0497
C(19)	0.0320(6)	-0.2125(17)	-0.3345(5)	0.0459
C(22)	-0.2396(6)	-0.0787(19)	-0.3353(5)	0.0529
C(23)	-0.2694(7)	0.0459(19)	-0.3776(5)	0.0530
C(25)	-0.1586(6)	0.2012(19)	-0.3721(5)	0.0472
C(26)	-0.1277(6)	0.0781(19)	-0.3298(5)	0.0513
C(28)	0.0842(6)	-0.5089(19)	-0.1919(5)	0.0523
C(29)	0.1434(6)	-0.6155(18)	-0.1968(5)	0.0520
C(31)	0.0861(6)	-0.7356(18)	-0.2912(5)	0.0475
C(32)	0.0274(6)	-0.6266(19)	-0.2856(5)	0.0484
H(1)	0.0337(6)	-0.1248(18)	-0.0117(5)	0.0350
H(21)	-0.2058(6)	-0.1437(18)	-0.2038(5)	0.0437
H(61)	-0.0526(6)	-0.5022(19)	-0.1445(5)	0.0635
H(81)	-0.2633(6)	-0.2850(18)	-0.1354(5)	0.0534
H(91)	-0.3145(7)	-0.3120(19)	-0.0427(5)	0.0930
H(111)	-0.1125(6)	-0.3688(19)	0.0439(5)	0.0600
H(121)	-0.0668(6)	-0.364(2)	-0.0495(5)	0.0642
H(151)	-0.1246(6)	-0.3662(19)	-0.3891(5)	0.0632
H(161)	-0.0741(9)	-0.316(2)	-0.4816(6)	0.0870
H(181)	0.1093(6)	-0.1507(19)	-0.3872(5)	0.0663
H(191)	0.0609(6)	-0.1810(17)	-0.2976(5)	0.0619
H(221)	-0.2703(6)	-0.1603(19)	-0.3177(5)	0.0517
H(231)	-0.3178(7)	0.0292(19)	-0.3961(5)	0.0686
H(251)	-0.1307(6)	0.2992(19)	-0.3837(5)	0.0509
H(261)	-0.0790(6)	0.0932(19)	-0.3119(5)	0.0704
H(281)	0.0840(6)	-0.4288(19)	-0.1585(5)	0.0556
H(291)	0.1846(6)	-0.6140(18)	-0.1669(5)	0.0684
H(311)	0.0888(6)	-0.8016(18)	-0.3277(5)	0.0594
H(321)	-0.0136(6)	-0.6328(19)	-0.3157(5)	0.0669
C(13)	-0.3135(6)	-0.332(2)	0.0725(5)	0.0570
H(131)	-0.3216(6)	-0.336(2)	0.1142(5)	0.0671
H(132)	-0.3366(6)	-0.431(2)	0.0514(5)	0.0671
H(133)	-0.3329(6)	-0.224(2)	0.0548(5)	0.0671
C(20)	0.0577(8)	-0.222(2)	-0.5042(6)	0.0766
H(201)	0.1071(8)	-0.187(2)	-0.4979(6)	0.0855
H(202)	0.0534(8)	-0.332(2)	-0.5258(6)	0.0855
H(203)	0.0302(8)	-0.133(2)	-0.5272(6)	0.0855
C(42)	0.0295(11)	0.022(3)	-0.1497(7)	0.1031
H(421)	0.0589(11)	-0.078(3)	-0.1565(7)	0.1041
H(422)	0.0527(11)	0.129(3)	-0.1607(7)	0.1041
H(423)	-0.0161(11)	0.011(3)	-0.1739(7)	0.1041

Table 2: Anisotropic temperature factors

Atom	u(11)	u(22)	u(33)	u(23)	u(13)	u(12)
I(1)	0.0825(7)	0.0672(9)	0.0677(6)	0.0167(5)	-0.0077(4)	0.0195(5)
I(2)	0.0691(6)	0.083(1)	0.0766(6)	0.0266(5)	0.0253(5)	0.0356(6)
O(1)	0.065(5)	0.093(9)	0.045(5)	0.003(4)	0.008(4)	-0.009(5)
O(11)	0.080(7)	0.132(14)	0.078(7)	0.023(7)	0.019(6)	-0.002(7)
C(1)	0.055(8)	0.031(9)	0.049(6)	-0.002(5)	0.014(5)	-0.005(6)
C(3)	0.038(6)	0.044(9)	0.044(6)	0.006(5)	-0.004(5)	0.013(5)
C(4)	0.040(6)	0.026(9)	0.046(6)	-0.003(5)	0.009(5)	-0.012(5)
C(5)	0.042(6)	0.060(12)	0.054(7)	0.007(6)	0.010(5)	-0.006(6)
C(7)	0.049(7)	0.026(8)	0.047(6)	0.006(5)	0.009(5)	0.004(5)
C(10)	0.076(9)	0.051(11)	0.034(6)	0.006(5)	0.013(6)	-0.020(7)
C(14)	0.038(6)	0.05(1)	0.044(6)	0.005(5)	0.010(5)	0.005(5)
C(17)	0.069(9)	0.047(11)	0.062(8)	0.002(6)	0.006(7)	0.011(7)
C(21)	0.036(6)	0.022(8)	0.060(7)	0.009(5)	0.017(5)	0.005(5)
C(24)	0.059(8)	0.04(1)	0.046(6)	0.009(5)	0.008(5)	0.007(6)
C(27)	0.050(7)	0.04(1)	0.057(7)	0.012(6)	0.015(6)	0.005(6)
C(30)	0.041(7)	0.05(1)	0.064(8)	0.008(6)	0.013(6)	0.012(5)
C(41)	0.089(12)	0.079(19)	0.074(12)	-0.01(1)	0.018(9)	-0.038(11)
O(12)	0.077(6)	0.100(11)	0.083(7)	0.003(6)	0.013(5)	-0.012(6)
C(2)	0.036(6)	0.05(1)	0.054(7)	0.004(6)	0.018(5)	-0.004(5)
C(6)	0.052(7)	0.050(11)	0.053(7)	0.004(6)	0.007(6)	-0.011(6)
C(8)	0.048(7)	0.05(1)	0.040(6)	-0.001(5)	0.001(5)	0.003(6)
C(9)	0.056(7)	0.062(11)	0.046(7)	-0.010(6)	0.012(6)	-0.006(7)
C(11)	0.037(7)	0.078(12)	0.049(7)	0.000(6)	0.008(5)	-0.010(6)
C(12)	0.031(6)	0.082(12)	0.057(7)	0.008(6)	-0.011(5)	-0.009(6)
C(15)	0.055(7)	0.057(11)	0.042(7)	0.004(6)	0.003(6)	-0.006(7)
C(16)	0.091(11)	0.043(11)	0.053(7)	-0.002(6)	0.008(7)	0.007(8)
C(18)	0.048(7)	0.03(1)	0.070(9)	0.009(6)	0.017(6)	0.011(5)
C(19)	0.046(6)	0.031(9)	0.060(7)	0.000(5)	0.005(5)	-0.005(5)
C(22)	0.030(5)	0.067(11)	0.061(7)	0.013(6)	0.000(5)	0.006(6)
C(23)	0.052(7)	0.05(1)	0.052(6)	-0.018(6)	-0.013(6)	0.001(6)
C(25)	0.040(7)	0.05(1)	0.053(7)	-0.001(6)	0.011(6)	0.004(6)
C(26)	0.031(6)	0.057(11)	0.064(7)	0.018(6)	0.002(5)	0.014(6)
C(28)	0.047(7)	0.065(11)	0.041(6)	0.007(5)	-0.011(5)	-0.000(6)
C(29)	0.046(7)	0.047(11)	0.060(7)	0.015(6)	-0.006(5)	-0.001(6)
C(31)	0.052(8)	0.05(1)	0.042(6)	0.001(5)	0.012(6)	0.001(6)
C(32)	0.047(6)	0.04(1)	0.056(7)	0.004(6)	0.013(5)	0.007(6)
C(13)	0.047(7)	0.074(12)	0.053(7)	0.012(6)	0.018(5)	0.007(6)
C(20)	0.091(11)	0.061(14)	0.09(1)	0.009(7)	0.045(8)	0.007(8)
C(42)	0.141(15)	0.089(18)	0.083(12)	0.013(9)	0.027(11)	-0.036(12)

Table 3: Bond lengths

Atoms	Length [Å]
I(1) - C(24)	2.090(12)
I(2) - C(30)	2.103(11)
O(1) - C(10)	1.382(13)
O(1) - C(13)	1.414(13)
O(11) - C(41)	1.28(2)
C(1) - C(7)	1.497(15)
C(1) - C(2)	1.387(16)
C(1) - C(6)	1.404(17)
C(3) - C(4)	1.427(15)
C(3) - C(21)	1.482(15)
C(3) - C(2)	1.397(14)
C(4) - C(5)	1.423(17)
C(4) - C(14)	1.498(14)
C(5) - C(27)	1.514(17)
C(5) - C(6)	1.390(16)
C(7) - C(8)	1.326(15)
C(7) - C(12)	1.378(15)
C(10) - C(9)	1.371(17)
C(10) - C(11)	1.384(17)
C(14) - C(15)	1.379(15)
C(14) - C(19)	1.373(16)
C(17) - C(16)	1.41(2)
C(17) - C(18)	1.344(17)
C(17) - C(20)	1.524(18)
C(21) - C(22)	1.397(15)
C(21) - C(26)	1.358(16)
C(24) - C(23)	1.392(18)
C(24) - C(25)	1.328(16)
C(27) - C(28)	1.397(15)
C(27) - C(32)	1.371(18)
C(30) - C(29)	1.390(18)
C(30) - C(31)	1.358(16)
C(41) - O(12)	1.27(2)
C(41) - C(42)	1.44(2)
C(8) - C(9)	1.421(16)
C(11) - C(12)	1.360(16)
C(15) - C(16)	1.421(17)
C(18) - C(19)	1.377(16)
C(22) - C(23)	1.387(18)
C(25) - C(26)	1.386(17)
C(28) - C(29)	1.374(17)
C(31) - C(32)	1.379(17)

Table 4: Bond angles

Atoms	Angles[°]
C(5) - C(4) - C(14)	121.3(10)
C(4) - C(5) - C(27)	119.6(9)
C(4) - C(5) - C(6)	121.3(11)
C(27) - C(5) - C(6)	119.0(11)
C(1) - C(7) - C(8)	121.0(10)
C(1) - C(7) - C(12)	121.5(10)
C(8) - C(7) - C(12)	117.5(10)
O(1) - C(10) - C(9)	124.5(12)
O(1) - C(10) - C(11)	115.5(10)
C(9) - C(10) - C(11)	119.8(10)
C(4) - C(14) - C(15)	119.9(10)
C(4) - C(14) - C(19)	121.5(9)
C(15) - C(14) - C(19)	118.6(10)
C(16) - C(17) - C(18)	115.5(12)
C(16) - C(17) - C(20)	119.0(12)
C(18) - C(17) - C(20)	125.5(13)
C(3) - C(21) - C(22)	119.7(11)
C(3) - C(21) - C(26)	120.8(10)
C(22) - C(21) - C(26)	119.2(10)
I(1) - C(24) - C(23)	119.7(9)
I(1) - C(24) - C(25)	120.4(10)
C(23) - C(24) - C(25)	119.9(11)
C(5) - C(27) - C(28)	117.7(11)
C(5) - C(27) - C(32)	124.0(10)
C(28) - C(27) - C(32)	118.3(11)
I(2) - C(30) - C(29)	119.2(8)
I(2) - C(30) - C(31)	119.2(9)
C(29) - C(30) - C(31)	121.6(11)
O(11) - C(41) - O(12)	119.5(14)
O(11) - C(41) - C(42)	118.4(20)
O(12) - C(41) - C(42)	122.1(20)
C(1) - C(2) - C(3)	123.4(11)
C(1) - C(6) - C(5)	122.2(11)
C(7) - C(8) - C(9)	123.3(10)
C(10) - C(9) - C(8)	117.4(11)
C(10) - C(11) - C(12)	119.8(10)
C(7) - C(12) - C(11)	122.1(11)
C(14) - C(15) - C(16)	119.2(11)
C(17) - C(16) - C(15)	121.8(12)
C(17) - C(18) - C(19)	124.2(12)
C(14) - C(19) - C(18)	120.7(11)
C(21) - C(22) - C(23)	118.8(12)
C(24) - C(23) - C(22)	120.4(11)
C(24) - C(25) - C(26)	120.6(13)
C(21) - C(26) - C(25)	121.0(10)
C(27) - C(28) - C(29)	120.1(12)
C(30) - C(29) - C(28)	119.3(10)
C(30) - C(31) - C(32)	118.0(11)
C(27) - C(32) - C(31)	122.5(11)

APPENDIX B

Form factor of a rod inventively thin and of length L

$$P(q) = A\left[2Si(qL)/qL - 4\sin^2(qL/2)/(q^2L^2)\right] \qquad \text{with } Si(x) = \int_0^x \frac{\sin t}{t}\,dt$$

Form factor of a cylinder of radius R and length L

$$P(q) = A\left\{\int_0^{\pi/2}\left[\frac{2B_1(qR\sin(\alpha))}{qR\sin(\alpha)}\cdot\frac{\sin((qL\cos(\alpha))/2}{(qL\cos(\alpha))/2}\right]\cdot\sin(\alpha)d\alpha\right\}$$

with B_1 Bessel function of the first order

Form factor of a sphere of radius R

$$F_1(q,R) = A\left\{\frac{3[\sin(qR) - qR\cos(qR)]}{(qR)^3}\right\}$$

Form factor of a distribution of rod

$$P_{ROD-Distribution}(q,A,L_M,\sigma) = \int_0^{\infty}\Pr ob_{\log norm}(L,L_M,\sigma)\cdot\left\{\frac{2Si(qL)}{qL}\cdot\frac{4\sin^2(qL/2)}{q^2L^2}\right\}dL$$

$$\Pr ob(L,L_m,\sigma) = \frac{1}{\sqrt{2\pi}\sigma x}\exp\left\{-\frac{(\ln(x)-\ln(x_M))^2}{2\sigma^2}\right\}$$

Form factor of a polydisperse hollow cylinder

$$\int_0^{\frac{\pi}{2}}\int_0^{\frac{R_a+R_i}{2}}\int_{\frac{R_a+R_i}{2}}^{\infty}\left((4r_a j_1(qr_a\sin(\alpha)) - 4r_i j_1(qr_i\sin(\alpha)))\sin(ql\cos(\alpha/2))/\left(q\sin(\alpha)ql\cos(\alpha)\left(r_a^2 - r_i^2\right)\right)\right)^2\sin(\alpha)_{dr_a dr_i d\alpha}$$
$$\bullet\exp\left(-(r_a - R_a)^2/\left(2\Delta r_a^2\right) - (r_i - R_i)^2/\left(2\Delta r_i^2\right)\right)$$

APPENDIX C

WAXS (first 6rows) and electron diffraction pattern data of copolymer 68 (dry sample cast from a cyclohexane solution).

X-ray, RT; Pulv.Diff.	**d obs**	**d obs**	**d obs**	**d obs**	**d obs**	**d obs**		**d obs**	**d calc (bragg18)**
0 1 0	71.0								71.60
0 2 0	35.7								35.80
0 4 0	17.8								17.90
0 6 0	11.9								11.93
0 8 0	8.7								8.95 R
0 10 0	7.2								7.16
ED pattern	**001685**	**011552**	**011554**	**011568**	**011570**	**001687**	**001686**	**001690**	
0 0 1	6.24					6.22		6.20	6.20
2 0 1	5.97					5.99/6.04	6.04	5.96/6.04	5.99
3 0 1									5.75
4 0 1	5.50					5.53/5.53		5.49/5.53	5.46
5 0 1	5.14							5.16/5.17	5.15
0 1 1		6.16	6.19				6.17		6.18
2 1 1							5.94		5.97
3 1 1									5.73
4 1 1		5.42					5.49		5.45
5 1 1						5.10			5.13
0 2 1									6.11
2 2 1									5.91
3 2 1									5.68
4 2 1									5.40
5 2 1		5.07			5.08	5.11			5.09
0 3 1				6.02	5.98				6.00
2 3 1									5.81
3 3 1		5.59	5.62	5.53 R	5.54		5.57		5.59
4 3 1				5.27 R					5.32
5 3 1									5.03
6 3 1		4.72		4.72					4.73
7 3 1		4.45		4.45					4.44
8 3 1		4.18		4.18	4.18				4.16
0 4 1									5.86
2 4 1									5.68
3 4 1									5.48
4 4 1			5.22		5.23				5.22
5 4 1									4.95
6 4 1					4.64				4.66
	011523	**011543/51**	**011553**	**011565**	**011567/68**				
0 2 2		3.08							
0 3 2			3.07	3.06					
0 5 2	3.03				3.03				

APPENDIX D

Spectra of coil-rod-coil block copolymers

Copolymer 65

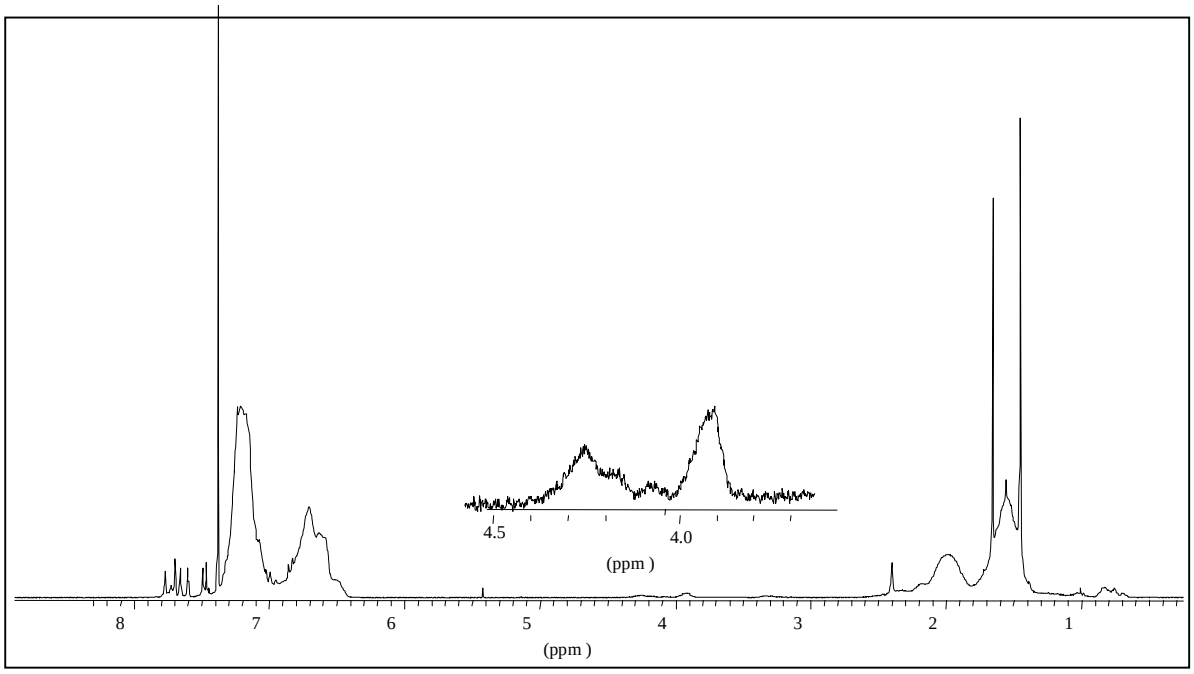

^{1}H NMR spectrum of the copolymer **65**.

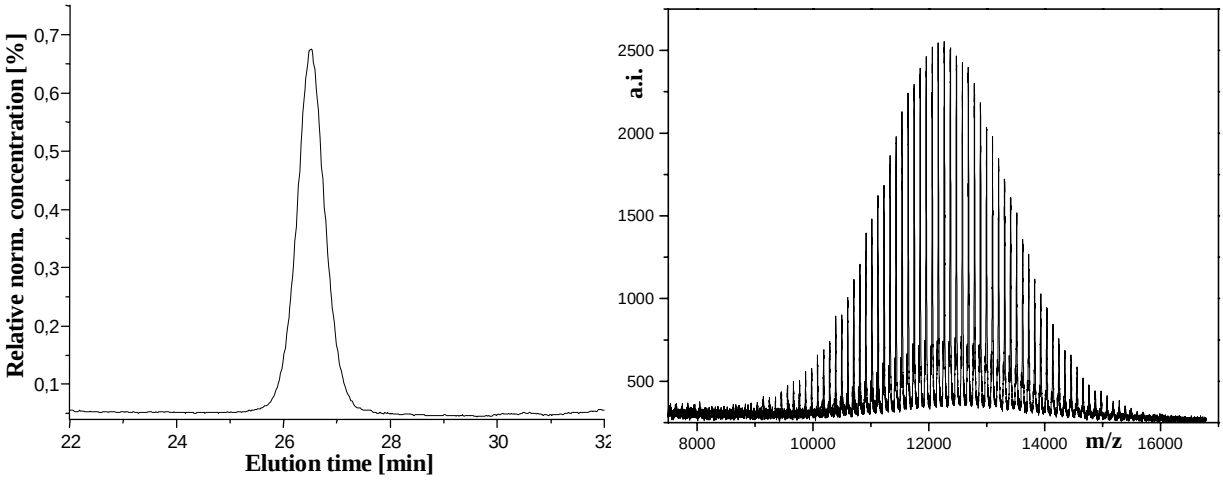

GPC data (left) and MALDI-TOF spectrum (Na) (right) of copolymer **65**.

Copolymer 66

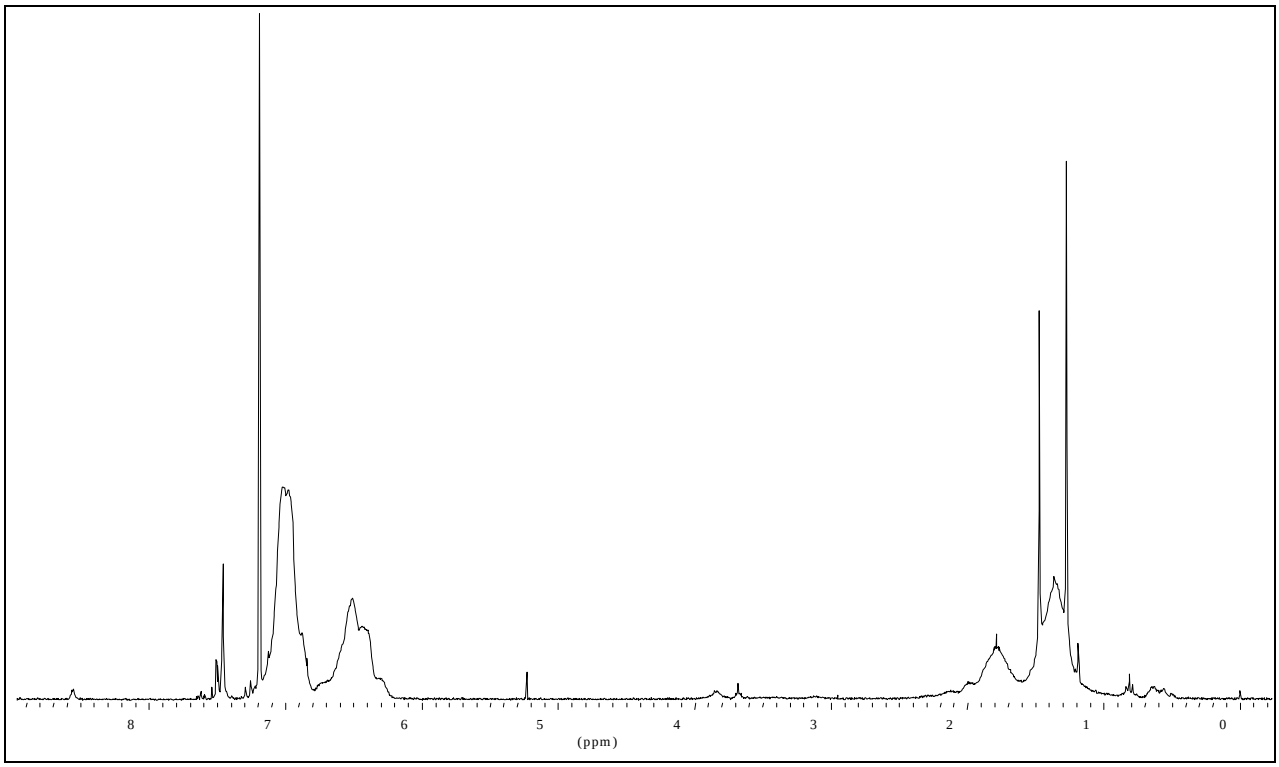

^{1}H NMR spectrum of the copolymer **66**.

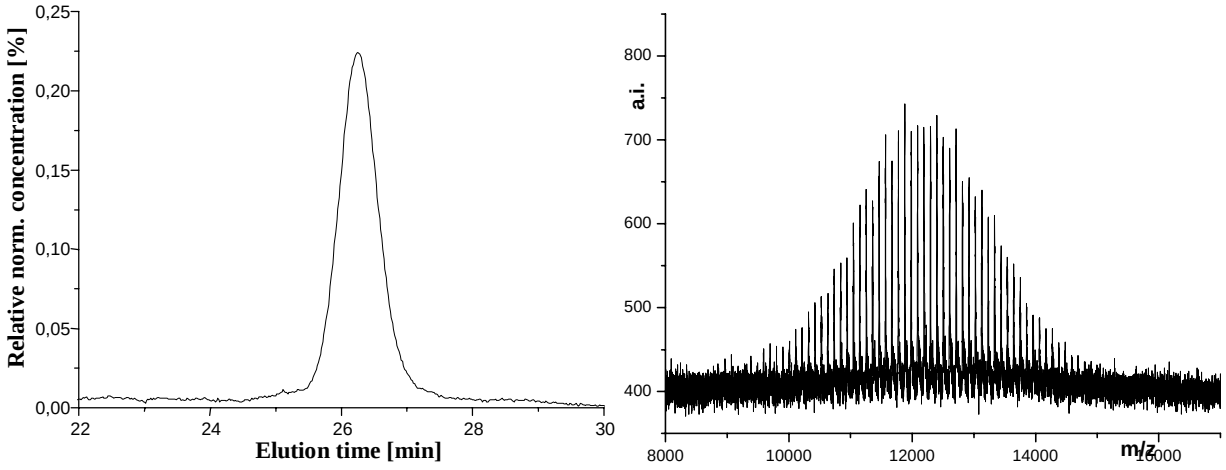

GPC data (left) and MALDI-TOF spectrum (Ag) (right) of copolymer **66**.

Copolymer 67

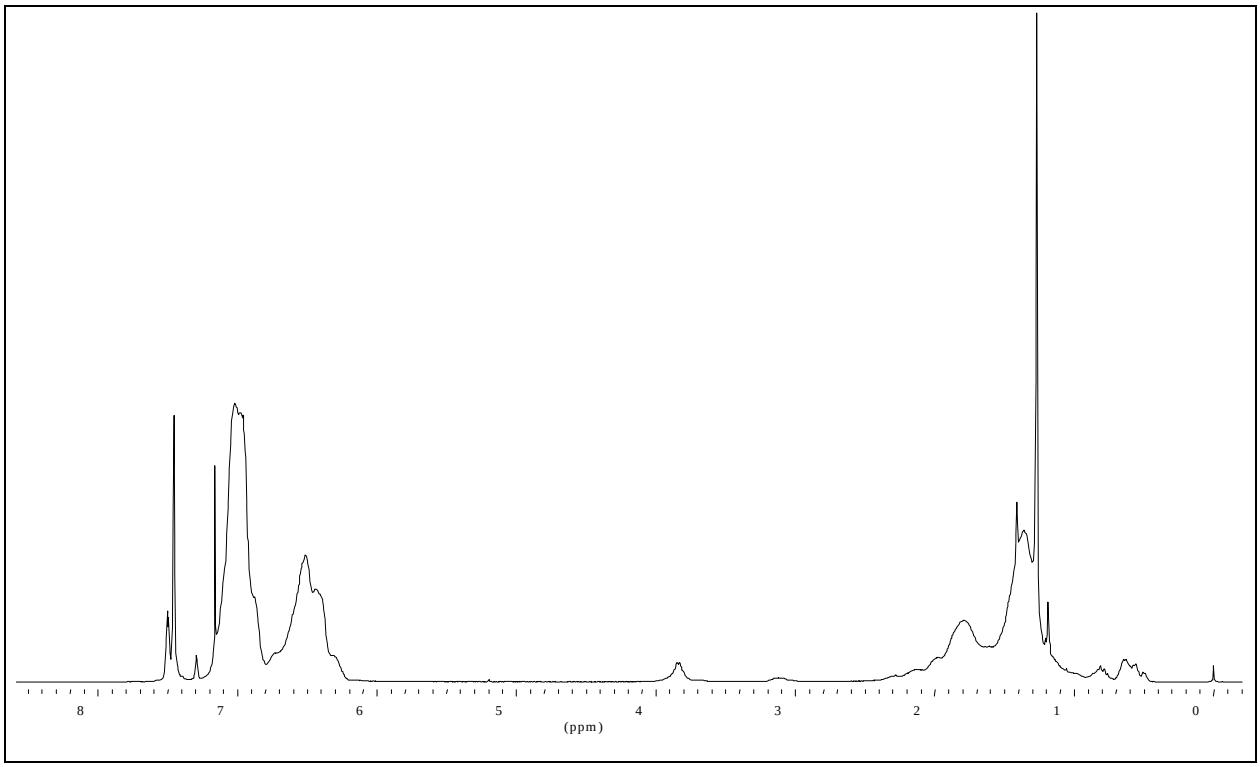

^{1}H NMR spectrum of the copolymer **67**.

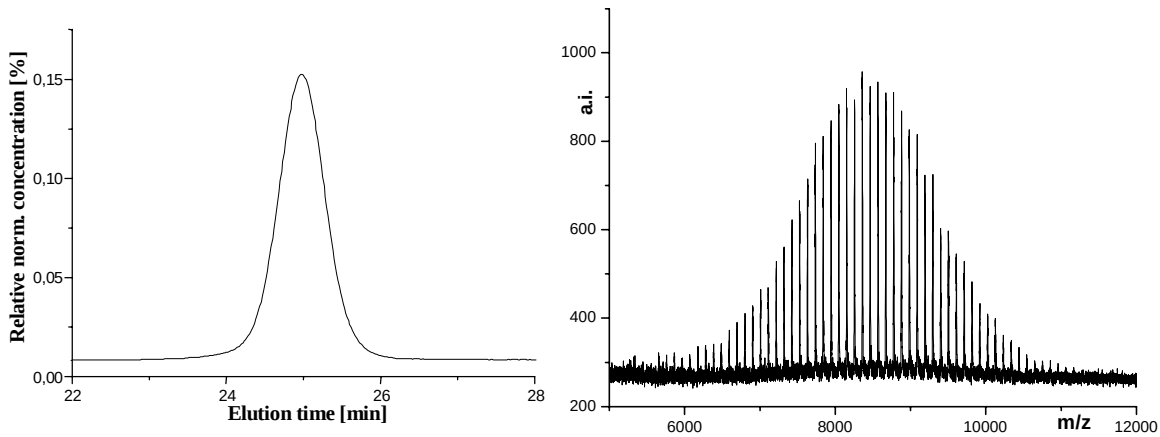

GPC data (left) and MALDI-TOF spectrum (Na) (right) of copolymer **67**.

Copolymer 68

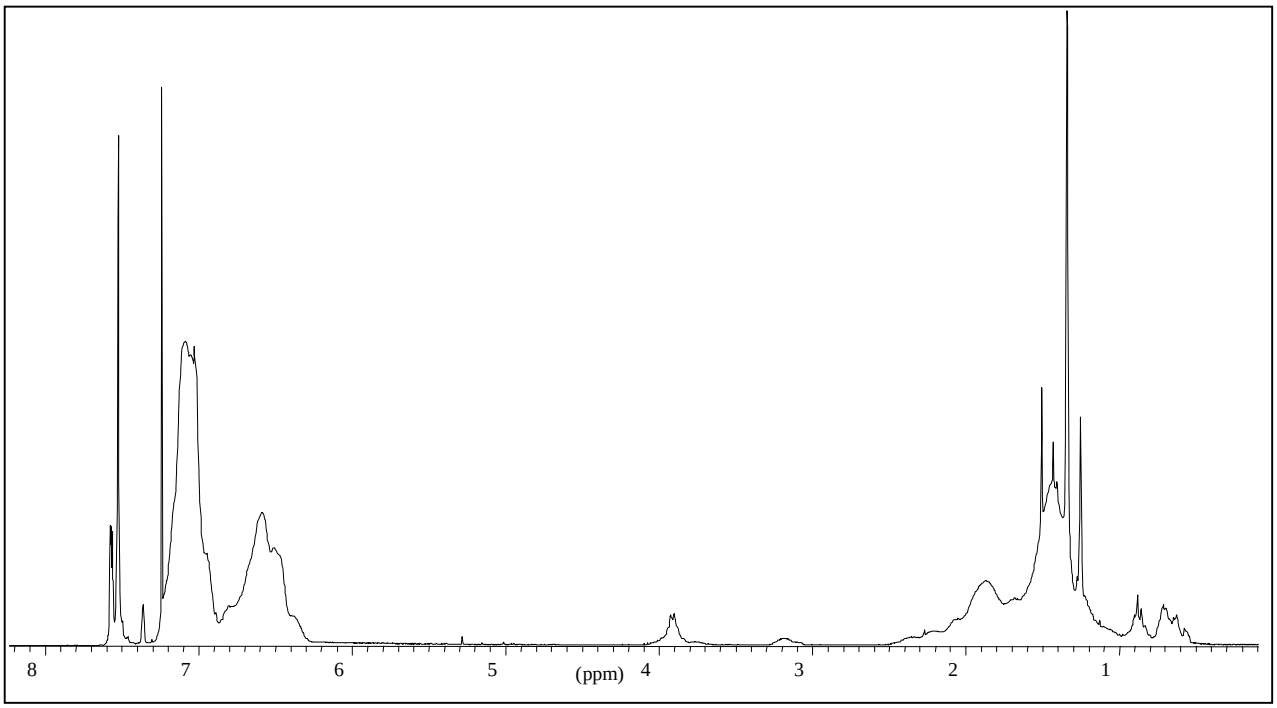

^{1}H NMR spectrum of copolymer **68**.

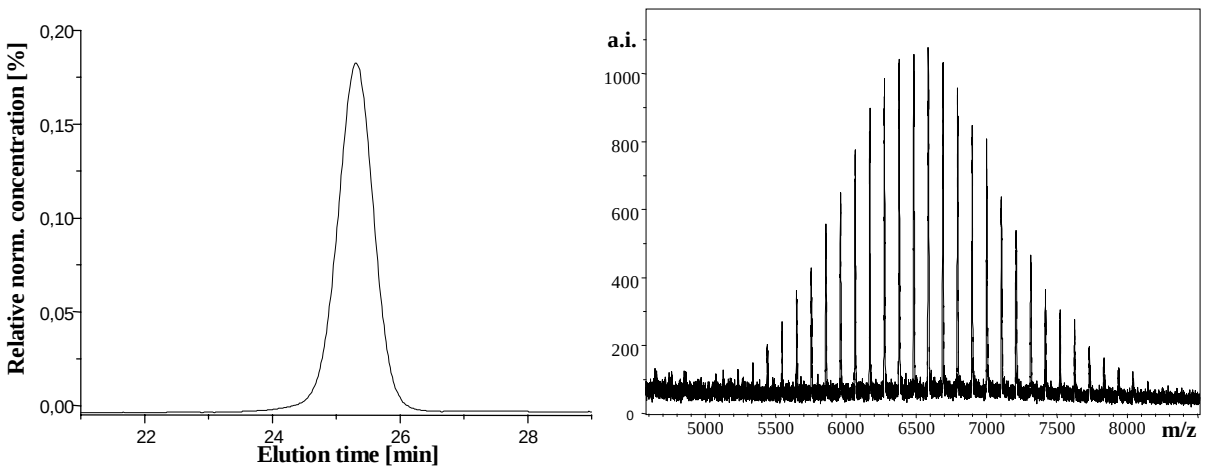

GPC data (left) and MALDI-TOF spectrum (Na) (right) of **68**.

Copolymer 69

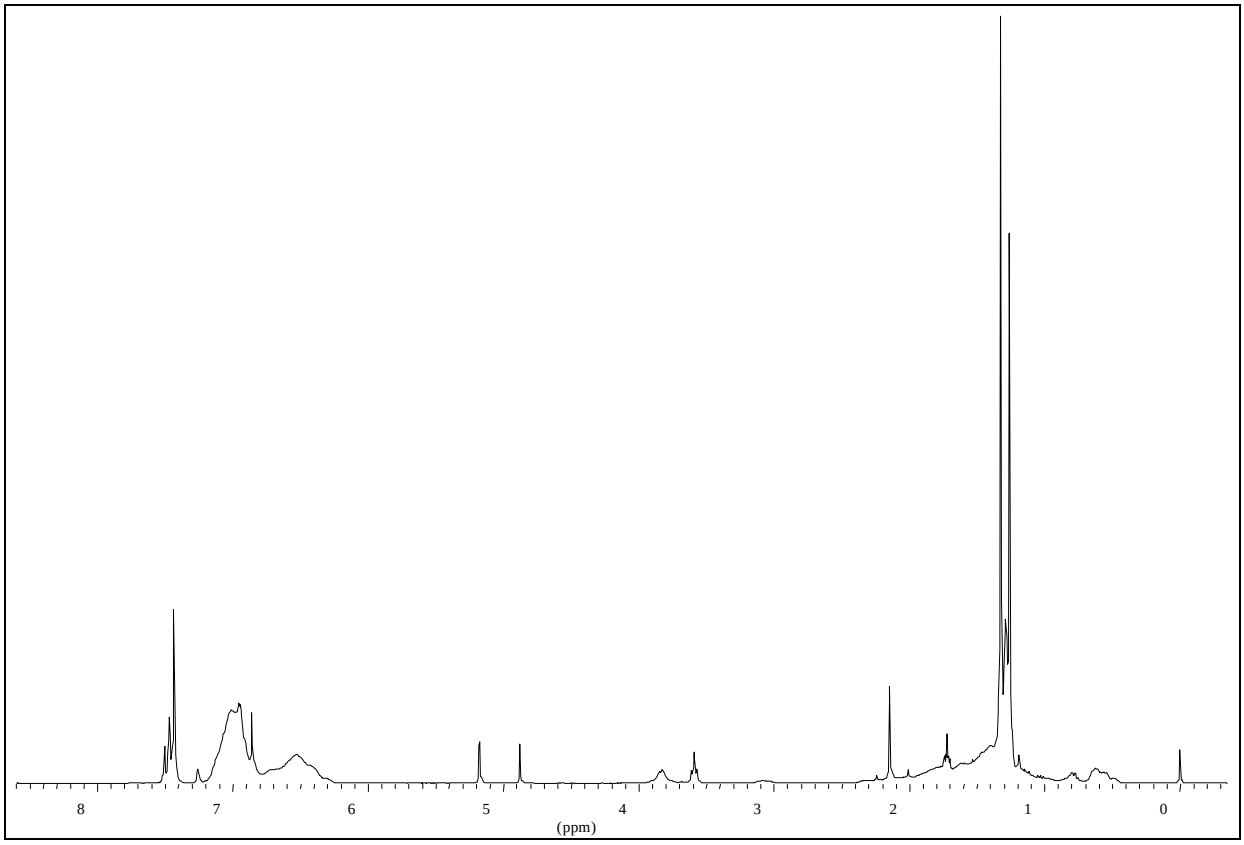

^{1}H NMR spectrum of copolymer **69**.

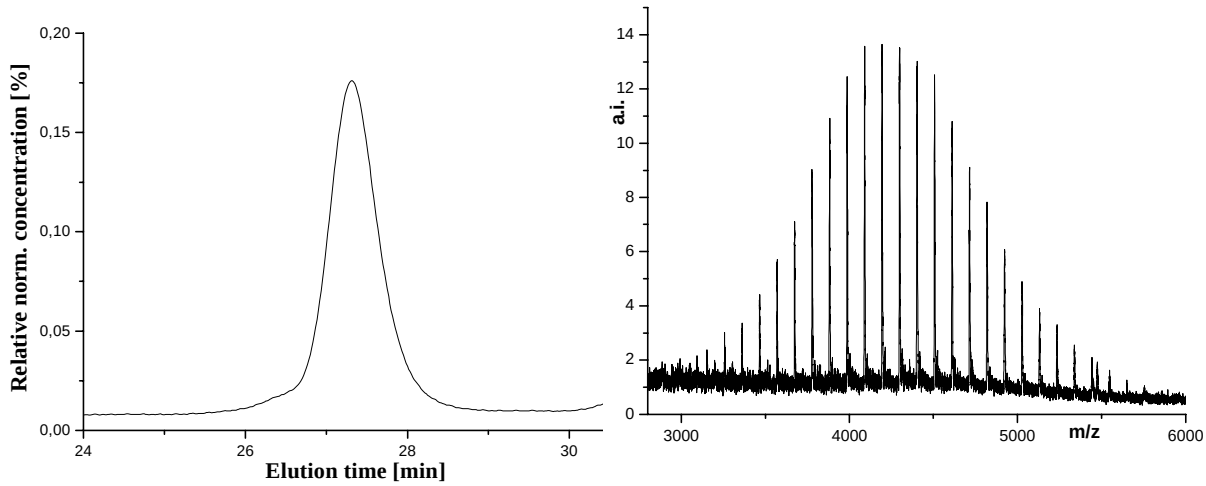

GPC data (left) and MALDI-TOF spectrum (Na) (right) of copolymer **69**.

Copolymer 70

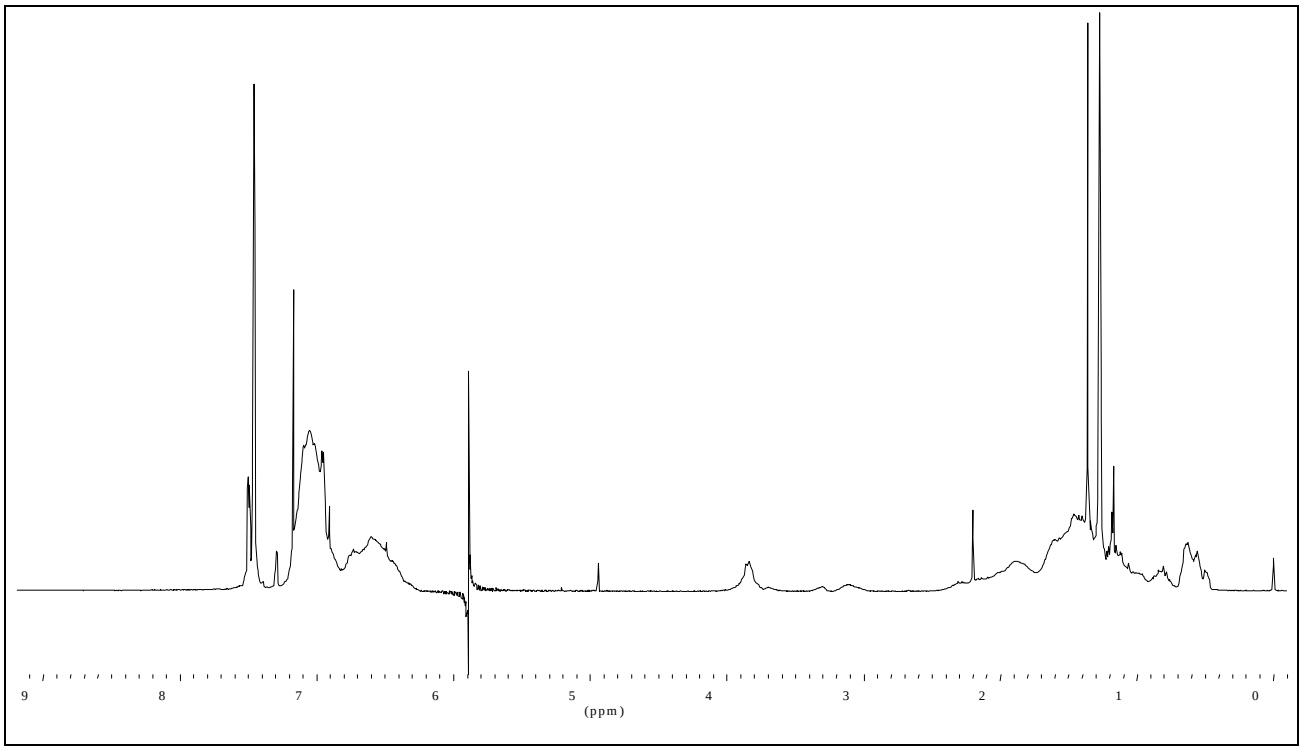

^{1}H NMR spectrum of copolymer **70**.

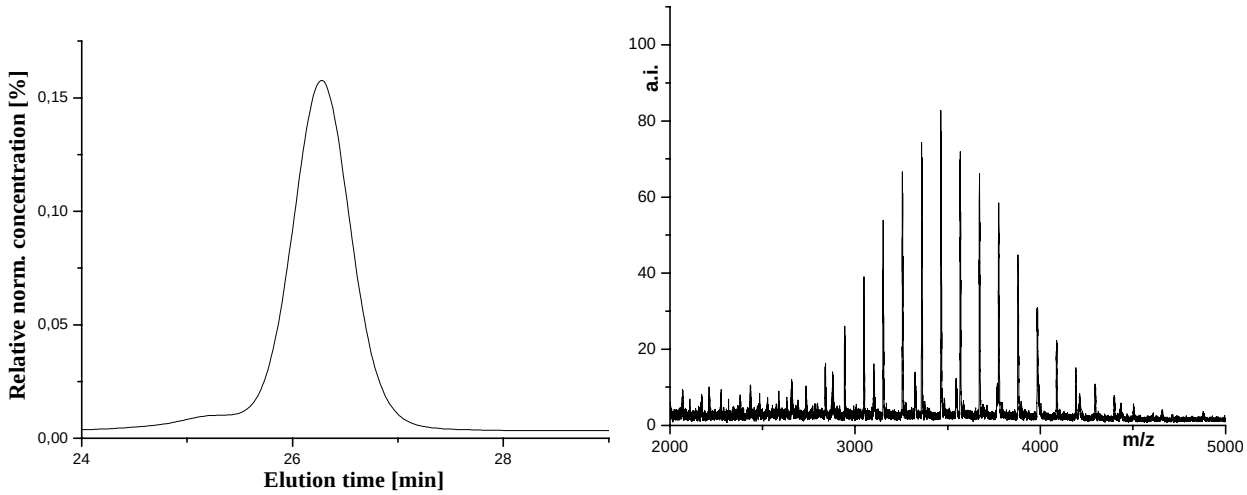

GPC data (left) and MALDI-TOF spectrum (Na) (right) of copolymer **70**.

.

Copolymer71

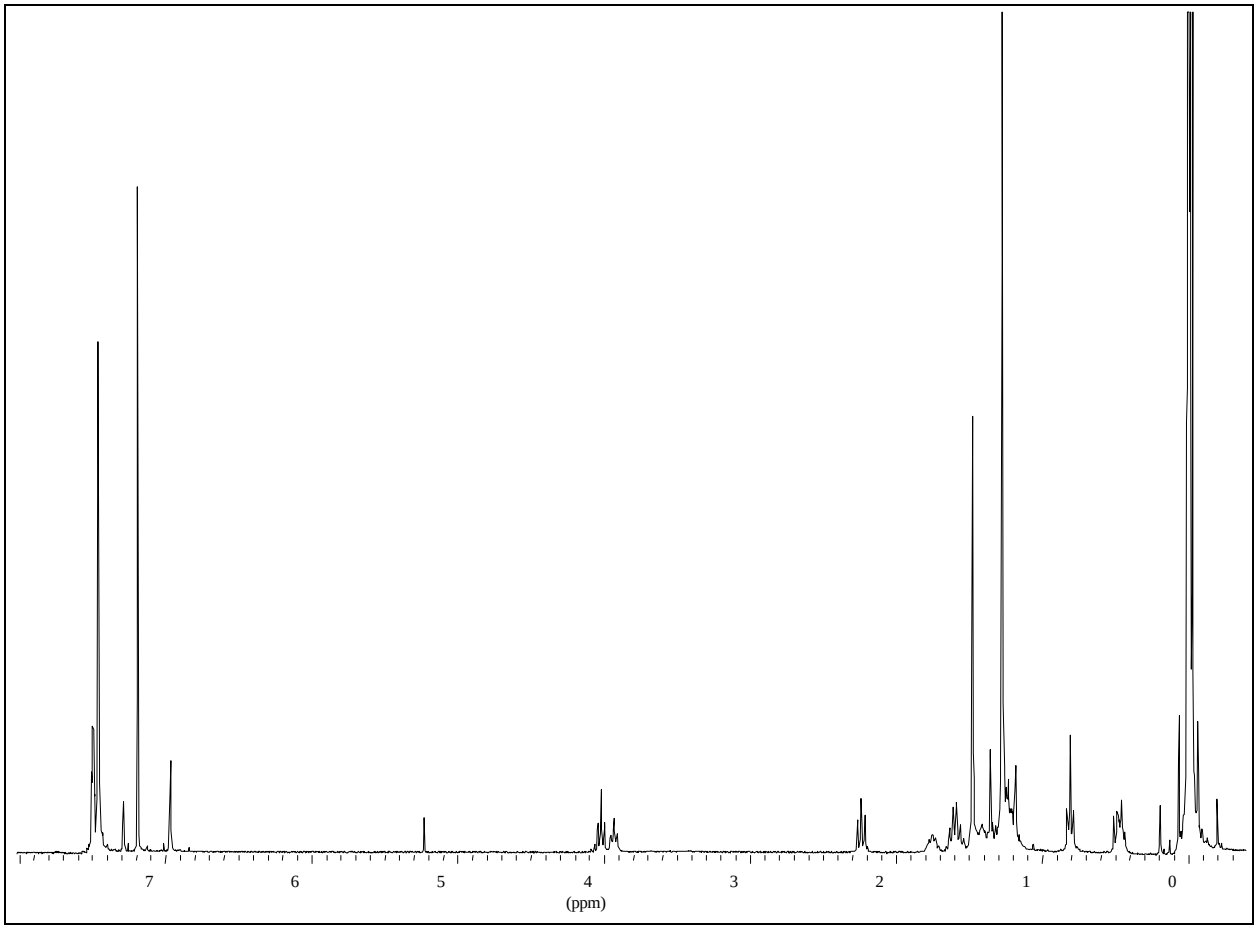

^{1}H NMR spectrum of copolymer **71**.

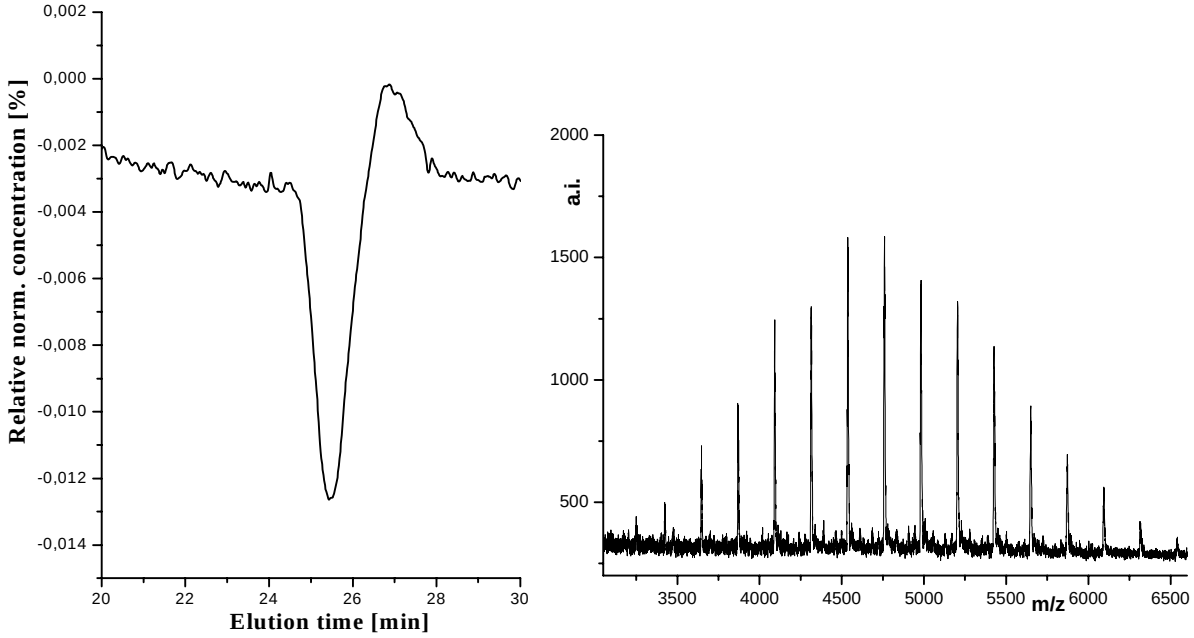

GPC data (left) and MALDI-TOF spectrum (K) (right) of copolymer **71**.

Copolymer 72

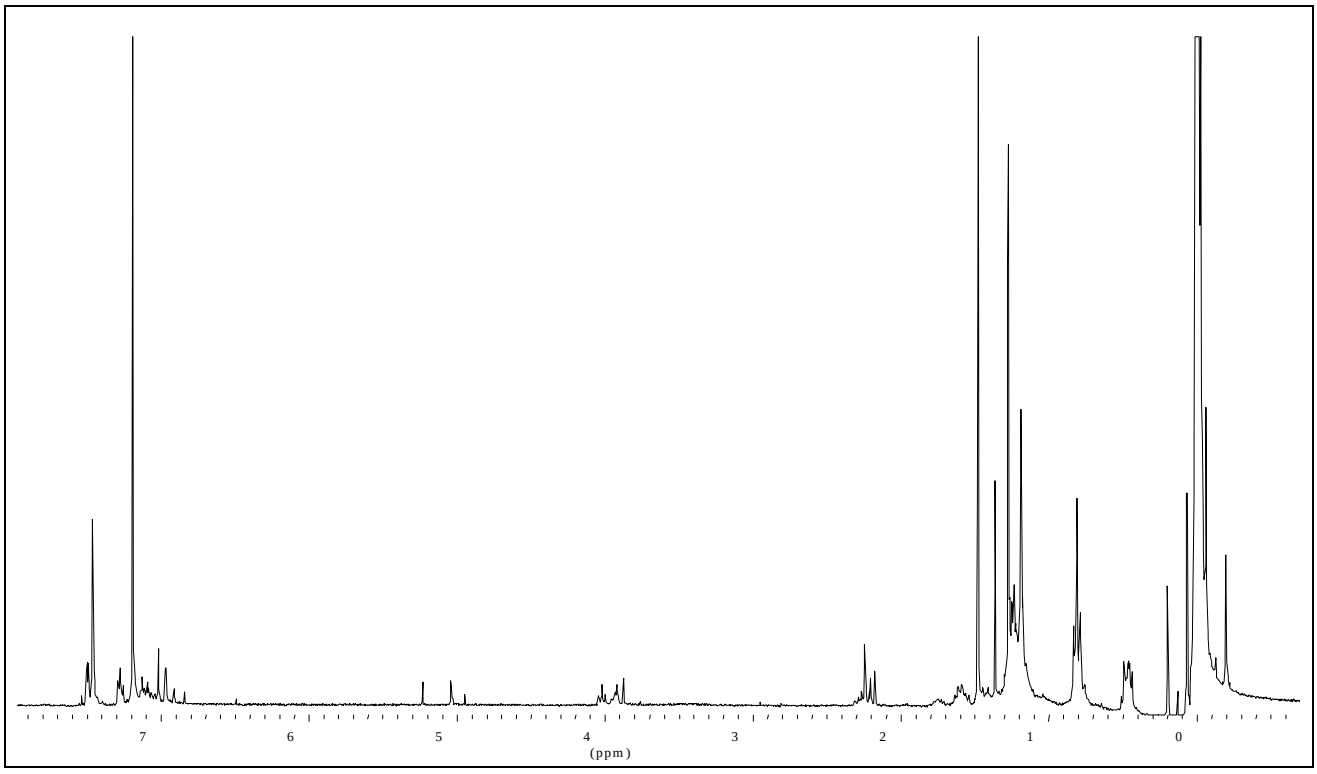

^{1}H NMR spectrum of copolymer **72**.

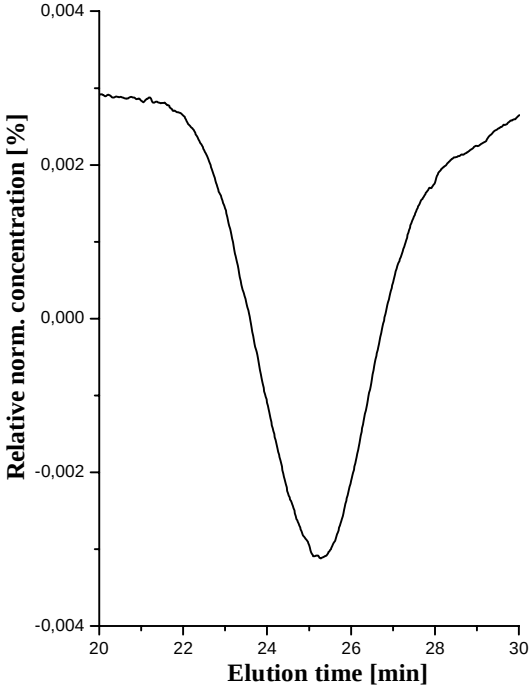

GPC data of copolymer **72.**

Copolymer 73

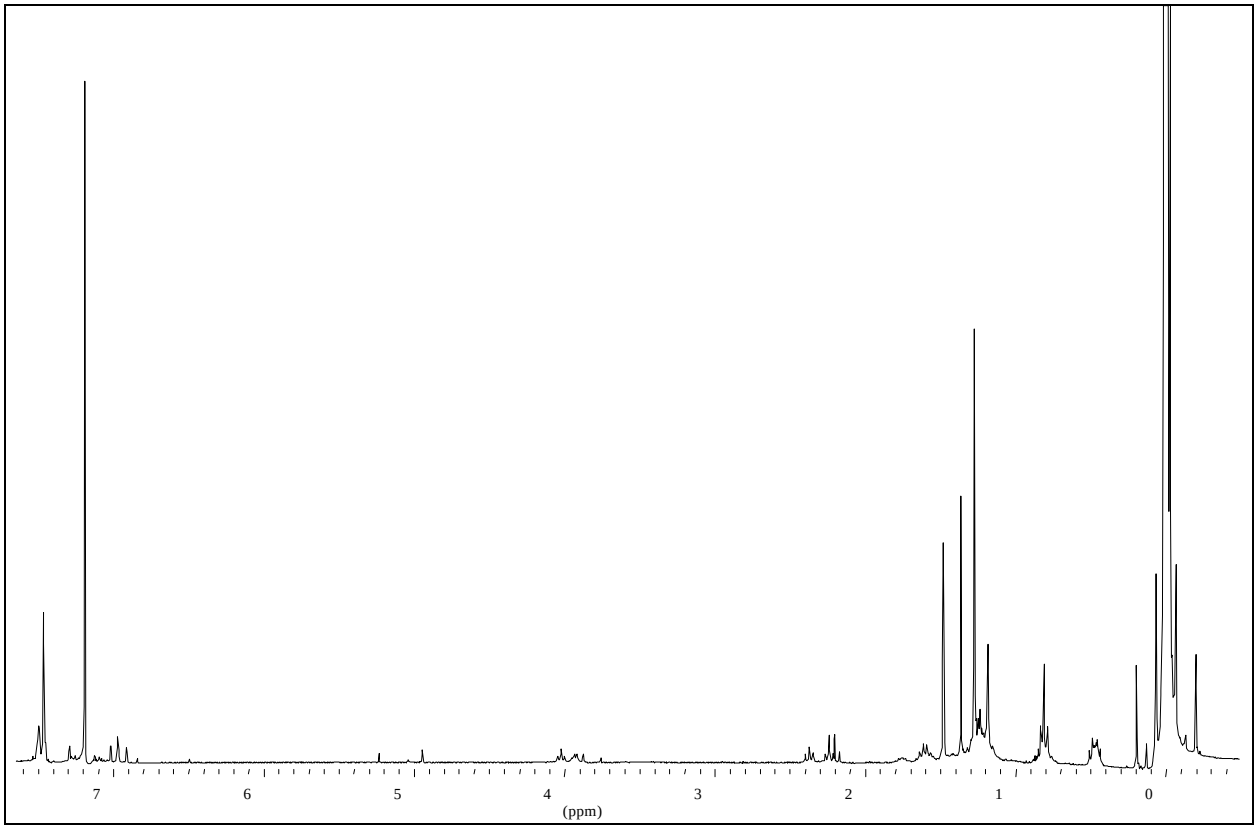

^{1}H NMR spectrum of copolymer **73**.

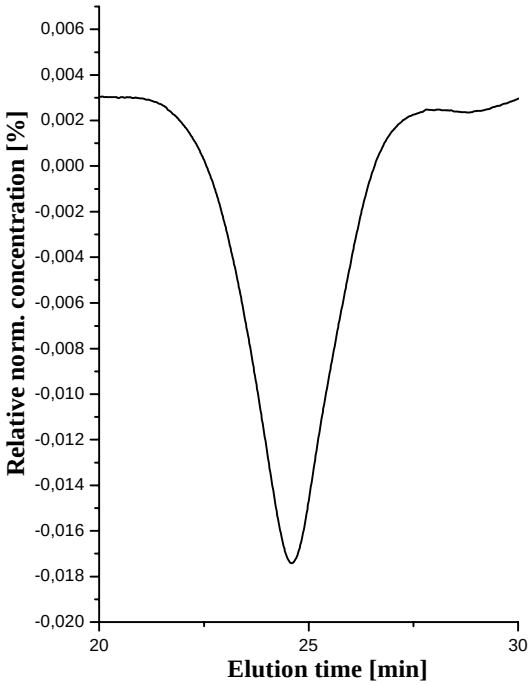

GPC data of copolymer **73**.

References

[1] J.-M. Lehn, "Supramolecular Chemistry, Concepts and Perspectives" VCH, Weinheim, **1995**; H. Ringsdorf, B. Schlarb, J. Venzmer *Angew. Chem. Int. Ed. Engl.* **1988**, 27, 113.

[2] V. Balsani, F. Scandola, *Supramolecular Photochemistry*, Ellis Horwood, Chichester **1991**.

[3] M. Antonietti, C. Göltener, *Angew. Chem. Int. Ed. Engl.* **1997**, 36, 910; M. Muthukumar, C. K. Ober, E. L. Thomas, *Science*, **1997**, 277, 1225; G. A. Ozin, *Adv. Mater* ,**1992**, 4, 612; A. W. Czarnik, *Acc. Chem. Rev.* **1994**, 27, 302; F. L. Dickert, H. Stathopoulos, M. Reif, . *Adv. Mat.* **1996**, 8, 525.

[4] A. E. Rowan, R.J. M. Nolte, *Angew. Chem.* **1998**, 110, 65; *Angew. Chem. Int. Ed. Engl.* **1998**, 37, 63; D. S. Lawrence, T. Jiang, M. Levett, *Chem. Rev.* **1995**, 95, 2229; V. Perec, J. Heck, G. Johansson, D. Tomazos, *Macromol. Symp.* **1994**, 77, 237; J. S. Weissmann, P. S. Kim, *Science*, **1991**, 253, 1386.

[5] A. E. Eschenmoser and C. E. Wintner, *Science*, **1977**, 196, 1410

[6] Y. Kishi et al., *J. Am. Chem. Soc*., **1989**, 111, 7525.

[7] G. Wulff, A. Matussek, C. Hanf, S. Gladow, C. Lehmann, R. Goddard, Angew. Chem. Int. Ed. **2000**, 39, 2275.

[8] A. Klug, *Angew. Chem. Int. Ed. Engl.*, **1983**, 22, 565.

[9] V. Perec, W. D. Cho, G. Ungar, D. J. P. Yeardely, *Angew. Chem. Int. Ed. Engl.*, **2000**, 39, 1598; V. Perec, D. Schlueter, G. Ungar, S. Z. D. Cheng, A. Zhang, *Macromolecules.*, **1998**, 31, 1745; S. D. Hudson, v. Perec, G. Ungar et al, *Science*, **1997**, 278, 449.

[10] M. R. Ghadiri, J. R. Granja, R. A. Milligan, D. E. Mcree, N. Khazanovich, *Nature* **1993**, 366, 324; D. S. Lawrence, T. Jiang, M. Levett, *Chem. Rev* **1995**, 95., 2229; G. Gattuso, S. Menzer, S.A. Nepogodiev, J. F. Stoddart, D. J. Williams, *Angew. Chem. Int. Ed. Engl.* **1997**, 36, 1451.

[11]A. Y. Grosberg, A. R. Khoklov, *Giant Molecules*, Accademic Press, San Diego, 1997, p.73.

[12] J. Zhang, J. S. Moore, *J. Am. Chem. Soc.* **1992**, 114, 9701; A. S. Shetty, J. Zhang, J. S. Moore, *J. Am. Chem. Soc.* **1996**, 118, 1019; Y. Tobe, N. Utsumi, K. Kawabata, K. Naemura, .*Tetrahedron Lett.*, **1996**, 37, 9325; Y. Tobe, N. Utsumi, K. Naemura, *Angew. Chem. Int. Ed. Engl.* **1998**, 37, 1285.

[13] R. B. Prince, S. A. Barnes, J. S. Moore, *J. Am. Chem. Soc.* **2000**, 122, 2758; M. S. Gin, T. Yokozawa, R. B. Price, J. S. Moore, *J. Am. Chem. Soc.* **1999**, 121, 2643; R. B. Price,T. Okada, J. S. Moore *Angew. Chem. Int. Ed. Engl.* 1999, 38, 233; J. C. Nelson, J. G. Saven, J. S. Moore, P. G. Wolynes, *Science* **1997**, 277, 1793.

[14] S. Höger, K. Bonrad, M. Möller, A. Mourran, U. Beginn, submitted

[15] Hamley , Ian W, " *The physics of block copolymers* ", Oxford University Press , 1998.

[16] B. Perly, A. Douvy, and B. Gallot, *Makromoleculaire Chemie*, **1976**, 177, 2569.

[17] S.-D. Lee, and R. B. Meyer, *Physical Review Letters*, **1998**, 61, 2217.

[18] A. Nakajiama, T. Hayashi, K. Kugo, K. Shinoda, *Macromolecules*, **1979**, 12, 840; A. Nakajiama, K. Kugo, T. Hayashi, *Macromolecules*, **1979**, 12, 844.

[19] K. Loos, R. Stadler, *Macromolecules*, **1997**, 30, 7641.

[20] D. Marsitzky, T. Brand, Y. Geerts, M. Klapper and K. Müllen, *Macromol. Rapid. Commun*., **1998**, 19, 385.

[21] S. A. Jenekhe and X. L. Chen, *Science*, **1998**, 279, 1903; S. A. Jenekhe and X. L. Chen, *Science*, **1999**, 283, 372.

[22] J. T. Chen, I. L. Thomas, C. K. Ober, and S. S. Hwang, *Macromolecules*, **1995**, 28, 1688; J. T. Chen, I. L. Thomas, C. K. Ober, and G.-P. Mao, *Science*, **1996**, 273, 343.

[23] L. H. Radzilowski, and S. I. Stupp, *Macromolecules*, **1994**, 27, 7747; L. H. Radzilowski, J. L. Wu, and S. I. Stupp, *Macromolecules*, **1993**, 26, 879.

[24] L. H. Radzilowski, B. O. Carragher and S. I. Stupp, *Macromolecules*, **1997**, 30, 2110.

[25] H. Kukula, U. Ziener, M. Schöps and A. Godt, *Macromolecules*, **1998**, 31, 5160.

[26] M. A. Hempenius, B. M. W. Langeveld-Yoss, J. A. E. H. van Harre, R. A. J. Janssen, S. S. Sheiko, J. P. Spatz, M. Möller and E. W. Meijer, *J. Am. Chem. Soc.*, **1998**, 120, 2798.

[27] A. Halperin, , *Macromolecules*, **1990**, 23, 2724; D. R. M. Willliams and G. H. Fredrickson, *Macromolecules*, **1992**, 25, 3561; M. Müller, M. Schick, *Macromolecules*, **1996**, 29, 8900.

[28] M. Lee, N.-K. Oh, H.-K. Lee and W.-C. Zin, *Macromolecules*, **1996**, 29, 5567.

[29] M. Lee, B.-K. Cho, H. Kim and W.-C. Zin, *Angew. Chem. Int. Ed*. **1998**, 37, 638.

[30] M. Lee, D.-W. Jang, Y.-S. Kang and W.-C. Zin, *Adv. Mater*. **1999**, 11, 1018.

[31] P. Leclère, A. Calderone, D. Marsitzky, V. Francke, Y. Geerts, K. Müllen, J. L. Brédas and R. Lazzaroni, *Adv. Mater*. **2000**, 12, 1042.

[32] J. A. Massey, K. N. Power, I. Manners and M. A. Winnik, *J. Am. Chem. Soc*., **1998**, 120, 9533.

[33] J. A. Massey, K. Temple, L. Cao, Y. Rharbi, J. Raez, M. A. Winnik and I. Manners, *J. Am. Chem. Soc*., **2000**, 122, 11577.

[34] J. Raez, R. Barjovanu, J. A. Massey, M. A. Winnik and I. Manners, *Angew. Chem. Int. Ed*. **2000**, 39, 3862.

[35] H. A. Staab, K. Neunhoeffer, *Synthesis*, **1974**, 424.

[36] J. Zhang, D. J. Pesak, J. L. Ludwig, J. S. Moore *J. Am. Chem. Soc.* **1994**, 116, 4227.

[37]T. Zimmermann, G. W. Fischer, *J. prakt. Chem*., **1987**, 329(6), 975.

[38] K. Bonrad, *PhD Thesis*, University of Mainz, **1999**.

[39] S. Höger, A-D. Meckenstock and H. Pellen, *J. Org. Chem.* **1997**, 62, 4556 see supporting information.

[40]C. Glaser, *Chem. Ber.* **1869**, 2, 422; b) C. Glaser, . *Ann. Chem.* **1870**, 137, 154.

[41]For a review on oxidative coupling of acetylenes see L. I. Simándi, "The chemistry of functional Groups, Supplement C" cap.13, John Wiley, New York, **1983.**

[42] A. Hirao, H. Nagahama, T. Ishizone, S. Nakahama, *Macromolecules*, **1993**, 26, 2145.

[43]J. C. M. van Hest, *PhD Thesis*, University of Eindhoven, **1996**; J. C. M van Hest., D. A. P.Delnoye, M. W. P. L. Baars, C. ElissenRoman, M. H. P. van Genderen, E. W. Meijer, *Chem. Eur. J.* **1996**, 12, 1616.

[44] a) J. S. Moore, S. I. Stupp, *Macromolecules* **1990**, 23, 65; b) A. Hasser, V. Axexanian, *Tetrahedron Lett.* **1978**, 19, 4475; c) E. P. Boden, G. E. Keck, *J. Org. Chem.* **1985**, 50, 2394; d) E. F. V. Scriven, *Chem. Soc. Rev.* **1983**, 12, 129.

[45] S. W. Provencher, *Comp. Physic Comm*, **1982**, 27, 229; S. W. Provencher, *Makromol. Chem.*, **1979**, 180, 201.

[46] P. Denkinger, W. Burchard, *J. Pol. Sci.* **1991**, 29, 589.

[47] D. Marquardt, *Journal the Society For Industrial and Applied Mathematics* **1963**, 11, 431.

[48] P. Bevington, *Data Reduction and Error Analysis for the Physical Sciences* , McGraw-Hill, New York, **1969**

[49] J. Pedersen, *Advances in Colloid and Interface Science* **1997**, 70, 171,

[50] a) M. Schmidt, W. H. Stockmayer, *Macromolecules* **1984**, 17, 509; b) H.-G. Elias, *Makromoleküle Bd. 1*, Verlag Hüthig & Wepf, Basel, **1990**.

[51] H. Höger, V. Enkelmann, *Angew. Chem. Int. Ed. Engl.* **1995**, 34, 2713; b) H. Höger, V. Enkelmann, K. Bonrad, C. Tschierske *Angew. Chem. Int. Ed. Engl.* **2000**, 39, 2268.

[52] a) P. Dziezok, S. S. Sheiko, K. Fischer, M. Schmidt, M. Möller *Angew. Chem. Int. Ed. Engl* **1997**, 36, 2812; b) A. D. Schlüter, J. P. Rabe, *Angew. Chem. Int. Ed. Engl* **2000**, 39, 864.

[53] A. W. Adamson *Physical Chemistry of Surfaces* , John Wiley & Sons, New York, **1990**

[54] a) A. S. Shetty, P. R. Fischer, K. F. Stork, P. W. Bohn, J. S. Moore *J. Am. Chem. Soc.* 1996, 118, 9409;b) O. Y. Mindyuk, M. R. Stetzer, D. Gidalvitz, P. A. Heiney, J. C. Nelson, J. S. Moore *Langmuir* **1999**, 15, 6897

[5555] S.J. Clarson, K. Dodgson, J.A. Semlyen, *Polymer* **1985**, 26, 930.

[56] M. Lee, B.-K. Cho, H. Kim, J.-Y. Yoon, W.-C. Zin, *J. Am. Chem. Soc.* **1998**, 120, 9168; M. Lee, D.-W. Lee,B.-K. Cho, *J. Am. Chem. Soc.* **1998**, 120, 13258.

[57] Dissertation Dr. Klaus Bonrad, Mainz, **1999**.

[58] S. Höger, A-D. Meckenstock and H. Pellen, *J. Org. Chem.* **1997**, 62, 4556 see supporting information.